

Cover Page



Universiteit Leiden



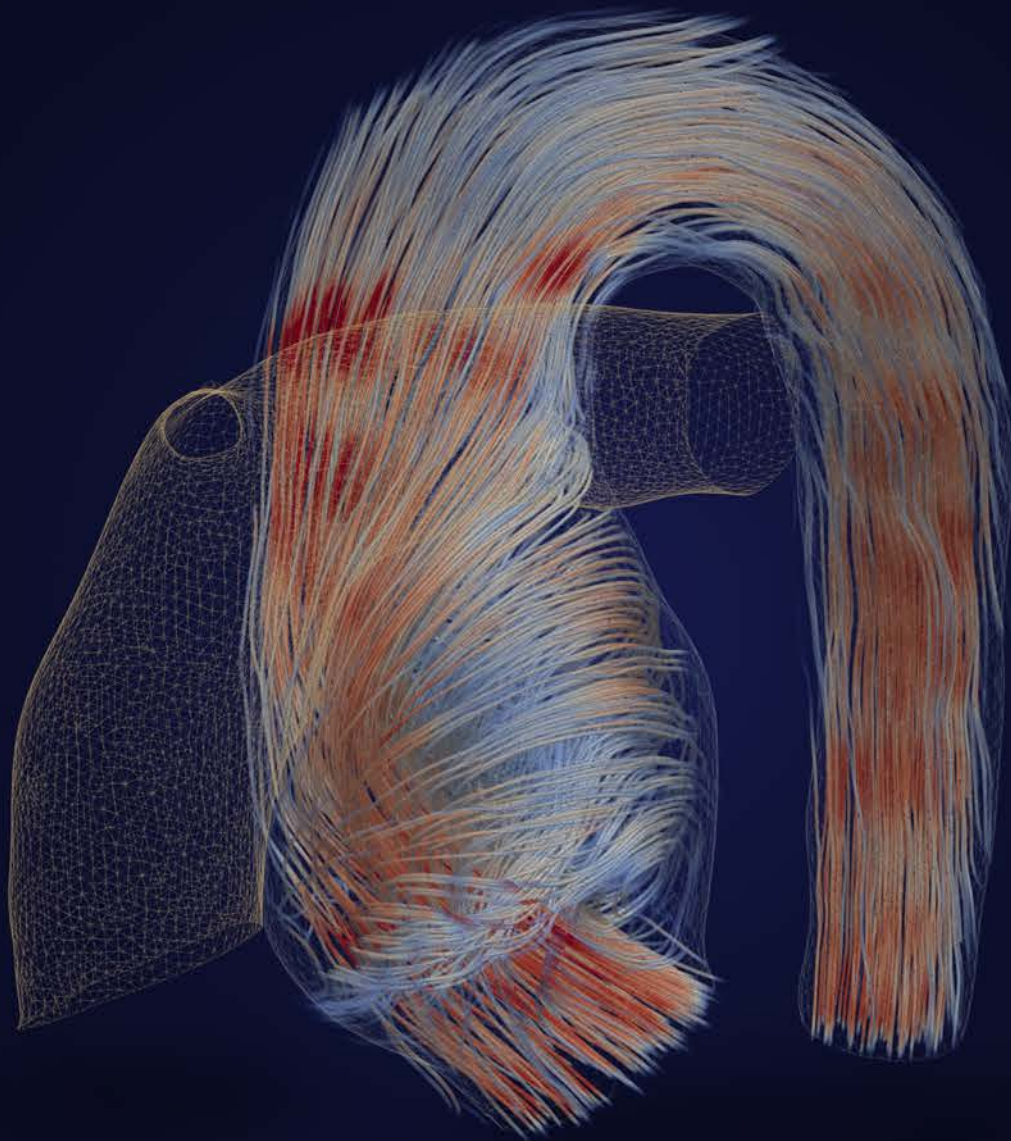
The handle <http://hdl.handle.net/1887/3185513> holds various files of this Leiden University dissertation.

**Author:** Palen, R.L.F. van der

**Title:** The aorta in transposition of the great arteries

**Issue date:** 2021-06-16

# THE AORTA IN TRANSPOSITION OF THE GREAT ARTERIES



Roel van der Palen



# **THE AORTA IN TRANSPOSITION OF THE GREAT ARTERIES**

**Roel Laurens Frederik van der Palen**

© Roel van der Palen, 2021

All rights reserved. No part of this thesis may be reproduced, stored or transmitted in any form or by any means without prior permission of the author, or the copyright-owning journals for previously published chapters.

ISBN: 978-94-6423-275-2

The research described in this thesis was supported by a grant of the Dutch Heart Foundation (DHF grant number 2014T087).

Financial support by the Dutch Heart Foundation for the publication of this thesis is gratefully acknowledged.

The printing of this thesis was financially supported by: Willem Alexander Children's Hospital and Pie Medical Imaging B.V.

Cover design & lay-out: Wendy Schoneveld || [www.wenziD.nl](http://www.wenziD.nl)

Cover image: Roel van der Palen en Friso Rijnberg

Printed by: ProefschriftMaken || [www.proefschriftmaken](http://www.proefschriftmaken)

# **THE AORTA IN TRANSPOSITION OF THE GREAT ARTERIES**

## **Proefschrift**

ter verkrijging van  
de graad van doctor aan de Universiteit Leiden,  
op gezag van rector magnificus prof. dr. ir. H. Bijl,  
volgens besluit van het college voor promoties  
te verdedigen op woensdag 16 juni 2021  
klokke 15.00 uur

door

**Roel Laurens Frederik van der Palen**

geboren te Valkenswaard

in 1982

Promotores: Prof. dr. N.A. Blom  
Prof. dr. M.G. Hazekamp

Co-promotor: Dr. A.A.W. Roest

Promotiecommissie: Prof. dr. H.J. Lamb  
Prof. dr. K. François (Universitair Ziekenhuis Gent, Gent, België)  
Prof. dr. W.A. Helbing (Erasmus Medisch Centrum, Rotterdam)

*Voor mijn familie*



# Contents

<b>CHAPTER 1</b>	General introduction and outline of the thesis	9
------------------	--	---

## **PART I The neo-aorta in TGA**

### Outcome after arterial switch operation

<b>CHAPTER 2</b>	Long-term outcome after the arterial switch operation: 43 years of experience	23
------------------	---	----

<b>CHAPTER 3</b>	Transposition of the great arteries: fetal pulmonary valve growth and postoperative neo-aortic root dilatation	53
------------------	--	----

<b>CHAPTER 4</b>	Progression of aortic root dilatation and aortic valve regurgitation after the arterial switch operation	75
------------------	--	----

<b>CHAPTER 5</b>	Neo-aortic growth rate and diameter as risk factors for neo-aortic valve regurgitation after arterial switch operation	99
------------------	--	----

## **PART II Aortic 4D flow MR imaging**

### The arterial switch operation for TGA and beyond

<b>CHAPTER 6</b>	Scan-rescan reproducibility of segmental aortic wall shear stress as assessed by phase-specific segmentation with 4D flow MRI in healthy volunteers	109
------------------	---	-----

<b>CHAPTER 7</b>	Altered ascending aorta hemodynamics in patients after arterial switch operation for transposition of the great arteries	131
------------------	--	-----

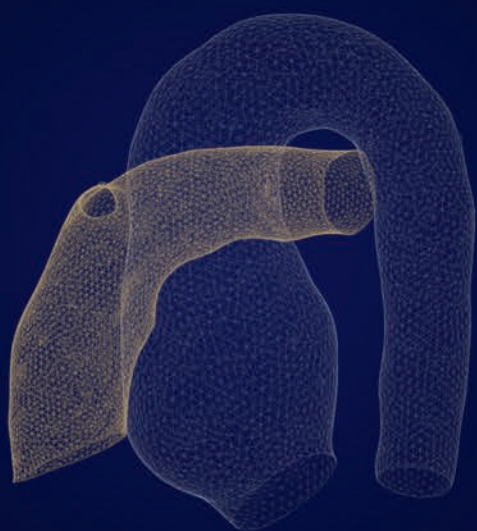
<b>CHAPTER 8</b>	Wall shear stress in the thoracic aorta at rest and with dobutamine stress after arterial switch operation	155
------------------	--	-----

<b>CHAPTER 9</b>	Altered aortic 3D hemodynamics and geometry in pediatric Marfan syndrome patients	177
------------------	---	-----

<b>CHAPTER 10</b>	Summary and future perspectives	197
<b>CHAPTER 11</b>	Nederlandse samenvatting	211

## **APPENDICES**

List of publications	226
Authors' affiliations	230
Dankwoord	233
Curriculum Vitae	236



# **CHAPTER 1**

General introduction

## Transposition of the great arteries

Transposition of the great arteries (TGA) is a congenital heart disease characterised by atrioventricular concordance and ventriculoarterial discordance: the right atrium is connected to the right ventricle from which the entire or most of the aorta originates; the left atrium is connected to the left ventricle from which the pulmonary artery arises. This results in a circulation in which the pulmonary and systemic circulation are running in parallel rather than in series. Postnatally, the blood with high oxygen content, coming from the lungs enters the left atrium, passes the left ventricle and is redirected to the lungs again; blood with low oxygen content returning from the body enters the right atrium and is redirected to the body again via the right ventricle, without passing the lungs. Cyanosis is often present directly after birth and survival is dependent on the presence of adequate communications between the two circulations (i.e. presence of an atrial septal defect or ventricular septal defect (VSD)). When these communications are too small or absent, neonates will deteriorate clinically with systemic acidosis, hypoxia and eventually leading to death. Neonates can be stabilized hemodynamically in the first days after birth by administration of prostaglandin E1, to maintain patency of the arterial duct ensuring sufficient pulmonary venous flow for mixing. In addition, a balloon atrial septostomy may be necessary to create an unrestrictive interatrial communication allowing adequate mixing between the systemic and pulmonary circulation.

Prenatal detection of TGA is of paramount importance as it may prevent hypoxia and acidosis early after birth thereby improving preoperative morbidity and mortality rates.<sup>1</sup> Ultimately, children with TGA need corrective cardiac surgery as only option for survival. A natural history study performed in California (1957-1964) showed that without intervention life expectancy in children with TGA is short and dependent on associated lesions: about 30% and 52% of the patients die within the first week and first month after birth respectively, 86% within 6 months and 89% within the first year of life.<sup>2</sup>

## The arterial switch operation – Leiden history

The current surgery of choice is the arterial switch operation (ASO). Before mid-eighties, children with TGA were treated by the *atrial* switch operation (according to dr. W.T. (William) Mustard or dr. A. (Åke) Senning). This surgical approach is based on an *atrial* rerooting of the systemic and pulmonary venous blood, by constructing an intraatrial baffle, leaving the right ventricle in the position to sustain the systemic circulation and the left ventricle in the position to sustain the pulmonary circulation. However, the systemic right ventricle is not developed to pump against high systemic arterial vascular resistance for many years and will fail sooner or later causing heart failure and ventricular arrhythmias.<sup>3,4</sup> Furthermore, the complex intraatrial surgery of the *atrial* switch procedure is also complicated by sinus node dysfunction, atrial arrhythmias, baffle stenosis<sup>5</sup> and baffle leakages during early-

mid- and long-term follow-up.<sup>3,6</sup> These complications contribute to a high risk of reoperations, interventions and a limited life expectancy.<sup>3,4,6,7</sup>

A significant milestone in congenital cardiac surgery was the introduction of a new surgical technique for TGA patients: the arterial switch operation (ASO). In Leiden, the ASO for the correction of TGA already started very early, only two years after the first successful ASO by dr. A.D. (Adib) Jatene in 1975.<sup>8</sup> Leiden's cardiothoracic surgeon prof. dr. A.G. (Gerard) Brom and the South African-born British cardiothoracic surgeon dr. D.N. (Donald) Ross performed the first ASO in a patient with TGA and VSD in May 1977 at the Academic Hospital Leiden. The ASO restores the ventriculoarterial concordance in such way that after repair the left and right ventricle support the systemic and pulmonary circulation respectively. During the ASO, the ascending aorta and pulmonary trunk are transected just above the commissures and relocated, leaving the semilunar valves and native roots in its original position. Consequently, the proximal part of the native pulmonary trunk becomes the neo-aorta and the native aortic root becomes the neo-pulmonary trunk. The coronary arteries are harvested from the native aortic root and are also relocated to the neo-aortic root. In the classical ASO as described by dr. Jatene, the reconstruction of the neo-pulmonary trunk was performed by a conduit.

Since the mid-eighties, after most high-volume surgical centers accomplished low perioperative mortality, the ASO technique replaced *atrial* switch operation worldwide. Leiden has played a role in this achievement, with its cardiothoracic surgeons prof. dr. Brom and prof. dr. J.M. (Jan) Quaegebeur as leading European pioneers and teachers of the ASO and other techniques in pediatric congenital heart surgery.<sup>9</sup>

## TGA subtypes and surgical refinements to the ASO

There is a so far unexplained male predominance in TGA patients with a male to female ratio of approximately 2:1. TGA is usually an isolated lesion (65% of the cases) but may be associated with a ventricular septal defect (VSD), left ventricular outflow tract obstruction, and abnormalities related to the pulmonary valve (i.e. bi-leaflet, asymmetrical three-leaflet or stenotic valve) or the aortic arch. A slightly different TGA subtype, also amenable for ASO, is double outlet right ventricle (DORV) with subpulmonary VSD (i.e. Taussig-Bing anomaly), which is frequently associated with an aortic arch abnormality and/or aortic outflow obstruction. Moreover, there is a large variation of coronary artery patterns in TGA patients. The international nomenclature for the structural description of these variants and its course, irrespective of the position of the great arteries, has been simplified by the introduction of the Leiden Convention coronary coding system invented by the Leiden professor of Anatomy and Embryology dr. A.C. (Adriana) Gittenberger-de Groot.<sup>10</sup>

Certain coronary variants necessitate different surgical techniques of coronary artery transfer. These techniques developed over time, as did other refinements that were implemented to optimize ASO. An important improvement was the application of the

Lecompte maneuver developed by dr. Y (Yves) Lecompte and his colleagues.<sup>11</sup> With this maneuver the pulmonary artery bifurcation is transferred to the front of the ascending aorta and made a direct reconstruction of the neo-pulmonary artery possible without the need of prosthetic conduits.<sup>11</sup> As a result, an altered spatial great artery relationship and geometry of the thoracic (neo-)aorta remains after ASO with Lecompte maneuver (Figure 1). Reconstruction of the neo-pulmonary artery after harvesting the coronary arteries is usually performed by using a pantaloons-shaped patch of fresh autologous pericardium.

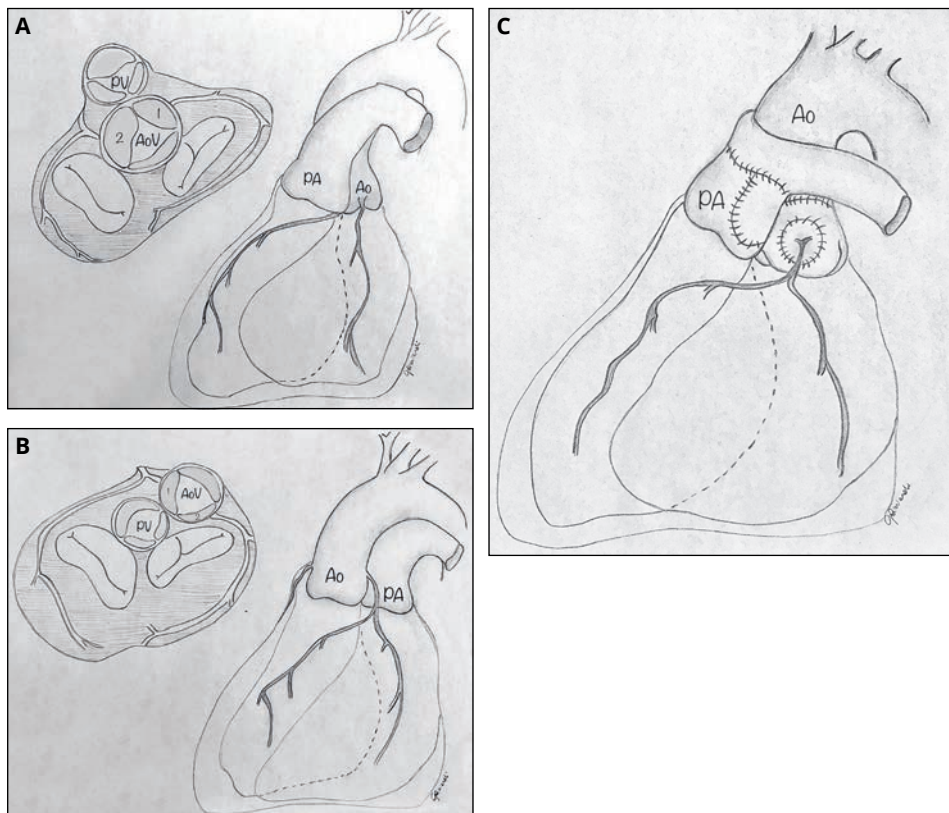


**Figure 1.** Representation of the great artery anatomy of the normal heart and the heart with transposition of the great arteries before and after the arterial switch operation.

*Drawings by Gabriella Ricciardi - adapted and expanded after Prêtre et al. Lancet 2001;357:1826–30.*

Normal heart (A); Transposition of the great arteries (B); Arterial switch operation (C). Note the anterior position of the pulmonary artery bifurcation over the ascending aorta after arterial switch operation and the translocation of the coronary arteries to the neo-aortic root (C). 1, *sinus 1* or right-hand facing sinus; 2, *sinus 2* or left-hand facing sinus (according to the Leiden Convention coronary coding system); Ao, aorta; AoV, aortic valve; PA, pulmonary artery; PV, pulmonary valve.

## Long-term outcome – the neo-aorta

From short- and mid-term follow-up studies after ASO<sup>9,12-14</sup> and mid- and long-term follow-up studies of the *atrial* switch cohort,<sup>3,6</sup> we may now conclude that the step towards the ASO technique was a good decision. Over the years, early mortality rates decreased significantly to current rates less than 5% in large international pediatric cardiac surgical centers. The question remains how the long-term cardiovascular status of these patients develops, with the first patients now reaching the age of 40 years post-ASO.

Residual problems are recognized during follow-up. The overall surgical and percutaneous intervention rates for right-sided lesions varies from 11-28% between different studies.<sup>15-17</sup> Less is known about the residual lesions and the need for interventions on the left side of the heart in the long-term. Neo-aortic root pathology plays a central role in the management of patients after ASO. Neo-aortic dilatation has been reported to be present in more than two-third of the patients but data on the progression of neo-aortic dilatation in adulthood are scarce and controversial.<sup>18-21</sup> There are concerns about impairment of neo-aortic valve function over time and whether neo-aortic root dilatation may play a key role in this. Furthermore, aortic expansion also enhances branch pulmonary artery stenosis<sup>22</sup> and is associated with a more acute angulation of the reimplanted coronary arteries possibly increasing the risk of coronary malperfusion, ventricular dysfunction and even sudden cardiac death.<sup>23,24</sup>

Neo-aortic valve repair with root reconstruction or even valve and/or root replacement is required when aortic complications progress. If valve replacement already needs to be done at very young age, the use of the autologous neo-pulmonary valve (the former aortic valve) is the preferred choice. This procedure for smaller children after ASO was first introduced by the Leiden cardiothoracic surgeon prof. dr. M.G. (Mark) Hazekamp and named this procedure the *switch back Ross operation*.<sup>25</sup> Together with cardiothoracic surgeon dr. D.R. (David) Koolbergen he reported that redo neo-aortic surgery for neo-aortic valve and root pathology can be performed with low risk taking into account the specific technical difficulties.<sup>26</sup> During these reoperations, remarkable thinning of the anterior wall of the ascending aorta was observed in many of these patients, located close to the level of the pulmonary artery embracement over the aorta after Lecompte maneuver.<sup>26</sup>

The course of neo-aortic root pathology in the long run is largely unknown and the contributors leading to neo-aortic valve and root problems are important to identify. In **part I** of this thesis, the unexplored questions regarding the long-term cardiovascular outcome and the fate of the neo-aortic valve and root are investigated. The incidence of adverse cardiovascular outcome, such as late death, presence of arrhythmias, coronary artery issues and the need for reoperations or catheter interventions are assessed in the cohort of the Center for Congenital Heart Disease Amsterdam-Leiden (CAHAL) with current 43-year experience of ASO. Neo-aortic valve function and the course of neo-aortic root dilatation during long-term follow-up for the various morphological subtypes of TGA after ASO are studied longitudinally. Furthermore, fetal growth of the semilunar valves is



investigated in order to understand the origin of the differences between the morphological subtypes of TGA (and with normal fetal semilunar growth), as starting point for the further course of neo-aortic valve and root growth beyond ASO. Finally, questions regarding the critical factor(s) for the neo-aortic root dilatation and impairment of neo-aortic valve function in the long-term are addressed.

## Evaluation of thoracic aorta hemodynamics with 4D flow MRI

The etiology of neo-aortic root pathology and anterior aortic wall thinning after ASO is not clear and the pathophysiological mechanisms leading to neo-aortic root dilatation have not been elucidated so far. The pulmonary root in the systemic circulation and the structural cell differences in the neo-aortic root wall itself, as described by the Leiden group,<sup>27,28</sup> have been reported previously as risk factors for dilatation.

Computational fluid dynamic model studies, simulating patient specific cardiac pathologies, have shown *in vitro* that altered hemodynamics can play a causative role in modelling of the heart and large blood vessels.<sup>29</sup> The concept that altered blood flow patterns with altered local shear stress acting on the vessel wall in a reconstructed neo-aortic root after ASO for TGA may contribute to the development of root dilatation is of importance. However, this has not been investigated so far.

Recently, four-dimensional flow magnetic resonance imaging (4D flow MRI) has been introduced as a novel non-invasive imaging tool that can be used for comprehensive *in vivo* assessment of blood flow in the large vessels.<sup>30</sup> It provides information about the spatial and temporal distribution of vascular blood flow and enables the quantification of flow related hemodynamic parameters. Using this technique, it has been shown that altered blood flow hemodynamics like blood flow profile and wall shear stress cause remodelling of the large vessels and dilation of the aorta in patients with bicuspid aortic valve disease.<sup>31,32</sup> The application of aortic 4D flow MRI can therefore be of great value for the evaluation of aortopathy in patients after ASO for TGA.

Leonardo da Vinci already demonstrated 500 years ago (~1507-1513) the flow patterns within the aortic root by his genius sketches (Figure 2A), presumably based on his observations from blood flow simulations in glass models with grass seeds suspended in water.<sup>33,34</sup> Da Vinci proposed that these observed vortical flow patterns in the aortic root aid in closure of the aortic valve and postulated that these secondary vortices do not occur more distal in the normal ascending aorta, where the flow is laminar.<sup>33</sup> With the use of the advanced 4D flow MRI technology, we can now prove that the flow phenomena expressed in his sketches show a highly accurate representation of the actual flow patterns in the proximal ascending aorta (Figure 2A and 2B).

4D flow MRI enables us to gain new insights in the contribution of flow dynamics on the development of aortic disease (i.e. pathophysiology) or disease progression in genetic inherited and congenital heart disease related aortopathies. In **part II** of this thesis, the 4D

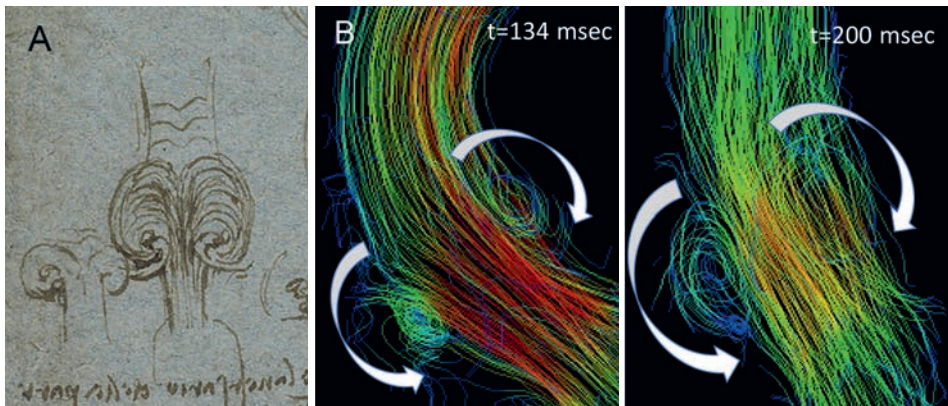


**Figure 2.** Vortex patterns in the aortic root and the laminar flow downstream the ascending aorta by a schematic sketch from Leonardo da Vinci (A) and by streamline visualization from 4D flow MRI of the proximal part of ascending aorta (B).

Figure 2A. Detail of RL19083 verso, Blood flow through the aortic valve. Leonardo da Vinci, c.1512-13. – Courtesy by Royal Collection Trust / © Her Majesty Queen Elizabeth II 2020; Figure 2B. 4D flow MRI illustration derived from Chapter 9 of this thesis. Altered aortic 3D hemodynamics and geometry in pediatric Marfan syndrome patients. *J Cardiovasc Magn Reson.* 2017;19(1):30.

flow MRI technique is used to study on aortic hemodynamics in healthy volunteers and in TGA patients after ASO. Furthermore, the application of 4D flow MRI to assess aortopathy is explored in patients at risk for aortic problems such as patients with Marfan syndrome. Blood flow patterns and 4D flow MRI-derived parameters, regional aortic wall shear stress and aortic flow displacement, within the thoracic aorta are investigated to unravel aortic flow abnormalities and their relationship with altered aortic geometry which may be indicative for vascular wall remodeling and root dilatation. The aortic flow hemodynamics are evaluated in rest and during dobutamine-induced stress conditions.

## Aim and outline of this thesis

The aim of this thesis is to investigate the prevalence and evolution of neo-aortic root pathology and surgical cardiovascular outcomes in patients after ASO for TGA in the long-term. Secondly, thoracic aortic blood flow hemodynamics are investigated in relation to post-ASO geometry and root pathology with advanced non-invasive 4D flow cardiovascular MR imaging techniques.

**Part I** of the thesis focuses on the fate of the neo-aortic valve and the course of neo-aortic root dimensions during fetal development and long-term post-ASO with echocardiographic imaging. Risk factors for the impairment of the neo-aortic valve function are assessed and long-term cardiovascular outcomes such as the prevalence of late mortality and the need for reoperations and interventions are investigated.

**Part II** of the thesis describes the thoracic aortic blood flow hemodynamics from 4D flow MR imaging in relation to post-ASO geometry and its potential role in the contribution to neo-aortic root dilatation and aortic wall thinning. Prior to these studies, aortic blood flow in healthy volunteers is investigated to test reproducibility of the 4D flow MRI-derived wall shear stress parameter. In addition, to further explore the use of aortic 4D flow MR imaging in patients with dilative aortopathy, a 4D flow MRI study is performed in patients with Marfan syndrome to assess aortic geometry in relation to aortic wall shear stress.

## Part I

**Chapter 2** reports the long-term surgical outcomes after ASO for TGA performed in the Center for Congenital Heart Disease Amsterdam-Leiden (CAHAL), based on 43 years of experience and follow-up. Prevalence of reoperations and interventions, arrhythmias and late mortality are described and risk factors for reoperation and intervention are identified.

**Chapter 3** addresses fetal semilunar valve growth in conjunction with short-term postoperative neo-aortic root dilatation.

**Chapter 4** shows the neo-aortic growth, neo-aortic valve function and the need for reoperations on the neo-aortic valve and/or root during long-term follow-up for the various morphological subtypes of TGA after ASO. Moreover, risk factors for neo-aortic root dilatation and neo-aortic valve regurgitation are determined.

**Chapter 5** demonstrates the effect of changing neo-aortic dimensions over time on the risk of neo-aortic valve regurgitation.

## Part II

**Chapter 6** describes the scan-rescan validation and reproducibility study on the hemodynamic parameter wall shear stress derived from aortic 4D flow MR imaging in healthy volunteers. These data serve as reference data for the knowledge about variability of the hemodynamic parameter and to judge whether differences between patients and healthy volunteers or hemodynamic changes in patients over time or between rest-rest examinations represent true (patho)physiological differences.

**Chapter 7** shows the altered ascending aorta hemodynamics in patients after ASO for TGA and the effect of differences in aortic geometry on hemodynamics.

**Chapter 8** further delineates the abnormalities in aorta hemodynamics within the entire thoracic aorta after ASO by a rest versus dobutamine-stress comparison.

**Chapter 9** describes the altered aorta hemodynamics and geometry in pediatric Marfan syndrome patients.

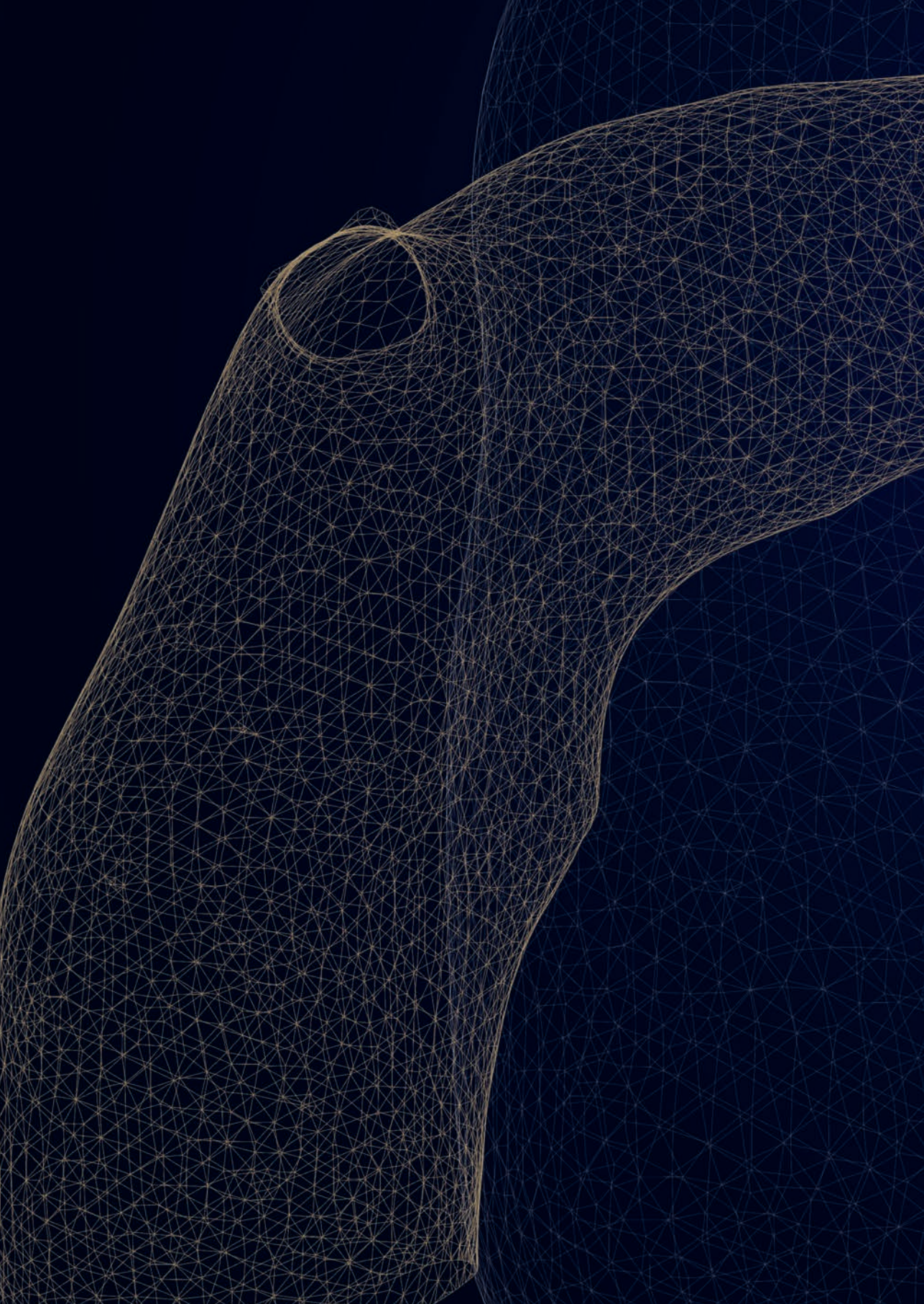
In **Chapter 10** the results of all studies from this thesis are summarized and clinical perspectives and future directions are discussed.

## References

1. van Velzen CL, Haak MC, Reijnders G, Rijlaarsdam ME, Bax CJ, Pajkrt E, Hruda J, Galindo-Garre F, Bilardo CM, de Groot CJ, et al. Prenatal detection of transposition of the great arteries reduces mortality and morbidity. *Ultrasound Obstet Gynecol*. 2015;45(3):320-5.
2. Liebman J, Cullum L, Belloc NB. Natural history of transposition of the great arteries. Anatomy and birth and death characteristics. *Circulation*. 1969;40(2):237-62.
3. Couperus LE, Vliegen HW, Zandstra TE, Kies P, Jongbloed MRM, Holman ER, Zeppenfeld K, Hazekamp MG, Schalij MJ, Scherp tong RWC. Long-term outcome after atrial correction for transposition of the great arteries. *Heart*. 2019;105(10):790-6.
4. Cuyper JA, Eindhoven JA, Slager MA, Opic P, Utens EM, Helbing WA, Witsenburg M, van den Bosch AE, Ouhlous M, van Domburg RT, et al. The natural and unnatural history of the Mustard procedure: long-term outcome up to 40 years. *Eur Heart J*. 2014;35(25):1666-74.
5. van der Palen RL, Westenberg JJ, Hazekamp MG, Kuipers IM, Roest AA. Four-dimensional flow cardiovascular magnetic resonance for the evaluation of the atrial baffle after Mustard repair. *Eur Heart J Cardiovasc Imaging*. 2016;17(3):353.
6. Gelatt M, Hamilton RM, McCrindle BW, Connelly M, Davis A, Harris L, Gow RM, Williams WG, Trusler GA, Freedom RM. Arrhythmia and mortality after the Mustard procedure: a 30-year single-center experience. *J Am Coll Cardiol*. 1997;29(1):194-201.
7. Venkatesh P, Evans AT, Maw AM, Pashun RA, Patel A, Kim L, Feldman D, Minutello R, Wong SC, Stribling JC, et al. Predictors of Late Mortality in D-Transposition of the Great Arteries After Atrial Switch Repair: Systematic Review and Meta-Analysis. *J Am Heart Assoc*. 2019;8(21):e012932.
8. Jatene AD, Fontes VF, Paulista PP, de Souza LC, Neger F, Galantier M, Souza JE. Successful anatomic correction of transposition of the great vessels. A preliminary report. *Arq Bras Cardiol*. 1975;28(4):461-64.
9. Quaegebeur JM, Rohmer J, Ottenkamp J, Buis T, Kirklin JW, Blackstone EH, Brom AG. The arterial switch operation. An eight-year experience. *J Thorac Cardiovasc Surg*. 1986;92(3 Pt 1):361-84.
10. Gittenberger-de Groot AC, Koenraadt WMC, Bartelings MM, Bokenkamp R, DeRuiter MC, Hazekamp MG, Bogers A, Quaegebeur JM, Schalij MJ, Vliegen HW, et al. Coding of coronary arterial origin and branching in congenital heart disease: The modified Leiden Convention. *J Thorac Cardiovasc Surg*. 2018;156(6):2260-9.
11. Lecompte Y, Neveux JY, Leca F, Zannini L, Tu TV, Dubois Y, Jarreau MM. Reconstruction of the pulmonary outflow tract without prosthetic conduit. *J Thorac Cardiovasc Surg*. 1982;84(5):727-33.
12. Hazekamp MG, Ottenkamp J, Quaegebeur JM, Hardjowijono R, Boot CA, Rohmer J, Huysmans HA. Follow-up of arterial switch operation. *Thorac Cardiovasc Surg*. 1991;39:166-9.
13. Lalezari S, Bruggemans EF, Blom NA, Hazekamp MG. Thirty-year experience with the arterial switch operation. *Ann Thorac Surg*. 2011;92(3):973-9.
14. Pretre R, Tamisier D, Bonhoeffer P, Mauriat P, Pouard P, Sidi D, Vouhe P. Results of the arterial switch operation in neonates with transposed great arteries. *Lancet*. 2001;357(9271):1826-30.
15. Cleuziou J, Vitanova K, Pabst von Ohain J, Ono M, Tanase D, Burri M, Lange R. Incidence and Risk Factors for Right Ventricular Outflow Tract Obstruction after the Arterial Switch Operation. *Thorac Cardiovasc Surg*. 2019;67(1):37-43.
16. Delmo Walter EM, Miera O, Nasser B, Huebler M, Alexi-Meskishvili V, Berger F, Hetzer R. Onset of pulmonary stenosis after arterial switch operation for transposition of great arteries with intact ventricular septum. *HSR Proc Intensive Care Cardiovasc Anesth*. 2011;3(3):177-87.
17. Nellis JR, Turek JW, Aldoss OT, Atkins DL, Ng BY. Intervention for Supravalvar Pulmonary Stenosis After the Arterial Switch Operation. *Ann Thorac Surg*. 2016;102(1):154-62.

18. Kempny A, Wustmann K, Borgia F, Dimopoulos K, Uebing A, Li W, Chen SS, Piorkowski A, Radley-Smith R, Yacoub MH, et al. Outcome in adult patients after arterial switch operation for transposition of the great arteries. *Int J Cardiol.* 2013;167(6):2588-93.
19. McMahon CJ, Ravekes WJ, Smith EO, Denfield SW, Pignatelli RH, Altman CA, Ayres NA. Risk factors for neo-aortic root enlargement and aortic regurgitation following arterial switch operation. *Pediatr Cardiol.* 2004;25(4):329-35.
20. van der Bom T, van der Palen RL, Bouma BJ, van Veldhuisen SL, Vliegen HW, Konings TC, Zwinderman AH, Blom NA, Koolbergen DR, Hazekamp MG, et al. Persistent neo-aortic growth during adulthood in patients after an arterial switch operation. *Heart.* 2014;100(17):1360-5.
21. Vandekerckhove KD, Blom NA, Lalezari S, Koolbergen DR, Rijlaarsdam ME, Hazekamp MG. Long-term follow-up of arterial switch operation with an emphasis on function and dimensions of left ventricle and aorta. *Eur J Cardiothorac Surg.* 2009;35(4):582-7.
22. Morgan CT, Mertens L, Grotenhuis H, Yoo SJ, Seed M, Grosse-Wortmann L. Understanding the mechanism for branch pulmonary artery stenosis after the arterial switch operation for transposition of the great arteries. *Eur Heart J Cardiovasc Imaging.* 2017;18(2):180-5.
23. Ou P, Khraiche D, Celermajer DS, Agnoletti G, Le Quan Sang KH, Thalabard JC, Quintin M, Raisky O, Vouhe P, Sidi D, et al. Mechanisms of coronary complications after the arterial switch for transposition of the great arteries. *J Thorac Cardiovasc Surg.* 2013;145(5):1263-9.
24. Veltman CE, Beeres SL, Kalkman DN, Kelder TP, Kies P, Vliegen HW, Hazekamp MG, Delgado V, Kroft LJ, van der Wall EE, et al. Variation in coronary anatomy in adult patients late after arterial switch operation: a computed tomography coronary angiography study. *Ann Thorac Surg.* 2013;96(4):1390-7.
25. Hazekamp MG, Schoof PH, Suys BE, Hutter PA, Meijboom EJ, Ottenkamp J, Huysmans HA. Switch back: using the pulmonary autograft to replace the aortic valve after arterial switch operation. *J Thorac Cardiovasc Surg.* 1997;114(5):844-6.
26. Koolbergen DR, Manshanden JS, Yazdanbakhsh AP, Bouma BJ, Blom NA, de Mol BA, Mulder BJ, Hazekamp MG. Reoperation for neo-aortic root pathology after the arterial switch operation. *Eur J Cardiothorac Surg.* 2014;46(3):474-9.
27. Lalezari S, Hazekamp MG, Bartelings MM, Schoof PH, Gittenberger-De Groot AC. Pulmonary artery remodeling in transposition of the great arteries: relevance for neo-aortic root dilatation. *J Thorac Cardiovasc Surg.* 2003;126(4):1053-60.
28. Lalezari S, Mahtab EA, Bartelings MM, Wisse LJ, Hazekamp MG, Gittenberger-de Groot AC. The outflow tract in transposition of the great arteries: an anatomic and morphologic study. *Ann Thorac Surg.* 2009;88(4):1300-5.
29. Morris PD, Narracott A, von Tengg-Kobligh H, Silva Soto DA, Hsiao S, Lungu A, Evans P, Bressloff NW, Lawford PV, Hose DR, et al. Computational fluid dynamics modelling in cardiovascular medicine. *Heart.* 2016;102(1):18-28.
30. Dyverfeldt P, Bissell M, Barker AJ, Bolger AF, Carlhall CJ, Ebbers T, Francios CJ, Frydrychowicz A, Geiger J, Giese D, et al. 4D flow cardiovascular magnetic resonance consensus statement. *J Cardiovasc Magn Reson.* 2015;17:72.
31. Guzzardi DG, Barker AJ, van Ooij P, Malaisrie SC, Puthumana JJ, Belke DD, Mewhort HE, Svystonyuk DA, Kang S, Verma S, et al. Valve-Related Hemodynamics Mediate Human Bicuspid Aortopathy: Insights From Wall Shear Stress Mapping. *J Am Coll Cardiol.* 2015;66(8):892-900.
32. Mahadevia R, Barker AJ, Schnell S, Entezari P, Kansal P, Fedak PW, Malaisrie SC, McCarthy P, Collins J, Carr J, et al. Bicuspid aortic cusp fusion morphology alters aortic three-dimensional outflow patterns, wall shear stress, and expression of aortopathy. *Circulation.* 2014;129(6):673-82.
33. Bissell MM, Dall'Armellina E, Choudhury RP. Flow vortices in the aortic root: in vivo 4D-MRI confirms predictions of Leonardo da Vinci. *Eur Heart J.* 2014;35(20):1344.
34. Gharib M, Kremers D, Koochesfahani MM, Kemp M. Leonardo's vision of flow visualization. *Experiments in Fluids.* 2002;33(1):219-23.



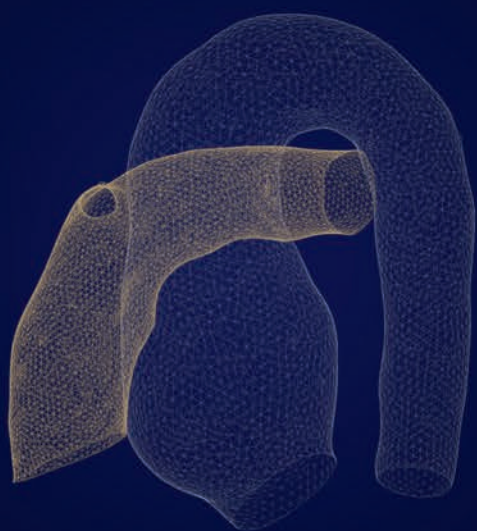




# PART I

**The neo-aorta in TGA**  
Outcome after arterial switch operation





## **CHAPTER 2**

# Long-term outcome after the arterial switch operation: 43 years of experience

European Journal of Cardio-Thoracic Surgery. 2021. Online ahead of print

Roel L.F. van der Palen  
Nico A. Blom  
Irene M. Kuipers  
Lukas A.J. Rammeloo  
Monique R.M. Jongbloed  
Thelma C. Konings  
Berto J. Bouma  
David R. Koolbergen  
Mark G. Hazekamp

## Abstract

### Objectives

The objective of this study was to assess our 43-year experience with arterial switch operation (ASO) for transposition of the great arteries (TGA) by analyzing cardiac outcome measures (hospital and late mortality, reoperations and catheter interventions, significant coronary artery obstruction) and to identify risk factors for reoperation and catheter interventions.

### Methods

A total of 490 patients who underwent ASO for TGA from 1977 to 2020 were included in this retrospective, single center study. Data on reoperation and catheter intervention of hospital survivors were estimated by the Kaplan-Meier method and compared using a long-rank test. Risk factors for reoperation and/or catheter intervention were assessed by multivariate Cox regression analysis.

### Results

Hospital mortality occurred in 43 patients (8.8%), late death in 12 patients (2.9%) and 43 patients were lost to follow-up. Median follow-up time of 413 hospital survivors was 15.6 (interquartile range 7.0-22.4) years. Reoperations were performed in 83 patients (117 reoperations). Neo-aortic valve regurgitation with root dilatation was the second most common indication for reoperation (15/83 patients, 18.1%) after right ventricular outflow tract obstruction (50/83 patients, 60.2%). Risk factors for any reoperation on multivariable analysis were: TGA morphological subtype [TGA with ventricular septal defect: hazard ratio (HR) = 1.99, 95% confidence interval (CI) 1.18-3.36,  $P = 0.010$  and TBA: HR = 2.17, 95% CI 1.02-4.64,  $P = 0.045$ ], aortic arch repair associated with ASO (HR = 3.03, 95% CI 1.62-5.69,  $P = 0.001$ ), and a non-usual coronary artery anatomy (HR = 2.41, 95% CI 1.45-4.00,  $P = 0.001$ ). One hundred and one catheter interventions were performed in 54 patients, usually for relief of supra-valvular pulmonary stenosis (44/54 patients, 81.5%) or arch obstruction (10/54 patients, 18.5%). Main risk factor for catheter intervention on multivariable analysis was aortic arch repair associated with ASO (HR = 2.95, 95% CI 1.37-6.36,  $P = 0.006$ ). Significant coronary artery stenosis was relatively uncommon (9/413 patients, 2.2%) but may be underrepresented.

### Conclusions

Patients after ASO typically have good long-term clinical outcomes but reoperations and interventions remain necessary in some patients. Neo-aortic valve regurgitation with root dilatation is the second most common indication for reoperation after right ventricular outflow tract obstruction and an increasing need for neo-aortic valve and root redo surgery in future is to be expected.

## Introduction

For more than forty years, the arterial switch operation (ASO) is the standard surgical treatment for transposition of the great arteries (TGA). Surgical results with low perioperative mortality over the last decades have now led to focus on the long-term outcomes. Health condition and quality-of-life assessments recently showed that most adult patients perceive normal functional health status, similar to healthy peers.<sup>1</sup> Cardiovascular outcome and survival from mid- and long-term follow-up studies are based on data from 20- up to 30-year post-ASO. In these reports residual lesions are reported such as supra-avalvular pulmonary stenosis,<sup>2-4</sup> neo-aortic root dilatation, neo-aortic valve insufficiency<sup>5, 6</sup> and coronary artery problems.<sup>7-9</sup> The purpose of this study was to assess our 43-year experience with ASO and to determine late mortality and morbidity, including coronary artery stenosis, arrhythmias and cardiac device implantations, as well as the need for reoperation and catheter intervention, and finally, to identify risk factors for cardiovascular reoperation and catheter intervention.

## Methods

### Study population

Patients who underwent ASO for TGA at the Leiden University Medical Center, Leiden, between January 1977 and January 2020 were included in this study. TGA subgroups based on anatomic differences included: TGA with intact ventricular septum (TGA-IVS); TGA with ventricular septal defect (TGA-VSD) and double outlet right ventricle with subpulmonary VSD (i.e. Taussig-Bing anomaly, TBA). Data on demographics, morphologic and surgical details, reoperations, catheter interventions, coronary artery problems, atrial or ventricular arrhythmias, the need for cardiac devices (pacemaker and implantable cardioverter-defibrillator) and mortality were collected from hospital and outpatient records. Hospital mortality was defined as death occurring before hospital discharge; late mortality was defined as death after hospital discharge. Reoperations and catheter interventions were subdivided in early (<30 days post-ASO) and late reoperations/interventions (>30 days post-ASO). Re-explorations for perioperative complications (e.g. for bleeding) were not included. Catheter ablations for arrhythmias were not included as catheter intervention but were reported separately. Rhythm disorders after hospital discharge were assessed. Left ventricular outflow tract obstruction was included as a separate variable; patients with TGA-VSD and (sub)pulmonary stenosis were only included when ASO had been performed ( $n = 4$ ) and were classified into the TGA-VSD group. The local Committee for Medical Ethics of the Amsterdam and Leiden University Medical Centers approved the study and waived the need for informed consent. Data collection was completed in January 2020.

**Surgical procedure**

A description of the ASO procedure in our center and indications for two-stage correction for TGA have been reported previously:<sup>10</sup> coronary artery translocation was performed by the button technique whenever feasible or by trap-door technique otherwise. In case of posterior common ostium (Yacoub types B and C), the technique as described by Yacoub was used.<sup>11</sup> The neo-pulmonary artery was reconstructed by using a pantaloony-shaped patch of fresh autologous pericardium. The Lecompte maneuver has been applied whenever possible since 1981; before that time, a classical Jatene procedure with implantation of a conduit between the right ventricle and pulmonary artery (PA) was performed. A Lecompte procedure was avoided when a side-to-side relationship of the great arteries was found, as this would lead to stretching and narrowing of the left PA. VSDs were closed via the right atrium or the aortic valve, and in TBA, the approach to the VSD was often from multiple sides sometimes including a limited right ventriculotomy. Arch repair was only by extended side-to-side anastomosis when a discrete coarctation was present; in all other cases, the arch was repaired with a xenopericardial curved patch which has the additional advantage of a better fit to the wider PA base.

**Statistical analysis**

Statistical analysis was performed using IBM SPSS Statistics 23.0. Clinical characteristics were presented as frequency (%) for categorical variables or as median (interquartile range, IQR or range). The normality of the distribution was tested using the Shapiro-Wilk test. Differences in frequencies of baseline characteristics and outcome parameters between TGA subgroups were assessed by the Fisher-Freeman-Halton exact test. A Kruskal-Wallis test was performed to test for differences in continuous data between the TGA subgroups. Primary outcome parameters were reoperations and catheter interventions. Secondary outcome parameters were hospital and late mortality, arrhythmias and coronary artery problems.

Kaplan-Meier analyses were performed to estimate overall survival and reoperation and catheter intervention-free survival of hospital survivors, and to estimate differences in reoperation rate and type based on era. Patients with late mortality, without having had reoperation (7/12 patients) or catheter intervention (10/12 patients) before death occurred, were censored at the age of death in this analysis (considering late death as competing risk resulted in similar percentages of freedom from reoperation/catheter intervention). The log-rank test was used to test for differences between intervention-free (reoperation, catheter intervention or both) survival curves among morphological TGA subtypes. A Cox regression model was used to assess the independent predictive values of different variables on primary outcome measures reoperation and/or catheter intervention, resulting in cause-specific hazard ratios (HRs) for the variables. Risk factors known from literature and potential explanatory variables were entered into the equation at the same time. Included risk factors from literature were: 'TGA morphological subtype'; 'arch abnormality', for which surgical repair was performed; 'left ventricular outflow tract obstruction'; PA banding prior to ASO,

'prior PA banding'; 'coronary artery anatomy', divided in 2 categories: (1) usual coronary artery anatomy: *1LCx-2R, 1L-2CxR and 1L-2R, no Cx* and (2) non-usual coronary artery anatomy: other than (1); 'weight at ASO'. Potential explanatory variables included in the models were: 'sex'; use of 'Lecompte maneuver' with the ASO. A  $P$  value  $<0.05$  (two-sided) was considered statistically significant.

## Results

### Patient characteristics and hospital mortality

During the study period, 490 patients underwent ASO. Thirty-four overseas patients were lost to follow-up. Hospital mortality was 8.8% (43 patients), highest from 1977 to 1987, and decreased to 3.3% between 2000 and 2020. Baseline patient characteristics of remaining 413 hospital survivors with follow-up are shown in Table 1. The morphological TGA subtypes were: TGA-IVS in 258 (62.5%), TGA-VSD in 117 (28.4%) and TBA in 38 (9.2%) patients. Arch anomalies for which surgical repair before or during ASO was necessary were present in 35 (8.5%) patients and consisted of hypoplastic aortic arch with ( $n = 25$ ) or without ( $n = 2$ ) coarctation, interrupted aortic arch ( $n = 7$ ) and double aortic arch with coarctation ( $n = 1$ ) (Table 1). The majority of the arch abnormalities were present in TBA patients ( $n = 18$ , 47.4%), in 14 (12.0%) of the TGA-VSD patients and in 3 (1.2%) of the TGA-IVS patients ( $P = 5.5 \times 10^{-16}$ ). Left ventricular outflow tract obstruction was not equally distributed across the TGA subgroups and present in 5 (13.2%) of the TBA patients, in 10 (8.5%) of the TGA-VSD patients and in 1 (0.4%) of the TGA-IVS patients ( $P = 3.0 \times 10^{-6}$ ). Median age at ASO was 8 days for the patients who underwent one-stage ASO. Forty-two patients had prior surgery before ASO (i.e. two-stage ASO). Median follow-up was 15.6 (IQR 7.0-22.4) years post-ASO, with a maximum follow-up of 41.1 years.

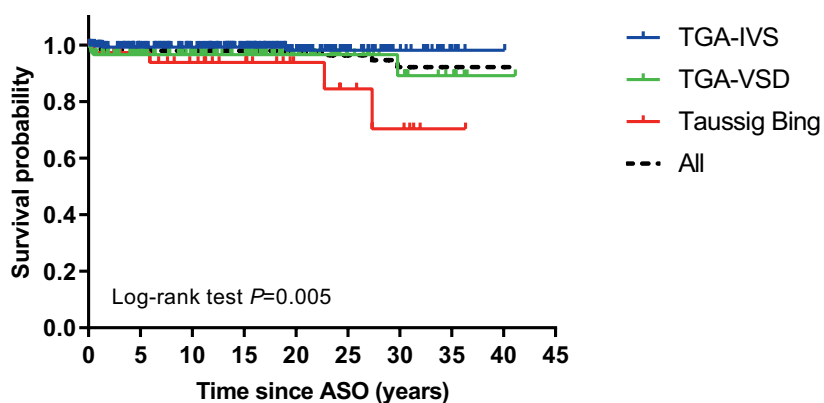
### Late mortality

Twelve patients died late during follow-up (2.9%). Median age of death was 10.6 (IQR 0.9-21.9) years. TGA morphology in these patients was as follows: TGA-IVS in 3 (1.2%), TGA-VSD in 5 (4.3%) and TBA in 4 (10.5%) patients ( $P = 0.006$ ). In 7 patients, the exact cause of death could not be retrieved retrospectively. Causes of mortality of the other patients were: recurrent *Staphylococcus Aureus* endocarditis of a Bentall prosthesis with severe neurological complication ( $n = 1$ , age 27.9 years); lymphocytic myocarditis with sudden cardiac death ( $n = 1$ , age 22.8 years); acute cardiac failure after PA embolism from a calcified in-stent vegetation by catheter intervention ( $n = 1$ , age 19.0 years); cardiac failure after reoperation for right ventricular outflow tract (RVOT) obstruction (RVOTO) ( $n = 1$ , age 0.4 years); and mediastinitis after pacemaker implantation ( $n = 1$ , age 0.2 years). The overall survival rate of the ASO hospital survivors was 97.9% at 10 years, 97.3% at 20 years and 94.5% at 30 and 40 years; the survival curve was significantly different between TGA subgroups ( $P = 0.005$ ) (Figure 1).

**Table 1.** Demographics and pre-operative anatomy

	Study cohort	TGA-IVS	TGA-VSD	TBA	P value
	<i>n</i> = 413	<i>n</i> = 258 (62.5%)	<i>n</i> = 117 (28.3%)	<i>n</i> = 38 (9.2%)	
Male, <i>n</i> (%)	280 (67.8)	184 (71.3)	72 (61.5)	24 (63.2)	0.133
Age follow-up, yrs <sup>a</sup>	15.6 (0.1-41.1)	15.7 (0.1-40.1)	15.8 (0.2-41.1)	12.3 (0.1-36.3)	0.661
Age follow-up, yrs <sup>b</sup>	15.6 (0.1-45.8)	15.7 (0.1-40.6)	15.8 (0.2-45.8)	12.4 (0.1-36.9)	0.706
<b>Coexisting findings, <i>n</i> (%)</b>					
Arch abnormality	35 (8.5)	3 (1.2)	14 (12.0)	18 (47.4)	5.5*10 <sup>-16</sup>
Bicuspid pulmonary valve	27 (6.5)	16 (6.2)	10 (8.5)	1 (2.6)	0.337
LVOTO	16 (3.9)	1 (0.4)	10 (8.5)	5 (13.2)	3.0*10 <sup>-6</sup>
<b>Coronary anatomy, <i>n</i> (%)<sup>c</sup></b>					
Usual (1LCx-2R, 1L-2CxR, 1L-2R-noCx)	341 (82.6)	224 (86.8)	94 (80.3)	23 (60.5)	3.1*10 <sup>-4</sup>
Other	67 (16.4)	31 (12.0)	21 (17.9)	15 (3.9)	
Unknown	5 (1.2)	3 (1.2)	2 (1.7)	0 (0)	
Intramural course of LAD	12 (2.9)	8 (3.1)	4 (3.4)	0 (0)	0.812
<b>Pre-operative procedures, <i>n</i> (%)</b>					
Balloon atrial septostomy	216 (52.3)	151 (58.5)	57 (48.7)	8 (21.1)	4.0*10 <sup>-5</sup>
Previous PAB	30 (7.2)	11 (4.3)	15 (12.8)	4 (10.5)	0.007
<b>Arterial switch operation</b>					
One-stage, <i>n</i> (%)	371 (89.8)	246 (95.3)	94 (80.3)	31 (81.6)	1.0*10 <sup>-5</sup>
median age (range)	8 d (0 d-0.9 yrs)	7 d (0 d-0.5 yrs)	11 d (1 d-0.9 yrs)	23 d (4 d-0.6 yrs)	9.2*10 <sup>-13</sup>
Two stage, <i>n</i> (%)	42 (10.2)	12 (4.7)	23 (19.7)	7 (18.4)	1.0*10 <sup>-5</sup>
median age (range)	166 d (7 d-12.7 yrs)	107 d (7 d-5.1 yrs)	238 d (46 d-12.7 yrs)	286 d (32 d-1.7 yrs)	0.256
<b>Lecompte maneuver, <i>n</i> (%)</b>	376 (91.0)	243 (94.2)	108 (92.3)	25 (65.8)	2.1*10 <sup>-7</sup>

<sup>a</sup> Median age (range) post-ASO; <sup>b</sup> Median age (range) post-birth; <sup>c</sup> Coronary anatomy description according to the Leiden Convention coronary coding system. *P* values based on Fisher-Freeman-Halton exact test for frequencies and Kruskal-Wallis test for median values of continue data. d, days; IVS, intact ventricular septum; L or LAD, left anterior descending coronary artery; LVOTO, left ventricular outflow tract obstruction; PAB, pulmonary artery banding; R, right coronary artery; TBA, Taussig-Bing anomaly; TGA, transposition of the great arteries; VSD, ventricular septal defect; yrs, years.



No. at risk	0	5	10	15	20	25	30	35	40
TGA-IVS	258	211	175	137	90	47	20	6	1
TGA-VSD	117	94	77	64	38	19	12	6	1
Taussig Bing	38	28	23	18	10	7	5	1	0

**Figure 1.** Kaplan-Meier estimates of overall survival of ASO hospital survivors by TGA morphology subgroups

### Arrhythmias, ablation and cardiac devices

Conduction disorders or late arrhythmias appeared in 26 patients post-ASO (6.3%). Details are presented in supplementary Table S1. In short, 8 patients had a complete atrioventricular block requiring pacemaker implantation (2 after reoperation). Eight patients presented with ventricular tachyarrhythmias at a median follow-up of 15.4 (IQR 12.3-18.5) years post-ASO. Supraventricular arrhythmias were diagnosed in 12 patients at a median age of 17.8 (IQR 8.1-24.1) years.

### Reoperations

In total, 117 reoperations (137 procedures) were performed in 83 patients (20.1%) (Table 2). Twenty-two patients needed 2 or more reoperations (Figure 2). Seven reoperations were performed within 30 days post-ASO (1.6%, 7/447 patients). Median age at reoperation was 2.0 (IQR 0.3-7.1) years post-ASO. Distribution of TGA morphology among patients who underwent reoperation was: TGA-IVS in 32 (32/258, 12.4%), TGA-VSD in 32 (32/117, 27.4%) and TBA in 19 (19/38, 50.0%) patients and reoperation-free survival differed significantly between TGA subgroups ( $P = 6.5 \times 10^{-10}$ ) (Figure 3A). Overall freedom from reoperation for the entire TGA population was 85% at 5 years, decreasing to 81%, 79%, 76%, 75%, 71% and 71% at 10, 15, 20, 25, 30 and 35 years after ASO, respectively (Figure 3A).

The most common indication for reoperation was RVOTO ( $n = 50$ , 68 procedures) (Table 2). A hybrid procedure with intraoperative stent implantation for relief of PA branch stenosis was performed in 7 of 50 patients. Median age at reoperation for RVOTO was 1.3 (IQR 0.3-4.5) years. Twenty-two of these patients had TGA-IVS (8.5%), 15 TGA-VSD (12.8%) and 13 TBA (34.2%) ( $P = 2.2 \times 10^{-4}$ ).



**Table 2.** Reoperation and catheter intervention procedures

<b>Reoperation (n = 83)</b>	<b>No. procedures (%)</b> <i>137 procedures / 117 reoperations</i>	<b>No. patients</b>
<b>RVOTO relief</b>	<b>68 (49.6)</b>	<b>50</b>
<b>Neo-aortic valve &amp; root surgery</b>	<b>21 (15.3)</b>	<b>15</b>
Neo-aortic valve plasty	1	
Neo-aortic valve replacement	3	
Bentall operation	12	
David operation	2	
Switchback Ross	1	
Replacement ascending aorta	2	
<b>Coronary revascularisation</b>	<b>8 (5.8)</b>	<b>8</b>
Ostial plasty	4	
CABG	4	
<b>Relief arch obstruction</b>	<b>12 (8.8)</b>	<b>12</b>
<b>LVOTO relief</b>	<b>4 (2.9)</b>	<b>4</b>
<b>Miscellaneous*</b>	<b>24 (17.5)</b>	<b>22</b>
<b>Catheter intervention (n = 54)</b>	<b>No. procedures (%)</b> <i>104 procedures / 101 interventions</i>	<b>No. patients</b>
<b>Relief supraaortic PS</b>	<b>80 (76.9)</b>	<b>44</b>
<i>Balloon angioplasty**</i>		<b>27</b>
MPA		5
RPA		8
LPA		5
Bilateral PA		9
<i>Stent implantation</i>		<b>39</b>
MPA only		1
RPA only		13
LPA only		11
Bilateral PA		13
MPA+RPA		1
<b>Relief arch obstruction</b>	<b>15 (14.4)</b>	<b>10</b>
Balloon angioplasty	14	
Stent implantation	1	
<b>Coronary artery intervention</b>	<b>2 (1.9)</b>	<b>2</b>
PTCA	1	
Stent implantation	1	
<b>Neo-aortic valve intervention</b>	<b>1 (1.0)</b>	<b>1</b>
TAVI	1	
<b>Closure shunts</b>	<b>6 (5.8)</b>	<b>5</b>
Atrial septal defect	5	
Aorta-pulmonary collaterals	1	

\* AV-valve plasty (n = 11), closure residual ASD/VSD (n = 5), relief supraaortic aortic stenosis (n = 1), relief MPA aneurysm (n = 3), relief pulmonary vein obstruction (n = 1), pulmonary artery endarterectomy (n = 1).

\*\* dilatation of native/in-stent PA (branch) stenosis. CABG, coronary artery bypass graft; LPA, left pulmonary artery; LVOTO, left ventricular outflow tract obstruction; MPA, main pulmonary artery; PA, pulmonary artery; PS, pulmonary stenosis; PTCA, percutaneous transluminal coronary angioplasty; RPA, right pulmonary artery; RVOTO, right ventricular outflow tract obstruction; TAVI, transcatheter aortic valve implantation.

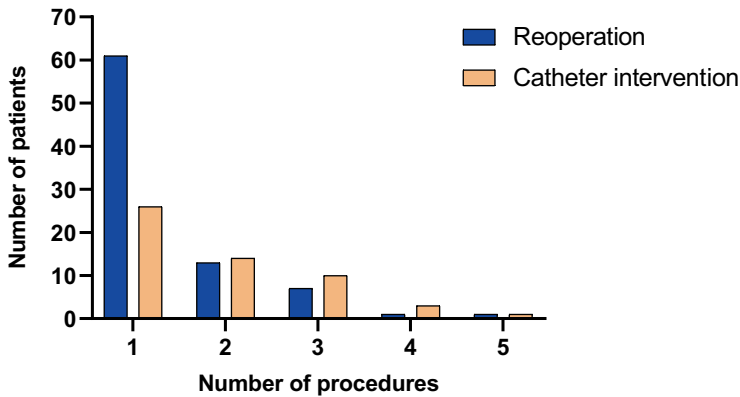


**Figure 2.** Histogram on the number of reoperations and catheter interventions

Neo-aortic valve, root or ascending aorta reoperations for neo-aortic valve insufficiency and/or root dilatation were performed in 15 patients (3.6%) and include 18% of all reoperations (21/117 reoperations). Median age at reoperation for these indications was 15.7 (IQR 11.4-20.0) years post-ASO. Ten patients underwent a Bentall operation, 2 patients had a valve-sparing root replacement, 1 patient had neo-aortic valve repair followed by later valve replacement, 1 patient underwent replacement of the neo-aortic root/ascending aorta by a supracoronary tubular prosthesis and in 1 patient, a switch back Ross operation was performed. Seven of these patients had TGA-IVS (2.7%), 5 TGA-VSD (4.3%) and 3 TBA (7.9%) ( $P = 0.193$ ).

Aortic arch repair after ASO was necessary in 12 of the 83 reoperated patients (14.5%) and consisted of either reoperations for recoarctation (in 7 patients, after ASO with arch repair) or reoperations for neo-coarctation (in 5 patients; i.e. aortic coarctation following ASO in patients who were not diagnosed with coarctation before or during initial ASO).

Reoperations for coronary artery problems were needed in 8 patients (1.9%) at median age of 11.5 (IQR 1.0-24.1) years. Patient-specific and surgical characteristics are summarized in supplementary Table S2. Number of coronary artery reoperations differed significantly between TGA subgroups: 2 patients had TGA-IVS (0.8%), 2 TGA-VSD (1.7%) and 4 TBA (10.5%) ( $P = 0.004$ ). Usual coronary artery anatomy (1LCx-2R) was present in 4 patients (50%).

Era-specific impact on reoperation rate and common reoperation types could not be detected, except for aortic arch repair due to recoarctation (supplementary Figures S1-S3). Patients who have been operated on for TGA with arch obstruction in the era '1977-1989' were more likely to require an aortic arch reoperation for recoarctation compared to patients with ASO and aortic arch repair performed in later eras ( $P=0.005$ ; supplementary Figure S3).

Univariable Cox regression analysis showed following factors associated with reoperation for any indication: TGA morphological subtype (TGA-VSD and TBA), weight at ASO, aortic arch repair associated with ASO, not having had a Lecompte maneuver and a non-usual

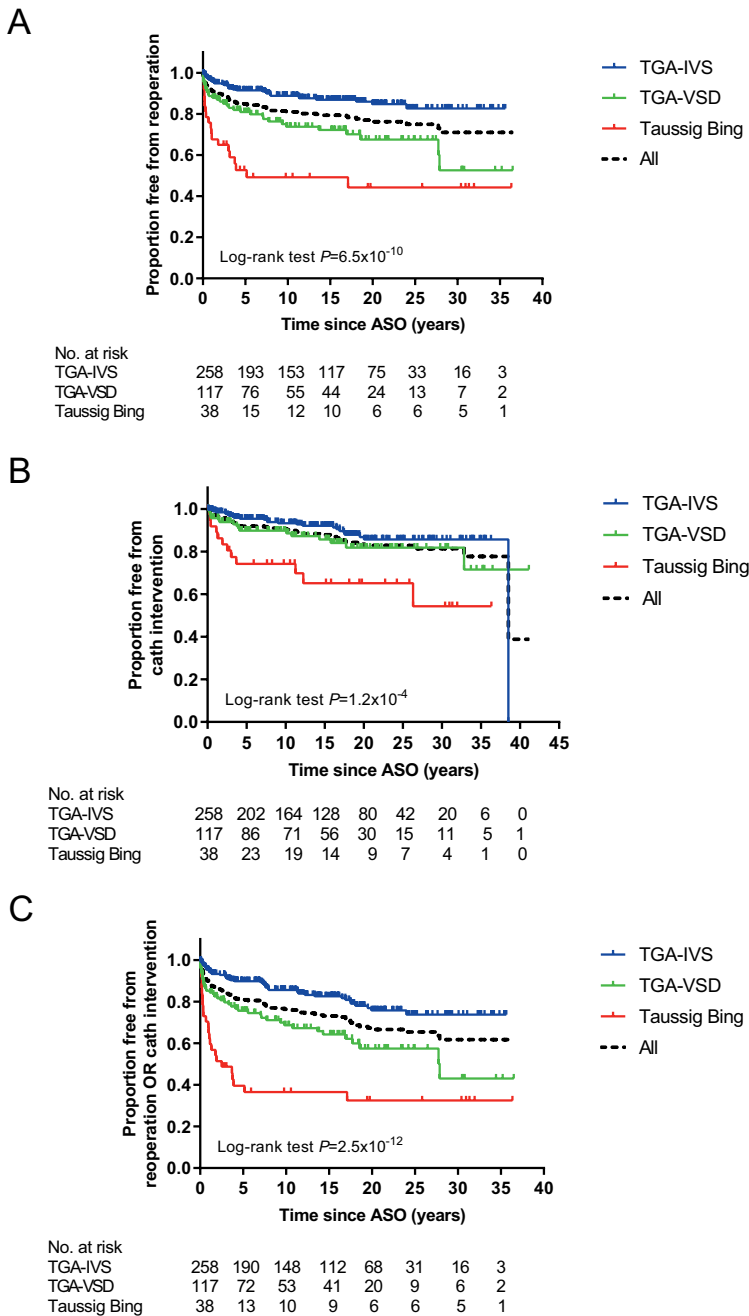


**Figure 3.** Kaplan-Meier estimates of freedom from reoperation (A), catheter intervention (B) and both reoperation and catheter intervention (C) by TGA morphology subgroups. IVS, intact ventricular septum; TGA, transposition of the great arteries; VSD, ventricular septal defect.

coronary artery anatomy. On multivariate analysis, TGA morphological subtype (TGA-VSD: HR = 1.99, 95% confidence interval (CI) 1.18-3.36,  $P = 0.010$  and TBA: HR = 2.17, 95% CI 1.02-4.64,  $P = 0.045$ ), aortic arch repair associated with ASO (HR = 3.03, 95% CI 1.62-5.69,  $P = 0.001$ ) and a non-usual coronary artery anatomy (HR = 2.41, 95% CI 1.45-4.00,  $P = 0.001$ ) were identified as independent risk factors for reoperation (supplementary Table S3).

### Catheter interventions

In total, 101 interventions were performed in 54 patients (13.1 %) (Table 2). Twenty-eight patients needed 2 or more interventions (Figure 2). Median age at first catheter intervention was 3.7 (IQR 1.3-12.8) years. Distribution of TGA morphology among patients who underwent catheter interventions was: TGA-IVS in 25 (25/258, 9.7%) patients, TGA-VSD in 17 (17/117, 14.5%) patients, TBA in 12 (12/38, 31.6%) patients and reoperation-free survival differed significantly between TGA subgroups ( $P = 1.2 \times 10^{-4}$ ) (Figure 3B). Overall freedom from catheter intervention for the entire TGA population was 92% at 5 years, decreasing to 91%, 88%, 84%, 83%, 81% and 78% at 10, 15, 20, 25, 30 and 35 years after ASO, respectively (Figure 3B).

The major indication for catheter intervention was relief of RVOTO ( $n = 44$ , 80 procedures). In 39 patients (9.4%), 1 or more stent implantation(s) in the PA system were performed to treat supravalvular pulmonary stenosis (including aforementioned intraoperative stent implantations in 7 patients). Distribution of TGA morphology among patients with stent implantations was: TGA-IVS in 21 (21/258, 8.1%) patients, TGA-VSD in 13 (13/117, 11.1%) patients and TBA in 5 (5/38, 13.2%) patients ( $P = 0.413$ ). One patient received a transcatheter pulmonary valve implantation (Melody®) in neo-pulmonary valve position.

Balloon angioplasty for aortic recoarctation was performed in 10 patients. Catheter interventions for significant coronary artery stenosis were done in 3 patients. As summarized in supplementary Table S2, percutaneous transluminal coronary angioplasty was performed in 2 patients (prior to or after coronary revascularization); in 1 patient, a drug-eluting stent was implanted for left anterior descending coronary artery ostial stenosis. A transcatheter aortic valve implantation (TAVI) was performed in a single TBA patient (with monocoronary ostium) for recurrent severe neo-aortic valve regurgitation, 1.5 year after a valve-sparing root replacement. Although originally developed for the treatment of aortic stenosis, TAVI has emerged as a viable alternative to surgical aortic valve replacement for patients with pure aortic regurgitation with a high-risk profile for surgery. Furthermore, this technique has proven to be technically feasible and successful for severe aortic regurgitation after David valve-sparing root replacement. With the large experience of TAVI for pure aortic regurgitation in our center and the patient's explicit wish to be treated via transcatheter procedure, TAVI was chosen over redo surgery.

Univariable Cox regression analysis showed following factors associated with catheter intervention: TGA morphological subtype (TBA), aortic arch repair associated with ASO and a non-usual coronary artery anatomy. On multivariable analysis, aortic arch repair associated with ASO (HR = 2.95, 95% CI 1.37-6.36,  $P = 0.006$ ) was identified as independent risk factor for catheter intervention (supplementary Table S4).

### Risk factors for any intervention - reoperations or catheter interventions

Of the 413 survivors with follow-up, 302 patients did not receive any reoperation or catheter intervention (73.1%) during follow-up (Figure 4). One hundred and eleven patients (26.9%) underwent at least 1 reoperation or catheter intervention; 26 patients (6.3%) underwent at least both a reoperation and catheter intervention. Distribution of the 111 patients over the TGA subgroups was: TGA-IVS in 46 (17.8%), TGA-VSD in 41 (35.0%), TBA in 24 (63.2%) patients and the combined reoperation/catheter intervention-free survival differed significantly between TGA subgroups ( $P = 2.5 \times 10^{-12}$ ) (Figure 3C). Overall freedom from reoperation or catheter intervention for the entire TGA population was 81% at 5 years, decreasing to 76%, 73%, 65%, 63%, 61% and 61% at 10, 15, 20, 25, 30 and 35 years after ASO, respectively (Figure 3C).

Risk analysis for the need of any reoperation(s) or catheter intervention(s) is presented in Table 3. TGA morphological subtype (TGA-VSD and TBA), aortic arch repair associated with ASO, weight at ASO, not having had a Lecompte maneuver, prior PA banding and a non-usual coronary artery anatomy were univariable risk factors for the risk of reoperation or catheter intervention. Independent risk factors for either reoperation or catheter intervention for all indications were TGA morphological subtype (TGA-VSD: HR = 1.84, 95% CI 1.18-2.89,  $P = 0.008$ ), aortic arch repair associated with ASO (HR = 3.72, 95% CI 2.13-6.50,  $P = 4.0 \times 10^{-6}$ ) and a non-usual coronary artery anatomy (HR = 1.92, 95% CI 1.20-3.07,  $P = 0.007$ ).

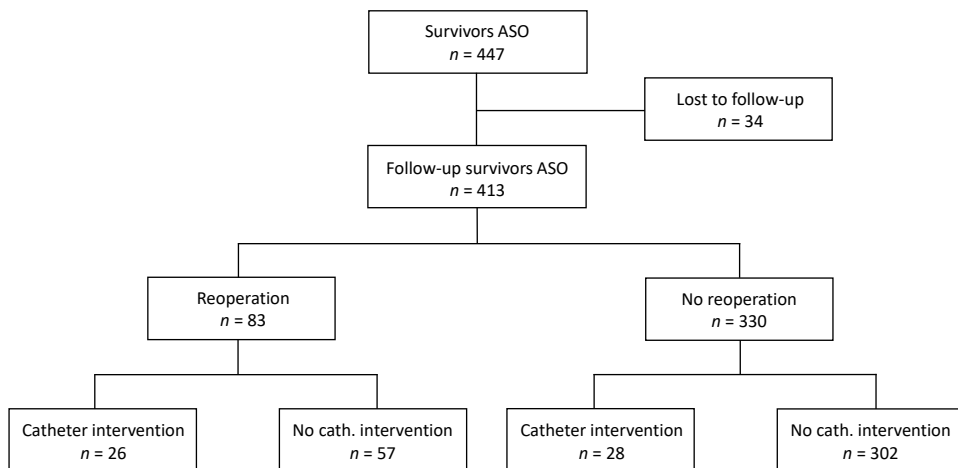


**Figure 4.** Flow diagram of reoperations and catheter interventions in ASO hospital survivors. ASO, arterial switch operation

**Table 3.** Univariable and multivariable Cox proportional hazard analysis for reoperation or catheter interventions

Risk factors	Univariable			Multivariable**			
	Events/total	Hazard ratio	95% CI	P value	Hazard ratio	95% CI	P value
<b>Morphological subtype</b>							<b>0.023</b>
TGA-IVS <sup>a</sup>	46/258	1		<b>1.35*10<sup>-10</sup></b>	1		
TGA-VSD	41/117	2.30	1.51–3.51	<b>1.06*10<sup>-4</sup></b>	1.84	1.18–2.89	<b>0.008</b>
TBA	24/38	5.33	3.25–8.76	<b>3.91*10<sup>-11</sup></b>	1.92	0.95–3.91	0.071
<b>Gender</b>							
Male <sup>b</sup>	72/280	1			1		
Female	39/133	1.19	0.80–1.75	0.39	1.18	0.79–1.77	0.41
<b>Weight at ASO (per 1 kg)</b>		1.10	1.04–1.17	<b>4.49*10<sup>-4</sup></b>	1.03	0.95–1.12	0.41
<b>LVOTO</b>							
No <sup>c</sup>	106/397	1			1		
Yes	5/16	1.13	0.54–3.23	0.55	1.01	0.39–2.62	0.99
<b>Aortic arch repair</b>							
No <sup>d</sup>	84/378	1			1		
Yes	27/35	5.75	3.69–8.95	<b>9.02*10<sup>-15</sup></b>	3.72	2.13–6.50	<b>4.0*10<sup>-6</sup></b>
<b>Lecompte</b>							
No <sup>e</sup>	17/29	1			1		
Yes	93/384	0.29	0.17–0.48	<b>3.00*10<sup>-6</sup></b>	0.74	0.38–1.43	0.37
<b>Prior PAB</b>							
No <sup>f</sup>	99/383	1			1		
Yes	12/30	2.00	1.10–3.65	<b>0.023</b>	1.24	0.59–2.61	0.57
<b>Coronary artery anatomy</b>							
Usual (1LcX-2R, 1L-2CxR, 1L-2R, noCx) <sup>g</sup>	79/341	1			1		
Other (non-usual)	31/67	2.65	1.74–4.02	<b>5.00*10<sup>-6</sup></b>	1.92	1.20–3.07	<b>0.007</b>

Cox proportional regression analysis - Enter inclusion model. Bold refers to statistically significant P values. Reference categories of covariate: <sup>a</sup> morphological subtype TGA-IVS; <sup>b</sup> male sex; <sup>c</sup> no left ventricular outflow tract obstruction; <sup>d</sup> no aortic arch repair associated with ASO; <sup>e</sup> no Lecompte maneuver; <sup>f</sup> no pulmonary artery banding prior to ASO; <sup>g</sup> usual coronary artery anatomy. \*\*Variables included for MV analysis: morphological subtype, sex, weight, aortic arch repair, pulmonary artery banding prior to ASO, and coronary artery anatomy. IVS, intact ventricular septum; \*\*Variables included for MV analysis: morphological subtype, sex, weight, aortic arch repair, pulmonary artery banding prior to ASO, and coronary artery anatomy. IVS, intact ventricular septum; OTO, outflow tract obstruction; PAB, pulmonary artery banding; TBA, Taussig-Bing anomaly; TGA, transposition of the great arteries; VSD, ventricular septal defect.

## Discussion

This study evaluated the long-term cardiac outcome in an ASO cohort with one of the longest reported follow-up and focussed on late mortality, reoperations and catheter interventions, coronary problems and late arrhythmias. During 43-year experience of ASO overall survival significantly improved over time, with a late mortality of 2.9% and a decline in hospital mortality to 3.3% for the past 2 decades. The need for 1 or more reoperations and 1 or more catheter interventions was 20% and 13%, respectively, and most reoperations and interventions were performed for RVOT problems. A more complex TGA morphology (TGA-VSD), aortic arch repair associated with ASO, and the presence of a non-usual coronary artery anatomy were found to be independent risk factors for the need for reoperation or intervention for any indication.

In 4 decades of ASO, a significant decrease in perioperative mortality to rates below 5% in high-volume cardiothoracic surgical centers has been achieved.<sup>2, 12, 13</sup> Although survival has greatly improved, recurrent and new lesions remain and require reoperations or catheter interventions. The reoperation rate in this study was 20% which is relatively high compared to other studies. These studies reported reoperation rates between 5% and 20%, but with shorter duration of follow-up.<sup>12-17</sup> Reoperation rates between studies may vary depending on the complexity of the included TGA patients (TGA-VSD and TBA included or not). Moreover, our early adoption of ASO (1977) has probably influenced the number of reinterventions. With longer follow-up, it is expected that more patients will need a reoperation or catheter intervention, confirmed by the 11% reoperation rate beyond childhood in a study of adult TGA patients post-ASO.<sup>17</sup>

### Right ventricular outflow tract procedures

RVOT problems are the most common indication for reoperations or catheter interventions and often occur in the first years after ASO, as already known from short- and intermediate-term follow-up studies.<sup>2-4</sup> Our data are in line with these reports, with a median age of 1.3 (IQR 0.3-4.5) years at the time of first RVOT reoperation. The overall surgical and percutaneous intervention rates for RVOTO varied from 5 to 28% between the different studies with at least 20-year follow-up,<sup>2-4, 14-16</sup> which is also similar to the results of this study.

Approximately 75% of the reoperations and all catheter interventions for RVOTO were performed for supravulvar obstruction in this study. Anatomical and surgical components may play a role in the development of PA stenosis. Patients with concomitant aortic arch obstruction (often TBA patients) are at increased risk for RVOTO.<sup>18, 19</sup> Moreover, the surgical technique and the material used for PA reconstruction, application of Lecompte maneuver, extent of mobilization of the PAs, and the age at operation impact the risk of RVOTO.<sup>2-4</sup>

Balloon angioplasty for supravulvar pulmonary stenosis is the least invasive option but usually has limited effect and stent implantation is eventually required in most cases, preferably performed at an older age. Although we have not seen complications of branch PA stenting after ASO (first procedures 1994), these procedures should be performed with

restraint because severe complications such as coronary artery compression and especially aortic erosion and aorto-pulmonary fistulas have been reported.<sup>20</sup>

### Neo-aortic reoperations

Twenty-one surgical procedures and 1 catheter intervention for neo-aortic valve regurgitation and/or root dilatation were performed in 15 patients (3.6%), approximately 20% of all reoperations. It is the second most common indication for reoperation, as has been reported in other studies with long follow-up duration.<sup>12, 16</sup> The main indication for neo-aortic root reoperation in this study was root dilatation with or without significant neo-aortic regurgitation.<sup>6, 21</sup> In two-thirds of cases, surgery was performed in the last decade (2009-2020). Although the total amount of reoperations on the neo-aortic valve/root is still low and comparable to other surgical centers,<sup>15, 16, 22</sup> we expect that with longer follow-up this may increase. Longitudinal follow-up studies on the neo-aortic valve function confirm this concern as root dilatation progresses over time and proved to be an independent risk factor for neo-aortic valve impairment.<sup>5, 6</sup> Recently, we showed in a subset of this cohort that 14% of patients had developed root diameters  $\geq 40$  mm, with moderate neo-aortic regurgitation in about 25% of them and one-quarter of these patients being below 18 years of age.<sup>6</sup>

Thresholds for root replacement in TGA patients after ASO are adapted from international guidelines on bicuspid aortic valve and connective-tissue disease-related aortopathy and are based on absolute diameters. No aortic dissections or ruptures have been reported after ASO to date. In our center root replacement is indicated if the neo-aortic root diameter reaches 55 mm according to the guidelines,<sup>23</sup> and at smaller sizes if significant neo-aortic valve regurgitation is present or if root diameter has rapidly progressed over time. A Bentall operation has been performed in most patients,<sup>6, 21</sup> but valve-sparing operation should be considered whenever possible.

### Coronary artery lesions

In our series, coronary artery reoperations or interventions for partial or total occlusion were required in only 9 patients (2.2%), suggesting that coronary problems do not frequently occur during follow-up so far. Moreover, late mortality was not related to acute coronary artery problems in the patients with identified causes of death. One patient had a near-fatal ventricular fibrillation due to ischemia based on coronary ostial stenosis. These findings are in line with the results of a systematic review on sudden cardiac death due to coronary complications late after ASO (at least more than 5 years).<sup>24</sup> From that review, sudden cardiac death was extremely rare with only a few possible cases and no proven cases of coronary artery-related sudden death. In our center, we do not systematically perform coronary surveillance imaging during childhood which might have influenced numbers of coronary artery problems. In general, children with complex coronary morphology or those with intraoperative difficulties of coronary artery transfer receive coronary computed tomography angiography (CTA) in the first year after ASO. Furthermore, patients undergo exercise tests in childhood and all asymptomatic patients underwent a coronary CTA at least once in early adolescence.<sup>25</sup>



The detection of coronary artery abnormalities in the patients who underwent intervention was based on symptoms, abnormal findings from echocardiography or an accidental finding by a surveillance CTA or catheter coronary angiography (all representing one-third of the causes of detection). Treatment for partial or total coronary occlusion was performed by either ostial plasty or by coronary artery bypass graft. Taussig-Bing anomaly patients had the highest prevalence of coronary artery reoperations in this study (4/38 patients, 10.5%). Remarkably, all coronary reoperations in this subgroup were performed during childhood, unlike most coronary procedures in the patients with other TGA subtypes. Given the small number of coronary reoperations, it is unclear whether TBA patients are at increased risk or whether this is related to the prevalent non-usual coronary artery pattern in TBA. Although abnormal coronary artery patterns have been reported as risk factor for early coronary artery obstruction,<sup>8, 9, 26</sup> it is suggested that the acquired coronary anatomy after ASO may be more important as a risk factor for late coronary artery obstruction.<sup>27</sup> Correspondingly, half of the patients necessitating coronary reoperation from this study had a usual coronary artery pattern without problems during coronary artery transfer. Acquired abnormal coronary anatomy may result from the surgically created pattern after reimplantation and changes by growth, arterial distortion or root dilatation.<sup>25, 27</sup>

### **Risk factors for reoperation, intervention or combined**

Independent risk factors for reoperation in this study were: TGA morphological subtype (TGA-VSD), aortic arch repair associated with ASO and a non-usual coronary artery anatomy. More complex TGA anatomy have been reported to be a risk factor for reoperation in previous studies.<sup>12-14</sup> Not surprisingly, aortic arch repair associated with ASO was reported as independent risk factor for surgical or catheter reintervention. A higher rate of reinterventions was previously described in TGA patients with arch obstruction by our group<sup>18</sup> and in other large series as well,<sup>12, 19, 22</sup> particularly indicated for right-sided obstructions next to residual arch obstruction. A non-usual coronary artery anatomy showed to be an independent risk factor for both reoperation and any reoperation or intervention for any indication in this study. Vargo et al.<sup>28</sup> hypothesized that this could be related to the fact that an abnormal coronary artery anatomy sometimes requires an unusual reconstructive technique to avoid compression of the coronary artery button. However, we were not able to prove this in our series. Differences in reoperation rate or type based on era of ASO could not be detected in this series, except for aortic arch reoperation due to recoarctation. Although these are relatively small numbers, patients operated on for TGA with arch obstruction in the early years after start of the ASO program (era '1977-1989') were more likely to require an aortic arch reoperation for recoarctation compared to patients operated on in later eras.

### **Rhythm disorders**

Arrhythmias requiring ablative therapy or device implantation are fairly uncommon after ASO in this study, which is in concordance with other studies.<sup>12, 14</sup> Most sustained ventricular

arrhythmias are related to coronary ischemia or post myocardial infarction necessitating preventive ventricular tachycardia ablation or implantable cardioverter-defibrillator implantation and, if present, relief of coronary artery obstruction. Supraventricular tachycardia episodes are usually more prevalent in the newborn period and directly after ASO and only very rarely occur later, as was also shown in this study. Pacemaker need for atrioventricular block was low and related to VSD closure (in TGA-VSD and TBA) from early surgical eras (before 2000).

### **Limitations**

Limitations of this study are related to the retrospective design from a single center. The prevalence of coronary artery stenosis or occlusion identified in this study may be underestimated because coronary surveillance imaging by CTA or coronary angiogram was not performed routinely in all cases.

### **Conclusion**

Patients after ASO typically have good clinical outcomes in the long term but reoperations and interventions remain necessary in some patients. Right ventricular outflow tract problems are the main indication for surgical and percutaneous interventions with neo-aortic valve or root reoperations as second most common reoperation indication. More complex TGA anatomy (TGA-VSD and TBA), aortic arch repair associated with ASO and non-usual coronary artery anatomy were independent risk factors for any reoperations or interventions of any indication. Reoperations for neo-aortic valve insufficiency and/or root dilatation are relatively low but revealed an increased incidence over the last decade. With the reported ongoing neo-aortic root dilatation in adulthood, this observation is of major concern for the future, as this implicate an expected increased need for neo-aortic valve or root redo surgery.

## References

1. Jegatheeswaran A, Devlin PJ, DeCampi WM, Welke KF, Williams WG, Blackstone EH, Fuller S, Jacobs ML, Mussatto KA, Woods RK, et al. Longitudinal functional health status in young adults with repaired dextro-transposition of the great arteries: A Congenital Heart Surgeons' Society study. *J Thorac Cardiovasc Surg.* 2020;159(2):604-14 e3.
2. Cleuziou J, Vitanova K, Pabst von Ohain J, Ono M, Tanase D, Burri M, Lange R. Incidence and Risk Factors for Right Ventricular Outflow Tract Obstruction after the Arterial Switch Operation. *Thorac Cardiovasc Surg.* 2019;67(1):37-43.
3. Delmo Walter EM, Miera O, Nasserri B, Huebler M, Alexi-Meskishvili V, Berger F, Hetzer R. Onset of pulmonary stenosis after arterial switch operation for transposition of great arteries with intact ventricular septum. *HSR Proc Intensive Care Cardiovasc Anesth.* 2011;3(3):177-87.
4. Nellis JR, Turek JW, Aldoss OT, Atkins DL, Ng BY. Intervention for Supravalvar Pulmonary Stenosis After the Arterial Switch Operation. *Ann Thorac Surg.* 2016;102(1):154-62.
5. Shepard CW, Germanakis I, White MT, Powell AJ, Co-Vu J, Geva T. Cardiovascular Magnetic Resonance Findings Late After the Arterial Switch Operation. *Circ Cardiovasc Imaging.* 2016;9(9):e004618.
6. van der Palen RLF, van der Bom T, Dekker A, Tsonaka R, van Geloven N, Kuipers IM, Konings TC, Rammeloo LA, Ten Harkel ADJ, Jongbloed MRM, et al. Progression of aortic root dilatation and aortic valve regurgitation after the arterial switch operation. *Heart.* 2019;105(22):1732-40.
7. Pasquali SK, Hasselblad V, Li JS, Kong DF, Sanders SP. Coronary artery pattern and outcome of arterial switch operation for transposition of the great arteries: a meta-analysis. *Circulation.* 2002;106(20):2575-80.
8. Ou P, Khraiche D, Celermajer DS, Agnoletti G, Le Quan Sang KH, Thalabard JC, Quintin M, Raisky O, Vouhe P, Sidi D, et al. Mechanisms of coronary complications after the arterial switch for transposition of the great arteries. *J Thorac Cardiovasc Surg.* 2013;145(5):1263-9.
9. Angeli E, Formigari R, Pace Napoleone C, Oppido G, Ragni L, Picchio FM, Gargiulo G. Long-term coronary artery outcome after arterial switch operation for transposition of the great arteries. *Eur J Cardiothorac Surg.* 2010;38(6):714-20.
10. Lalezari S, Bruggemans EF, Blom NA, Hazekamp MG. Thirty-year experience with the arterial switch operation. *Ann Thorac Surg.* 2011;92(3):973-9.
11. Yacoub MH, Radley-Smith R. Anatomy of the coronary arteries in transposition of the great arteries and methods for their transfer in anatomical correction. *Thorax.* 1978;33(4):418-24.
12. Khairy P, Clair M, Fernandes SM, Blume ED, Powell AJ, Newburger JW, Landzberg MJ, Mayer JE, Jr. Cardiovascular outcomes after the arterial switch operation for D-transposition of the great arteries. *Circulation.* 2013;127(3):331-9.
13. Losay J, Touchot A, Serraf A, Litvinova A, Lambert V, Piot JD, Lacour-Gayet F, Capderou A, Planche C. Late outcome after arterial switch operation for transposition of the great arteries. *Circulation.* 2001;104(12 Suppl 1):1121-6.
14. Fricke TA, d'Udekem Y, Richardson M, Thuys C, Dronavalli M, Ramsay JM, Wheaton G, Grigg LE, Brizard CP, Konstantinov IE. Outcomes of the arterial switch operation for transposition of the great arteries: 25 years of experience. *Ann Thorac Surg.* 2012;94(1):139-45.
15. Oda S, Nakano T, Sugiura J, Fusazaki N, Ishikawa S, Kado H. Twenty-eight years' experience of arterial switch operation for transposition of the great arteries in a single institution. *Eur J Cardiothorac Surg.* 2012;42(4):674-9.
16. Raju V, Burkhart HM, Durham LA, 3rd, Eidem BW, Phillips SD, Li Z, Schaff HV, Dearani JA. Reoperation after arterial switch: a 27-year experience. *Ann Thorac Surg.* 2013;95(6):2105-12.
17. Tobler D, Williams WG, Jegatheeswaran A, Van Arsdell GS, McCrindle BW, Greutmann M, Oechslin EN, Silversides CK. Cardiac outcomes in young adult survivors of the arterial switch operation for transposition of the great arteries. *J Am Coll Cardiol.* 2010;56(1):58-64.

18. Bokenkamp R, Aguilar E, van der Palen RL, Sojak V, Bruggemans EF, Hruda J, Kuipers IM, Hazekamp MG. Reoperation for right ventricular outflow tract obstruction after arterial switch operation for transposition of the great arteries and aortic arch obstruction. *Eur J Cardiothorac Surg.* 2016;49(5):e91-6.
19. Fricke TA, Donaldson S, Schneider JR, Menahem S, d'Udekem Y, Brizard CP, Konstantinov IE. Outcomes of the arterial switch operation in patients with aortic arch obstruction. *J Thorac Cardiovasc Surg.* 2020;159(2):592-9.
20. Vida VL, Biffanti R, Stellin G, Milanese O. Iatrogenic aortopulmonary fistula occurring after pulmonary artery balloon angioplasty: a word of caution. *Pediatr Cardiol.* 2013;34(5):1267-8.
21. Koolbergen DR, Manshanden JS, Yazdanbakhsh AP, Bouma BJ, Blom NA, de Mol BA, Mulder BJ, Hazekamp MG. Reoperation for neo-aortic root pathology after the arterial switch operation. *Eur J Cardiothorac Surg.* 2014;46(3):474-9.
22. Baruteau AE, Vergnat M, Kalfa D, Delpey JG, Ly M, Capderou A, Lambert V, Belli E. Long-term outcomes of the arterial switch operation for transposition of the great arteries and ventricular septal defect and/or aortic arch obstruction. *Interact Cardiovasc Thorac Surg.* 2016;23(2):240-6.
23. Baumgartner H, De Backer J, Babu-Narayan SV, Budts W, Chessa M, Diller GP, Lung B, Kluin J, Lang IM, Meijboom F, et al. 2020 ESC Guidelines for the management of adult congenital heart disease. *Eur Heart J.* 2021;42(6):563-645.
24. van Wijk SWH, van der Stelt F, Ter Heide H, Schoof PH, Doevendans P, Meijboom FJ, Breur J. Sudden Death Due to Coronary Artery Lesions Long-term After the Arterial Switch Operation: A Systematic Review. *Can J Cardiol.* 2017;33(9):1180-7.
25. Veltman CE, Beeres SL, Kalkman DN, Kelder TP, Kies P, Vliegen HW, Hazekamp MG, Delgado V, Kroft LJ, van der Wall EE, et al. Variation in coronary anatomy in adult patients late after arterial switch operation: a computed tomography coronary angiography study. *Ann Thorac Surg.* 2013;96(4):1390-7.
26. Pretre R, Tamisier D, Bonhoeffer P, Mauriat P, Pouard P, Sidi D, Vouhe P. Results of the arterial switch operation in neonates with transposed great arteries. *Lancet.* 2001;357(9271):1826-30.
27. Michalak KW, Sobczak-Budlewska K, Moll JJ, Szymczyk K, Moll JA, Niwald M, Dryzek P, Moll M. Can we predict potentially dangerous coronary patterns in patients with transposition of the great arteries after an arterial switch operation? *Cardiol Young.* 2019;29(11):1350-5.
28. Vargo P, Mavroudis C, Stewart RD, Backer CL. Late complications following the arterial switch operation. *World J Pediatr Congenit Heart Surg.* 2011;2(1):37-42.



## Supplementary material

**Supplementary Table S1.** Conduction disorders, arrhythmias post-discharge and therapy

	<i>n</i>	Age (years)* median (IQR)	Treatment
<b>Total AV-block</b>	<b>8</b>		Pacemaker ( <i>n</i> = 8)
Post-ASO ( <i>n</i> = 5 before year 2000)	6		
After reoperation**	2	15.2 and 32.1	
<b>Ventricular tachyarrhythmia</b>	<b>8</b>	15.4 (12.3-18.5)	ICD ( <i>n</i> = 5), catheter ablation ( <i>n</i> = 5)
Ventricular tachycardia	7		
Ventricular fibrillation - aborted sudden cardiac death	1		
<b>Supraventricular tachyarrhythmia</b>	<b>12***</b>	17.8 (8.1-24.1)	Catheter ablation ( <i>n</i> = 4; redo in <i>n</i> = 1)
AV(N)RT	3		
Atrial flutter	8		
Atrial fibrillation	1		

AV(N)RT, AV(nodal) reentrant tachycardia; ICD, implantable cardioverter defibrillator; *n*, number of patients.  
\* age post-ASO.

\*\* reoperation: mitral valve replacement (*n* = 1, age 15.2 years), Bentall procedure (*n* = 1, age 31.1 years).

\*\*\* 2/12 patients also suffered from ventricular tachyarrhythmia.

**Supplementary Table S2.** Patients requiring surgical and catheter intervention for coronary artery lesions

Management coronary artery stenosis												
Arterial switch operation												
Pt	Diagnosis	Additional defects	Gender	Age (days)	CA anatomy <sup>a</sup>	CA transfer	Inter-vention	Age (years post-ASO)	Detection CA problem	Procedure(s)	Indication	Follow-up
1.	TGA-IVS	-	M	180	1LCx-2R	2 buttons	S	29.2	Routine catheter procedure for elevated RV pressure and supravulvar PS	CABG: LIMA on LCA	LCA ostial stenosis (filling LCA via collaterals from RCA)	Coronary CTA: Patent LIMA anastomosis (9 yrs after CABG)
2.	TGA-VSD	Double AA with CoA	M	3	1LCx-2R	2 trapdoors	S	9.8	Chest pain	LCA angioplasty	LCA ostial stenosis	Coronary CTA: Patent LCA ostium (12 yrs after LCA angioplasty)
3.	TBA	CoA with hypoplastic distal AA	F	46	1RL-2Cx	1RL button, 2LCx trapdoor	S&C	13.1	Decline in condition with systolic RV failure on echocardiography	Root reconstruction with CABG: RIMA to RCA. (1-month before PTCA RCA)	Total occlusion RCA	Coronary CTA: Patent RIMA anastomosis (4 yrs after CABG)
4.	TBA	CoA with hypoplastic distal AA	M	12	1L-2CxR	2 buttons	S	0.4 (131 days)	Supravulvar PS and moderate MV regurgitation. Hypokinesia LV posterior wall	Enlargement plasty LAD ostium	Reoperation for supravulvar PS. Ostium LAD and RCA small but not stenotic. Due to post-operative problems enlargement plasty LAD ostium was performed	Death after surgery due to massive subendocardial ischemia
5.	TBA	-	M	42	1R-2LCx	1R trapdoor, 2LCx button	S	0.2 (84 days)	LV dilatation and diminished cardiac function	LCA reimplantation with resection stenotic proximal part of the LCA and a side-to-side anastomosis	LCA ostial stenosis	Coronary CTA: Subtotal occlusion LCA (16 yrs after CA surgery)
6.	TBA	IAA type A	F	19	1LCx-2R	2 buttons	S&C	3.0	Angina pectoris	Ostial plasty LCA and RCA IV. saphena magna) and CABG: RIMA to mid-RCA	Severe proximal RCA stenosis, LCA ostial stenosis	PTCA for residual RCA ostium stenosis (3 yrs after CABG & ostial plasty)

Supplementary Table S2. Continued

7.	TGA-IVS	-	M	8	1L*-2CxR, (*intramural course LAD and slitlike LAD ostium)	2 buttons, LAD enlargement and plasty	S	13.3	Routine catheterization: total occlusion proximal LAD with adequate retrograde filling (1 yr post-ASO); No filling defects on perfusion scintigraphy (1 and 5yrs post-ASO); Myocardial ischemia on SPECT myocardial perfusion imaging (13 yrs post-ASO)	CABG: LIMA on LAD	Total occlusion LAD ostium	Follow-up CABG patency planned (2 yrs after CABG)
8.	TGA-VSD	-	F	15	1LCx-2R	2 buttons	S	27.7	S/p small posterolateral infarction post-ASO; S/p ICD implantation and VT ablation. OHCA with ICD shock	CABG: RIMA on RCA	RCA ostial stenosis	Well condition (1 yr after CABG)
9.	TGA-VSD	-	M	13	1L-2CxR	2 buttons	C	19.5	No complaints. Routine coronary CTA	PTCA drug eluting stent in LAD ostium	LAD ostial stenosis	CAG: patent stent without stenosis, no calcification (6 yrs after stent implantation)
10.	TGA-VSD	-	M	15	1L-2CxR	2 buttons	N	10.9	No complaints. Routine coronary CTA	No intervention	Total occlusion LAD ostium, retrograde filling	CAG: retrograde filling LCA (4 yrs after diagnosis)
11.	TBA	-	F	3	1L-2CxR	2 buttons	N	24.4	Chest pain during exercise, followed by coronary CTA	No intervention	Total occlusion LAD ostium, retrograde filling	Well condition (2 yrs after diagnosis)

<sup>a</sup> Coronary anatomy description according to the Leiden Convention coronary coding system. AA, aortic arch; C, catheter intervention; CA, coronary artery; CABG, coronary artery bypass graft; CAG, coronary angiography; CTA, computed tomography angiography; TBA, Taussig-Bing anomaly; F, female; IAA, interruption of the aortic arch; ICD, implantable cardioverter defibrillator; IVS, intact ventricular septum; L or LAD, left anterior descending coronary artery; LIMA, left internal mammary artery; LV, left ventricle; M, male; N, no intervention; OHCA, out of hospital cardiac arrest; PS, pulmonary stenosis; PTCA, percutaneous transluminal coronary angioplasty; RCA, right coronary artery; RIMA, right internal mammary artery; RV, right ventricular; S, surgery; S&C, surgery and catheter intervention; S/p, status praesens; SPECT, single-photon emission computerized tomography; TGA, transposition of the great arteries; VSD, ventricular septal defect; VT, ventricular tachycardia; Y, yes; yrs, years.



**Supplementary Table S3.** Univariable and multivariable Cox proportional hazard analysis for reoperation

Risk factors	Events/total	Univariable			Multivariable**		
		Hazard ratio	95% CI	P value	Hazard ratio	95% CI	P value
<b>Morphological subtype</b>							
TGA-IVS <sup>a</sup>	32/258	1		<b>1.66*10<sup>3</sup></b>		1	<b>0.028</b>
TGA-VSD	32/117	2.50	1.53-4.09	<b>2.45*10<sup>4</sup></b>	1.18-3.36	1.99	<b>0.010</b>
TBA	19/38	5.48	3.10-9.69	<b>4.92*10<sup>9</sup></b>	1.02-4.64	2.17	<b>0.045</b>
<b>Gender</b>							
Male <sup>b</sup>	56/280	1				1	
Female	27/133	1.04	0.66-1.64	0.87	0.62-1.61	1.00	1.00
<b>Weight at ASO (per 1 kg)</b>		1.12	1.06-1.18	<b>9.90*10<sup>5</sup></b>	0.98-1.15	1.07	0.12
<b>Left ventricular OTO</b>							
No <sup>c</sup>	78/397	1				1	
Yes	5/16	1.77	0.72-4.38	0.22	0.51-3.65	1.36	0.54
<b>Aortic arch repair</b>							
No <sup>d</sup>	62/378	1				1	
Yes	21/35	4.92	2.99-8.10	<b>4.00*10<sup>10</sup></b>	1.62-5.69	3.03	<b>0.001</b>
<b>Lecompte</b>							
No <sup>e</sup>	16/29	1					
Yes	67/384	0.22	0.13-0.38	<b>6.37*10<sup>3</sup></b>			
<b>Prior PAB</b>							
No <sup>f</sup>	74/383	1				1	
Yes	9/30	1.99	1.00-3.99	0.051	0.42-2.46	1.02	0.97
<b>Coronary artery anatomy</b>							
Usual (1LCx-2R, 7L-2CxR, 1L-2R,noCx) <sup>g</sup>	56/341	1				1	
Other	26/67	3.04	1.91-4.85	<b>3.00*10<sup>6</sup></b>	1.45-4.00	2.41	<b>0.001</b>

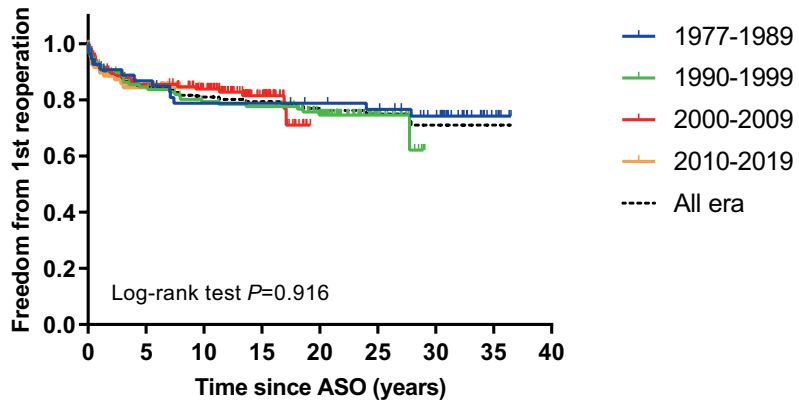
Cox proportional regression analysis - Enter inclusion model. Bold refers to statistically significant *P* values. Reference categories of covariate: <sup>a</sup> morphological subtype TGA-IVS, <sup>b</sup> male sex, <sup>c</sup> no left ventricular outflow tract obstruction, <sup>d</sup> no aortic arch repair associated with ASO, <sup>e</sup> no Lecompte maneuver, <sup>f</sup> no pulmonary artery banding prior to ASO, <sup>g</sup> usual coronary artery anatomy. \*\* Variables included for MV analysis: morphological subtype, sex, weight, aortic arch repair, pulmonary artery banding prior to ASO, and coronary artery anatomy. IVS, intact ventricular septum; OTO, outflow tract obstruction; PAB, pulmonary artery banding; TBA, Taussig-Bing anomaly; TGA, transposition of the great arteries; VSD, ventricular septal defect.

**Supplementary Table S4.** Univariable and multivariable Cox proportional hazard analysis for catheter intervention

Risk factors	Univariable			Multivariable**			
	Events/total	Hazard ratio	95% CI	P value	Hazard ratio	95% CI	P value
<b>Morphological subtype</b>							
TGA-IVS <sup>a</sup>	25/258	1		<b>3.51*10<sup>-4</sup></b>	1		0.30
TGA-VSD	17/117	1.56	0.84-2.89	0.16	1.31	0.68-2.51	0.41
TBA	12/38	4.07	2.04-8.12	<b>6.60*10<sup>-5</sup></b>	2.08	0.82-5.27	0.12
<b>Gender</b>							
Male <sup>b</sup>	33/280	1			1		
Female	21/133	1.36	0.79-2.36	0.27	1.16	0.66-2.04	0.60
<b>Weight at ASO (per 1 kg)</b>							
Left ventricular OTO		0.96	0.83-1.11	0.56	0.85	0.67-1.08	0.18
No <sup>c</sup>	53/397	1					
Yes	1/16	0.57	0.08-4.09	0.57			
<b>Aortic arch repair</b>							
No <sup>d</sup>	41/378	1			1		
Yes	13/35	4.24	2.27-7.94	<b>6.00*10<sup>-6</sup></b>	2.95	1.37-6.36	<b>0.006</b>
<b>Lecompte</b>							
No <sup>e</sup>	4/29	1					
Yes	50/384	1.29	0.40-4.15	0.67			
<b>Prior PAB</b>							
No <sup>f</sup>	48/383	1			1		
Yes	6/30	1.55	0.65-3.71	0.32	2.19	0.74-6.47	0.16
<b>Coronary artery anatomy</b>							
Usual (1LcX-2R, 1L-2CxR, 1L-2R, noCx)*	39/341	1			1		
Other	15/67	3.61	2.24-5.81	<b>1.30*10<sup>-7</sup></b>	1.74	0.89-3.42	0.11

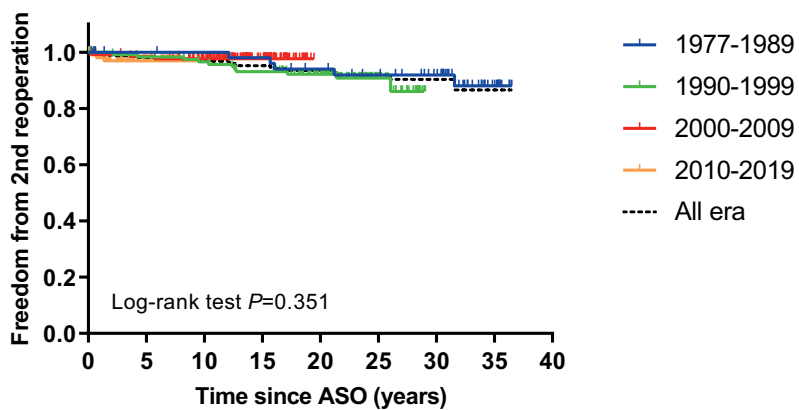
Cox proportional regression analysis - Enter inclusion model. Bold refers to statistically significant *P* values. Reference categories of covariate: <sup>a</sup> morphological subtype TGA-IVS, <sup>b</sup> male sex, <sup>c</sup> no left ventricular outflow tract obstruction, <sup>d</sup> no aortic arch repair associated with ASO, <sup>e</sup> no Lecompte maneuver, <sup>f</sup> no pulmonary artery banding prior to ASO, <sup>g</sup> usual coronary artery anatomy. \*\*Variables included for MV analysis: morphological subtype, sex, weight, aortic arch repair, pulmonary artery banding prior to ASO, and coronary artery anatomy. IVS, intact ventricular septum; OTO, outflow tract obstruction; PAB, pulmonary artery banding; TBA, Taussig-Bing anomaly; TGA, transposition of the great arteries; VSD, ventricular septal defect.

A

1st reoperation ( $n = 83$ )

No. at risk	0	5	10	15	20	25	30	35	40
1977-1989	55	44	39	39	37	35	28	6	
1990-1999	118	98	91	89	57	17	0		
2000-2009	131	110	90	43	0				
2010-2019	109	32	0						

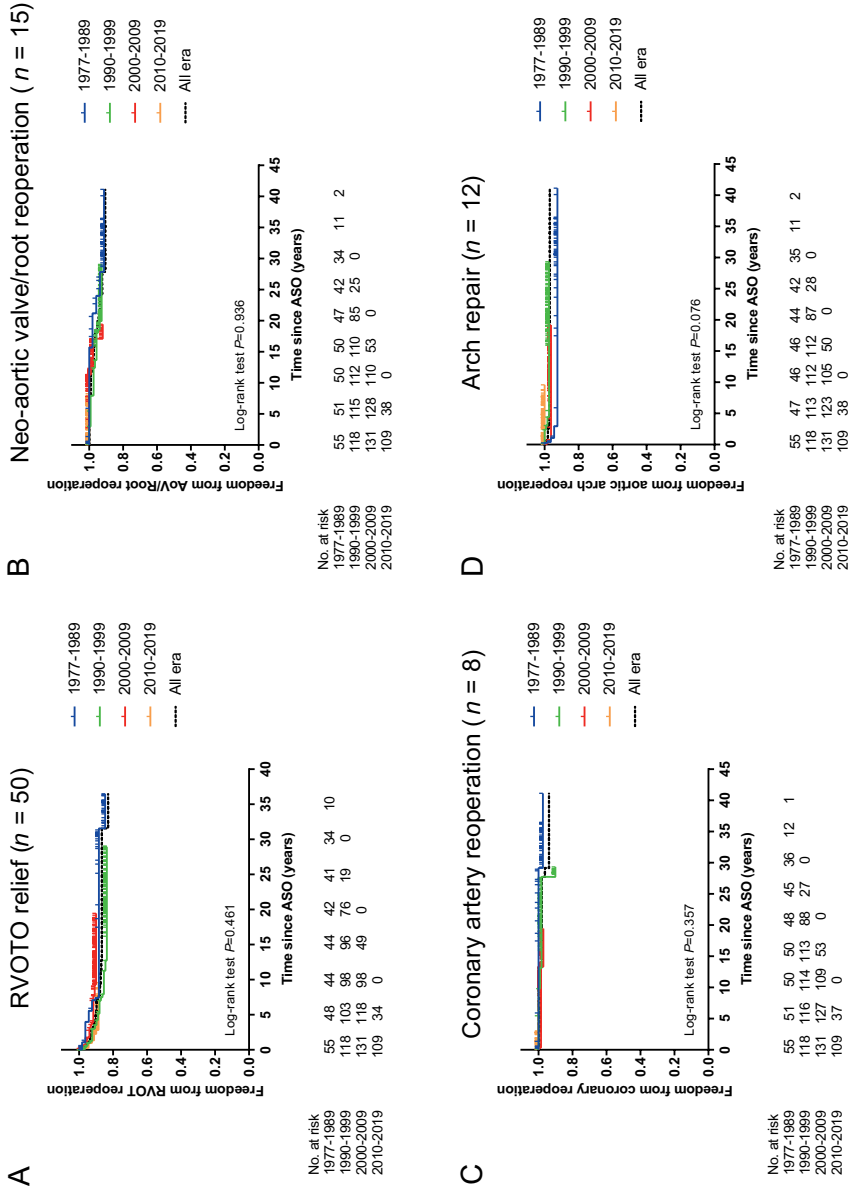
B

2nd reoperation ( $n = 22$ )

No. at risk	0	5	10	15	20	25	30	35	40
1977-1989	55	51	50	49	45	41	34	10	
1990-1999	118	114	111	107	83	25	0		
2000-2009	131	126	107	51	0				
2010-2019	109	37	0						

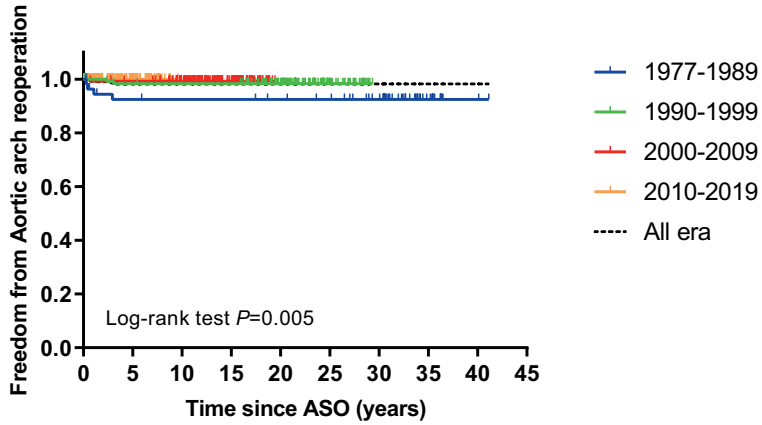
**Supplementary Figure S1.** Differences in reoperation rate by era.

Differences in reoperation rates of 1<sup>st</sup> reoperation (A) and 2<sup>nd</sup> reoperation (B) post-ASO between eras.



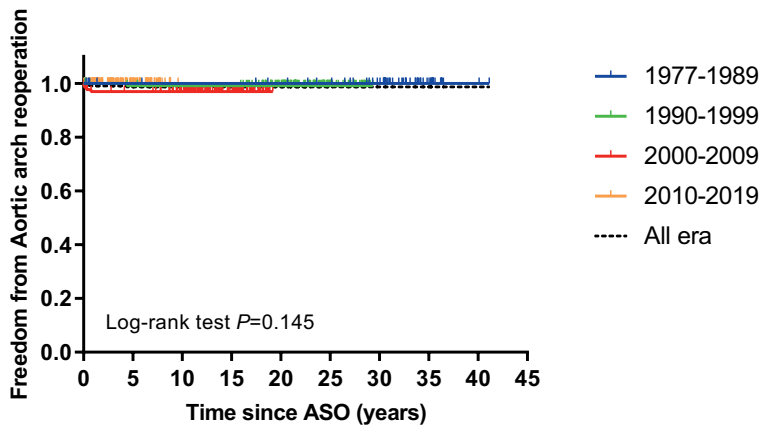
**Supplementary Figure S2.** Differences in reoperation type by era. Differences in type of reoperation post-ASO between eras for: relief right ventricular outflow tract obstruction (RVOTO) (A), neo-aortic valve or neo-aortic root reoperation (B), coronary artery reoperation (C) and aortic arch repair post-ASO (all indications: both recoarctation and neo-coarctation) (D).

**A** Arch repair for recoarctation ( $n = 7$ )



No. at risk	0	5	10	15	20	25	30	35	40	45
1977-1989	55	47	46	46	44	42	35	11	2	
1990-1999	118	114	113	113	88	28	0			
2000-2009	131	127	109	53	0					
2010-2019	109	38	0							

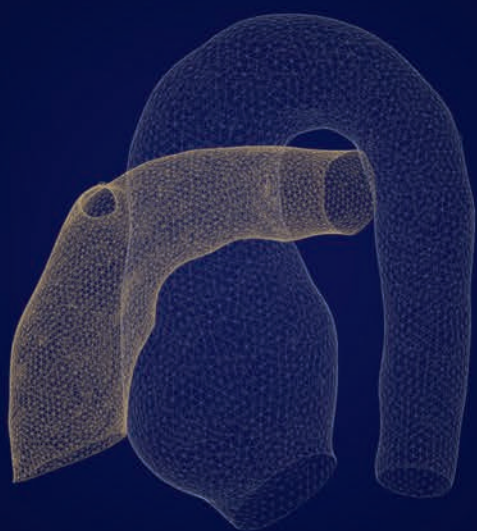
**B** Arch repair for neo-coarctation ( $n = 5$ )



No. at risk	0	5	10	15	20	25	30	35	40	45
1977-1989	55	51	50	50	48	45	37	13	2	
1990-1999	118	115	114	114	89	28	0			
2000-2009	131	124	106	51	0					
2010-2019	109	38	0							

**Supplementary Figure S3.** Differences between arch repair post-ASO by era: recoarctation (A) versus neo-coarctation (B)





## CHAPTER 3

# Transposition of the great arteries: fetal pulmonary valve growth and postoperative neo-aortic root dilatation

Prenatal Diagnosis. 2019;39:1054-63

Roel L.F. van der Palen\*

Carlijn van der Zee\*

Arja S. Vink

Ingmar Knobbe

Sean J. Jurgens

Elizabeth van Leeuwen

Caroline J. Bax

Gideon J. du Marchie Sarvaas

Nico A. Blom

Monique C. Haak

Caterina M. Bilardo

Sally-Ann B. Clur

\* shared first authorship



## Abstract

### Objectives

Documentation of semilunar valve growth in fetal transposition of the great arteries (TGA) and the relationship between neo-aortic root dilatation, a cause for postoperative reinterventions after the arterial switch operation (ASO), and pulmonary valve (PV) annulus dimensions prenatally.

### Methods

This retrospective multicenter observational study included TGA fetuses suitable for ASO. Semilunar valve annuli pre-ASO and neo-aortic root diameters (post-ASO) were measured. Trends in annulus diameters were analyzed using a linear mixed-effects model and compared with normal values. Prenatal semilunar valve Z-scores were correlated with neo-aortic root diameters post-ASO.

### Results

We included 137 TGA fetuses (35.8% with significant ventricular septal defects (VSDs)). One hundred twenty-one underwent ASO. Fetal TGA-PV diameters were significantly larger than control aortic valve (AoV) and PV annuli from 23 and 27 weeks, respectively, especially when a VSD was present. Fetal TGA-AoV annuli were significantly larger than control AoV and PV annuli from 26 and 30 weeks, respectively. Z-scores of fetal TGA-PV and neo-aortic root diameter at last follow-up correlated significantly, ( $P < 0.001$  at 26-30 weeks).

### Conclusion

Fetal TGA semilunar valve annuli are larger than control annuli, especially when there is a significant VSD. Factors besides postoperative hemodynamics, including fetal anatomy, PV Z-score, prenatal flow, connective tissue properties and genetics may influence the risk for late reintervention in these fetuses.

## Introduction

Transposition of the great arteries (TGA) is a frequently seen cyanotic cardiac anomaly, occurring in 1 in 3,500 to 5,000 live births per year.<sup>1</sup> The pulmonary and systemic circulations are in parallel not series, and blood with a higher saturation is ejected into the pulmonary circulation instead of the systemic circulation.<sup>2,3</sup> Historically, low prenatal TGA detection rates have contributed to a relatively limited knowledge of fetal TGA pathophysiology.<sup>4</sup> With the inclusion of additional views in prenatal screening protocols, the prenatal detection rate of TGA is improving.<sup>5</sup> Fetal cardiologists are required to discuss long-term postoperative outcomes of TGA more frequently.

Currently, the arterial switch operation (ASO) is the preferred intervention for TGA and Taussig-Bing anomaly (TBA) worldwide with an operative mortality less than 5%.<sup>6-8</sup> Despite this encouraging figure, some troubling complications do occur.<sup>8</sup> Problems with coronary perfusion and peripheral pulmonary artery stenosis may occur in the short term. The growth of the anastomoses of the great arteries and the competence of the native pulmonary valve (PV) and root, now functioning as the neo-aortic valve and root in the systemic circulation, are important in the long term.<sup>6-8</sup> Neo-aortic root dilatation has been reported,<sup>8-17</sup> even in the first year post-ASO,<sup>9-11</sup> and the root continues to grow excessively,<sup>15-17</sup> at a rate  $\geq 4$  times normal.<sup>9</sup> The resulting neo-aortic valve regurgitation and aneurysm formation may require a reintervention.<sup>15-17</sup> The 25-year reintervention-free survival for the neo-aortic valve or root after ASO is reported to be 95%.<sup>15</sup>

The underlying etiology of neo-aortic root dilatation is not completely understood and is probably multifactorial. Prior pulmonary artery banding, presence of a ventricular septal defect (VSD), TBA, gender, the technique used for the transfer of the coronary buttons and the length of follow-up have been implicated.<sup>11-20</sup> The study aim was to document the natural growth of the semilunar valves in fetuses with TGA and to compare it to normal semilunar valve growth. We also wished to determine if neo-aortic root dilatation post-ASO is related to the prenatal semilunar valve growth. This knowledge could be important to understand the pathophysiology of fetal TGA and the long-term post-ASO complications.

## Methods

### Study population

All fetuses diagnosed between 2000 and 2017 with TGA or TBA (TGA without pulmonary stenosis with a large VSD and overriding of the PV  $\leq 50\%$ ) suitable for ASO at four academic centers in the Netherlands (Amsterdam University Medical Centers [Academic Medical Center and VU Medical Center], Leiden University Medical Center, and the University Medical Center Groningen), were included in this observational study. The patients were divided into two subgroups: (1) TGA with a hemodynamically significant VSD and (2) TGA with an intact interventricular septum (IVS). The study was approved by the Medical Ethics Committee of the Academic Medical Center, Amsterdam University Medical Centers, Amsterdam.

### Clinical data

The collected clinical data included sex, gestational age at prenatal follow-ups, prenatal and final diagnosis after birth, gestational age at birth, birth weight, surgical procedures performed, and outcome (alive or dead). The age, weight, and height of the patients at 1-year post-ASO and/or last follow-up moment were also collected.

### Echocardiographic measurements

The diameters of the semilunar valve annuli at each prenatal follow-up visit and on the first postnatal day were measured in millimeters. The prenatal and pre-ASO measurements were made with the valves open using outflow tract views and compared with the normal data of Vigneswaran et al.<sup>21</sup> and Schneider et al.<sup>22</sup> as Vigneswaran et al. measured the annuli with the valve closed and Schneider et al. with the valves open. Fetal and pre-ASO Z-scores for the PV and aortic valve (AoV) annular diameters were calculated from Vigneswaran et al.<sup>21</sup> and Schneider et al.<sup>22</sup>

Measurements post-ASO included the neo-aortic annulus, neo-aortic root at the level of the sinuses, and sinotubular (ST) junction at the follow-up closest to 1-year post-ASO and at the last follow-up visit. The measurements were made with the valves open from inner-edge to inner-edge (Figure 1). The Haycock formula was used to calculate the body surface area,<sup>23</sup> and the Z-scores were determined according to a pediatric reference dataset.<sup>24</sup> Measurements were performed by two observers (SAC and RvdP) using stored images. The prenatal images were recorded using Voluson E8 and E10 ultrasound machines (General Electric). The postnatal echo images were recorded on Vivid 7 echomachines (General Electric) and measured using the EchoPac workstation.

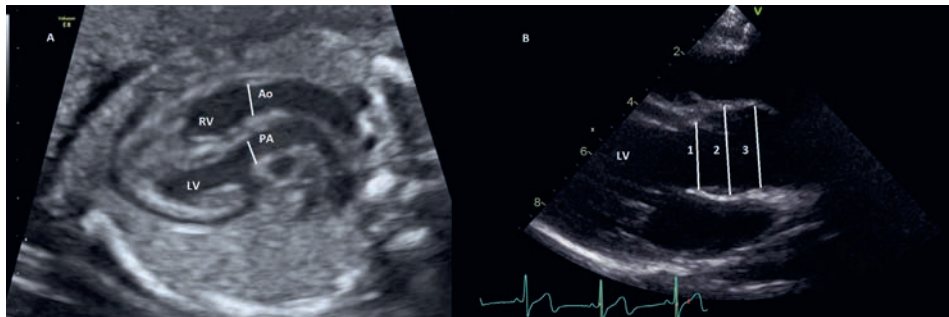


**Figure 1.** Echocardiographic measurements prenatally and post arterial switch. Prenatal measurements at the level of the semilunar valve annulus with the valve open (A). Post arterial switch measurements of the neo-aortic root from the parasternal long-axis view with the neo-aortic valve open (B). Dimensions: 1 = annulus, 2 = neo-aortic root and 3 = sinotubular junction. Ao, aorta; LV, left ventricle; PA, pulmonary artery; RV, right ventricle.

## Statistical analysis

### *Population characteristics*

Statistical analysis was performed using IBM SPSS Statistics 23.0 (SPSS Inc., Chicago, IL, USA) and R version 3.3.2.<sup>25</sup> Clinical characteristics and echocardiographic parameters were presented as a number (percentage) for categorical variables, mean (standard deviation) for continuous variables with an approximately symmetric distribution, and median (interquartile range, IQR) for continuous data with a skewed distribution. Comparisons between baseline characteristics for TGA fetuses with IVS and VSD were performed using the chi-square test for categorical variables and for continuous variables, the Welch approximate t-test or the Mann Whitney test, as appropriate.

### *Prenatal trends in PV and AoV annular diameters*

A repeated measurements analysis with a linear mixed-effects model was used to assess average age trends in PV and AoV annular diameters, using all available prenatal echocardiograms per fetus and the first postnatal echocardiogram. This was also done for the Z-scores of the PV and AoV annular diameters, using only the fetal data. A mixed-effects model takes account of repeated measurements per fetus over time during which the number and timing of the measurements may vary per fetus. Natural cubic splines were modeled to evaluate the variations in time. Knots were placed at five fixed quintiles of the predictor's distribution as suggested by Stone and Koo.<sup>26</sup> The intercept was allowed to differ per fetus and was assumed to follow a multivariate normal distribution (random effect). Since the slope and the intercept of both semilunar valve models had a correlation of 1.0, no random effect for the slope was used. Control lines for PV and AoV annular diameters were plotted on the basis of regression equations described by Vigneswaran et al.<sup>21</sup> and Schneider et al.<sup>22</sup>

Several comparisons were performed for the PV and AoV annular diameters: (1) the average trend in PV annular diameters of the TGA fetuses compared with the trend in PV annular diameters of controls and (2) with the AoV annulus of the controls. Further, (3) the average trend in AoV annulus of the TGA fetuses was compared with the trend in PV annulus of the controls and (4) the AoV annulus of controls. The average trends in (5) the PV and AoV annuli of the TGA fetuses were additionally allowed to differ by the presence or absence of a VSD as well as (6) by the presence of TBA. A sensitivity analysis was also performed for the TGA-PV annulus trend where only measurements made during fetal life were included. For the Z-scores of the PV and AoV annular diameters, the average trend was analyzed and the trends were allowed to differ by the presence or absence of a VSD. Sampling uncertainty was quantified via 95% confidence intervals and *P* values. A *P* value <0.05 was considered statistically significant.

### *Correlation between prenatal and postnatal measurements*

Correlations between the Z-scores of the prenatal semilunar valve annuli and the neo-aortic dimensions 1-year post-ASO and last outpatient follow-up were performed, stratified for

gestational age: 18 to 22, 26 to 30, and 32 to 36 weeks' gestation. Each group included only one measurement of PV and AoV annulus per fetus. Correlation between prenatal and postnatal measurements was tested by the Spearman correlation coefficient ( $r$ ).

#### *Prediction of neo-aortic root dilatation post-ASO*

Receiver-operating characteristic (ROC) analyses were performed, and the area under the curves (AUCs) were determined for neo-aortic root dilatation (defined as Z-score  $\geq 2.0$ ) at 1-year post-ASO or the last post-ASO follow-up visit for all gestational age groups (i.e. 8-22, 26-30, and 32-36 weeks' gestation), based on the fetal PV and AoV Z-score of one measurement per age group. An AUC  $> 0.700$  was considered to be of a good predictive value, and of these values, an optimal cut-off value was defined (Youden's index). A logistic regression analysis was additionally performed to stratify the predictive value for sex.

## Results

### **Population characteristics**

One hundred forty-nine fetuses were identified with a prenatal diagnosis of TGA suitable for ASO. There were no fetal echocardiograms available for revision in 12 (8.1%). One hundred thirty-seven fetuses were included in the analyses of whom 90 (65.7%) were male and 46 were female. The gender of one fetus, where the pregnancy was interrupted, was not recorded. Eighty-eight fetuses (64.2%) had an IVS and 49 (35.8%) a significant VSD of which 12 (8.8%) had a TBA. In total, 15 fetuses (11%) died (Figure 2). One hundred twenty-one underwent an ASO. There were three post-ASO deaths related to coronary perfusion problems giving an operative mortality of 2.5%. Table 1 shows the baseline characteristics of the included fetuses. There were 384 fetal and 119 postnatal echocardiograms analyzed giving pre-ASO data from 503 echocardiograms. The median number of included echocardiograms was 5 (range 1-10) per patient. Follow-up data post-ASO was available from 118 fetuses. The median follow-up was 2.9 years (range 1 month - 14.3 years).

### **Trends in PV annular diameters**

A statistically significant trend in PV annular diameter ( $P < 0.0001$ ) was seen in the TGA fetuses through gestation. The average trend in PV annular diameter in TGA fetuses compared with controls was different from 27 weeks' gestation, with the PV-annuli being larger in the TGA fetuses (Figure 3A and supplementary Figure S1). In late gestation, the PV annular growth rate reduced (change in slope of curve). The sensitivity analysis with the exclusion of the first postnatal measurements showed a subtler reduction in PV annular growth rate in late gestation (supplementary Figure S2).

When compared with the AoV annular diameter of the controls (Figure 3B and supplementary Figure S1), TGA fetuses had a larger PV annular diameter from 23 weeks' gestation onwards. There was a statistically significant difference in the PV annular diameter

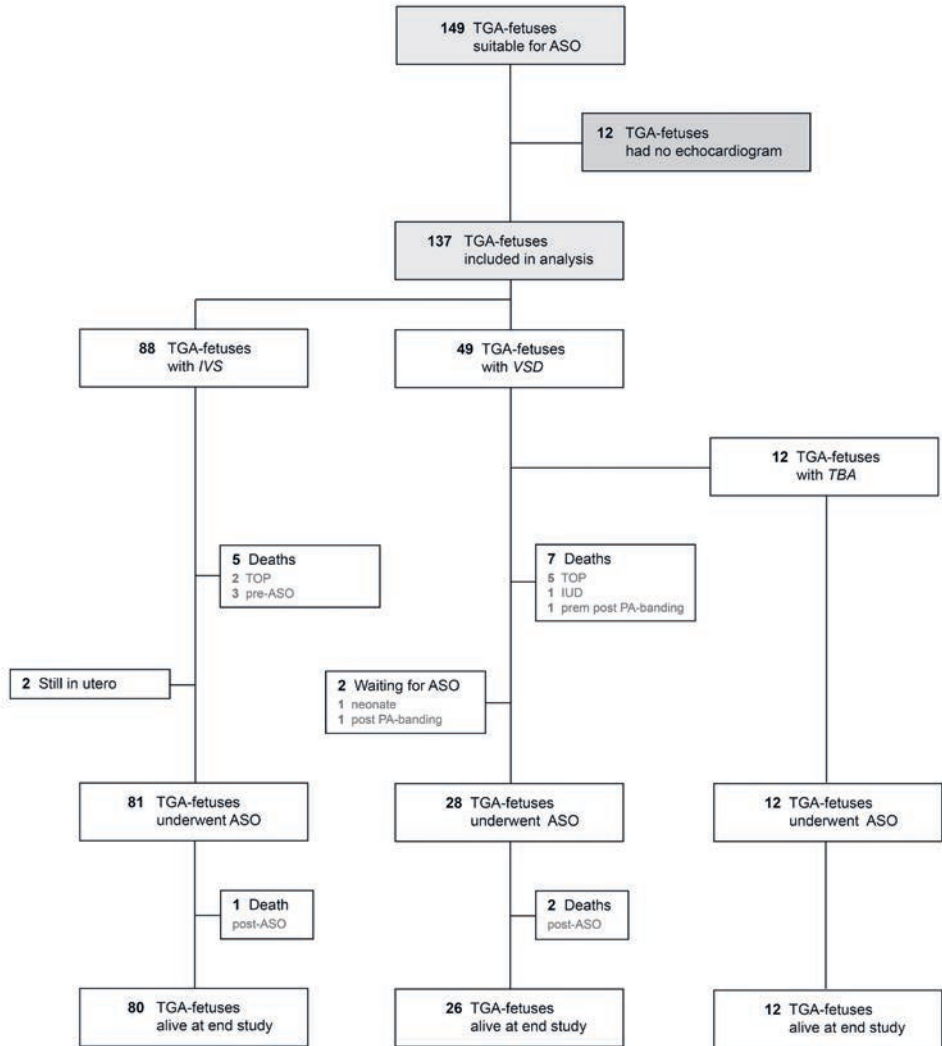


**Figure 2.** Flow diagram of included patients.

ASO, arterial switch operation; IUD, intra-uterine death; IVS, intact interventricular septum; TBA, Taussig-Bing anomaly; TGA, transposition of the great arteries; TOP, termination of pregnancy; VSD, ventricular septal defect.

of TGA-fetuses with and without a VSD ( $P = 0.005$ ) (Figure 3C). TGA fetuses with VSD had, on average, larger PV annular dimensions. When the TGA-VSD fetuses were further stratified on the basis of a TBA or non-TBA anatomy, there was a statistically significant difference in the trend in PV annular diameter between the subgroups ( $P < 0.0001$ ) (Figure 3D).

**Table 1.** Baseline characteristics

	All (n = 137)	TGA-IVS (n = 88)	TGA-VSD (n = 49)	P value TGA- IVS vs TGA-VSD
Male <sup>a</sup>	90 (65.7%)	63 (71.6%)	27 (55.1%)	0.0001
Female <sup>a</sup>	46 (33.6%)	25 (28.4%)	21 (42.9%)	0.55
Number of echocardiograms*	5 (4-7)	6 (4-7)	5 (4-6)	0.007
Gestation age at birth, weeks**	39.1 ± 1.2 (n = 126)	39.2 ± 0.9 (n = 83)	39.0 ± 1.5 (n = 43)	0.43
Birth weight, kg**	3.359 ± 0.442 (n = 126)	3.380 ± 0.438 (n = 83)	3.320 ± 0.454 (n = 43)	0.47
Balloon atrial septostomy	65 (51.6%) (n = 126)	49 (59%) (n = 83)	16 (37.2%) (n = 43)	0.03
Deaths	15 (10.9%)	6 (6.8%)	9 (18.4%)	0.07

<sup>a</sup> The gender of one fetus, where the pregnancy was interrupted, was not recorded and is therefore missing from these numbers. \* Median (IQR), \*\* Mean ± standard deviation. IVS, intact interventricular septum; VSD, ventricular septal defect.

### Trends in AoV annular diameters

A statistically significant trend was seen in the AoV annular diameter in the TGA fetuses ( $P < 0.0001$ ). There was a significant difference between the average trend in AoV annulus in TGA fetuses compared with the PV annular diameter of the controls from 30 weeks' gestation (Figure 3E). TGA fetuses had a significantly larger AoV annular diameter compared with the AoV annular diameter of the controls from 26 weeks' gestation onwards (Figure 3F).

### Prenatal trends in Z-score of PV and AoV annular diameters

A statistically significant trend was seen in the semilunar valve Z-scores in the TGA fetuses ( $P < 0.0001$  for both valves). The trends in the Z-scores of the PV and AoV annular diameters were not different for the presence or absence of a VSD ( $P = 0.052$  and  $P = 0.078$ , respectively) (Figure 4 and supplementary Figure S3).

### Correlation between prenatal and postnatal measurements

All correlations are documented in Table 2. Most importantly, at 26 to 30 weeks gestation, Z-scores of the PV and AoV annular diameters correlated with the Z-score of the neo-aortic root measurement at the last follow up visit ( $r = -0.49$ ,  $P < 0.001$  and  $r = -0.35$ ,  $P = 0.003$ , respectively).

### Prediction of neo-aortic root dilatation post-ASO

Only the PV annulus Z-score at 26 to 30 weeks' gestation was considered to be of a predictive value for neo-aortic root dilatation at the last follow-up visit (AUC = 0.761) (supplementary Table S1). The optimal cutoff value to predict neo-aortic root dilatation at the last follow-up visit post-ASO was a PV annulus Z-score of -0.04 at 26 to 30 weeks' gestation (sensitivity

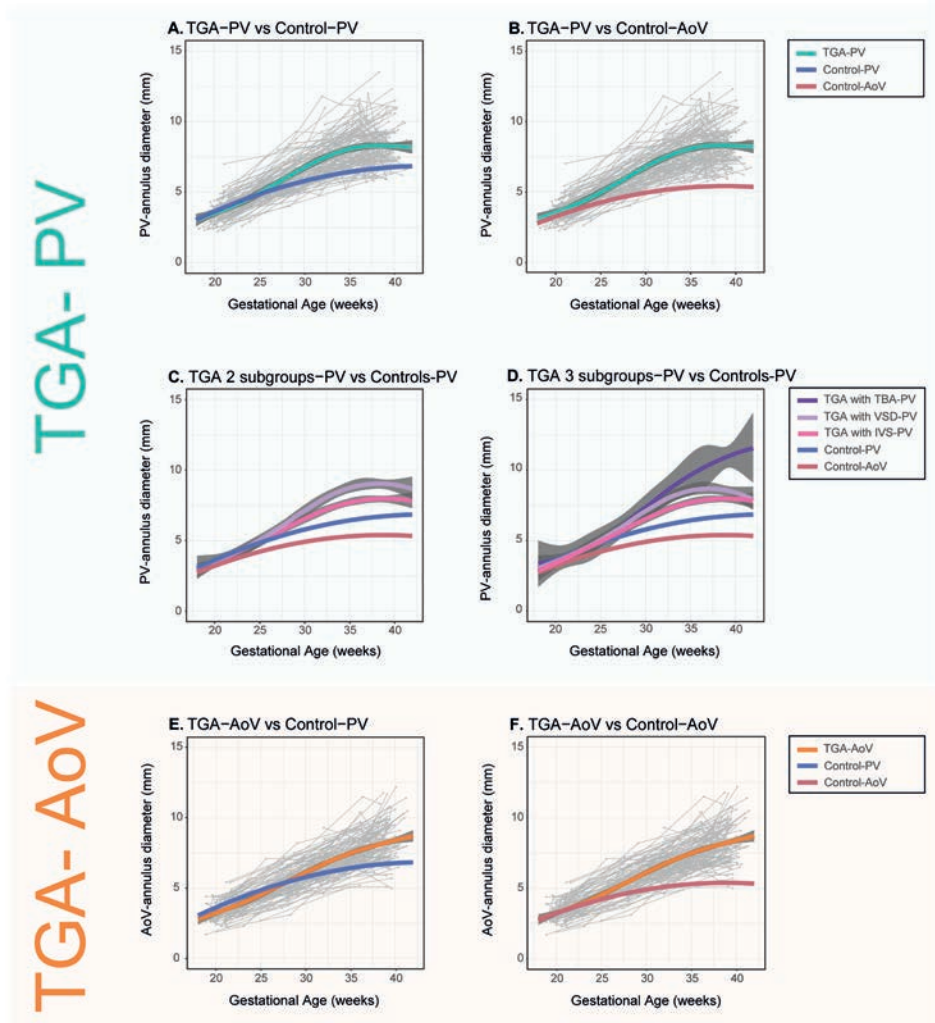


**Figure 3.** Average trends in semilunar valve diameters in TGA fetuses versus controls (Vigneswaran et al.). Average trends in PV annular diameters in TGA fetuses (TGA-PV) (A) versus trends in controls PV annular diameter (Control-PV); (B) versus AoV annular diameter (Control-AoV); (C) TGA with an IVS (TGA with IVS-PV) and a VSD (TGA with VSD-PV); and (D) with the TGA-VSD fetuses further stratified on the basis of a TBA or non-TBA anatomy (TGA with TBA-PV). Average trend in AoV annular diameters in TGA fetuses (TGA-AoV): (E) versus trends in controls of PV annular diameter (Control-PV); and (F) AoV annular diameter (Control-AoV). Trends in PV and AoV annular diameters in controls are shown (Control-PV and Control-AoV). Grey dots are individual measurements, and grey lines are individual trends. The 95% confidence intervals for both the fitted model and the control line as described by Vigneswaran et al.<sup>21</sup> are shown in blue (pulmonary valve) and red (aortic valve). Note that the 95% confidence intervals for the controls are smaller than the thickness of the line. AoV, aortic valve; IVS, intact interventricular septum; PV, pulmonary valve; TBA, Taussig-Bing anomaly; TGA, transposition of the great arteries; VSD, ventricular septal defect.



73%, specificity 69%) (supplementary Figure S4). There was no statistically significant difference between males and females in the prediction of neo-aortic root dilatation at last follow-up visit post-ASO based on the PV annulus Z-score at 26 to 30 weeks' gestation ( $P = 0.395$ ).

**Table 2.** Comparisons between Z-scores of semilunar valve annulus and left ventricular outflow tract measurements at 1 year and last follow-up

Comparisons	r	P value	Comparisons	r	P value
<b>18-22 weeks</b>					
1 year FU			Last FU		
Z-fPV vs Z-AoV	-0.18	0.142	Z-fPV vs Z-AoV	-0.10	0.370
Z-fPV vs Z-Root	<b>-0.27</b>	<b>0.027</b>	Z-fPV vs Z-Root	<b>-0.29</b>	<b>0.009</b>
Z-fPV vs Z-STjunction	-0.09	0.491	Z-fPV vs Z-STjunction	0.01	0.949
Z-fAoV vs Z-AoV	<b>-0.35</b>	<b>0.002</b>	Z-fAoV vs Z-AoV	-0.21	0.062
Z-fAoV vs Z-Root	-0.16	0.171	Z-fAoV vs Z-Root	-0.12	0.338
Z-fAoV vs Z-STjunction	-0.09	0.501	Z-fAoV vs Z-STjunction	-0.03	0.794
<b>26-30 weeks</b>					
1 year FU			Last FU		
Z-fPV vs Z-AoV	<b>-0.31</b>	<b>0.020</b>	Z-fPV vs Z-AoV	<b>-0.32</b>	<b>0.008</b>
Z-fPV vs Z-Root	<b>-0.28</b>	<b>0.035</b>	Z-fPV vs Z-Root	<b>-0.49</b>	<b>&lt;0.001</b>
Z-fPV vs Z-STjunction	-0.20	0.150	Z-fPV vs Z-STjunction	<b>-0.39</b>	<b>0.019</b>
Z-fAoV vs Z-AoV	<b>-0.31</b>	<b>0.019</b>	Z-fAoV vs Z-AoV	<b>-0.29</b>	<b>0.016</b>
Z-fAoV vs Z-Root	-0.13	0.333	Z-fAoV vs Z-Root	<b>-0.35</b>	<b>0.003</b>
Z-fAoV vs Z-STjunction	-0.08	0.574	Z-fAoV vs Z-STjunction	-0.10	0.441
<b>32-36 weeks</b>					
1 year FU			Last FU		
Z-fPV vs Z-AoV	-0.24	0.054	Z-fPV vs Z-AoV	<b>-0.27</b>	<b>0.024</b>
Z-fPV vs Z-Root	-0.24	0.063	Z-fPV vs Z-Root	<b>-0.28</b>	<b>0.019</b>
Z-fPV vs Z-STjunction	-0.06	0.658	Z-fPV vs Z-STjunction	-0.11	0.394
Z-fAoV vs Z-AoV	-0.11	0.410	Z-fAoV vs Z-AoV	-0.24	0.056
Z-fAoV vs Z-Root	-0.21	0.112	Z-fAoV vs Z-Root	-0.17	0.164
Z-fAoV vs Z-STjunction	-0.17	0.228	Z-fAoV vs Z-STjunction	-0.02	0.877

Significant results are shown in bold ( $P < 0.05$ ). Fetal Z-scores based on Vigneswaran et al.<sup>21</sup>  
 FU, follow-up; Z-AoV, Z-score of neo-aortic valve annulus diameter post arterial switch operation; Z-fAoV, Z-score of the fetal aortic valve annulus diameter; Z-fPV, Z-score of the fetal pulmonary valve annulus diameter; Z-Root, Z-score of the neo-aortic root; Z-STjunction, Z-score of the sinotubular junction.

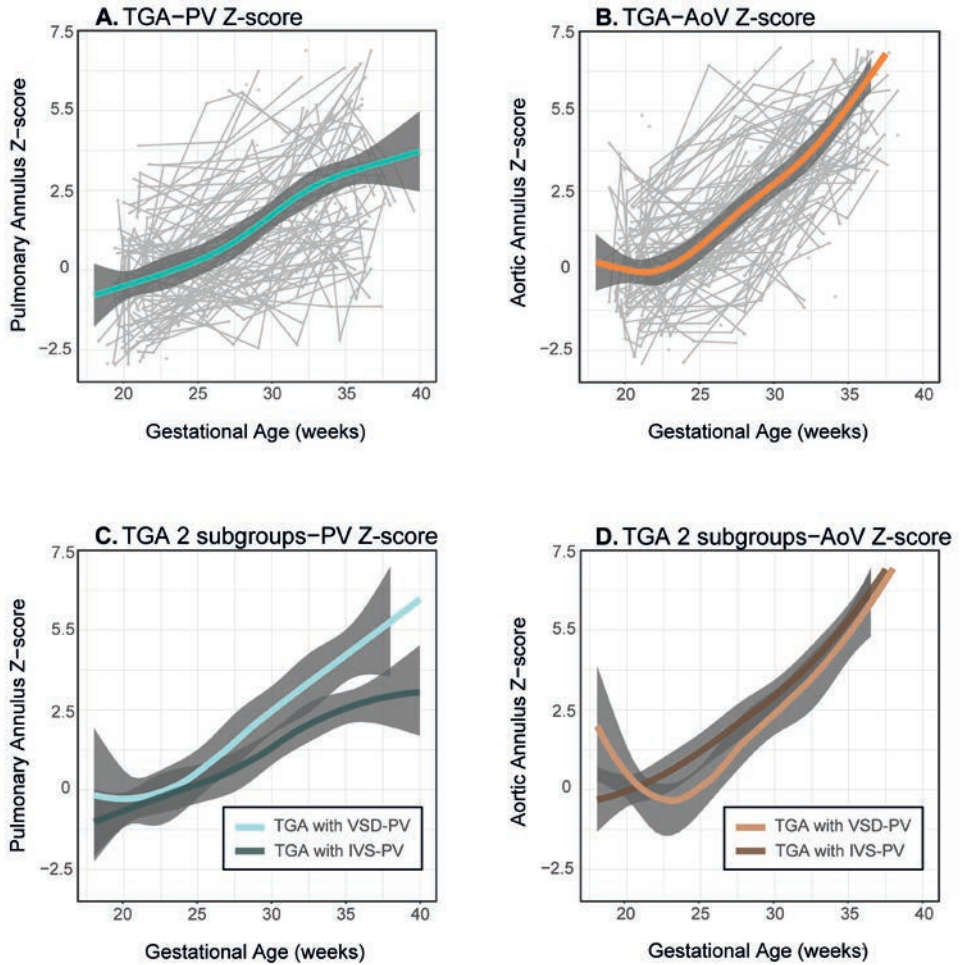


**Figure 4.** Average trend in semilunar valve Z-scores in TGA fetuses (based on Vigneswaran et al.). Average trend in TGA fetal (A) PV annular diameter Z-score (TGA-PV Z-score) and (B) AoV annular diameter Z-score (TGA-AoV Z-score). Fetal Z-scores based on data from Vigneswaran et al.<sup>21</sup> Grey dots are individual measurements and grey lines are individual trends. Both trends were stratified on the basis of the presence (TGA with VSD) or absence (TGA with IVS) of a VSD (C and D). AoV, aortic valve; IVS, intact interventricular septum; PV, pulmonary valve; TGA, transposition of the great arteries; VSD, ventricular septal defect.

## Discussion

This study has shown that the semilunar valves are larger in TGA fetuses compared with fetuses with normal hearts. PV annular diameters in the TGA fetuses were significantly larger than controls from 27 weeks' gestation, especially when a VSD was present. They were also significantly larger than control AoV annular diameters from 23 weeks' gestation. The Z-scores of the PV-annulus and neo-aortic root diameter at last follow-up post-ASO correlated significantly, but only the PV annulus Z-score at 26 to 30 weeks' gestation was considered to be of a predictive value for neo-aortic root dilatation at the last follow-up visit (AUC = 0.761). Additionally, the AoV annular diameters were significantly larger in TGA fetuses than controls from 26 weeks' gestation and larger than control PV annular measurements from 30 weeks' gestation.

### Flow and growth of the semilunar valves

The size of a vessel can be related to the flow through it,<sup>27,28</sup> growing larger with more flow. The PV annulus is usually larger than the AoV annulus in a normal fetal heart. This correlates with the larger proportion of the combined cardiac output (CCO) ejected by the right ventricle compared with the left ventricle, which increases with gestation to about 66% for the right ventricle.<sup>3,29-31</sup> In the fetus, oxygenated blood from the venous duct is preferentially streamed across the oval fossa into the left atrium and left ventricle. In TGA, this blood, with a higher oxygen saturation, is ejected into the pulmonary artery and may cause pulmonary vasodilatation and potential ductal constriction. Increased pulmonary blood flow, pulmonary venous return to the left atrium and left ventricular filling then follows.<sup>2,3,5</sup> The percentage of the CCO ejected by the left ventricle increases as a consequence to about 50%.<sup>2,3,5</sup>

So, if only flow determines growth, the PV annular diameter in fetal TGA hearts should be smaller than control PV annuli but larger than control AoV annuli. However, we found the diameters of fetal TGA-PV annuli to be significantly larger than controls from 27 weeks and also larger than the control AoV annuli from 23 weeks onwards. A previous study has also shown PV Z-scores smaller than the AoV Z-scores (-0.65 vs 1.13), in TGA-fetuses with IVS,<sup>4</sup> in concordance with our findings. Furthermore, the fetal TGA-AoV annuli were not smaller than control PV annuli as may be expected if only flow determines annular growth.

Our findings suggest that other factors besides flow also play a role in the growth of the semilunar valve annuli in fetal TGA. Lalezari et al. have shown that the amount of collagen was diminished in unoperated neonatal TGA hearts and the anchorage and embedding of both arterial roots in the myocardium was less extensive.<sup>32</sup> This deficiency in support for the great vessels possibly contributes to the increased size of the semilunar valves. Furthermore, the pulmonary artery in unoperated TGA hearts showed a clear trend in loss of actin-positive smooth muscle cells with age,<sup>33</sup> which may further contribute to neo-aortic root dilatation post-ASO.

**Effect of a VSD**

The enlargement of the PV annulus was especially marked when there was a significant VSD from about 30 weeks' gestation. In TBA, the PV annular diameter is larger than the AoV annulus as the subpulmonary VSD allows a proportion of the right ventricular output, in addition to the left ventricular output, to cross the PV, encouraging growth. Larger PV annular diameters in non-TBA TGA hearts with a significant VSD were also found, suggesting a net right to left shunt across the fetal VSD and increased flow over the PV, coinciding with the fall in pulmonary resistance that is seen in the fetus around 28 weeks' gestation.<sup>30, 31</sup>

**Late gestational changes in PV annular growth**

We found a reduced growth rate in the PV annulus at the end of gestation. A corresponding leveling in the prenatal PV Z-score was seen from 35 weeks onwards. Godfrey et al. have also described a significant reduction in the PV annular Z-score in fetal TGA between the second and third trimesters.<sup>4</sup> The reason for this is not entirely clear. After 30 weeks, the proportion of the CCO passing through the lungs and oval fossa is stable in normal fetal hearts, but the pulmonary vascular resistance increases.<sup>31</sup> In TGA fetuses, the pulmonary venous return may be increased elevating left atrial pressure and encouraging restriction of the oval foramen,<sup>2</sup> reducing right to left shunting at atrial level, left ventricular filling and flow over the PV in later gestation with possible reduced growth of the PV as a result. When the postnatal measurements were not included in our model, the late gestational trend for reduction in PV annular growth was less evident.

**Neo-aortic root**

The long-term prognosis of the ASO depends on the adequate growth of the repaired arteries and the adaption of the neo-aortic valve.<sup>6, 8, 9</sup> We have shown that the size of the PV-annulus at 26 to 30 weeks correlated with the size of the neo-aortic root at last follow-up visit post-ASO and that the PV annulus in fetal TGA is already larger than a normal AoV annulus. However, this correlation was not strong enough to be clinically useful for a prenatal prediction of neo-aortic root dilatation post-ASO. Measuring the PV annulus at 28 weeks' gestation will not influence the immediate postnatal management of the baby. In countries where there are constraints on prenatal echo facilities, the emphasis should rather lie on the initial diagnosis of the transposition of the great arteries around 20 weeks of gestation with the use of the outflow tract views. A follow-up echo in the last two weeks of pregnancy is also important to evaluate the oval fossa size and risk for a postnatal Rashkind procedure and pulmonary hypertension.<sup>34</sup>

Hourihan et al. also observed that the neo-aortic root and PV annulus are already larger than in normal infants before the ASO.<sup>8</sup> An increased risk of neo-aortic root dilation in TBA and TGA with VSD has previously been recognized,<sup>13, 16, 18</sup> highlighting the role of a significant VSD in the pathophysiology of neo-aortic root dilatation. This is clinically relevant as the reintervention rate is higher in TGA patients with a VSD compared to those with an IVS.<sup>14, 17</sup> Furthermore, the neo-aortic root growth rate post-ASO is  $\geq 4$  times the normal rate.<sup>9</sup> The resultant valve regurgitation may require reintervention.<sup>7, 15-17</sup>

**Strengths and limitations**

This was a multicenter study of one of the largest cohorts of fetal TGA reported to date and presents serial data. As with all retrospective studies, it has limitations. Not all cases had stored data that could be analyzed. The fetal echocardiograms were made by different observers, and there was no predetermined protocol, which may have biased the results. However, two researchers performed all the measurements. We did not have our own control group and used the normal data of Vigneswaran et al. based on a cohort of more than 7000 fetuses.<sup>21</sup> As the semilunar valves were measured in closed position by Vigneswaran et al.<sup>21</sup> and they had no measurement data after 36 weeks' gestation, we also plotted our cohort against the normal data of Schneider et al.<sup>22</sup> where the semilunar valves were measured in the open position in 130 fetuses. The trends and our conclusions using the different control data were similar.

**Conclusions**

In conclusion, fetal TGA semilunar valve annuli are larger than normal, especially when there is a significant VSD. This research adds to our understanding of the pathophysiology of fetal TGA and the long-term complications post-ASO.

## References

1. Samanek M, Slavik Z, Zborilova B, Hrobonova V, Voriskova M, Skovranek J. Prevalence, treatment, and outcome of heart disease in live-born children: a prospective analysis of 91,823 live-born children. *Pediatr Cardiol.* 1989;10(4):205-11.
2. Rudolph AM. Congenital cardiovascular malformations and the fetal circulation. *Arch Dis Child Fetal Neonatal Ed.* 2010;95(2):F132-6.
3. Rudolph AM. *Congenital Diseases of the Heart: Clinical-Physiological Considerations.* 3rd ed. Chichester, UK: Wiley Blackwell; 2009.
4. Godfrey ME, Friedman KG, Drogosz M, Rudolph AM, Tworetzky W. Cardiac output and blood flow redistribution in fetuses with D-loop transposition of the great arteries and intact ventricular septum: insights into pathophysiology. *Ultrasound Obstet Gynecol.* 2017;50(5):612-7.
5. Everwijn SMP, van Nesselrooij AEL, Rozendaal L, Clur SB, Pajkrt E, Hruđa J, Linskens IH, van Lith JM, Blom NA, Haak MC. The effect of the introduction of the three-vessel view on the detection rate of transposition of the great arteries and tetralogy of Fallot. *Prenat Diagn.* 2018;38(12):951-7.
6. Rodrigues C, Cerejo R. Arterial Switch: How to Predict Reoperation. *Rev Port Cir Cardiorac Vasc.* 2017;24(3-4):124.
7. de Koning WB, van Osch-Gevers M, Ten Harkel AD, van Domburg RT, Spijkerboer AW, Utens EM, Bogers AJ, Helbing WA. Follow-up outcomes 10 years after arterial switch operation for transposition of the great arteries: comparison of cardiological health status and health-related quality of life to those of the a normal reference population. *Eur J Pediatr.* 2008;167(9):995-1004.
8. Hourihan M, Colan SD, Wernovsky G, Maheswari U, Mayer JE, Jr., Sanders SP. Growth of the aortic anastomosis, annulus, and root after the arterial switch procedure performed in infancy. *Circulation.* 1993;88(2):615-20.
9. van der Bom T, van der Palen RL, Bouma BJ, van Veldhuisen SL, Vliegen HW, Konings TC, Zwinderman AH, Blom NA, Koolbergen DR, Hazekamp MG, et al. Persistent neo-aortic growth during adulthood in patients after an arterial switch operation. *Heart.* 2014;100(17):1360-5.
10. Marino BS, Wernovsky G, McElhinney DB, Jawad A, Kreb DL, Mantel SF, van der Woerd WL, Robbers-Visser D, Novello R, Gaynor JW, et al. Neo-aortic valvar function after the arterial switch. *Cardiol Young.* 2006;16(5):481-9.
11. van der Palen RLF, van der Bom T, Dekker A, Tsonaka R, van Geloven N, Kuipers IM, Konings TC, Rammeloo LAJ, Ten Harkel ADJ, Jongbloed MRM, et al. Progression of aortic root dilatation and aortic valve regurgitation after the arterial switch operation. *Heart.* 2019;105(22):1732-40.
12. McMahon CJ, Ravekes WJ, Smith EO, Denfield SW, Pignatelli RH, Altman CA, Ayres NA. Risk factors for neo-aortic root enlargement and aortic regurgitation following arterial switch operation. *Pediatr Cardiol.* 2004;25(4):329-35.
13. Michalak KW, Moll JA, Moll M, Dryzek P, Moszura T, Kopala M, Mludzik K, Moll JJ. The neo-aortic root in children with transposition of the great arteries after an arterial switch operation. *Eur J Cardiothorac Surg.* 2013;43(6):1101-8.
14. Co-Vu JG, Ginde S, Bartz PJ, Frommelt PC, Tweddell JS, Earing MG. Long-term outcomes of the neo-aorta after arterial switch operation for transposition of the great arteries. *Ann Thorac Surg.* 2013;95(5):1654-9.
15. Koolbergen DR, Manshanden JS, Yazdanbakhsh AP, Bouma BJ, Blom NA, de Mol BA, Mulder BJ, Hazekamp MG. Reoperation for neo-aortic root pathology after the arterial switch operation. *Eur J Cardiothorac Surg.* 2014;46(3):474-9.
16. Raju V, Burkhart HM, Durham LA, 3rd, Eidem BW, Phillips SD, Li Z, Schaff HV, Dearani JA. Reoperation after arterial switch: a 27-year experience. *Ann Thorac Surg.* 2013;95(6):2105-12.
17. Fricke TA, d'Udekem Y, Richardson M, Thuys C, Dronavalli M, Ramsay JM, Wheaton G, Grigg LE, Brizard CP, Konstantinov IE. Outcomes of the arterial switch operation for transposition of the great arteries: 25 years of experience. *Ann Thorac Surg.* 2012;94(1):139-45.

18. Schwartz ML, Gauvreau K, del Nido P, Mayer JE, Colan SD. Long-term predictors of aortic root dilation and aortic regurgitation after arterial switch operation. *Circulation*. 2004;110(11 Suppl 1):II128-32.
19. Baruteau AE, Vergnat M, Kalfa D, Delpey JG, Ly M, Capderou A, Lambert V, Belli E. Long-term outcomes of the arterial switch operation for transposition of the great arteries and ventricular septal defect and/or aortic arch obstruction. *Interact Cardiovasc Thorac Surg*. 2016;23(2):240-6.
20. Formigari R, Toscano A, Giardini A, Gargiulo G, Di Donato R, Picchio FM, Pasquini L. Prevalence and predictors of neo-aortic regurgitation after arterial switch operation for transposition of the great arteries. *J Thorac Cardiovasc Surg*. 2003;126(6):1753-9.
21. Vigneswaran TV, Akolekar R, Syngelaki A, Charakida M, Allan LD, Nicolaides KH, Zidere V, Simpson JM. Reference Ranges for the Size of the Fetal Cardiac Outflow Tracts From 13 to 36 Weeks Gestation: A Single-Center Study of Over 7000 Cases. *Circ Cardiovasc Imaging*. 2018;11(7):e007575.
22. Schneider C, McCrindle BW, Carvalho JS, Hornberger LK, McCarthy KP, Daubeney PE. Development of Z-scores for fetal cardiac dimensions from echocardiography. *Ultrasound Obstet Gynecol*. 2005;26(6):599-605.
23. Haycock GB, Schwartz GJ, Wisotsky DH. Geometric method for measuring body surface area: a height-weight formula validated in infants, children, and adults. *J Pediatr*. 1978;93(1):62-6.
24. Pettersen MD, Du W, Skeens ME, Humes RA. Regression equations for calculation of z scores of cardiac structures in a large cohort of healthy infants, children, and adolescents: an echocardiographic study. *J Am Soc Echocardiogr*. 2008;21(8):922-34.
25. R Core Team (2017). R: A language and environment for statistical computing. R Foundation for Statistical Computing, Vienna, Austria. URL <https://www.R-project.org/>.
26. Stone CJ, Koo CY. Additive splines in statistics. . In: *Proceedings of the Statistical Computing Section ASA*. Washington, DC: American Statistical Association; 1985:45-48.
27. Fishman NH, Hof RB, Rudolph AM, Heymann MA. Models of congenital heart disease in fetal lambs. *Circulation*. 1978;58(2):354-64.
28. Lev M. Pathologic anatomy and interrelationship of hypoplasia of the aortic tract complexes. *Lab Invest*. 1952;1(1):61-70.
29. Clur SA, Oude Rengerink K, Mol BW, Ottenkamp J, Bilardo CM. Fetal cardiac function between 11 and 35 weeks' gestation and nuchal translucency thickness. *Ultrasound Obstet Gynecol*. 2011;37(1):48-56.
30. Kiserud T, Acharya G. The fetal circulation. *Prenat Diagn*. 2004;24(13):1049-59.
31. Rasanen J, Wood DC, Weiner S, Ludomirski A, Huhta JC. Role of the pulmonary circulation in the distribution of human fetal cardiac output during the second half of pregnancy. *Circulation*. 1996;94(5):1068-73.
32. Lalezari S, Mahtab EA, Bartelings MM, Wisse LJ, Hazekamp MG, Gittenberger-de Groot AC. The outflow tract in transposition of the great arteries: an anatomic and morphologic study. *Ann Thorac Surg*. 2009;88(4):1300-5.
33. Lalezari S, Hazekamp MG, Bartelings MM, Schoof PH, Gittenberger-De Groot AC. Pulmonary artery remodeling in transposition of the great arteries: relevance for neo-aortic root dilatation. *J Thorac Cardiovasc Surg*. 2003;126(4):1053-60.
34. Authors/Task Force M, Sarris GE, Balmer C, Bonou P, Comas JV, da Cruz E, Di Chiara L, Di Donato RM, Fragata J, Jokinen TE, et al. Clinical guidelines for the management of patients with transposition of the great arteries with intact ventricular septum. *Cardiol Young*. 2017;27(3):530-69.

## Supplementary material

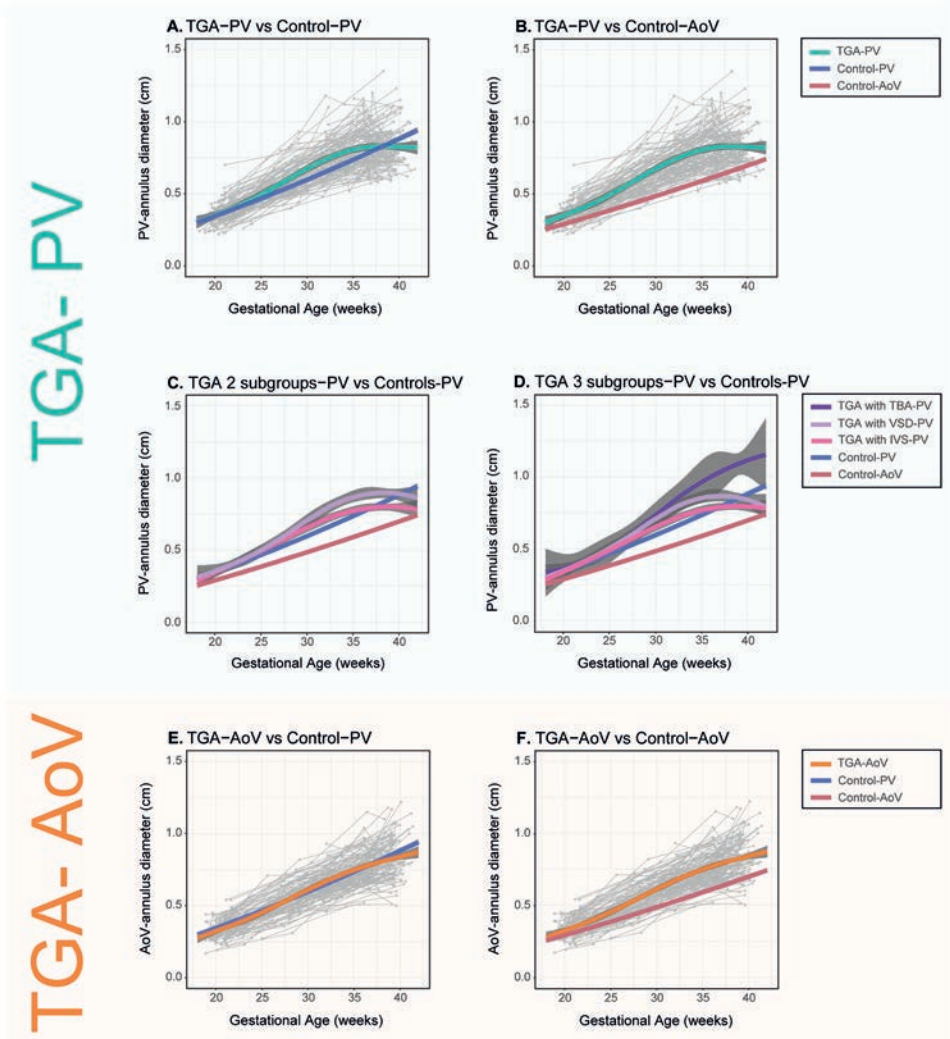


**Figure S1.** Average trends in semilunar valve diameters in TGA fetuses versus controls (Schneider et al.). Average trends in PV annular diameters in TGA fetuses (TGA-PV): (A) versus trends in controls PV annular diameter (Control-PV); (B) versus AoV annular diameter (Control-AoV); (C) TGA with an IVS (TGA with IVS-PV) and a VSD (TGA with VSD-PV); and (D) with the TGA-VSD fetuses further stratified on the basis of a TBA or non-TBA anatomy (TGA with TBA-PV). Average trend in AoV annular diameters in TGA fetuses (TGA-AoV): (E) versus trends in controls of PV annular diameter (Control-PV); and (F) AoV annular diameter (Control-AoV). Trends in PV and AoV annular diameters in controls are shown (Control-PV and Control-AoV). Grey dots are individual measurements, and grey lines are individual trends. The 95% confidence intervals for both the fitted model and the control line as described by Schneider et al.<sup>22</sup> are shown in blue (pulmonary valve) and red (aortic valve). Note that the 95% confidence intervals for the controls are smaller than the thickness of the line. AoV, aortic valve; IVS, intact interventricular septum; PV, pulmonary valve; TBA, Taussig-Bing anomaly; TGA, transposition of the great arteries; VSD, ventricular septal defect.



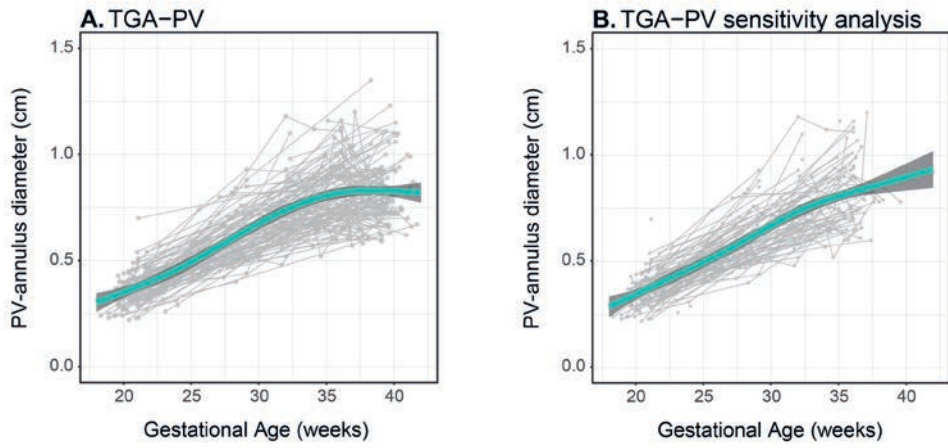


**Figure S2.** Sensitivity analysis.

Average trend in PV annular diameters in TGA fetuses (A) including first postnatal measurements and (B) including fetal measurements only. Grey dots are individual measurements and grey lines are individual trends. The 95% confidence intervals for both of the fitted models are shown in dark grey. PV, pulmonary valve; TGA, transposition of the great arteries.

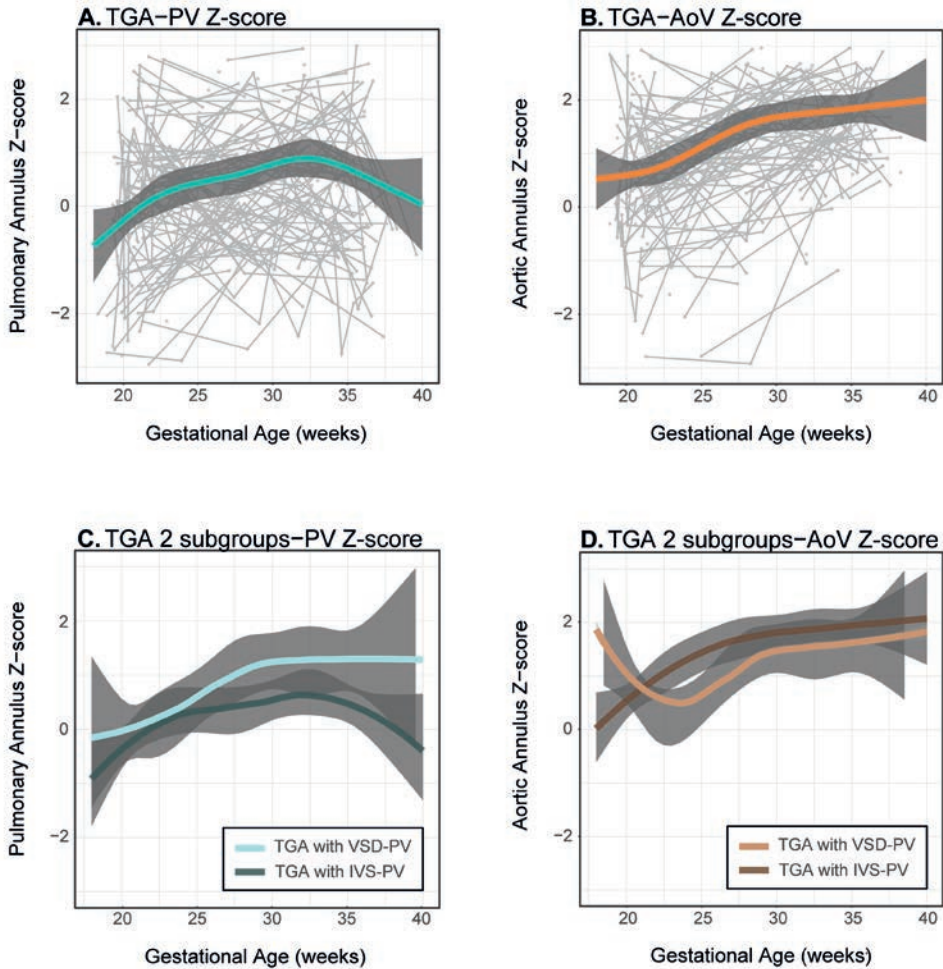


**Figure S3.** Average trend in semilunar valve Z-scores in TGA fetuses (based on Schneider et al.). Average trend in TGA fetal (A) PV annular diameter Z-score (TGA-PV Z-score) and (B) AoV annular diameter Z-score (TGA-AoV Z-score). Fetal Z-scores based on data from Schneider et al.<sup>22</sup> Grey dots are individual measurements and grey lines are individual trends. Both trends were stratified based on the presence (TGA with VSD) or absence (TGA with IVS) of a VSD (C and D). AoV, aortic valve; IVS, intact interventricular septum; PV, pulmonary valve; TGA, transposition of the great arteries; VSD, ventricular septal defect.

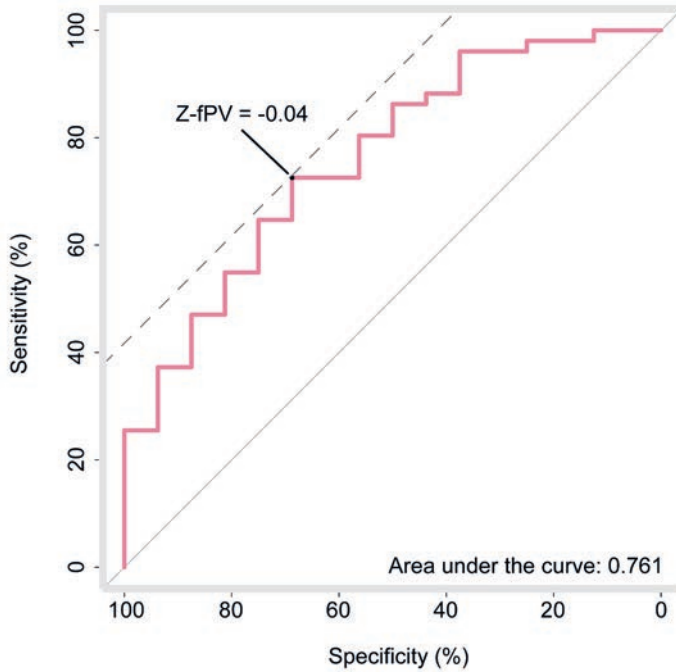
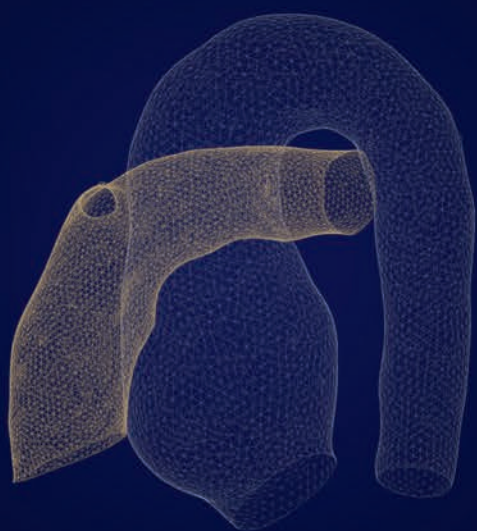


**Figure S4.** ROC for the prediction of neo-aortic root dilatation post-ASO at the last follow-up visit postnatally based on the PV-annular Z-score at 26-30 weeks gestation. Fetal Z-scores based on Vigneswaran et al.<sup>21</sup> Z-fPV, Z-score of the fetal pulmonary valve annular diameter.





## **CHAPTER 4**

# Progression of aortic root dilatation and aortic valve regurgitation after the arterial switch operation

Heart 2019;105:1732-40

Roel L.F. van der Palen  
Teun van der Bom  
Annika Dekker  
Roula Tsonaka  
Nan van Geloven  
Irene M. Kuipers  
Thelma C. Konings  
Lukas A.J. Rammeloo  
Arend D.J. ten Harkel  
Monique R.M. Jongbloed  
David R. Koolbergen  
Barbara J.M. Mulder  
Mark G. Hazekamp  
Nico A. Blom

## Abstract

### Objective

To study neo-aortic growth and the evolution of neo-aortic valve regurgitation (AR) in patients with transposition of the great arteries (TGA) after arterial switch operation (ASO) from newborn to adulthood and to identify patients at risk.

### Methods

Neo-aortic dimensions (annulus/root/sinotubular junction) and neo-aortic valve regurgitation were assessed serially in 345 TGA patients that underwent ASO between 1977-2015. Linear mixed-effect models were used to assess increase of neo-aortic dimensions over time and to identify risk factors for dilatation. Risk factor analysis for AR by using time-dependent Cox regression models.

### Results

After a rapid increase in the first year after ASO and proportional growth in childhood, neo-aortic dimensions continue to increase in adulthood without stabilization. Annual diameter increase in adulthood was  $0.39 \pm 0.06$ ,  $0.63 \pm 0.09$  and  $0.54 \pm 0.11$  mm for respectively neo-aortic annulus, root and sinotubular junction, all significantly exceeding normal growth. AR continues to develop over time: freedom from AR  $\geq$ moderate during the first 25 years post-ASO was 69%. Risk factors for root dilatation were complex TGA anatomy (TGA-VSD, double outlet right ventricle with subpulmonary ventricular septal defect (DORV-SP-VSD)) and male gender. Risk factors for AR  $\geq$ moderate were: complex TGA anatomy and neo-aortic growth. Per mm increase in aortic root dimension there was a 9% increase in the hazard of AR  $\geq$ moderate. Bicuspid pulmonary valve did not relate to the presence of root dilatation or AR.

### Conclusion

After ASO, neo-aortic dilatation proceeds beyond childhood and is associated with an increase in AR incidence over time. Careful follow-up of the neo-aortic valve and root function is mandatory, especially in males and in patients with complex TGA anatomy.

## Introduction

The arterial switch operation (ASO) has been a significant milestone in the evolution of surgery for transposition of the great arteries (TGA) and after its introduction in 1975<sup>1</sup> has gradually replaced the atrial switch procedure worldwide. Despite excellent late survival with good functional ability, residual problems are increasingly recognized during long-term follow-up and include dilatation of the neo-aortic root and neo-aortic valve regurgitation (AR) that may result in neo-aortic root replacement.<sup>2-4</sup> It has been reported that the neo-aortic root dilates in more than two-thirds of patients after ASO.<sup>5, 6</sup> However, data on progression of neo-aortic dilatation in adulthood are scarce and controversial.<sup>4, 7</sup> Similar to root dilatation, concerns have risen about the neo-aortic valve function over time and AR has been described as an important cause for reoperation.<sup>8</sup> The purpose of this study was to assess neo-aortic growth, neo-aortic valve function and the need for reoperations on neo-aortic valve and/or root during long-term follow-up for the various morphological subtypes of TGA after ASO and, finally, to identify risk factors for root dilatation and neo-aortic valve regurgitation.

## Methods

### Study population

All patients who underwent ASO for TGA with intact ventricular septum (TGA-IVS), TGA with ventricular septal defect (TGA-VSD) or double outlet right ventricle with subpulmonary ventricular septal defect (DORV-SP-VSD) at the Center for Congenital Heart Disease Amsterdam-Leiden, The Netherlands, between 1977 and 2015 with two or more echocardiographic follow-up examinations were included in the study. Hospital and outpatient records were reviewed to obtain information on demographics, anthropometrics, morphologic and surgical details, aortic re-interventions and mortality. The local Committee for Medical Ethics of the academic centers approved the study and waived the need for informed consent.

### Echocardiographic measurements

Retrospective measurements were performed on images derived from transthoracic echocardiograms by two observers. Echocardiographic images were analysed from videocassette tapes (before 2006) and from digital recordings (after 2006) using an offline workstation (EchoPac v11.1.8., GE Vingmed Ultrasound AS, Norway). Available and good quality images were assessed at the following intervals after ASO: 3, 6, 9 and 12 months, at 2, 3 and 5 years and thereafter with 5-year intervals up to the last available follow-up recordings. End of follow-up was defined as the date of the last available echocardiogram or the last echocardiogram before root and/or aortic valve reoperation. Neo-aortic diameters were measured from two-dimensional mid-systolic parasternal long-axis views at three



levels: 1. neo-aortic valve annulus, from hinge-point to hinge-point; 2. neo-aortic root, at mid-sinus level from internal edge to internal edge; 3. neo-aortic sinotubular junction (STJ), from internal edge to internal edge (Figure 1). To account for the range in body size for neo-aortic measurements during childhood (0-18 years), Z-scores were calculated for each patient by using pediatric reference values and BSA (DuBois method).<sup>9</sup> Dilatation was defined as Z-score  $\geq 2.0$ .

Neo-aortic regurgitation (AR) severity was assessed semi-quantitatively by one pediatric cardiologist based on the width of the color Doppler regurgitation jet at the level of neo-aortic valve on the parasternal long-axis view.<sup>10</sup> The regurgitation jet width was graded as follows: 0-1 mm (none-trivial), 1-4 mm (mild), 5-6 mm (moderate), >6 mm (severe). Additionally, left ventricular end-diastolic diameter as well as the presence of diastolic flow reversal in the proximal descending aorta was verified to distinguish moderate from severe AR. This method is used in clinical practice and has been described and applied in previous echocardiographic studies on follow-up of AR.<sup>11-13</sup>

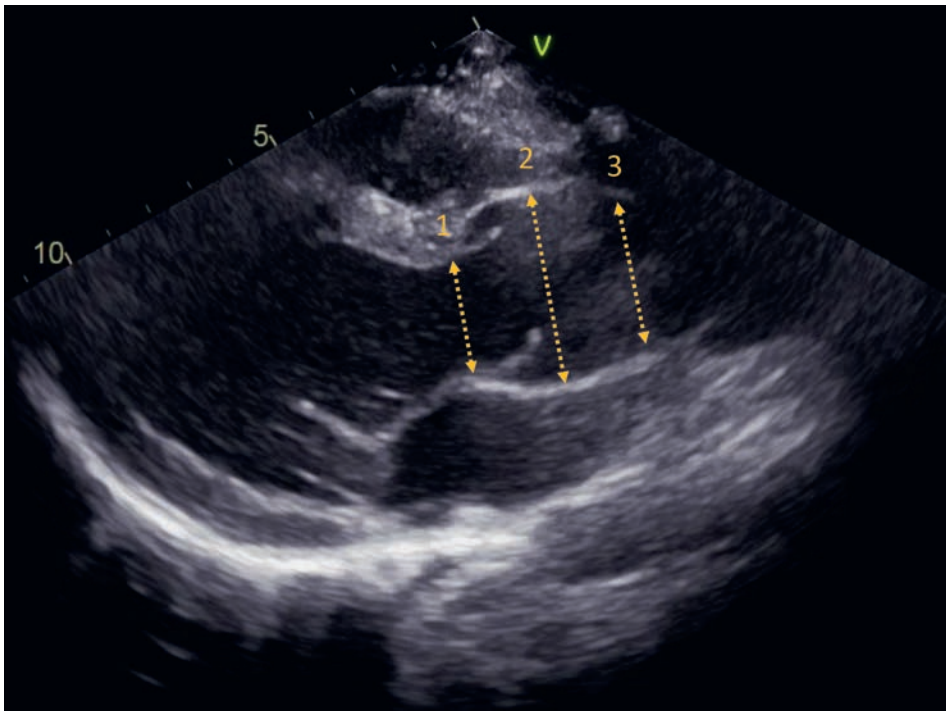


**Figure 1.** Measurement of neo-aortic dimensions from parasternal long-axis view. Dimensions: 1 = neo-aortic valve annulus, 2 = neo-aortic root and 3 = sinotubular junction.

### Statistical analysis

Statistical analysis was performed using IBM SPSS Statistics 23.0 and R versions 3.4.0/3.4.2. Clinical characteristics were presented as number (%) for categorical variables, mean  $\pm$  standard deviation for continuous variables or as median (range) where appropriate. To analyse the progression of neo-aortic dimensions at three neo-aortic levels over time, linear mixed-effects models were used. To adequately capture non-linear progression over time and the between subject variability, natural cubic splines both in the fixed and random-effects term with 3 knots located at the sample quantiles were used. Potential risk factors known from literature for neo-aortic dilatation were incorporated in the models for the different neo-aortic levels (see details on risk factor inclusion in supplementary material). The likelihood ratio test including Bonferroni correction was used to test for differences in mean neo-aortic profiles over time between TGA subtypes.

Kaplan-Meier analysis was performed to assess the probability of freedom from AR  $\geq$ mild and AR  $\geq$ moderate. The log-rank test was used to test for differences of event-free survival curves among morphological TGA subtypes. To assess the independent predictive value of different covariates (from Table 1) on the occurrence of AR, Cox regression models were used. A time-dependent Cox model was used to evaluate the effect of the changing aortic dimensions over time on risk of AR (see details on inclusion of variables in Supplementary section 1). All *P* values were 2 sided with a significance threshold  $<0.05$ .

## Results

During the study period, 452 patients underwent ASO. Fifty-two patients (11.5%) died during follow-up. Mortality in the first postoperative month was 9.3% (42 patients) and late deaths ( $>30$  days post-ASO) occurred in 10 patients. Early-mortality was highest from 1977-1987 after start of the ASO program and early-mortality incidence decreased to 3.3% between 1995 and 2015. Fifty overseas patients were lost to follow-up directly post-surgery and in five patients echocardiographic examinations were either lacking ( $n = 3$ ) or of poor image quality ( $n = 2$ ), leaving 345 patients for the analysis. Baseline patient characteristics are shown in Table 1. The morphological TGA subtypes were: TGA-IVS in 230 (66.7%) patients, TGA-VSD in 89 (25.8%) patients and DORV-SP-VSD in 26 (7.5%) patients. Baseline characteristics did not significantly differ between the study population and patients lost to follow-up or those who did not survive. Median number of repeated neo-aortic measurements and AR grading was 4 (range 2-9) per patient.

### Neo-aortic growth from neonate to adult

Averaged time-related evolution of the neo-aortic dimensions for all TGA patients are depicted in Figure 2A-C. The neo-aortic annulus, neo-aortic root and the STJ all showed similar growth patterns: a rapid increase in the first year after ASO, followed by a nearly linear increase of neo-aortic dimensions in childhood with an ongoing increased growth

**Table 1.** Demographics and pre-operative anatomy

	Study cohort (n = 345), no. (%)
Male	228 (66.1)
Age at 1 <sup>st</sup> assessment, median (range)	1.9 (0.04-31.5) years
Age at last follow-up, median (range)	12.2 (1.0-39.0) years
<b>Morphological TGA subtype</b>	
TGA-IVS	230 (66.7)
TGA-VSD	89 (25.8)
DORV-SP-VSD	26 (7.5)
<b>Coexisting findings</b>	
Arch abnormality	24 (7.0)
Bicuspid pulmonary valve	21 (6.1)
Left ventricular OTO	12 (3.5)
<b>Coronary anatomy<sup>a</sup></b>	
Usual (1LCx-2R, 1L-2CxR)	275 (79.7)
Other	60 (17.4)
Intramural course of LAD	4 (1.2)
Unknown	6 (1.7)
<b>Pre-operative procedures</b>	
Balloon atrial septostomy	182 (52.8)
Previous PAB	18 (5.2)
<b>Arterial switch operation</b>	
One-stage	319 (92.5)
Median age (range)	8 days (0 days-0.6 years)
Two stage	26 (7.5)
Median age (range)	143 days (36 days-5.1 years)
<b>Coronary artery transfer technique</b>	
Double button	197 (57.1)
Single trapdoor, single button	96 (27.9)
Double trapdoor	31 (9.0)
Aortic sinus pouch technique	4 (1.2)
Unknown	17 (4.9)
<b>Lecompte maneuver</b>	320 (92.8)

<sup>a</sup> Coronary anatomy description according to the Leiden Convention coronary coding system. Cx, circumflex artery; DORV-SP-VSD, double outlet right ventricle with subpulmonary ventricular septal defect; IVS, intact ventricular septum; L or LAD, left anterior descending coronary artery; OTO, outflow tract obstruction; PAB, pulmonary artery banding; R, right coronary artery; TGA, transposition of the great arteries; VSD, ventricular septal defect.

rate in adulthood. The average diameter progression in adulthood (18-30 years post-ASO) for all TGA patients was 0.39 mm/year for the neo-aortic annulus (95% CI: 0.33-0.46 mm/year), 0.63 mm/year for the neo-aortic root (95% CI: 0.54-0.71 mm/year), and 0.54 mm/year for the STJ (95% CI: 0.43-0.65 mm/year).

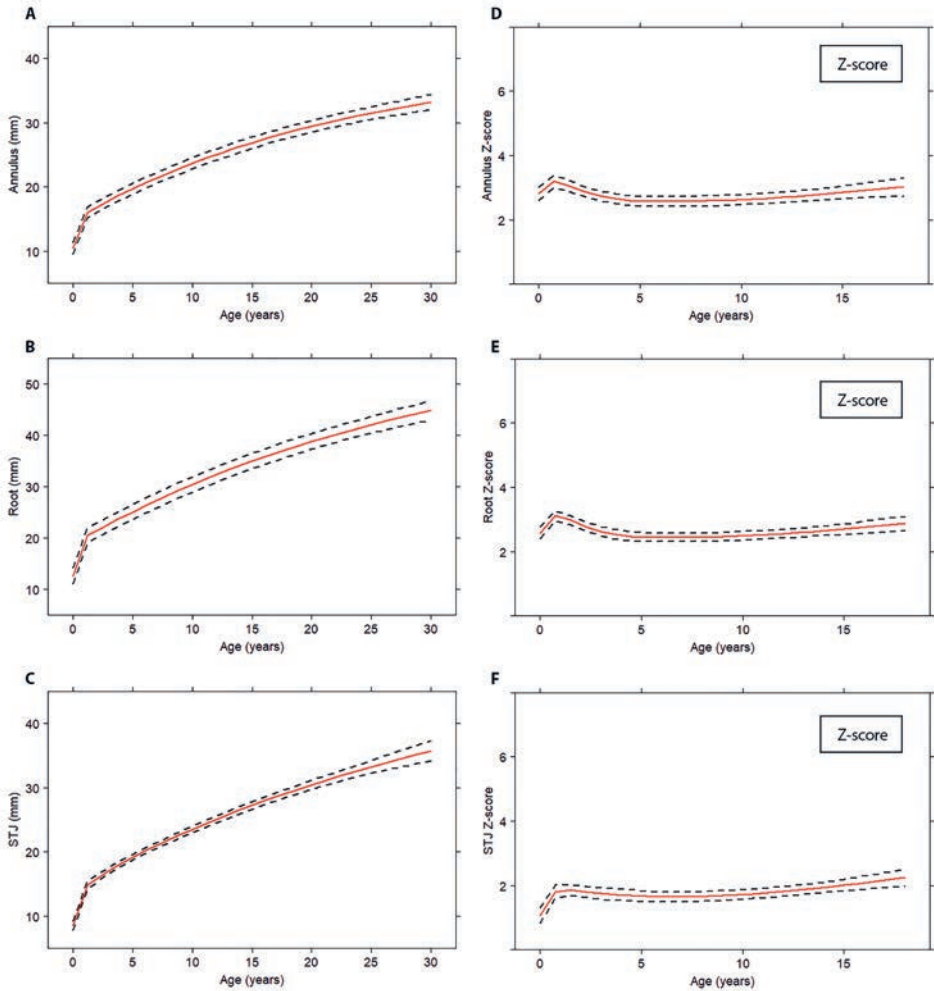


**Figure 2.** Mean progression of neo-aortic dimensions over time for all patients with TGA. Absolute neo-aortic diameters (A-C); neo-aortic Z-scores (D-F). Mean profiles are plotted with the described risk factors set to the reference level; dashed lines represent 95% confidence interval. Annulus, neo-aortic valve annulus; Root, neo-aortic root; STJ, sinotubular junction; TGA, transposition of the great arteries.

For the childhood period, neo-aortic diameters were indexed to body size and depicted as Z-scores (Figure 2D-F). A rapid increase in neo-aortic Z-scores was observed for all neo-aortic dimensions in the first year after ASO (average Z-score >2.5 for neo-aortic annulus and neo-aortic root and average Z-score of 2.0 for STJ), followed by stabilization at these high Z-score levels during childhood. From 2-18 years, no Z-score increase was observed for neo-aortic annulus ( $P = 0.53$ ) and neo-aortic root ( $P = 0.79$ ). The Z-score for STJ slightly increased within this period ( $P = 0.005$ ), between 15-18 years post-ASO (Figure 2D-F).

### Neo-aortic progression between TGA subtypes

Figure 3A-C depicts the time-related evolution of the neo-aortic dimensions at three aortic levels for the different TGA subtypes (CI in supplementary Figure S1A-C). The mean profiles for neo-aortic annulus and neo-aortic root diameters showed significant differences between the three TGA subtypes ( $P = 3.7 \times 10^{-4}$  and  $P = 7.6 \times 10^{-6}$  respectively). No difference in mean profiles between TGA subgroups for STJ was found ( $P = 0.37$ ).

Mean increase of the neo-aortic dimensions beyond childhood for the TGA subtypes is depicted in supplementary Table S1. The growth rate slightly decreases after 18 years post-ASO but remained high for the different neo-aortic dimensions in all subtypes. The smallest neo-aortic diameter increase was observed in the TGA-IVS patients and the largest increase in the DORV-SP-VSD patients.

### Risk factors for neo-aortic dilatation

Morphological TGA subtype and gender were independent risk factors for root dilatation (Figure 3A-F). Male TGA patients tend to have larger neo-aortic roots compared to female TGA patients (Annulus  $P = 3.0 \times 10^{-6}$ ; Root  $P = 8.5 \times 10^{-6}$ ; STJ  $P = 0.008$ ), of which the effect starts 13 years after ASO (Figure 3D-F; CI in supplementary Figure S1D-F). Explorative risk factor analysis showed that none of the other anatomical and surgical variables from Table 1 were associated with progression of neo-aortic root dimensions (supplementary Table S2).

### Neo-aortic valve regurgitation

Neo-aortic valve regurgitation was assessed serially. At last follow-up or just before reoperation for neo-aortic root pathology, thirty-three of the 345 TGA patients (9.6%) had at least moderate AR (AR  $\geq$  moderate). Moderate or more AR was present in 7.4% ( $n = 17$ ) of the TGA-IVS, in 11.2% ( $n = 10$ ) of the TGA-VSD and in 23.1% ( $n = 6$ ) of the DORV-SP-VSD patients. Mild or more AR was present in 28.2% ( $n = 65$ ) of the TGA-IVS, in 36.0% ( $n = 32$ ) of TGA-VSD and in 53.8% ( $n = 14$ ) of the DORV-SP-VSD patients. The Kaplan-Meier curves for AR  $\geq$  mild and AR  $\geq$  moderate are shown in Figure 4. The overall probability of freedom from AR  $\geq$  moderate was 96% at 5 years, which decreased to 95%, 88%, 78% and 69% at 10, 15, 20 and 25 years after ASO, respectively. The overall freedom from AR  $\geq$  mild was 79% at 5 years, which decreased to 64%, 50%, 39% and 33% at 10, 15, 20 and 25 years after ASO, respectively. Log-rank test showed significant differences between the TGA subtypes ( $P = 0.037$  and  $P = 0.013$  for AR  $\geq$  moderate and AR  $\geq$  mild respectively).

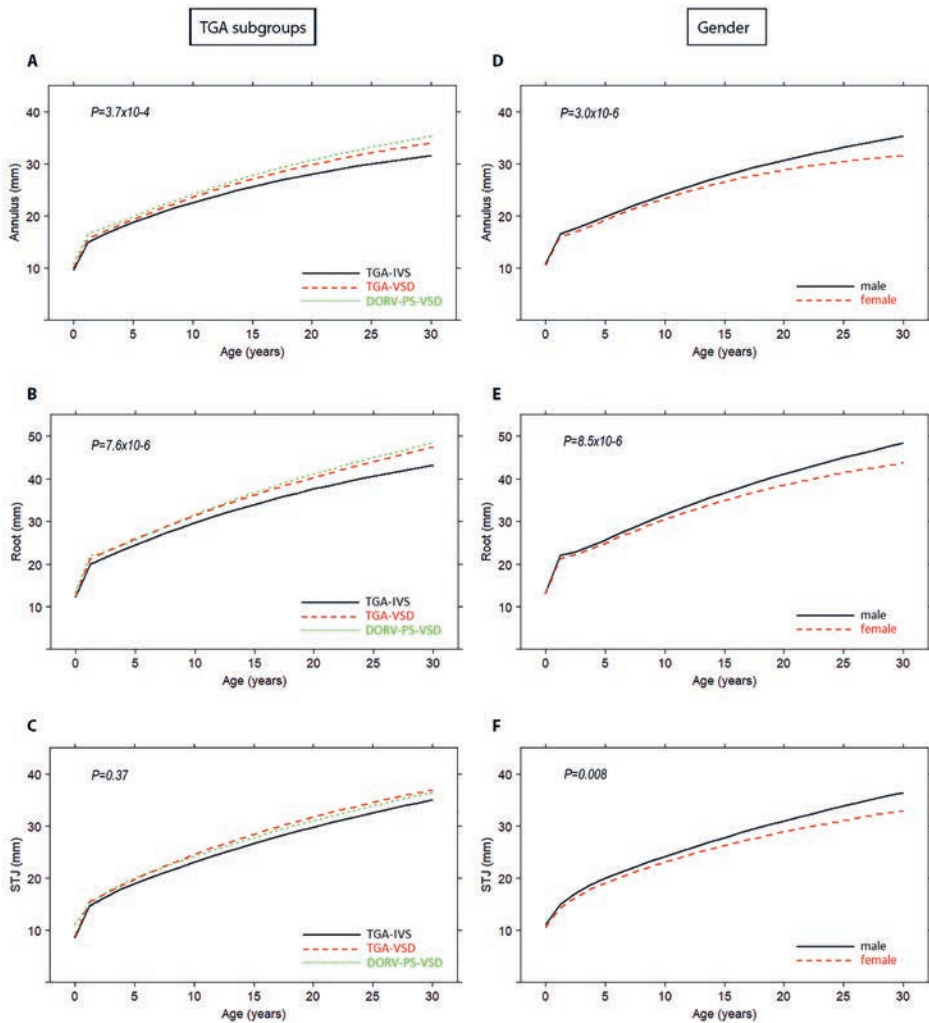


**Figure 3.** Mean progression of neo-aortic dimensions over time for different TGA subtypes (A-C) and gender (D-F).

Mean profiles are plotted with the described risk factors set to the reference level. For confidence intervals (supplementary Figure S1). Annulus, neo-aortic valve annulus; DORV-SP-VSD, double outlet right ventricle with subpulmonary ventricular septal defect; IVS, intact ventricular septum; Root, neo-aortic root; STJ, sinotubular junction; TGA, transposition of the great arteries; VSD, ventricular septal defect.

Results from Cox regression and time-dependent Cox regression analysis for the development of AR are depicted in Table 2. TGA morphological subtype was a univariable risk factor for the occurrence of both AR  $\geq$ mild and AR  $\geq$ moderate ( $P = 0.009$  and  $P = 0.02$  respectively). Furthermore, late ASO (ASO  $\geq 6$  months of age) was significantly associated with the occurrence of AR  $\geq$ mild. Aortic diameter increase over time (for neo-aortic annulus

and root) were risk factors for development of AR  $\geq$  moderate in the univariable time-dependent Cox analysis. Multivariable models for the diameters showed a 9% (95% CI 1-17%) increase in the hazard of AR  $\geq$  moderate per mm increase in aortic root diameter dimension (Table 2).

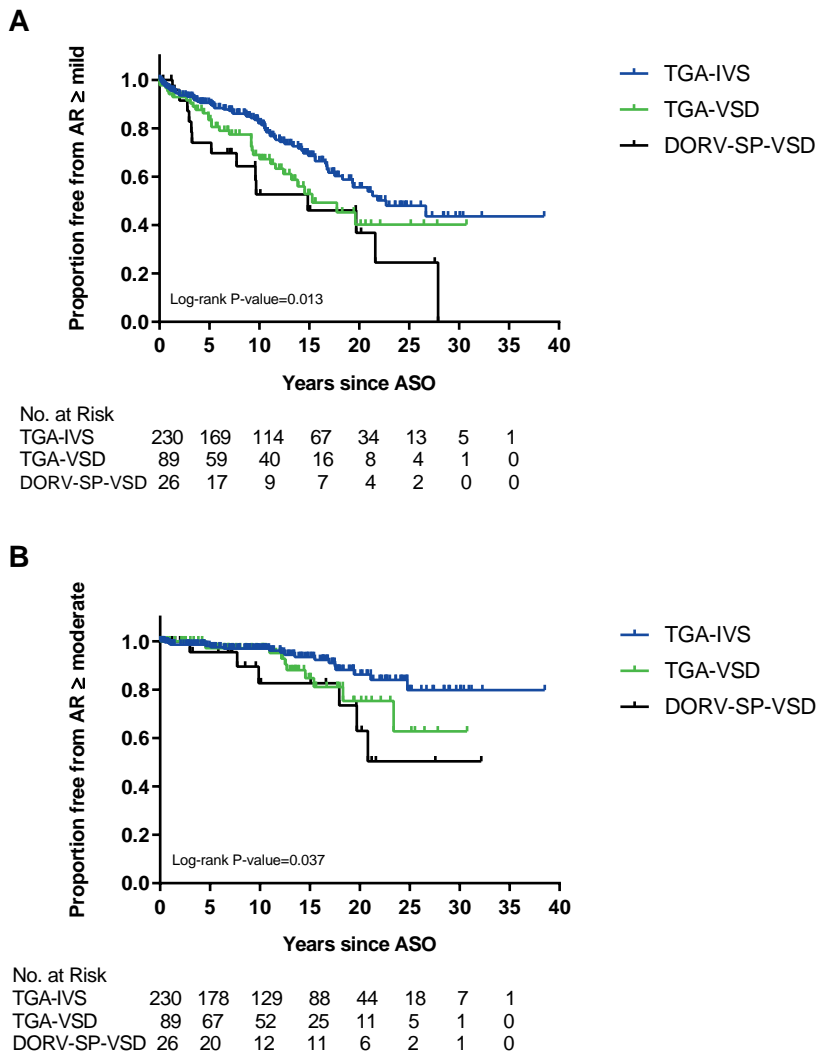


**Figure 4.** Freedom from at least mild (A) and at least moderate (B) neo-aortic valve regurgitation after ASO. AR, neo-aortic valve regurgitation; ASO, arterial switch operation; DORV-SP-VSD, double outlet right ventricle with subpulmonary ventricular septal defect; IVS, intact ventricular septum; TGA, transposition of the great arteries; VSD, ventricular septal defect.

**Table 2.** Cox model (univariable model) and time-dependent Cox model for the risk on neo-aortic valve regurgitation

Risk factors	AR $\geq$ moderate (n = 33)			AR $\geq$ mild (n = 111)		
	Events/total	Hazard ratio (95% CI)	P value	Events/total	Hazard ratio (95% CI)	P value
<b>Morphological subtype</b>						
TGA-IVS <sup>a</sup>	17/230	ref (1)	0.02	65/230	ref (1)	0.009
TGA-VSD	10/89	2.01 (0.92 – 4.38)	0.08	32/89	1.71 (1.08 – 2.71)	0.02
DORV-SP-VSD	6/26	3.55 (1.38 – 9.15)	0.01	14/26	2.28 (1.21 – 4.28)	0.01
<b>Gender</b>						
Male <sup>b</sup>	26/228	ref (1)		72/228	ref (1)	
Female	7/117	0.49 (0.21 – 1.17)	0.11	39/117	1.03 (0.67 – 1.58)	0.89
<b>Pulmonary valve</b>						
Tricuspid <sup>c</sup>	31/324	ref (1)		105/324	ref (1)	
Bicuspid	2/21	1.16 (0.25 – 5.48)	0.85	5/21	0.89 (0.34 – 2.30)	0.49
<b>Left ventricular OTO</b>						
No <sup>d</sup>	33/333	ref (1)		106/333	ref (1)	
Yes	0/12	N/A	N/A	5/12	1.25 (0.48 – 3.25)	0.65
<b>Previous PAB</b>						
No <sup>e</sup>	31/327	ref (1)		103/327	ref (1)	
Yes	2/18	2.02 (0.48 – 8.46)	0.34	8/18	1.94 (0.87 – 4.33)	0.11
<b>Age ASO <math>\geq</math> 6 months</b>						
No <sup>f</sup>	32/333	ref (1)		104/333	ref (1)	
Yes	1/12	0.83 (0.09 – 7.55)	0.87	7/12	2.97 (1.10 – 8.04)	0.03



Table 2. Continued

<i>Time-dependent Cox model</i>		AR $\geq$ moderate		AR $\geq$ mild	
Diameter increase	UV/MV	Hazard ratio (95% CI)	P value	Hazard ratio (95% CI)	P value
Annulus (per mm)	UV	1.14 (1.04 – 1.25)	0.004	1.04 (0.98 – 1.10)	0.16
	MV	1.09 (0.99 – 1.21)*	0.09	1.03 (0.97 – 1.09)**	0.31
Root (per mm)	UV	1.12 (1.05 – 1.21)	0.001	1.04 (1.00 – 1.10)	0.07
	MV	1.09 (1.01 – 1.17)*	0.04	1.04 (0.99 – 1.09)**	0.10
STJ (per mm)	UV	1.06 (0.94 – 1.18)	0.35	0.99 (0.93 – 1.06)	0.88
	MV	1.04 (0.93 – 1.15)*	0.52	0.99 (0.93 – 1.06)**	0.84

Reference categories of covariate: <sup>a</sup> Morphological subtype TGA-IVS, <sup>b</sup> Male sex, <sup>c</sup> Tricuspid pulmonary valve, <sup>d</sup> No left ventricular outflow tract obstruction. <sup>e</sup> No previous PAB, <sup>f</sup> Age ASO <6 months.

\* Multivariable analysis adjusted for morphological subtype and gender.

\*\* Multivariable analysis adjusted for morphological subtype, gender, pulmonary valve, previous pulmonary artery banding and age ASO  $\geq$  6 months of age. Annulus, neo-aortic valve annulus; AR, neo-aortic valve regurgitation; ASO, arterial switch operation; CI, confidence interval; DORV-SP-VSD, double outlet right ventricle with subpulmonary ventricular septal defect; HR, Hazard Ratio; IVS, intact ventricular septum; MV, multivariable analysis; N/A, not applicable; OTO, outflow tract obstruction; PAB, pulmonary artery banding; Root, neo-aortic root; STJ, sinotubular junction; TGA, transposition of the great arteries; UV, univariable analysis; VSD, ventricular septal defect.

**Table 3.** Aortic dimensions and patient characteristics for aortic reoperation

Pt	Arterial switch operation				Aortic reoperation				Aortic dimensions		
	Diagnosis	Gender	PVm	One-stage	Age (days)	Lecompte	Age (years)	Procedure	Main indication	Annulus (mm) (Z-score)*	Root (mm) (Z-score)*
1.	TGA-IVS	M	T	Y	2	Y	7.9	AVR + PApI	Root dilatation + AR	26.0 (5.40)	35.8 (5.06)
2.	TGA-VSD	M	T	Y	101	Y	16.0	AVR	Root dilatation + AR	31.7 (4.46)	40.2 (3.38)
3.	TGA-IVS	M	T	Y	3	Y	8.0	Switchback	Root dilatation + AR	22.1 (4.06)	29.4 (3.52)
4.	TGA-VSD	M	T	N (Blalock)	403	Y	29.0	SCT + MVP	Root dilatation + MR	25.2 (N/A)	42.3 (N/A)
5.	TGA-IVS	M	T	Y	7	Y	24.0	Bentall	Root dilatation + AR	32.7 (N/A)	47.2 (N/A)
6.	TGA-VSD	M	T	Y	6	N	20.0	Bentall	Root dilatation	31.9 (N/A)	53.6 (N/A)
7.	TGA-VSD	M	T	Y	95	Y	13.9	Bentall + Asc	Root dilatation + AR	28.5 (4.87)	49.4 (6.63)
8.	DORV-SP-VSD	M	T	Y	210	Y	21.8	Bentall + VSDc	Root dilatation	27.4 (N/A)	47.7 (N/A)
9.	DORV-SP-VSD	M	T	N (PAB+CoAR)	607	N	14.0	Bentall + PVR	Root dilatation + RVOTO	24.1 (3.34)	45.1 (5.93)
10.	TGA-VSD	F	T	Y	115	Y	18.9	Bentall + MVP	Root dilatation + AR + MR	31.9 (N/A)	48.0 (N/A)

\* Z-scores available for patients <18 years.

AR, neo-aortic valve regurgitation; Asc, ascending aorta replacement; AVR, aortic valve replacement; Blalock, Blalock shunt; CoAR, repair of aortic coarctation; DORV-SP-VSD, double outlet right ventricle with subpulmonary ventricular septal defect; F, female; IVS, intact ventricular septum; M, male; MVP, mitral valve plasty; N, no; N/A, not applicable; PAB, pulmonary artery banding; PApI, pulmonary artery plasty for supravalvular pulmonary stenosis; Pt, patients; PVm, pulmonary valve morphology; PVR, neo-pulmonary valve replacement; RVOTO, right ventricular outflow tract obstruction; SCT, supracoronary tube; TGA, transposition of the great arteries; T, tricuspid; VSD, ventricular septal defect; VSDc, closure residual ventricular septal defect; Y, yes.

### **Neo-aortic reoperation**

Ten patients (2.9%) from the study cohort underwent reoperation on the neo-aortic valve and/or root (Table 3). Median age at reoperation was 17.4 (range 7.9-29.0) years. Original diagnoses were TGA-IVS in 3 (1.3%), TGA-VSD in 5 (5.6%) and DORV-SP-VSD in 2 patients (7.7%). Primary indications for neo-aortic reoperations were root dilatation ( $n = 4$ ) or root dilatation with AR ( $n = 6$ ). Surgical procedures performed were: Bentall operation ( $n = 6$ ), neo-aortic valve replacement ( $n = 2$ ), supracoronary tubular prosthesis for repair of root/STJ ( $n = 1$ ) and switch back operation ( $n = 1$ ). Additional details on neo-aortic diameters, patient and surgical characteristics are depicted in Table 3.

## **Discussion**

This is the first study that investigated long-term neo-aortic growth and neo-aortic valve function in TGA patients by analysing serial measurements using a linear mixed model approach from birth up to 39 years post-ASO. This study demonstrates that neo-aortic root dilatation is progressive and does not stabilize in adulthood and that AR progresses over time. Dilatation did not only involve the neo-aortic root but also the neo-aortic valve annulus and STJ. Morphological TGA subtype (TGA-VSD and DORV-SP-VSD) and male gender were found to be independent risk factors for aortic root dilatation. Furthermore, the progression of root dilatation was a critical factor for impairment of neo-aortic valve function: per mm increase in aortic root dimension over time there is an average 9% increase in the hazard of AR  $\geq$  moderate.

### **Neo-aortic root dilatation**

Discussion about the neo-aortic growth pattern after ASO in childhood is still ongoing. In the present study we show that a disproportional increase of neo-aortic sizes occurs in the first year after ASO, followed by a neo-aortic growth rate comparable to normal somatic growth from 2 till 18 years of age albeit at a higher Z-score level. Similar findings were reported by smaller mid-term follow-up studies.<sup>14, 15</sup> In contrast, other studies reported ongoing disproportional neo-aortic root growth during the entire childhood period<sup>13</sup> or disproportionate growth till the age of 10 years followed by stabilization until 18 years of age.<sup>16</sup> This study extends the current knowledge on aortic growth patterns by its unique serial evaluation of neo-aorta dimensions in these patients from birth till adulthood. A major finding of this study and a concern for the future is the ongoing growth of the neo-aortic root beyond childhood, after somatic growth stops. Our findings are in agreement with those of a cardiac MRI study using longitudinal data from two consecutive MRI examinations in patients between 0-29 years post-ASO.<sup>17</sup>

The rate of progression of the aortic root in healthy adult individuals is estimated 0.08 mm/year<sup>18</sup> whereas in TGA patients the growth rate, depending on its exact morphological subtype, is on average 0.63 mm/year as shown by this study. This growth rate is similar to

the yearly aortic root growth rate in patients with other diseases associated with aortopathy: for Marfan disease average aortic root growth is reported 0.41 up to  $0.49 \pm 0.5$  mm/year before the era of preventive beta-blocker and losartan therapies,<sup>19,20</sup> in bicuspid aortic valve related aortopathy  $0.42 \pm 0.6$  up to 0.5 mm/year for the ascending aorta<sup>20</sup> and after Ross operation in adulthood 0.43 mm/year for the neo-aortic root.<sup>21</sup> The annual growth of the neo-aortic annulus and STJ in adult patients after Ross operation is estimated between 0.33-0.40 mm and 0.49-0.51 mm respectively.<sup>21,22</sup> Likewise, after Ross operation there is also an initial rapid increase in neo-aortic root dimension followed by a slower ongoing progression.

In this study, we demonstrated complex TGA anatomy (TGA-VSD and DORV-SP-VSD) and male gender to be independent risk factors for neo-aortic root dilatation. Complex TGA anatomy is more often reported as risk factor in smaller studies with shorter follow-up duration.<sup>5,14,15,23</sup> Other reported risk factors could not be found in this study, including pulmonary artery banding (PAB) prior to ASO<sup>5,16,23</sup> and presence of an aortic arch anomaly.<sup>15</sup> Remarkably, male gender appeared to be an independent risk factor for larger neo-aortic root growth after ASO. The onset of the differences in aortic diameters between TGA males and females coincides with the age of puberty onset which suggests a possible relation with hormonal changes. Although male gender is known to be related with larger aortic diameters from population studies on aortic sizes in healthy adults,<sup>18,24</sup> this association has only been reported in one cross-sectional study in complex TGA patients after ASO.<sup>8</sup>

The etiology of ongoing root dilatation most likely has a multifactorial origin. From a post-mortem specimen study it is known that the arterial roots in unoperated TGA patients have a diminished amount and altered distribution of collagen and that the root and neo-aortic valve are less firmly embedded in the myocardium.<sup>25</sup> Furthermore, the neo-aortic root and pulmonary valve annulus already start larger in TGA patients immediately after birth (pre-ASO) compared to healthy infants.<sup>23</sup> This finding is more pronounced in TGA-VSD and DORV-SP-VSD patients as compared to TGA-IVS patients. The role of hemodynamic factors in aortic dilatation is unknown. Important geometric alterations in the ascending neo-aorta after ASO with Lecompte maneuver may have hemodynamic consequences which potentially impacts on the root diameter. Four-dimensional flow MR imaging in pediatric post-ASO patients has already shown abnormal systolic flow patterns in the ascending aorta in two-thirds of the TGA patients<sup>26</sup> but a causal relation still has to be demonstrated.

### **Neo-aortic valve regurgitation and reoperation**

The occurrence of AR becomes increasingly evident long-term after ASO. Several factors are reported to be associated with AR in literature. These include neo-aortic root dilatation (certain Z-scores:  $\geq 2.5$  or  $\geq 3.0$ ),<sup>11,14,16</sup> TGA subtype,<sup>5,11,14,16,27,28</sup> older age at ASO,<sup>16,27,29</sup> previous PAB<sup>16,27,28</sup> and left ventricular outflow tract obstruction.<sup>11,16,29</sup> In this study we could only confirm morphological TGA subtype and ASO  $\geq 6$  months as risk factors for the development of AR by univariable analysis. More importantly, this study is the first to show an increase in neo-aortic valve annulus and root diameter over time (i.e. annulus and root growth) as

independent risk factors for moderate or more AR. Every mm increase in neo-aortic root size significantly increases the hazard of at least moderate AR. These data suggest that in this group of patients an important underlying mechanism for AR is impaired leaflet coaptation due to progression of the neo-aortic root and valve-annulus dimensions. In addition, the anatomical pulmonary valve itself may be more at risk for valvar incompetence due to differences in histology and anchoring compared to a native aortic valve.<sup>25</sup> Nevertheless, bicuspid native pulmonary valve morphology was not associated with AR in this study which endorses that a pre-operative competent bicuspid valve itself is not a contraindication for ASO when it comes to long-term valve function.

To date, no cases have been reported with aortic rupture or dissection after ASO but in several re-operated patients the anterior wall of the aneurysmatic aorta was observed to be paper-thin and fragile.<sup>3,30</sup> Indications for reoperation for aortic root dilatation after ASO to prevent rupture, dissection or progressive aortic regurgitation are unclear. The threshold and timing for aortic root repair are mainly based on absolute diameters rather than indexed aortic diameters (Z-scores) and are adapted from guidelines for aortopathy due to bicuspid aortic valve or connective tissue disease. The current incidence of neo-aortic reoperations in this study and in a recent multicenter study is low.<sup>30</sup> However, in the present study already 47 patients (14%) developed a root diameter  $\geq 40$  mm, and moderate AR was present in 26% of them. One quarter of these patients have not even reached adulthood. The ongoing neo-aortic dilatation, AR progression and its mutual relationship beyond childhood as shown in this study may predict an increased number of root and valve reoperations in the future.

### **Limitations**

This is a retrospective study and is therefore subject to limitations inherent to the design. A complete series of measurements from birth to adulthood was not available in all patients, with an average of 4 measurements per patient. In general, in the oldest group of patients fewer images at young ages after ASO were available. Therefore, the aortic measurements at young age after ASO (<5 years) mainly consisted of data from patients operated in the last two decades. However, as long as those that were followed for a period can be seen as representative for the whole population of similar age, our linear mixed-effect models will provide an unbiased estimate of aortic diameter trends over time. Echocardiographic imaging systems have improved the last decades that might affect accuracy of the measurements. However, only good quality images were used for analysis. Finally, AR grading remains a semi-quantitative estimation and may therefore be subject to observer variability that needs to be taken into account.

## Conclusions

After ASO, neo-aortic root dilatation is progressive over time and does not stabilize in adulthood with male gender and complex TGA morphology as risk factors. The progressive root dilatation is a critical factor for the impairment of AR long-term after ASO. Based on this data, concerns exist for the neo-aortic root function and the expected increasing need for neo-aortic root and/or neo-aortic valve reoperations in this aging group of patients of which the firsts have now reached the age of 40 years.

## ACKNOWLEDGMENT

We thank Dan Dyar for his collaboration in providing Z-score equations.

## References

1. Jatene AD, Fontes VF, Paulista PP, de Souza LC, Neger F, Galantier M, Souza JE. Successful anatomic correction of transposition of the great vessels. A preliminary report. *Arq Bras Cardiol.* 1975;28(4):461-64.
2. Lalezari S, Bruggemans EF, Blom NA, Hazekamp MG. Thirty-year experience with the arterial switch operation. *Ann Thorac Surg.* 2011;92(3):973-9.
3. Koolbergen DR, Manshanden JS, Yazdanbakhsh AP, Bouma BJ, Blom NA, de Mol BA, Mulder BJ, Hazekamp MG. Reoperation for neo-aortic root pathology after the arterial switch operation. *Eur J Cardiothorac Surg.* 2014;46(3):474-9.
4. Kempny A, Wustmann K, Borgia F, Dimopoulos K, Uebing A, Li W, Chen SS, Piorkowski A, Radley-Smith R, Yacoub MH, et al. Outcome in adult patients after arterial switch operation for transposition of the great arteries. *Int J Cardiol.* 2013;167(6):2588-93.
5. McMahon CJ, Ravekes WJ, Smith EO, Denfield SW, Pignatelli RH, Altman CA, Ayres NA. Risk factors for neo-aortic root enlargement and aortic regurgitation following arterial switch operation. *Pediatr Cardiol.* 2004;25(4):329-35.
6. Vandekerckhove KD, Blom NA, Lalezari S, Koolbergen DR, Rijlaarsdam ME, Hazekamp MG. Long-term follow-up of arterial switch operation with an emphasis on function and dimensions of left ventricle and aorta. *Eur J Cardiothorac Surg.* 2009;35(4):582-7.
7. van der Bom T, van der Palen RL, Bouma BJ, van Veldhuisen SL, Vliegen HW, Konings TC, Zwinderman AH, Blom NA, Koolbergen DR, Hazekamp MG, et al. Persistent neo-aortic growth during adulthood in patients after an arterial switch operation. *Heart.* 2014;100(17):1360-5.
8. Baruteau AE, Vergnat M, Kalfa D, Delpey JG, Ly M, Capderou A, Lambert V, Belli E. Long-term outcomes of the arterial switch operation for transposition of the great arteries and ventricular septal defect and/or aortic arch obstruction. *Interact Cardiovasc Thorac Surg.* 2016;23(2):240-6.
9. Pettersen MD, Du W, Skeens ME, Humes RA. Regression equations for calculation of z scores of cardiac structures in a large cohort of healthy infants, children, and adolescents: an echocardiographic study. *J Am Soc Echocardiogr.* 2008;21(8):922-34.
10. Jenkins KJ, Hanley FL, Colan SD, Mayer JE, Jr., Castaneda AR, Wernovsky G. Function of the anatomic pulmonary valve in the systemic circulation. *Circulation.* 1991;84(5 Suppl):III173-9.
11. Co-Vu JG, Ginde S, Bartz PJ, Frommelt PC, Tweddell JS, Earing MG. Long-term outcomes of the neo-aorta after arterial switch operation for transposition of the great arteries. *Ann Thorac Surg.* 2013;95(5):1654-9.
12. Cohen MS, Marino BS, McElhinney DB, Robbers-Visser D, van der Woerd W, Gaynor JW, Spray TL, Wernovsky G. Neo-aortic root dilation and valve regurgitation up to 21 years after staged reconstruction for hypoplastic left heart syndrome. *J Am Coll Cardiol.* 2003;42(3):533-40.
13. Marino BS, Wernovsky G, McElhinney DB, Jawad A, Krebs DL, Mantel SF, van der Woerd WL, Robbers-Visser D, Novello R, Gaynor JW, et al. Neo-aortic valvar function after the arterial switch. *Cardiol Young.* 2006;16(5):481-9.
14. Bove T, De Meulder F, Vandenplas G, De Groot K, Panzer J, Suys B, DeWolf D, Francois K. Midterm assessment of the reconstructed arteries after the arterial switch operation. *Ann Thorac Surg.* 2008;85(3):823-30.
15. Hutter PA, Thomeer BJ, Jansen P, Hitchcock JF, Faber JA, Meijboom EJ, Bennink GB. Fate of the aortic root after arterial switch operation. *Eur J Cardiothorac Surg.* 2001;20(1):82-8.
16. Schwartz ML, Gauvreau K, del Nido P, Mayer JE, Colan SD. Long-term predictors of aortic root dilation and aortic regurgitation after arterial switch operation. *Circulation.* 2004;110(11 Suppl 1):II128-32.
17. Shepard CW, Germanakis I, White MT, Powell AJ, Co-Vu J, Geva T. Cardiovascular Magnetic Resonance Findings Late After the Arterial Switch Operation. *Circ Cardiovasc Imaging.* 2016;9(9).

18. Vasan RS, Larson MG, Levy D. Determinants of echocardiographic aortic root size. The Framingham Heart Study. *Circulation*. 1995;91(3):734-40.
19. Meijboom LJ, Timmermans J, Zwinderman AH, Engelfriet PM, Mulder BJ. Aortic root growth in men and women with the Marfan's syndrome. *Am J Cardiol*. 2005;96(10):1441-4.
20. Detaint D, Michelena HI, Nkomo VT, Vahanian A, Jondeau G, Sarano ME. Aortic dilatation patterns and rates in adults with bicuspid aortic valves: a comparative study with Marfan syndrome and degenerative aortopathy. *Heart*. 2014;100(2):126-34.
21. Hanke T, Stierle U, Boehm JO, Botha CA, Matthias Bechtel JF, Erasmi A, Misfeld M, Hemmer W, Rein JG, Robinson DR, et al. Autograft regurgitation and aortic root dimensions after the Ross procedure: the German Ross Registry experience. *Circulation*. 2007;116(11 Suppl):I251-8.
22. Takkenberg JJ, van Herwerden LA, Galema TW, Bekkers JA, Kleyburg-Linkers VE, Eijkemans MJ, Bogers AJ. Serial echocardiographic assessment of neo-aortic regurgitation and root dimensions after the modified Ross procedure. *J Heart Valve Dis*. 2006;15(1):100-6.
23. Hourihan M, Colan SD, Wernovsky G, Maheswari U, Mayer JE, Jr., Sanders SP. Growth of the aortic anastomosis, annulus, and root after the arterial switch procedure performed in infancy. *Circulation*. 1993;88(2):615-20.
24. Wolak A, Gransar H, Thomson LE, Friedman JD, Hachamovitch R, Gutstein A, Shaw LJ, Polk D, Wong ND, Saouaf R, et al. Aortic size assessment by noncontrast cardiac computed tomography: normal limits by age, gender, and body surface area. *JACC Cardiovasc Imaging*. 2008;1(2):200-9.
25. Lalezari S, Mahtab EA, Bartelings MM, Wisse LJ, Hazekamp MG, Gittenberger-de Groot AC. The outflow tract in transposition of the great arteries: an anatomic and morphologic study. *Ann Thorac Surg*. 2009;88(4):1300-5.
26. Geiger J, Hirtler D, Burk J, Stiller B, Arnold R, Jung B, Langer M, Markl M. Postoperative pulmonary and aortic 3D haemodynamics in patients after repair of transposition of the great arteries. *Eur Radiol*. 2014;24(1):200-8.
27. Losay J, Touchot A, Capderou A, Piot JD, Belli E, Planche C, Serraf A. Aortic valve regurgitation after arterial switch operation for transposition of the great arteries: incidence, risk factors, and outcome. *J Am Coll Cardiol*. 2006;47(10):2057-62.
28. Delmo Walter EM, Huebler M, Alexi-Meshkishvili V, Sill B, Berger F, Hetzer R. Fate of the aortic valve following the arterial switch operation. *J Card Surg*. 2010;25(6):730-6.
29. Lange R, Cleuziou J, Horer J, Holper K, Vogt M, Tassani-Prell P, Schreiber C. Risk factors for aortic insufficiency and aortic valve replacement after the arterial switch operation. *Eur J Cardiothorac Surg*. 2008;34(4):711-7.
30. Vida VL, Zanutto L, Zanutto L, Stellin G, European Congenital Heart Surgeons Association Study G, Padalino M, Sarris G, Protopapas E, Prospero C, Pizarro C, et al. Left-Sided Reoperations After Arterial Switch Operation: A European Multicenter Study. *Ann Thorac Surg*. 2017;104(3):899-906



## Supplementary material

### Detailed description of Statistical analysis

To analyse the progression of neo-aortic dimensions at three neo-aortic levels over time, linear mixed-effects models were used. To adequately capture non-linear progression over time and the between subject variability, natural cubic splines both in the fixed and random-effects term with 3 knots located at the sample quantiles were used. Potential risk factors known from literature for neo-aortic dilatation were incorporated in the models for the different neo-aortic levels. For all models, risk factors 'morphological TGA subtype' (i.e. TGA-IVS, TGA-VSD and DORV-SP-VSD) and 'gender' were included as main effects and in interaction with time. Additional risk factors were included as main effects in the models for the following neo-aortic levels: for the neo-aortic valve model, 'presence of aortic arch abnormality'; for the neo-aortic root model, 'previous pulmonary artery banding' (PAB) and 'method of coronary artery transfer'; for the STJ model, none. Normality was tested on the model residuals. To assess whether additional candidate risk factors (covariates from Table 1) are associated with neo-aortic diameter progression, these factors were included simultaneously as main effects in the models.

To assess the independent predictive value of different covariates (from Table 1) on the occurrence of AR, Cox regression models were used. A time-dependent Cox model was used to evaluate the effect of the changing aortic dimensions over time on risk of AR. For the multivariable time-dependent Cox model regarding the effect of aortic diameter on AR certain factors were included; for AR  $\geq$ mild: 'morphological subtype', 'gender', 'presence of pulmonary valve abnormality', 'previous PAB' and 'ASO performed  $\geq$ 6 months post birth'. For AR  $\geq$ moderate, the lower number of events only allowed inclusion of the two strongest univariable risk factors: 'morphological TGA subtype' and 'gender'. All *P* values were 2 sided with a significance threshold  $<0.05$ .

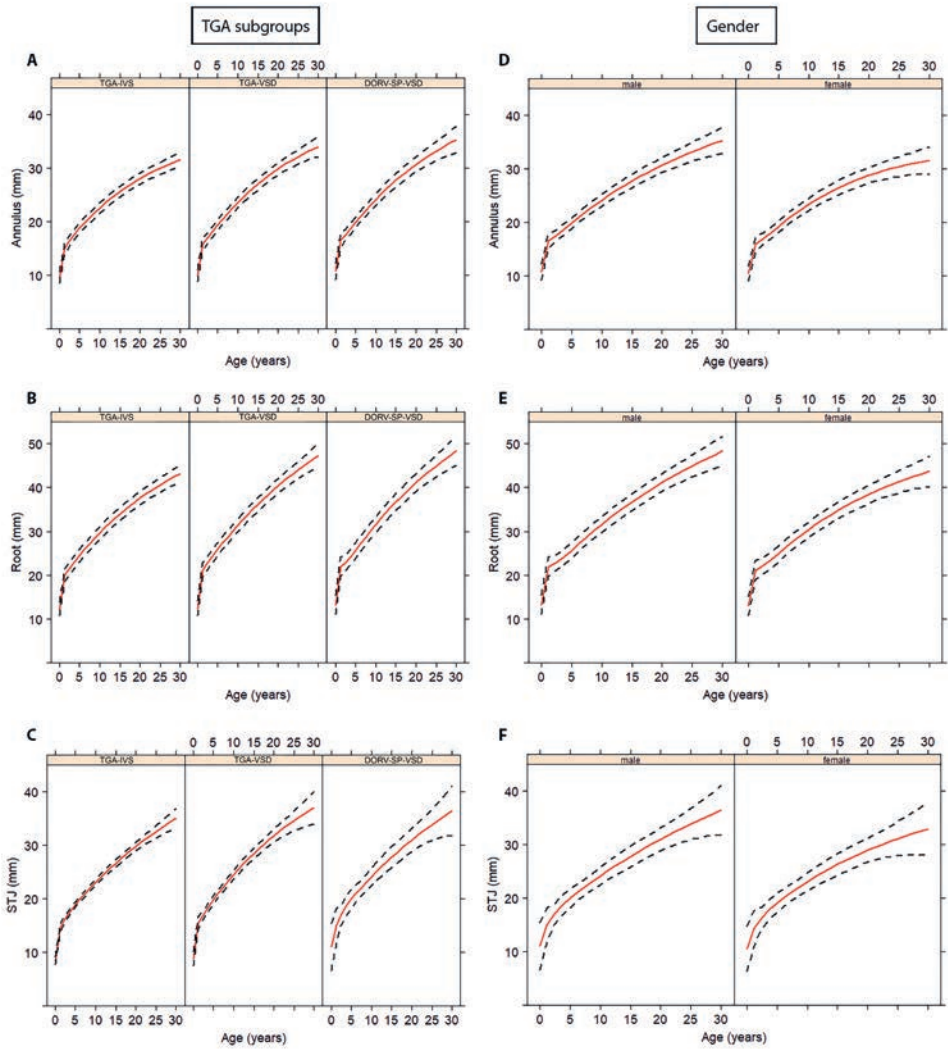


**Figure S1.** Mean progression of neo-aortic dimensions over time for different TGA subtypes (A-C) and gender (D-F), including confidence intervals.

Mean profiles are plotted with the described risk factors set to the reference level; dashed lines represent 95% confidence interval. Annulus, neo-aortic valve annulus; DORV-SP-VSD, double outlet right ventricle with subpulmonary ventricular septal defect; IVS, intact ventricular septum; Root, neo-aortic root; STJ, sinotubular junction; TGA, transposition of the great arteries; VSD, ventricular septal defect.

**Table S1.** Mean neo-aortic progression in adulthood per TGA subtype

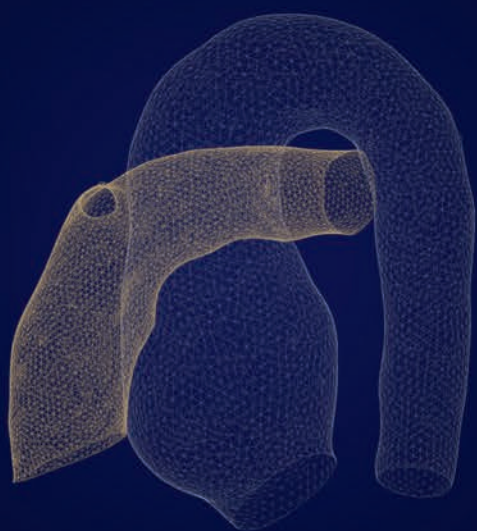
	<b>Annulus</b> mm/year (95% CI)	<b>Root</b> mm/year (95% CI)	<b>STJ</b> mm/year (95% CI)
<b>TGA-IVS (18-26 yrs)</b>	0.40 (0.34-0.46)	0.61 (0.53-0.70)	0.56 (0.44-0.68)
18-20 yrs	0.45 (0.40-0.51)	0.67 (0.61-0.75)	0.60 (0.50-0.70)
20-22 yrs	0.42 (0.36-0.48)	0.63 (0.55-0.71)	0.57 (0.46-0.68)
22-24 yrs	0.38 (0.31-0.45)	0.59 (0.50-0.68)	0.54 (0.42-0.67)
24-26 yrs	0.35 (0.27-0.43)	0.55 (0.45-0.66)	0.52 (0.38-0.66)
<b>TGA-VSD (18-26 yrs)</b>	0.47 (0.36-0.57)	0.75 (0.60-0.90)	0.57 (0.37-0.77)
18-20 yrs	0.52 (0.44-0.61)	0.80 (0.68-0.92)	0.63 (0.47-0.79)
20-22 yrs	0.48 (0.38-0.58)	0.76 (0.62-0.90)	0.59 (0.40-0.77)
22-24 yrs	0.44 (0.33-0.56)	0.73 (0.57-0.89)	0.55 (0.34-0.76)
24-26 yrs	0.41 (0.28-0.54)	0.70 (0.52-0.87)	0.52 (0.28-0.75)
<b>DORV-SP-VSD (18-26 yrs)</b>	0.51 (0.36-0.66)	0.78 (0.58-0.97)	0.58 (0.27-0.89)
18-20 yrs	0.56 (0.44-0.68)	0.84 (0.68-1.00)	0.61 (0.37-0.86)
20-22 yrs	0.52 (0.38-0.67)	0.80 (0.61-0.98)	0.59 (0.30-0.88)
22-24 yrs	0.49 (0.33-0.65)	0.75 (0.55-0.96)	0.56 (0.23-0.90)
24-26 yrs	0.46 (0.28-0.64)	0.72 (0.49-0.95)	0.54 (0.16-0.92)

Data represent average annual growth over the depicted time-interval. Annulus, neo-aortic valve annulus; CI, confidence interval; DORV-SP-VSD, double outlet right ventricle with subpulmonary ventricular septal defect; IVS, intact ventricular septum; Root, neo-aortic root; STJ, sinotubular junction; TGA, transposition of the great arteries; VSD, ventricular septal defect; yrs, years.

**Table S2.** Additional determinants of neo-aortic diameter progression

	Annulus		Root		STJ	
	Coefficient	P value	Coefficient	P value	Coefficient	P value
<b>Previous PAB</b>						
No	ref (1)		ref (1)		ref (1)	
Yes	-0.213	0.681	0.026	0.967	0.111	0.876
<b>Arch abnormality<sup>a</sup> - No</b>						
DORV-SP-VSD	ref (1)		ref (1)		ref (1)	
TGA-IVS	-0.935	0.487	-2.022	0.229	-0.181	0.940
TGA-VSD	-0.950	0.402	-0.896	0.527	1.659	0.405
<b>Pulmonary valve</b>						
Tricuspid	ref (1)		ref (1)		ref (1)	
Bicuspid	0.028	0.949	0.211	0.696	0.002	0.997
<b>Balloon atrial septostomy<sup>a</sup> - No</b>						
DORV-SP-VSD	ref (1)		ref (1)		ref (1)	
TGA-IVS	0.363	0.654	0.542	0.608	1.417	0.311
TGA-VSD	1.207	0.159	1.600	0.138	2.234	0.124
<b>Lecompte maneuver</b>						
No	ref (1)		ref (1)		ref (1)	
Yes	-0.797	0.145	-0.078	0.913	-0.026	0.976
<b>Coronary artery transfer</b>						
(sinus 1, sinus 2)						
2 buttons	N/A	N/A	ref (1)		ref (1)	
2 trapdoor OR	N/A	N/A	0.251	0.368	0.515	0.091
1 button, 1 trapdoor						

<sup>a</sup> Arch abnormality and need for balloon atrial septostomy have been modelled in interaction with the three morphological TGA subtypes. Annulus, neo-aortic valve annulus; DORV-SP-VSD, double outlet right ventricle with subpulmonary ventricular septal defect; IVS, intact ventricular septum; N/A, not applicable; PAB, pulmonary artery banding; Root, neo-aortic root; STJ, sinotubular junction; TGA, transposition of the great arteries; VSD, ventricular septal defect.



## **CHAPTER 5**

# Neo-aortic growth rate and diameter as risk factors for neo-aortic valve regurgitation after arterial switch operation

Adapted from: Heart. 2020; 106(24):1950

Roel L.F. van der Palen  
Sara J. Baart  
Nan van Geloven  
Mark G. Hazekamp  
Nico A. Blom

## To the Editor

Patients after arterial switch operation (ASO) for transposition of the great arteries (TGA) usually have excellent late survival with good quality of life. However, residual sequelae may develop post-ASO of which neo-aortic root dilatation and neo-aortic valve regurgitation (AR) are common and require longitudinal monitoring on severity and progression. Although current reoperation rates for neo-aortic root dilatation or AR are relatively low,<sup>1,2</sup> it is reported to be the second most common cause for reoperation in the long-term follow-up.<sup>3</sup>

In our recently published paper<sup>4</sup> we reported on the ongoing progression of neo-aortic root dilatation beyond childhood (Figure, panels A and B) and identified TGA morphological subtype and male sex as risk factors for neo-aortic root dilatation. In that paper, neo-aortic dimensions and neo-aortic valve function derived from echocardiographic imaging were longitudinally assessed from birth till adulthood in 345 TGA patients after ASO. Thirty-three

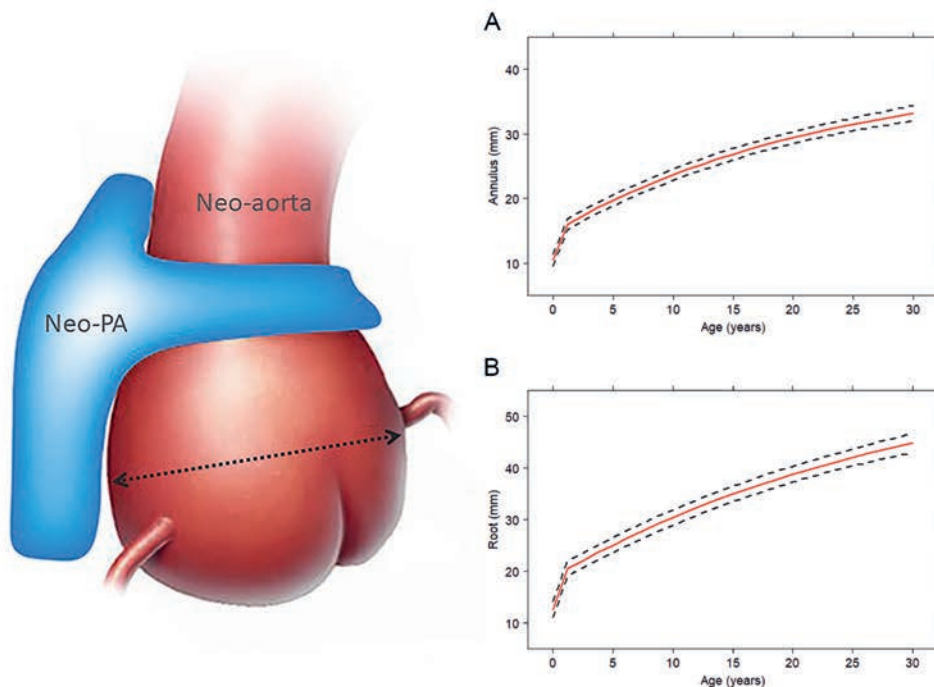


**Figure.** The great arteries after arterial switch operation and mean progression of neo-aortic dimensions. Neo-pulmonary artery and pulmonary artery branches (neo-PA) running in front and embracing the neo-aorta with its dilated neo-aortic root (dashed arrow). Panels A and B derived from van der Palen et al.<sup>4</sup> represent mean progression of neo-aortic dimensions over time for all patients after arterial switch operation for transposition of the great arteries: neo-aortic annulus (A), neo-aortic root (B). Mean profiles are plotted with the described risk factors set to the reference level; dashed lines represent 95% confidence intervals.

of the 345 patients (9.6%) developed at least moderate AR ( $AR \geq \text{moderate}$ ) and mild or more AR ( $AR \geq \text{mild}$ ) was present in one hundred and eleven patients (32.2%). From these data, the mutual relationship between the neo-aortic root dilatation and the development of neo-aortic valve regurgitation was demonstrated. Univariate time-dependent Cox-regression (TD-Cox) analysis to assess the effect of changing aortic dimensions over time on the risk of  $AR \geq \text{moderate}$  showed a clear relationship between neo-aortic annulus and root dimensions and  $AR \geq \text{moderate}$ . However, with the multivariate TD-Cox analysis only neo-aortic root dimensions were independently associated with the development of  $AR \geq \text{moderate}$  (HR = 1.09 (1.01-1.17),  $P = 0.040$ ). No significant association could be established for the development of  $AR \geq \text{mild}$ , neither in the univariate nor in the multivariate analysis.

Recent developments in biostatistics allow a more comprehensive statistical approach for the evaluation of the association between longitudinal markers and time-to-event outcomes by means of joint modeling.<sup>5</sup> A major advantage of the joint model compared to the TD-Cox analysis is that the joint model reconstructs the complete trajectory of the longitudinal marker instead of assuming it to remain constant between two measurement points. This assumption of the TD-Cox model might have had an effect on the results and conclusions from our series. The joint model method combines a mixed effect submodel for the longitudinal marker with a time-to-event submodel for the risk of the event. The mixed effect submodel estimates the trajectory of a marker (i.e. neo-aortic diameter in our dataset), and the estimated marker value at the time of the event (i.e. reaching certain degree of neo-aortic valve regurgitation) is used to estimate the hazard of the event. Non-linear terms, such as quadratic terms or splines, can be included in the mixed effect submodel to obtain a modelled trajectory of the marker that follows the natural evolution over time. Since the event of neo-aortic regurgitation is only diagnosed at a visit, the exact time point of the event is unknown, but takes place somewhere between the last two measurements. This interval-censored nature of the data can be taken into account by the joint model. Another advantage of joint modeling over TD-Cox analysis is that it additionally easily allows for modeling of different associations between the marker and the event. For example, the slope of the marker can be additionally included. Therefore, analysis of the valve function over time in relation to neo-aortic dimensions with the joint modeling statistical approach is preferable to the TD-Cox model for the analysis of our dataset and the dataset was therefore re-analyzed.

In accordance with the previous analysis,<sup>4</sup> cubic splines with knots at 2 and 10 years were used in the mixed effect model to capture non-linear evolutions over time. The mixed effect models were estimated for both neo-aortic annulus and root dimensions over time, and the event data were classified as either  $AR \geq \text{mild}$  or  $AR \geq \text{moderate}$ . In addition to the estimated neo-aortic dimensions, the slope of this marker was added to the survival submodel, representing the estimated growth rate at each point in time. Additional risk factors measured at baseline were included in the risk submodel, which was estimated taking the interval censoring into account. Statistical analysis was performed with the JMbayes software package in R.<sup>6,7</sup>



From the multivariable analysis using the joint modeling approach, it was confirmed that the neo-aortic root dimensions showed a positive significant association with AR  $\geq$ moderate, but the association was much stronger than was determined by the previous TD-Cox analysis (Joint modeling: HR = 1.25 (1.13-1.39),  $P < 0.001$  vs TD-Cox: HR = 1.09 (1.01-1.17),  $P = 0.040$  (Table). Furthermore, with joint modeling the neo-aortic root dimension was also shown to be an independent risk factor for the development of AR  $\geq$ mild (HR = 1.15 (1.08-1.22),  $P < 0.001$ ), where previously no association was found. Moreover, the neo-aortic annulus dimension was an independent risk factor for the development of AR  $\geq$ mild and AR  $\geq$ moderate (AR  $\geq$ mild: HR = 1.18 (1.10-1.27),  $P < 0.001$ ; AR  $\geq$ moderate: HR = 1.22 (1.08-1.38),  $P < 0.001$ ). Apart from this, we identified that the neo-aortic annular growth rate as well as the neo-aortic root growth rate were independently associated with the development of at least mild neo-aortic regurgitation (Table). This means that a faster growth of the neo-aortic annulus and neo-aortic root, in addition to the neo-aortic dimensions itself, was associated with a higher risk of AR  $\geq$ mild. For AR  $\geq$ moderate, growth rate of the neo-aortic annulus and

**Table.** Time-dependent Cox models and Joint models for the risk on neo-aortic valve regurgitation

<i>TD Cox model</i> <sup>§</sup>		<b>AR <math>\geq</math>moderate*</b>		<b>AR <math>\geq</math>mild**</b>	
<b>Diameter increase</b>		<b>Hazard ratio (95% CI)</b>	<b>P value</b>	<b>Hazard ratio (95% CI)</b>	<b>P value</b>
Annulus (per mm)		1.09 (0.99 – 1.21)	0.09	1.03 (0.97– 1.09)	0.31
Root (per mm)		1.09 (1.01 – 1.17)	0.04	1.04 (0.99 – 1.09)	0.10
<i>Joint model</i>		<b>AR <math>\geq</math>moderate*</b>		<b>AR <math>\geq</math>mild**</b>	
<b>Diameter increase</b>		<b>Hazard ratio (95% CI)</b>	<b>P value</b>	<b>Hazard ratio (95% CI)</b>	<b>P value</b>
Annulus (per mm) - dimension	dimension	1.22 (1.08 – 1.38)	<0.001	1.18 (1.10 – 1.27)	<0.001
	dimension	1.20 (1.07 – 1.37)	0.006	1.11 (1.03 – 1.20)	0.008
Annulus (per mm) - dimension and slope	slope	1.75 (0.44 – 6.24)	0.376	3.06 (1.40 – 6.45)	0.004
	dimension	1.25 (1.13 – 1.39)	<0.001	1.15 (1.08 – 1.22)	<0.001
Root (per mm) - dimension and slope	dimension	1.25 (1.13 – 1.38)	<0.001	1.10 (1.04 – 1.18)	0.006
	slope	1.26 (0.36 – 3.72)	0.647	2.28 (1.28 – 4.02)	0.008

<sup>§</sup> Results from time-dependent Cox model as reported by van der Palen et al.<sup>4</sup>

\* Multivariable analysis adjusted for morphological subtype and gender.  $n = 31/323$  (annulus);  $n = 32/323$  (root).

\*\* Multivariable analysis adjusted for morphological subtype, gender, pulmonary valve, previous pulmonary artery banding and age ASO  $\geq 6$  months of age.  $n = 105/323$  (annulus and root).

AR, neo-aortic valve regurgitation.

root did not show such an association next to its absolute neo-aortic dimensions. This could be related to a lack of power as less than 10% of the patients developed AR  $\geq$  moderate.

Data on the evaluation of the neo-aortic growth rate next to neo-aortic dimensions is new in the clinical risk factor assessment on the development of neo-aortic valve regurgitation in patients after congenital heart surgery. This report is the first to show the effect of neo-aortic growth rate in addition to neo-aortic dimensions as critical factors for the impairment of neo-aortic valve function. These results, with stronger and additional effect measures compared to the previously reported outcomes by traditional TD-Cox regression analysis,<sup>4</sup> support the knowledge and concept of AR mechanisms by root dilatation as presented previously by Grande et al. using computational modeling.<sup>8</sup> From that study, progressive root dilatation has been shown to reveal a significant increase in stress and strain on the aortic valve leaflets, leading to significantly reduced leaflet coaptation and valve regurgitation.<sup>8</sup>

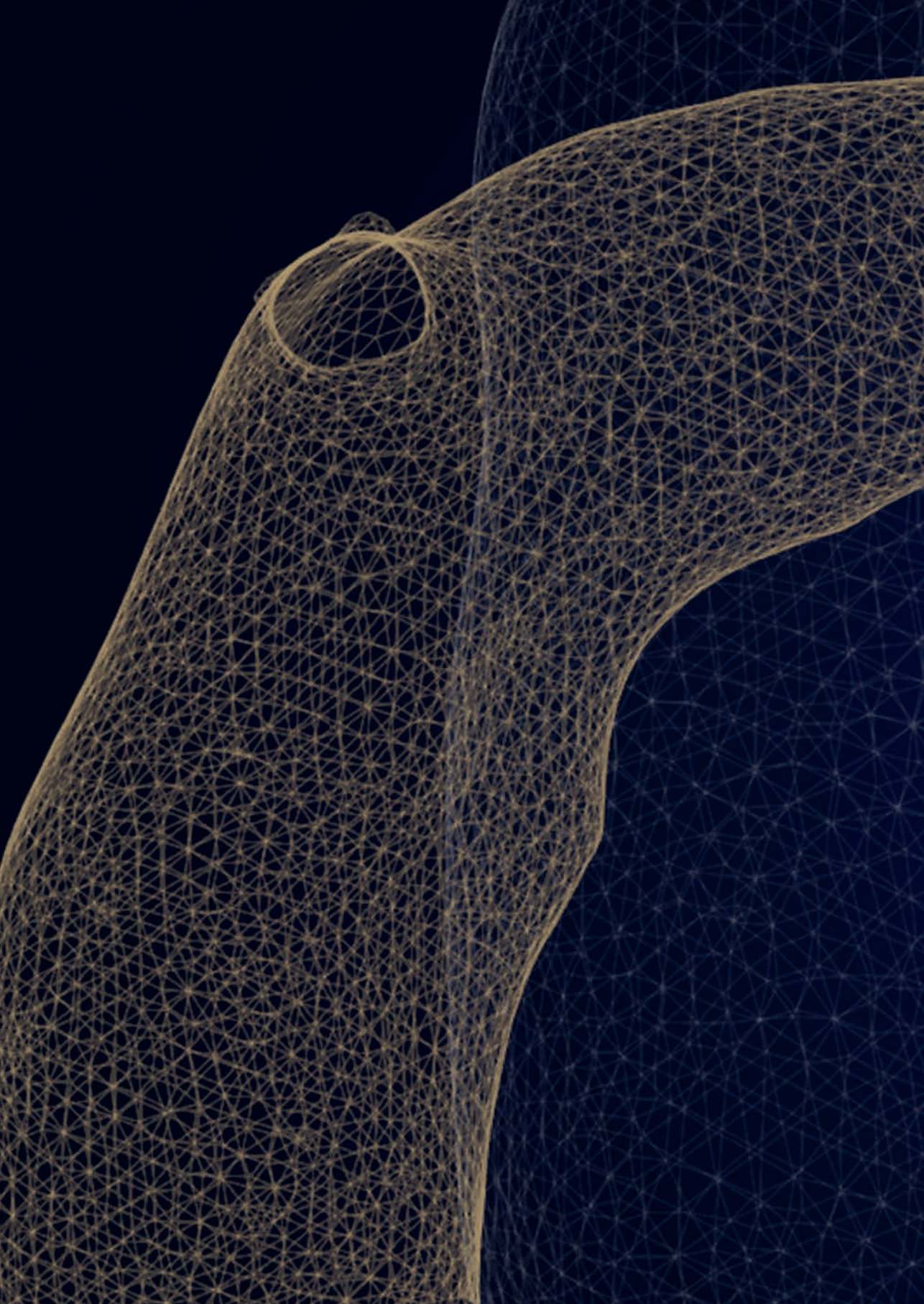
The advantages of multimarker analysis from joint modeling on large population data ultimately might help in tailoring surgical decision making for neo-aortic valve and/or root reinterventions after ASO. Furthermore, extensions to this joint model approach can also help for individual prediction of the occurrence of a defined event in future (i.e. reaching certain degree of AR), by the use of dynamic predictions of the repeated measures in the joint model. With this technique, for each individual patient the probability of a certain degree of valve regurgitation over time can be estimated. Each time new information on the patient's aortic dimensions is available, the probabilities can be updated.

In conclusion, based on the joint model analysis, both annulus and root dimensions are independently associated with AR and, additionally, growth rate of the former native pulmonary valve annulus and adjacent root is associated with AR as well. The fact that neo-aortic dilatation after ASO is progressive over time without stabilization in adulthood, predicts an increasing incidence of neo-aortic regurgitation in future with an expected growing need for surgical reinterventions on the neo-aortic valve and/or root.

## References

1. Koolbergen DR, Manshanden JS, Yazdanbakhsh AP, Bouma BJ, Blom NA, de Mol BA, Mulder BJ, Hazekamp MG. Reoperation for neo-aortic root pathology after the arterial switch operation. *Eur J Cardiothorac Surg*. 2014;46(3):474-9.
2. Vida VL, Zanotto L, Zanotto L, Stellin G, European Congenital Heart Surgeons Association Study G, Padalino M, Sarris G, Protopapas E, Prospero C, Pizarro C, et al. Left-Sided Reoperations After Arterial Switch Operation: A European Multicenter Study. *Ann Thorac Surg*. 2017;104(3):899-906.
3. Kempny A, Wustmann K, Borgia F, Dimopoulos K, Uebing A, Li W, Chen SS, Piorkowski A, Radley-Smith R, Yacoub MH, et al. Outcome in adult patients after arterial switch operation for transposition of the great arteries. *Int J Cardiol*. 2013;167(6):2588-93.
4. van der Palen RLF, van der Bom T, Dekker A, Tsonaka R, van Geloven N, Kuipers IM, Konings TC, Rammeloo LAJ, Ten Harkel ADJ, Jongbloed MRM, et al. Progression of aortic root dilatation and aortic valve regurgitation after the arterial switch operation. *Heart*. 2019;105(22):1732-40.
5. Rizopoulos D. Joint Models for Longitudinal and Time-to-Event Data with Applications in R2012.
6. R Core Team (2017). R: A language and environment for statistical computing. R Foundation for Statistical Computing, Vienna, Austria. URL <https://www.R-project.org/>.
7. Rizopoulos D. The R Package JMBayes for Fitting Joint Models for Longitudinal and Time-to-Event Data Using MCMC. *J Stat Softw*. 2016(72):1-46.
8. Grande KJ, Cochran RP, Reinhall PG, Kunzelman KS. Mechanisms of aortic valve incompetence: finite element modeling of aortic root dilatation. *Ann Thorac Surg*. 2000;69(6):1851-7.

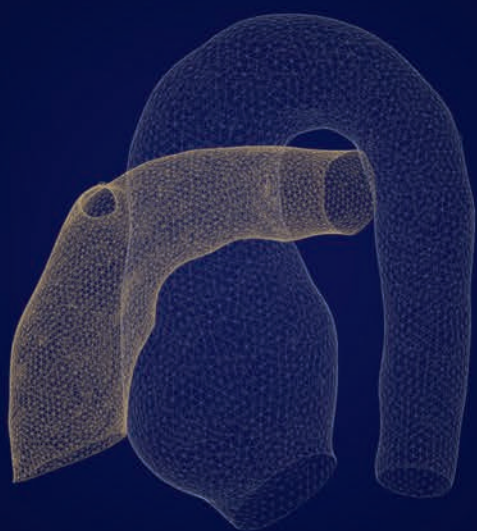




A 3D wireframe model of a heart and aorta, rendered in a dark blue color. The model is composed of a dense grid of lines forming a mesh. The heart is on the left, and the aorta is on the right. The aorta is highlighted in a lighter blue color. The background is a dark blue gradient.

## PART II

**Aortic 4D flow MR imaging**  
The arterial switch operation for TGA and beyond



## **CHAPTER 6**

# Scan-rescan reproducibility of segmental aortic wall shear stress as assessed by phase-specific segmentation with 4D flow MRI in healthy volunteers

Magnetic Resonance Materials in Physics, Biology and Medicine. 2018;31:653-63

Roel L.F. van der Palen  
Arno A.W. Roest  
Pieter J. van den Boogaard  
Albert de Roos  
Nico A. Blom  
Jos J.M. Westenberg



## Abstract

### Objective

The aim was to investigate scan-rescan reproducibility and observer variability of segmental aortic 3D systolic wall shear stress (WSS) by phase-specific segmentation with 4D flow MRI in healthy volunteers.

### Materials and Methods

Ten healthy volunteers (age  $26.5 \pm 2.6$  years) underwent aortic 4D flow MRI twice. Maximum 3D systolic WSS (WSS<sub>max</sub>) and mean 3D systolic WSS (WSS<sub>mean</sub>) for 5 thoracic aortic segments over 5 systolic cardiac phases by phase-specific segmentations were calculated. Scan-rescan analysis and observer reproducibility analysis were performed.

### Results

Scan-rescan data showed overall good reproducibility for WSS<sub>mean</sub> (coefficient of variation, COV 10-15%) with moderate-to-strong intraclass correlation coefficient (ICC 0.63-0.89). The variability in WSS<sub>max</sub> was high (COV 16-31%) with moderate-to-good ICC (0.55-0.79) for different aortic segments. Intra- and interobserver reproducibility was good-to-excellent for regional aortic WSS<sub>max</sub> (ICC  $\geq 0.78$ ; COV  $\leq 17\%$ ) and strong-to-excellent for WSS<sub>mean</sub> (ICC  $\geq 0.86$ ; COV  $\leq 11\%$ ). In general, ascending aortic segments showed more WSS<sub>max</sub>/WSS<sub>mean</sub> variability compared to aortic arch or descending aortic segments for scan-rescan, intraobserver and interobserver comparison.

### Conclusions

Scan-rescan reproducibility was good for WSS<sub>mean</sub> and moderate for WSS<sub>max</sub> for all thoracic aortic segments over multiple systolic phases in healthy volunteers. Intra/interobserver reproducibility for segmental WSS assessment was good-to-excellent. Variability of WSS<sub>max</sub> is higher and should be taken into account in case of individual follow-up or in comparative rest-stress studies to avoid misinterpretation.

## Introduction

Four-dimensional flow magnetic resonance imaging (4D flow MRI) is a non-invasive imaging method to investigate in-vivo cardiovascular flow and is used to better understand cardiovascular physiology and pathophysiology. Besides simple measures of flow,<sup>1-3</sup> this technique allows for quantification of more comprehensive hemodynamic parameters, such as wall shear stress (WSS).<sup>4,5</sup> WSS is defined as the viscous shear force of flowing blood acting tangentially to the vessel wall and can be estimated in both small and large vessels. Alterations in WSS within the aorta have been associated with vascular wall remodelling and dysfunction<sup>6</sup> and this hemodynamic parameter is therefore of interest in patients with aortopathy.

Aortic WSS can be calculated from 4D flow MRI data based on 2D cross-sectional planes at specific locations along the vessel wall<sup>7</sup> or by volumetric 3D WSS computational algorithms.<sup>8</sup> It is known that several acquisition and post-processing factors may influence the estimation of WSS, e.g. spatial resolution, settings of encoding velocity (VENC parameter), signal-to-noise ratio and segmentation inaccuracies.<sup>9,10</sup> Estimation of WSS from 4D flow MRI data necessitates analysis of velocity data within a geometric representation of the 3D vascular structure of interest through segmentation (i.e. creating a cast of the vessel of interest).<sup>11</sup> Currently, thoracic aorta segmentations in most studies are based on phase contrast MR angiograms averaged over all cardiac time frames or manually drawn for every cardiac time frame in 2D planes. Using these approaches, accurate WSS reproducibility has been proven in healthy volunteers.<sup>7,12</sup> However, due to movement of the aorta during the cardiac cycle, aortic compliance and peak systolic time-differences of the propagating blood flow wave front along the thoracic aorta, calculations of WSS throughout the systolic cardiac cycle from a time frame averaged aortic cast could lead to an incorrect assessment of true aortic border velocities for aortic segments along the thoracic aorta.

Therefore, the aim of the study was to assess scan-rescan reproducibility and observer variability of segmental aortic 3D WSS based on semi-automatic, systolic phase-specific 3D aortic segmentation from 4D flow MRI in healthy volunteers. To put the reproducibility analysis of segmental WSS approach into clinical perspective, aortic WSS analyses of two patient cases with congenital aortic abnormalities were compared to the healthy volunteers.

## Materials and methods

### Study population

The study protocol was approved by the Medical Ethics Committee of the Leiden University Medical Center and informed consent was obtained from all participants. Ten healthy volunteers (age  $26.5 \pm 2.6$  yrs) without history of cardiovascular disease were included. All subjects underwent a cardiovascular MR examination including aortic 4D flow MRI. The same scanning protocol was performed twice (i.e. scan and rescan) in the same session with a 10-minute break between the scans and repositioning and replanning for every volunteer.

### **Cardiovascular MR imaging acquisition and 4D flow data processing**

Cardiovascular MR imaging, including aortic 4D flow imaging, was performed on a 3.0 Tesla scanner (Ingenia, Philips Medical Systems, the Netherlands with Software Stream 4.1.3.0) with FlexCoverage Posterior coil in the table top with a dStream Torso coil, providing up to 32 coil elements for signal reception. Aortic 4D flow MRI was acquired during free breathing using respiratory navigator gating based on hemidiaphragm excursion and retrospective ECG gating with full 3D coverage of the thoracic aorta in an oblique sagittal orientation. 4D flow MRI sequence parameters were as follows: velocity-encoding of 200 cm/s in three directions, acquired spatial resolution: 2.5 x 2.5 x 2.5 mm, temporal resolution: 35.1-36.5 ms, echo time/repetition time: 2.5-2.7 ms/4.4-4.6 ms, flip angle: 10°, field of view: 350 x 250 x 75 mm, TFE factor: 2, Sensitivity encoding (SENSE) factor 2.5 in anterior-posterior direction. Concomitant gradient correction and local phase correction was performed from standard available scanner software. Acquisition time was on average 12 minutes.

4D flow MRI data was imported into the commercially available software program CAAS MR 4D flow v1.1 (Pie Medical Imaging BV, Maastricht, the Netherlands). Additional phase offset correction and anti-aliasing was performed in the CAAS MR software package.

The peak systolic cardiac phase was automatically detected by the CAAS MR Flow software program by identification of the cardiac phase with the highest variance in the 3D velocity dataset. For this phase, the segmentation was initialized by manual placing two delimiter points (start and endpoint): one in the subaortic region of the left ventricular outflow tract (start point) and one in the descending aorta (end point), at the same level as the start point. A phase-specific 3D aortic volume was automatically segmented for this peak systolic phase plus two consecutive phases before and two phases after this peak systolic phase (i.e. peak systolic phase-2, peak systolic phase-1, peak systolic phase, peak systolic phase+1 and peak systolic phase+2). The 3D segmentation uses a deformable model algorithm<sup>13</sup> that recursively optimizes the location of the surface towards the vessel luminal boundary based on image gradients, extracted from the appropriate phase within the 4D flow MRI data, while simultaneously maintaining local smoothness of the 3D segmented surface. Manual delineation of the vessel lumen boundary was applied with the available adaptation tool from the software in case of segmentation incorrectness.

### **Segmental WSS assessment**

The surface of the 3D segmented aorta consisted of wall points and for each wall point the 3D systolic WSS vector was calculated based on a quadratic approximation of the axial velocity profile perpendicular to the surface of the 3D segmented aorta. For the regional assessment of maximum aortic 3D systolic WSS (WSSmax) and mean 3D systolic WSS (WSSmean) the thoracic aorta was manually divided into 5 aortic segments based on anatomic landmarks (Figure 1). This aortic subdivision was applied to each of the five phase-specific segmentations. Segment 1: proximal ascending aorta (pAAo, from the sinotubular junction to the mid-ascending aorta); segment 2: distal ascending aorta (dAAo, from mid-ascending aorta to the origin of the innominate artery); segment 3: aortic arch (Arch, from

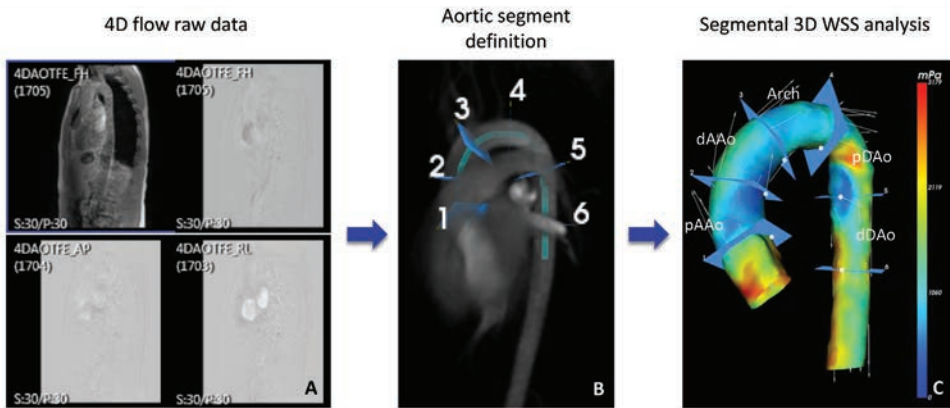


**Figure 1.** Aortic 4D flow MRI processing and analysis.

4D flow MRI raw data including anatomical and flow data (A). Automatic segmentation of 3D aortic volume after manually defining start and endpoint of the thoracic aorta and aortic segment definition (B). 3D color-coded aortic segmentation representing WSSmax distribution for one systolic cardiac phase (C).

origin innominate artery until left subclavian artery); segment 4: proximal descending aorta (pDAo, beyond the left subclavian artery to the mid-descending thoracic aorta); and segment 5: distal descending aorta (dDAo, from mid-descending thoracic aorta to the descending aorta at the level of the aortic valve). Of note, supra-aortic arch branches were excluded from segmental WSS measurements. WSSmax was defined as the maximum WSS vector of all wall points within the defined aortic segment. WSSmean was defined as the average of all WSS vectors of all wall points within the defined aortic segment.

To assess scan-rescan reproducibility, the two consecutively acquired 4D flow MRI scans for each healthy volunteer were analyzed and compared: segmental aortic WSS analysis (i.e. including segmentation and adaptation, and subsequent division of the aorta into 5 segments) for 5 systolic cardiac phases (peak systolic phase  $\pm$  2 phases) was performed for the first and second 4D flow MRI scan data (i.e. scan and rescan) by a single observer (RvdP) in all volunteers. All data was presented blinded to the observers who analyzed the data in a random order. To assess intraobserver variability, segmental aortic WSS analysis was performed twice for 5 systolic cardiac phases (peak systolic phase  $\pm$  2 phases) from the first acquired 4D flow MRI scan by a single observer (RvdP) in all volunteers. To assess interobserver variability, segmental aortic WSS analysis was performed for 5 systolic cardiac phases (peak systolic phase  $\pm$  2 phases) from the first acquired 4D flow MRI scan by two observers (RvdP and PvdB) in all volunteers. The analysis took approximately 18 minutes per systolic phase per volunteer.

To put the reproducibility analysis of segmental WSS approach into clinical perspective, two patient cases with congenital aortic abnormalities were included: Case 1. A 13-year-old male patient with non-stenotic residual narrow proximal descending aortic segment after surgical correction for aortic coarctation at the age of 1 month; and Case 2. A 17-year-old

male patient with ascending aortic dilation after arterial switch operation for transposition of the great arteries prior to replacement of the proximal ascending aorta. Cardiovascular MR imaging, including 4D flow MRI and post-processing, was performed in these cases according to above described methods. An aortic segmentation was made and WSS calculations (WSSmax and WSSmean) were performed for the peak systolic cardiac phase for the aortic segments of interest for the two patients. For patient case 1 this included the pDAo segment, for patient case 2 the ascending aortic segments (pAAo and dAAo).

### Statistical analysis

Statistical analysis was performed using IBM SPSS Statistics 20.0 (SPSS Inc., Chicago, IL, USA). Normality assumptions for all variables were assessed using a Shapiro-Wilk test. All continuous parameters were expressed as mean  $\pm$  standard deviation (SD). Paired t-test was used to determine heart rate differences and differences in time-points of the systolic cardiac phases between the scan and rescan data. To assess the degree of agreement for scan-rescan and intra- and interobserver comparison, mean differences and limits of agreement ( $\pm$  2SD of mean difference) of WSSmean and WSSmax for the different aortic segments from 5 consecutive cardiac systolic phases were calculated by Bland-Altman analysis.<sup>14</sup> Correlation between measurements of the scan and rescan as well as for intra- and interobserver comparison was tested by the Spearman correlation coefficient (*r*). To evaluate the extent of variability in relation to the mean, the coefficient of variation (COV) was calculated as: standard deviation of mean difference for the WSS parameter (WSSmean or WSSmax) between scan-rescan divided by the group average of that WSS parameter for each aortic segment. Reliability between two scans was assessed by the intra-class correlation (ICC) coefficient. Correlation and agreement were classified as follows: *r* or ICC  $\geq$  0.95: excellent, 0.94-0.85: strong, 0.84-0.70: good, 0.69-0.50: moderate,  $<$  0.50: poor. The COV was classified as: low ( $\leq$  10%), intermediate (11-20%), high (21-30%) and very high ( $\geq$  31%). A *P* value  $<$  0.05 was considered statistically significant.

## Results

Baseline characteristics of the volunteers are shown in Table 1. Average heart rate (HR) was similar in the volunteers for the scan and rescan ( $60.8 \pm 7.7$  vs  $61.6 \pm 6.0$  bpm, *P* = 0.65). Average time-points of the 5 systolic phases (ms) throughout the cardiac cycle were not significant different between the scan and rescan data from the volunteers (Table 1).

### Scan-rescan reproducibility

Figure 2 shows the group averaged WSS measurements over 5 systolic cardiac phases (peak systolic phase  $\pm$  2 phases) across the 5 thoracic aortic segments for all volunteers for the scan and rescan. The average WSSmean shows very similar values for scan and rescan and both average WSSmean and average WSSmax closely follow similar trend during the 5 systolic cardiac phases.

**Table 1.** Baseline characteristics

	Volunteers	Scan	Rescan	P value*
<i>n</i>	10			
Male (%)	5 (50%)			
Age, years	26.5 ± 2.6			
Height, cm	175.6 ± 6.6			
Weight, kg	68.3 ± 12.7			
BSA, m <sup>2</sup>	1.8 ± 0.2			
Heart rate, bpm		61 ± 8	62 ± 6	0.65
Time-points throughout cardiac cycle (ms)				
Peak systolic phase-2		104.1 ± 19.2	103.4 ± 19.0	0.91
Peak systolic phase -1		136.8 ± 18.4	135.4 ± 18.1	0.86
Peak systolic phase		169.0 ± 17.5	167.5 ± 17.6	0.85
Peak systolic phase +1		201.5 ± 17.6	199.9 ± 17.2	0.83
Peak systolic phase +2		233.6 ± 17.6	232.0 ± 17.1	0.83

Data presented as mean ± standard deviation. \* paired sample t-test.  
BSA, body surface area; bpm, beats per minute; ms, milliseconds.

Results from the scan-rescan reproducibility analysis for regional aortic WSS<sub>mean</sub> and WSS<sub>max</sub> are presented in Table 2. For all thoracic aortic segments, moderate to good ICCs and Spearman correlations were found for WSS<sub>max</sub> and overall good to strong ICCs with good to strong correlation for WSS<sub>mean</sub>. COV of segmental systolic WSS measurements between the scan and rescan were 16-31% for WSS<sub>max</sub> and 10-15% for WSS<sub>mean</sub>. For the WSS<sub>max</sub>, this degree of variation was higher for the ascending aortic segments compared to the descending aortic segments, on average 26-31% versus 16-18% respectively. Bland-Altman plots and correlation diagrams for scan-rescan analysis for WSS<sub>max</sub> and WSS<sub>mean</sub> of all aortic segments during 5 systolic cardiac phases were depicted in Figure 3.

### Intraobserver analysis

Table 3 and supplementary Tables S1-S4 show the results of the intraobserver reproducibility analysis. Both WSS<sub>max</sub> and WSS<sub>mean</sub> showed overall good to excellent correlation for the different aortic segments (WSS<sub>max</sub>:  $r = 0.66-0.99$ ,  $P < 0.001-0.038$ ); WSS<sub>mean</sub>:  $r = 0.82-1.00$ ,  $P < 0.001-0.004$ ) with overall strong to excellent ICC and low COV indicating excellent reproducibility (range COV WSS<sub>max</sub> 1-14%; range COV WSS<sub>mean</sub> 1-7%) (supplementary Tables S1-S4). Larger variability for WSS measurements of the ascending aortic segments was shown compared to the measurements of the aortic arch and descending aortic segments, more pronounced for the WSS<sub>max</sub> than for WSS<sub>mean</sub>.

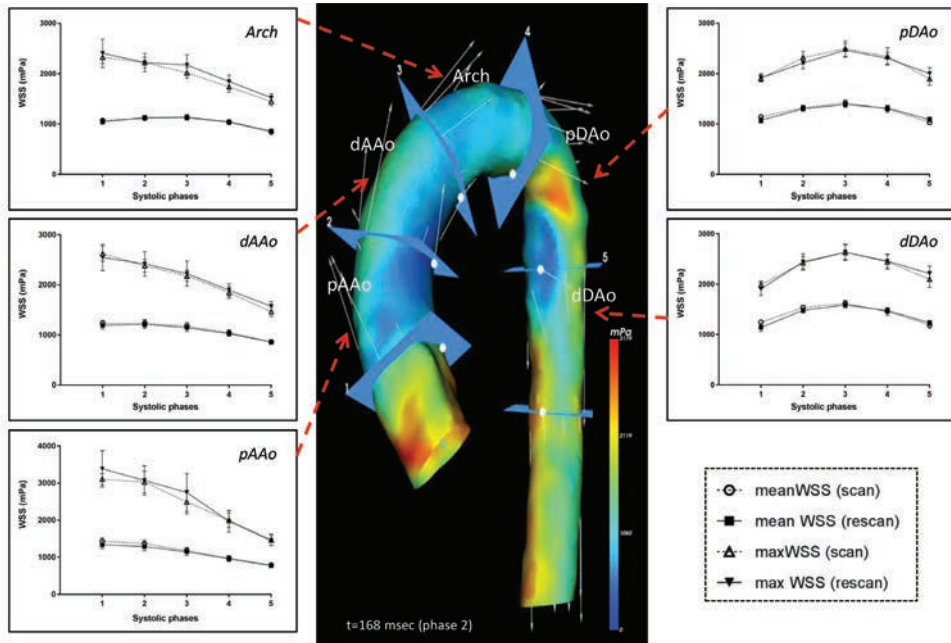


**Figure 2.** Mean and max systolic WSS over 5 systolic cardiac phases around peak systole (peak systolic phase  $\pm 2$  phases) across the 5 thoracic aortic segments for all volunteers. Error bars represent standard error of the mean (SEM).

### Interobserver analysis

Results from the interobserver reproducibility analysis are depicted in Table 4 and supplementary Tables S5-S8. WSSmax between the two observers shows overall good to excellent correlation ( $r = 0.77-0.99$ ,  $P < 0.001-0.009$ ) with strong to excellent ICC and low to intermediate COV (2-17%), indicating good reproducibility. WSSmean between the two observers shows good to excellent correlation ( $r = 0.76-1.00$ ,  $P < 0.001-0.011$ ) with overall excellent ICC and low COV (1-11%), indicating excellent reproducibility (supplementary Tables S5-S8). Least variability in WSS parameters is seen in the aortic arch and descending aortic segments.

### Clinical application of segmental WSS assessment - patient cases

Figure 4 shows two examples of aortic WSS assessment by 4D flow MRI in patients with congenital heart disease involving the aorta. Panel 4A shows the color-coded aortic model of the WSSmax distribution from a 13-year-old patient after neonatal aortic coarctation repair with a residual non-stenotic narrow proximal descending aortic segment (patient 1). Peak systolic WSSmax and WSSmean in the post-coarctation region were 7023 mPa and 3444 mPa, respectively. These WSS values are high and far above the upper 95% confidence

**Table 2.** Segmental WSS analysis (WSSmax and WSSmean) scan versus rescan

	WSSmax (mPa)			WSSmean (mPa)								
	Bland-Altman	COV (%)	Correlation*	ICC	Bland-Altman	COV (%)	Correlation*	ICC				
	Mean difference (mPa)	Limits of agreement ( $\pm 2\sigma$ ) (mPa)	r	P	Mean difference (mPa)	Limits of agreement ( $\pm 2\sigma$ ) (mPa)	r	P				
Proximal AAO	-107	1536	31	0.86	<0.001	0.79	50	323	14	0.90	<0.001	0.89
Distal AAO	-32	1115	26	0.68	<0.001	0.63	23	229	10	0.89	<0.001	0.88
Aortic arch	-84	1066	27	0.71	<0.001	0.55	-4	260	13	0.72	<0.001	0.70
Proximal DAO	12	700	16	0.68	<0.001	0.69	10	359	15	0.64	<0.001	0.63
Distal DAO	-12	815	18	0.65	<0.001	0.66	26	342	12	0.79	<0.001	0.76

\* Spearman correlation coefficient.

AAo, ascending aorta; COV, coefficient of variation; DAO, descending aorta; ICC, intraclass correlation coefficient.

**Table 3.** Intraobserver variability of segmental WSS analysis of the peak systolic cardiac phase from the scan exams

	WSSmax (mPa)			WSSmean (mPa)								
	Bland-Altman	COV (%)	Correlation*	ICC	Bland-Altman	COV (%)	Correlation*	ICC				
	Mean difference (mPa)	Limits of agreement ( $\pm 2\sigma$ ) (mPa)	r	P	Mean difference (mPa)	Limits of agreement ( $\pm 2\sigma$ ) (mPa)	r	P				
Proximal AAO	47.4	628.3	13	0.96	<0.001	0.94	21.1	100.6	5	0.99	<0.001	0.98
Distal AAO	87.4	369.6	9	0.78	0.008	0.87	17.8	48.3	2	0.95	<0.001	0.99
Aortic arch	69.1	157.4	4	0.95	<0.001	0.97	14.9	48.3	2	0.99	<0.001	0.99
Proximal DAO	-1.6	139.9	3	0.99	<0.001	0.99	12.3	68.7	2	1.00	<0.001	0.98
Distal DAO	-51.7	495.9	8	0.93	<0.001	0.89	-16.3	82.2	3	0.98	<0.001	0.98

\* Spearman correlation coefficient.

AAo, ascending aorta; COV, coefficient of variation; DAO, descending aorta; ICC, intraclass correlation coefficient.



limit compared to the average WSS measures in the proximal descending aortic segment of the 10 healthy volunteers (scan/rescan: WSSmax  $2492 \pm 497/ 2466 \pm 431$  mPa; WSSmean  $1418 \pm 199/ 1386 \pm 180$  mPa) (Figure 2).

Panel 4B shows the color-coded aortic model of WSSmax distribution from a 17-year-old male patient after neonatal arterial switch operation for transposition of the great arteries (TGA) with severely dilated proximal ascending aortic segment (52 mm) prior to ascending aorta replacement (patient 2). Regional peak systolic WSS values in this TGA patient: WSSmax 2564 mPa; WSSmean 842 mPa. These WSS values were lower compared to the average WSS measures found in the proximal ascending aortic segment in the 10 healthy volunteers (scan/rescan: WSSmax  $3106 \pm 479/ 3385 \pm 1553$  mPa and WSSmean  $1432 \pm 273/ 1340 \pm 335$  mPa) (Figure 2).

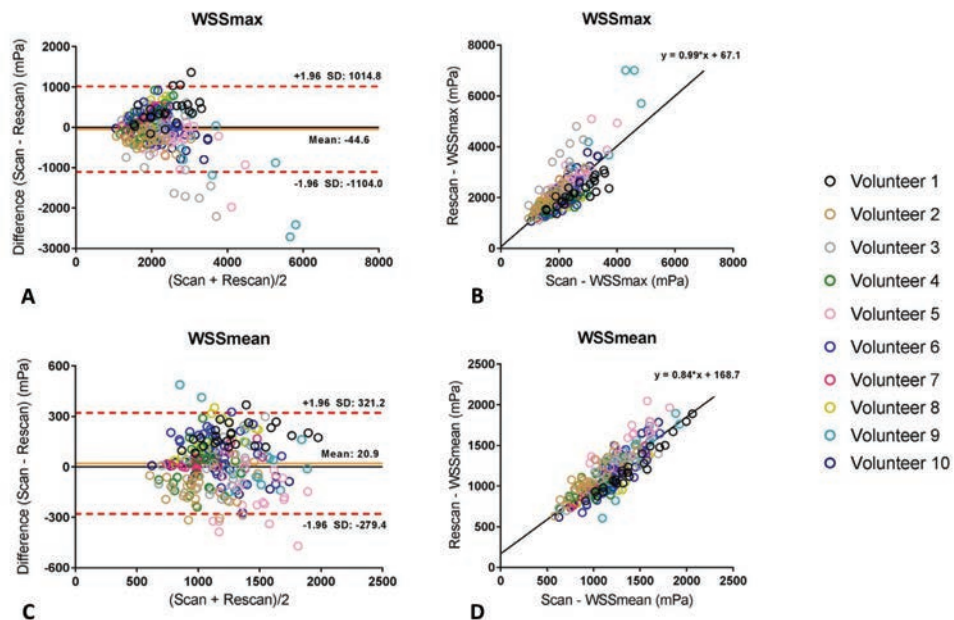


**Figure 3.** Bland-Altman and correlation plots for scan-rescan analysis for the WSSmax (A-B) and WSSmean (C-D) for 5 systolic cardiac phases (peak systolic phase  $\pm 2$  phases)

**Table 4.** Interobserver variability of segmental WSS analysis of the *peak systolic cardiac phase* from the scan exams

	WSSmax (mPa)				WSSmean (mPa)					
	Bland-Altman Mean difference (mPa)	Limits of agreement ( $\pm 2\sigma$ ) (mPa)	COV (%)	Correlation* r	ICC	Bland-Altman Mean difference (mPa)	Limits of agreement ( $\pm 2\sigma$ ) (mPa)	COV (%)	Correlation* r	ICC
Proximal AAO	-182.4	924.7	17	0.81	0.89	-59.8	197.1	8	0.82	0.94
Distal AAO	-27.3	466.3	11	0.81	0.85	11.2	35.5	2	0.96	1.00
Aortic arch	58.8	234.7	6	0.94	0.93	26.3	40.3	2	0.99	0.99
Proximal DAO	-44.6	229.7	5	0.98	0.97	1.6	103.7	4	0.96	0.96
Distal DAO	-155.0	418.1	8	0.93	0.90	-22.7	94.1	3	0.96	0.97

\* Spearman correlation coefficient.

AAo, ascending aorta; COV, coefficient of variation; DAO, descending aorta; ICC, intraclass correlation coefficient.

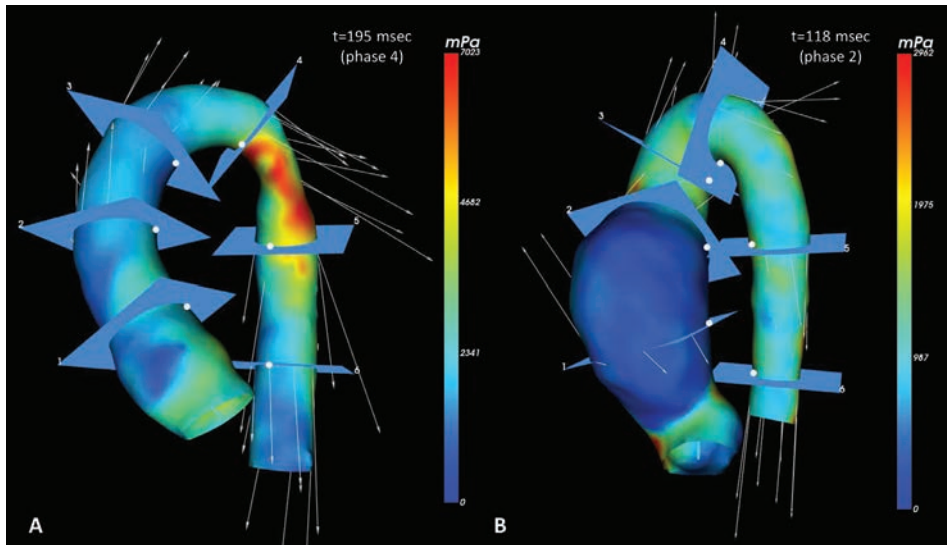


**Figure 4.** Color-coded aortic model representing WSSmax distribution from two patients with congenital heart disease involving the aorta.

Aortic model from a 13-year-old male patient with non-stenotic residual narrow proximal descending aortic segment after surgical correction for aortic coarctation (A). Aortic model from a 17-year-old male patient with severe dilation of the proximal ascending aorta after neonatal arterial switch operation for transposition of the great arteries (B).

## Discussion

The results of this study demonstrate reproducibility of segmental aortic systolic 3D WSS measures in the thoracic aorta of healthy volunteers, by phase-specific 4D flow MRI segmentation. Scan-rescan reproducibility was good for WSSmean for all thoracic aortic regions but scan-rescan reproducibility for WSSmax was moderate with higher variability up to 31% in the proximal ascending aorta. The intraobserver and interobserver reproducibility for segmental systolic WSS analysis of WSSmax and WSSmean was good to excellent. In general, the ascending aortic segments showed more variability in WSSmax and WSSmean measurements compared to aortic arch or descending aortic segments for scan-rescan, intraobserver and interobserver comparison.

Deriving accurate WSS from 4D flow MR velocity data remains challenging and delineation of the aortic wall influences the accuracy of this WSS estimation.<sup>9, 10</sup> Most of the previously reported studies on 3D WSS assessment make use of segmentations based on phase contrast MR angiograms averaged over all cardiac time frames to assess aortic WSS over the entire systolic cardiac cycle.<sup>12, 15-17</sup> In this study, we used a phase-specific segmentation approach for 3D WSS calculations from velocity data for 5 consecutive systolic cardiac phases. A major advantage of this phase-specific segmentation approach is that it will

approximate the aortic wall of the thoracic aorta more accurate in order to better estimate true border WSS. Due to the aortic compliance and movement of the aorta, calculations from a segmentation from averaged phase contrast MR angiograms over all cardiac time frames could lead to an incorrect assessment of WSS along the thoracic aortic wall. Furthermore, the phase-specific segmentations enable identification of peak systolic WSS for each aortic segment along the thoracic aorta, which for every aortic segment is reached at a different time frame throughout systole.

The ability to measure advanced aortic hemodynamic parameters make 4D flow MRI potentially valuable for patients with different entities of aortopathy: to assess disease severity, to better anticipate disease progression and potentially stratify patients at risk for adverse events. However, knowledge of scan-rescan variability for regional WSS measures is essential to study interactions between hemodynamic parameters and aortic geometry and to judge whether hemodynamic changes in patients over time represent true (patho) physiological changes.

Few studies have investigated scan-rescan reproducibility and/or observer variability of aortic WSS measurements *in vivo*.<sup>7,12,18</sup> Similar to our findings, these studies reported good scan-rescan reproducibility for WSSmean measures with relatively higher scan-rescan variability for WSSmax measures. However, these WSS reproducibility studies used different approaches for WSS estimation varying from a time-resolved 2D planar WSS quantification method with manual 2D aortic segmentation<sup>7</sup> to a volumetric 3D WSS assessment from an aortic segmentation from phase contrast MRAs averaged over all cardiac time frames.<sup>12</sup> Furthermore, different time intervals between first and second scan in these studies were chosen compared to this study and varied from 2-4 weeks<sup>12</sup> to 1 year.<sup>7</sup> Moreover, in the study by van Ooij et al.<sup>12</sup> anisotropic voxels of different sizes for different subjects were used, that might have resulted in accuracy problems of WSS estimations between subjects. Our study extends the WSS reproducibility knowledge with its phase-specific, semi-automated 3D WSS segmentation approach with segmental aortic WSS assessment from a non-contrast enhanced 4D flow MRI data acquisition. The good to excellent intra- and interobserver reproducibility from this study is in accordance with these reported studies<sup>7,12</sup> and a study by Bieging et al.,<sup>18</sup> in which observer reproducibility was evaluated by a time-resolved volumetric 3D aortic WSS approach for contrast-enhanced 4D flow MRI.

In general, ascending aortic segments showed more variability in WSSmax and WSSmean compared to aortic arch or descending aortic segments for scan-rescan, intra- and interobserver comparison. Operator and subject dependent factors may have contributed to the differences found in WSS reproducibility for different aortic segments. First, the sub-optimal anatomic information within the 4D flow dataset hampers the exact manual determination of the aortic segments based on anatomic landmarks; especially identifying the sinotubular junction to determine the proximal ascending aortic segment proved to be challenging. Second, variability due to movement and systolic longitudinal stretch of the ascending aorta cannot entirely be ruled out as an influencing factor, despite the phase-specific segmentation has been applied. Heart-beat related motion and longitudinal stretch

during systole has been reported to be more present in the ascending aorta compared to the aortic arch and descending aorta.<sup>19,20</sup> Third, small individual variations in heart rate might have affected WSS differences between scan and rescan, although the averaged heart rate of each individual volunteer was not significantly different between the consecutive scans. Greater variability was found in WSS<sub>max</sub> for both scan-rescan, but in general WSS<sub>max</sub> values are more subject to noise than WSS<sub>mean</sub> values. Furthermore, the VENC setting affects the velocity-to-noise ratio and therefore may have influence on the WSS calculations in low velocity range near the aortic wall. In this study, VENC was 200 cm/s, which was chosen with respect to the anticipated peak velocity in the full aorta, in order to avoid phase wrapping. However, the VENC setting was identical between both scan and rescan and therefore differences due to the velocity sensitivity between both scans are unlikely.

In patients with aortopathy, the aorta can be regionally affected or being entirely involved in the disease, depending on its expression. Aortic WSS disturbances have been shown to strongly correlate with molecular and architectural medial aortic wall alterations<sup>6</sup> or show a direct relation with its regional aortic geometry.<sup>16,21</sup> The regional WSS analysis by phase-specific segmentation models in the presented patient cases provides its clinical applicability in locally diseased aortas, as the WSS values in patient 1 fall far beyond the confidence these intervals of the healthy controls and the WSS values in patient 2 are considerably lower than of the healthy controls with this WSS approach. Using this method, it shows that segment-specific aortic WSS estimation is discriminative and emphasizes the importance of accurate knowledge of WSS reproducibility and consistency across different aortic segments for each applied WSS method.

A limitation of this study is that the study consisted of only 10 healthy volunteers with a relatively small age range. A larger number of volunteers with a larger variation of age could have provided more information about the robustness of this method over ages. The study did not include patients with aortopathy for a scan-rescan comparison which could have provided more insight in the reproducibility of this method for clinical use in patients with aortic disease. The spatial and temporal resolution was similar for the scan-and rescan and both were performed without use of contrast agents. The latter could be considered as a limitation as the use of contrast agents might have increased our signal-to-noise ratio and therefore our reproducibility. However, in the light of the recent discussions on the use of contrast agents in cardiovascular MR we tested the robustness of the WSS assessment method with 4D flow MRI without contrast.<sup>22</sup> The scan and rescan for every volunteer in this study was performed on the same day, which is the most ideal circumstance for a reproducibility analysis, as the volunteers were in the same cardiovascular, neurohormonal and mental status, at the same scanner, the similar moment of the day. Repeated scans on separate days would have been more comparable with clinical practice and may have resulted in a more realistic estimation of reproducibility. However, these assessments have already been performed in other WSS reproducibility studies with time intervals between first and second scan varying from 2-4 weeks<sup>12</sup> to 1 year.<sup>7</sup>

In conclusion, reproducibility of phase-specific WSS assessment in this scan-rescan study in healthy volunteers was good for mean 3D systolic WSS for all thoracic aortic segments over multiple systolic phases. Maximum 3D systolic WSS showed more variability, up to 31% for the proximal ascending aortic region. Although intra- and interobserver reproducibility is good to excellent, these scan-rescan WSS variations should be considered to avoid misinterpretation by investigators in case of individual follow-up or in comparative rest-stress studies.

## References

1. Westenberg JJ, Roes SD, Ajmone Marsan N, Binnendijk NM, Doornbos J, Bax JJ, Reiber JH, de Roos A, van der Geest RJ. Mitral valve and tricuspid valve blood flow: accurate quantification with 3D velocity-encoded MR imaging with retrospective valve tracking. *Radiology*. 2008;249(3):792-800.
2. Hope MD, Hope TA, Meadows AK, Ordovas KG, Urbana TH, Alley MT, Higgins CB. Bicuspid aortic valve: four-dimensional MR evaluation of ascending aortic systolic flow patterns. *Radiology*. 2010;255(1):53-61.
3. Calkoen EE, Roest AA, Kroft LJ, van der Geest RJ, Jongbloed MR, van den Boogaard PJ, Blom NA, Hazekamp MG, de Roos A, Westenberg JJ. Characterization and improved quantification of left ventricular inflow using streamline visualization with 4DFlow MRI in healthy controls and patients after atrioventricular septal defect correction. *J Magn Reson Imaging*. 2015;41(6):1512-20.
4. Kamphuis VP, Westenberg JJM, van der Palen RLF, Blom NA, de Roos A, van der Geest R, Elbaz MSM, Roest AAW. Unravelling cardiovascular disease using four dimensional flow cardiovascular magnetic resonance. *Int J Cardiovasc Imaging*. 2017;33(7):1069-81.
5. Markl M, Schnell S, Wu C, Bollache E, Jarvis K, Barker AJ, Robinson JD, Rigsby CK. Advanced flow MRI: emerging techniques and applications. *Clin Radiol*. 2016;71(8):779-95.
6. Guzzardi DG, Barker AJ, van Ooij P, Malaisrie SC, Puthumana JJ, Belke DD, Mewhort HE, Svystonyuk DA, Kang S, Verma S, et al. Valve-Related Hemodynamics Mediate Human Bicuspid Aortopathy: Insights From Wall Shear Stress Mapping. *J Am Coll Cardiol*. 2015;66(8):892-900.
7. Markl M, Wallis W, Harloff A. Reproducibility of flow and wall shear stress analysis using flow-sensitive four-dimensional MRI. *J Magn Reson Imaging*. 2011;33(4):988-94.
8. Potters WV, van Ooij P, Marquering H, vanBavel E, Nederveen AJ. Volumetric arterial wall shear stress calculation based on cine phase contrast MRI. *J Magn Reson Imaging*. 2015;41(2):505-16.
9. Petersson S, Dyverfeldt P, Ebbers T. Assessment of the accuracy of MRI wall shear stress estimation using numerical simulations. *J Magn Reson Imaging*. 2012;36(1):128-38.
10. Stalder AF, Russe MF, Frydrychowicz A, Bock J, Hennig J, Markl M. Quantitative 2D and 3D phase contrast MRI: optimized analysis of blood flow and vessel wall parameters. *Magn Reson Med*. 2008;60(5):1218-31.
11. Dyverfeldt P, Bissell M, Barker AJ, Bolger AF, Carlhall CJ, Ebbers T, Francios CJ, Frydrychowicz A, Geiger J, Giese D, et al. 4D flow cardiovascular magnetic resonance consensus statement. *J Cardiovasc Magn Reson*. 2015;17:72.
12. van Ooij P, Powell AL, Potters WV, Carr JC, Markl M, Barker AJ. Reproducibility and interobserver variability of systolic blood flow velocity and 3D wall shear stress derived from 4D flow MRI in the healthy aorta. *J Magn Reson Imaging*. 2016;43(1):236-48.
13. Delingette H. General object reconstruction based on simplex meshes. *Research report RR-3111, Inria, February 1997*.
14. Bland JM, Altman DG. Statistical methods for assessing agreement between two methods of clinical measurement. *Lancet*. 1986;1(8476):307-10.
15. Farag ES, van Ooij P, Planken RN, Dukker KCP, de Heer F, Bouma BJ, Robbers-Visser D, Groenink M, Nederveen AJ, de Mol B, et al. Aortic valve stenosis and aortic diameters determine the extent of increased wall shear stress in bicuspid aortic valve disease. *J Magn Reson Imaging*. 2018;48(2):522-30.
16. van der Palen RL, Barker AJ, Bollache E, Garcia J, Rose MJ, van Ooij P, Young LT, Roest AA, Markl M, Robinson JD, et al. Altered aortic 3D hemodynamics and geometry in pediatric Marfan syndrome patients. *J Cardiovasc Magn Reson*. 2017;19(1):30.
17. van Ooij P, Markl M, Collins JD, Carr JC, Rigsby C, Bonow RO, Malaisrie SC, McCarthy PM, Fedak PWM, Barker AJ. Aortic Valve Stenosis Alters Expression of Regional Aortic Wall Shear Stress: New Insights From a 4-Dimensional Flow Magnetic Resonance Imaging Study of 571 Subjects. *J Am Heart Assoc*. 2017;6(9).

18. Biegling ET, Frydrychowicz A, Wentland A, Landgraf BR, Johnson KM, Wieben O, Francois CJ. In vivo three-dimensional MR wall shear stress estimation in ascending aortic dilatation. *J Magn Reson Imaging*. 2011;33(3):589-97.
19. Bell V, Mitchell WA, Sigurethsson S, Westenberg JJ, Gotal JD, Torjesen AA, Aspelund T, Launer LJ, de Roos A, Gudnason V, et al. Longitudinal and circumferential strain of the proximal aorta. *J Am Heart Assoc*. 2014;3(6):e001536.
20. Rengier F, Weber TF, Henninger V, Bockler D, Schumacher H, Kauczor HU, von Tengg-Kobligk H. Heartbeat-related distension and displacement of the thoracic aorta in healthy volunteers. *Eur J Radiol*. 2012;81(1):158-64.
21. Hope TA, Kvitting JP, Hope MD, Miller DC, Markl M, Herfkens RJ. Evaluation of Marfan patients status post valve-sparing aortic root replacement with 4D flow. *Magn Reson Imaging*. 2013;31(9):1479-84.
22. Rogosnitzky M, Branch S. Gadolinium-based contrast agent toxicity: a review of known and proposed mechanisms. *Biometals*. 2016;29(3):365-76.



## Supplementary material

**Supplementary Table S1.** Intraobserver variability of segmental WSS analysis of the peak systolic cardiac phase-2 from the scan exams

	WSSmax (mPa)			WSSmean (mPa)								
	Bland-Altman	COV (%)	Correlation*	ICC	Bland-Altman	COV (%)	Correlation*	ICC				
	Mean difference (mPa)	Limits of agreement ( $\pm 2\sigma$ ) (mPa)	r	P	Mean difference (mPa)	Limits of agreement ( $\pm 2\sigma$ ) (mPa)	r	P				
Proximal Aao	53.2	250.0	4	0.95	<0.001	0.97	71.1	127.1	5	0.96	<0.001	0.98
Distal Aao	-51.7	483.3	9	0.76	0.011	0.91	5.6	53.8	2	0.99	<0.001	0.99
Aortic arch	-11.6	164.8	4	0.98	<0.001	0.97	-3.0	50.0	2	0.94	<0.001	0.98
Proximal DAO	1.2	115.9	3	0.93	<0.001	0.95	-6.1	46.9	2	0.94	<0.001	0.98
Distal DAO	-39.9	239.0	6	0.94	<0.001	0.89	-10.4	95.6	4	0.92	<0.001	0.94

\* Spearman correlation coefficient.

AAo, ascending aorta; COV, coefficient of variation; DAO, descending aorta; ICC, intraclass correlation coefficient.

**Supplementary Table S2.** Intraobserver variability of segmental WSS analysis of the peak systolic cardiac phase-1 from the scan exams

	WSSmax (mPa)			WSSmean (mPa)								
	Bland-Altman	COV (%)	Correlation*	ICC	Bland-Altman	COV (%)	Correlation*	ICC				
	Mean difference (mPa)	Limits of agreement ( $\pm 2\sigma$ ) (mPa)	r	P	Mean difference (mPa)	Limits of agreement ( $\pm 2\sigma$ ) (mPa)	r	P				
Proximal Aao	182.6	815.1	14	0.92	<0.001	0.87	81.0	114.5	4	0.98	<0.001	0.98
Distal Aao	-40.8	295.3	6	0.89	0.001	0.94	11.0	47.0	2	0.96	<0.001	1.00
Aortic arch	27.6	159.8	4	0.99	<0.001	0.97	14.8	50.7	2	0.96	<0.001	0.98
Proximal DAO	-24.7	184.6	4	0.99	<0.001	0.97	-1.0	62.8	2	0.95	<0.001	0.98
Distal DAO	-137.3	532.5	11	0.66	0.038	0.78	-10.5	120.9	4	0.82	0.004	0.91

\* Spearman correlation coefficient.

AAo, ascending aorta; COV, coefficient of variation; DAO, descending aorta; ICC, intraclass correlation coefficient.

**Supplementary Table S3.** Intraobserver variability of segmental WSS analysis of the *peak systolic cardiac phase+1* from the scan exams

	WSSmax (mPa)			WSSmean (mPa)								
	Bland-Altman	COV (%)	Correlation*	ICC	Bland-Altman	COV (%)	Correlation*	ICC				
	Mean difference (mPa)	Limits of agreement ( $\pm 2\sigma$ ) (mPa)	r	P	Mean difference (mPa)	Limits of agreement ( $\pm 2\sigma$ ) (mPa)	r	P				
Proximal AAO	111.1	327.8	8	0.92	<0.001	0.97	49.4	74.9	4	0.99	<0.001	0.99
Distal AAO	5.9	149.9	4	0.95	<0.001	0.98	3.2	25.4	1	0.99	<0.001	1.00
Aortic arch	-27.5	152.0	4	0.93	<0.001	0.98	9.5	43.6	2	0.99	<0.001	0.99
Proximal DAO	-15.0	148.2	3	0.96	<0.001	0.99	-0.1	88.7	3	0.95	<0.001	0.98
Distal DAO	-22.5	252.0	5	0.72	0.018	0.97	-24.7	86.7	3	0.99	<0.001	0.98

\* Spearman correlation coefficient.

AAO, ascending aorta; COV, coefficient of variation; DAO, descending aorta; ICC, intraclass correlation coefficient.

**Supplementary Table S4.** Intraobserver variability of segmental WSS analysis of the *peak systolic cardiac phase+2* from the scan exams

	WSSmax (mPa)			WSSmean (mPa)								
	Bland-Altman	COV (%)	Correlation*	ICC	Bland-Altman	COV (%)	Correlation*	ICC				
	Mean difference (mPa)	Limits of agreement ( $\pm 2\sigma$ ) (mPa)	r	P	Mean difference (mPa)	Limits of agreement ( $\pm 2\sigma$ ) (mPa)	r	P				
Proximal AAO	16.4	153.9	5	0.94	<0.001	0.99	51.5	85.8	6	1.00	<0.001	0.97
Distal AAO	-1.1	30.6	1	0.99	<0.001	1.00	1.6	28.9	2	0.99	<0.001	1.00
Aortic arch	25.1	136.6	5	0.96	<0.001	0.97	2.3	51.7	3	0.98	<0.001	0.98
Proximal DAO	-38.9	209.8	5	0.89	0.001	0.97	-15.6	137.8	7	0.92	<0.001	0.92
Distal DAO	-49.2	334.8	8	0.93	<0.001	0.94	-18.1	113.9	5	0.99	<0.001	0.96

\* Spearman correlation coefficient.

AAO, ascending aorta; COV, coefficient of variation; DAO, descending aorta; ICC, intraclass correlation coefficient.

**Supplementary Table S5.** Interobserver variability of segmental WSS analysis of the peak systolic cardiac phase-2 from the scan exams

	WSSmax (mPa)				WSSmean (mPa)					
	Bland-Altman		COV (%)	Correlation*	Bland-Altman		COV (%)	Correlation*	ICC	
	Mean difference (mPa)	Limits of agreement ( $\pm 2\sigma$ ) (mPa)	r	P	Mean difference (mPa)	Limits of agreement ( $\pm 2\sigma$ ) (mPa)	r	P	ICC	
Proximal AAO	-61.9	578.1	9	0.84	0.002	0.86	11	0.76	0.011	0.86
Distal AAO	-99.0	387.1	7	0.82	0.004	0.94	2	0.99	<0.001	0.99
Aortic arch	-1.5	205.8	4	0.96	<0.001	0.96	4	0.95	<0.001	0.95
Proximal DAO	-70.2	234.2	6	0.84	0.002	0.84	2	0.98	<0.001	0.98
Distal DAO	-142.4	230.7	6	0.95	<0.001	0.90	4	0.93	<0.001	0.94

\* Spearman correlation coefficient.

AAO, ascending aorta; COV, coefficient of variation; DAO, descending aorta; ICC, intraclass correlation coefficient.

**Supplementary Table S6.** Interobserver variability of segmental WSS analysis of the peak systolic cardiac phase-1 from the scan exams

	WSSmax (mPa)				WSSmean (mPa)					
	Bland-Altman		COV (%)	Correlation*	Bland-Altman		COV (%)	Correlation*	ICC	
	Mean difference (mPa)	Limits of agreement ( $\pm 2\sigma$ ) (mPa)	r	P	Mean difference (mPa)	Limits of agreement ( $\pm 2\sigma$ ) (mPa)	r	P	ICC	
Proximal AAO	-27.7	710.2	12	0.94	<0.001	0.91	9	0.88	0.001	0.92
Distal AAO	-150.8	468.5	10	0.79	0.006	0.88	2	0.99	<0.001	1.00
Aortic arch	33.1	114.0	3	0.99	<0.001	0.99	1	0.99	<0.001	0.99
Proximal DAO	-78.4	194.0	4	0.95	<0.001	0.97	2	0.96	<0.001	0.98
Distal DAO	-302.2	496.3	10	0.78	0.008	0.81	3	0.95	<0.001	0.93

\* Spearman correlation coefficient.

AAO, ascending aorta; COV, coefficient of variation; DAO, descending aorta; ICC, intraclass correlation coefficient.

**Supplementary Table S7.** Interobserver variability of segmental WSS analysis of the *peak systolic cardiac phase+1* from the scan exams

	WSSmax (mPa)			WSSmean (mPa)				
	Bland-Altman	COV (%)	Correlation*	ICC	Bland-Altman	COV (%)	Correlation*	ICC
	Mean difference (mPa)	Limits of agreement ( $\pm 2\sigma$ ) (mPa)	r	P	Mean difference (mPa)	Limits of agreement ( $\pm 2\sigma$ ) (mPa)	r	P
Proximal AAO	-60.3	517.0	14	0.77	0.009	0.89	0.89	0.92
Distal AAO	7.6	272.5	7	0.92	<0.001	0.94	0.98	<0.001
Aortic arch	1.0	159.7	5	0.90	<0.001	0.97	0.99	<0.001
Proximal DAO	-26.3	98.5	2	0.96	<0.001	1.00	0.99	<0.001
Distal DAO	-237.9	552.4	11	0.82	0.004	0.85	0.96	<0.001

\* Spearman correlation coefficient.

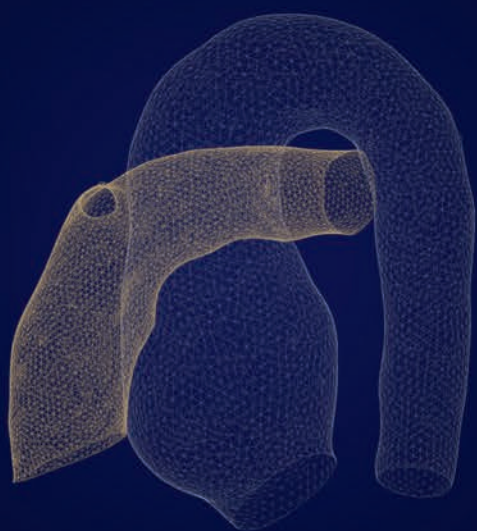
AAo, ascending aorta; COV, coefficient of variation; DAO, descending aorta; ICC, intraclass correlation coefficient.

**Supplementary Table S8.** Interobserver variability of segmental WSS analysis of the *peak systolic cardiac phase+2* from the scan exams

	WSSmax (mPa)			WSSmean (mPa)				
	Bland-Altman	COV (%)	Correlation*	ICC	Bland-Altman	COV (%)	Correlation*	ICC
	Mean difference (mPa)	Limits of agreement ( $\pm 2\sigma$ ) (mPa)	r	P	Mean difference (mPa)	Limits of agreement ( $\pm 2\sigma$ ) (mPa)	r	P
Proximal AAO	-99.3	407.6	13	0.81	0.005	0.91	0.89	<0.001
Distal AAO	-22.3	125.5	4	0.98	<0.001	0.98	1.0	<0.001
Aortic arch	42.6	153.1	5	0.94	<0.001	0.96	0.98	<0.001
Proximal DAO	-75.0	192.9	5	0.84	0.002	0.97	0.92	<0.001
Distal DAO	-164.0	494.3	11	0.77	0.009	0.88	0.95	<0.001

\* Spearman correlation coefficient.

AAo, ascending aorta; COV, coefficient of variation; DAO, descending aorta; ICC, intraclass correlation coefficient.



## CHAPTER 7

# Altered ascending aorta hemodynamics in patients after arterial switch operation for transposition of the great arteries

Journal of Magnetic Resonance Imaging. 2020;51:1105-16

Roel L.F. van der Palen  
Quirine S. Deurvorst  
Lucia J.M. Kroft  
Pieter J. van den Boogaard  
Mark G. Hazekamp  
Nico A. Blom  
Hildo J. Lamb  
Jos J.M. Westenberg\*  
Arno A.W. Roest\*

\* shared last authorship

## Abstract

### Background

Patients with transposition of the great arteries (TGA) have an altered aortic geometry after an arterial switch operation (ASO), with neo-aortic root dilatation as an important complication. Geometry-related aortic hemodynamics have been assumed to contribute to pathology of the ascending aorta (AAo).

### Purpose

To evaluate aortic flow displacement (FD) and regional wall shear stress (WSS) in relation to ascending neo-aortic geometry in children after ASO.

### Study type

Prospective.

### Population

Twenty-eight TGA patients after ASO and ten healthy volunteers.

### Field Strength/Sequence

3.0T/4D flow (segmented fast-spoiled echo pulse), non-contrast enhanced MR angiography (Dixon), and anatomic images (SSFP).

### Assessment

Aortic diameters and body surface area-indexed aortic dimensions (Z-scores), normalized FD and planar ascending aortic WSS.

### Statistical tests

Mann Whitney and chi-square tests for differences in FD magnitude, WSS, and FD directionality between groups, respectively. Spearman rank correlation to assess the degree of association between aortic geometry, FD and WSS parameters. Shapiro-Wilk test to evaluate distribution normality on the absolute differences in octant location between FD and WSS.

### Results

TGA patients showed a significantly dilated proximal AAo and relatively small mid-AAo dimensions at the level of the pulmonary arteries (Z-scores neo-aortic root:  $4.38 \pm 1.96$  vs  $1.52 \pm 0.70$ ,  $P < 0.001$ ; sinotubular junction:  $3.48 \pm 2.67$  vs  $1.38 \pm 1.30$ ,  $P = 0.010$ ; mid-AAo:  $0.32 \pm 3.06$  vs  $1.69 \pm 1.24$ ,  $P = 0.001$ ). FD magnitude was higher in TGA patients (neo-aortic root:  $0.048 \pm 0.027$  vs  $0.021 \pm 0.006$ ,  $P < 0.001$ ; sinotubular junction:  $0.054 \pm 0.037$  vs  $0.029 \pm 0.013$ ,  $P < 0.05$ ) and was related to the neo-aortic Z-score. Clear areas of higher WSS at the right and anterior aortic wall regions along the distal AAo were detected in TGA patients, most pronounced in those with relatively smaller mid-AAo diameters.

**Data conclusion**

TGA-specific geometry related to the ASO, evidenced by neo-aortic root dilatation and a sudden change in vessel diameter at mid-AAo level, leads to more aortic flow asymmetry in the proximal AAo and WSS distribution with higher WSS at the right and anterior aortic wall regions along the distal AAo.

**Introduction**

The arterial switch operation (ASO) is currently the operation of choice for patients with transposition of the great arteries (TGA).<sup>1</sup> The ASO replaced the atrial switch operation with excellent early and long-term survival and good function outcome in most of the patients. However, studies on large cohorts of patients show progressive neo-aortic root dilatation over time with an associated increased incidence of neo-aortic regurgitation and the need for root and/or valve re-operation.<sup>2,3</sup> Factors involved in the pathophysiological mechanisms for neo-aortic root dilatation are largely unknown.

The ASO with the Lecompte maneuver restores ventriculo-arterial concordance; however, the spatial relation between the aorta and pulmonary artery is still abnormal, with the pulmonary trunk situated anterior to the ascending aorta and the two pulmonary arteries embracing the ascending aorta. During the ASO, the aorta and pulmonary trunk are transected just above the commissures and relocated, leaving the semilunar valves and native root in its original position. Subsequently, the proximal part of the native pulmonary trunk becomes the proximal neo-aorta and the native aortic root becomes the neo-pulmonary root. The arterial relocation leads to an abnormal angulation between the neo-aortic valve and the newly formed sinotubular junction (STJ) in TGA patients compared with healthy subjects, and geometric alterations in the ascending neo-aorta after ASO have hemodynamic consequences.<sup>4,5</sup>

Currently, 4D flow magnetic resonance imaging (4D flow MRI) allows visualization and quantification of abnormal hemodynamics within the ascending aorta<sup>6</sup> which has led to better knowledge of cardiovascular hemodynamics and disease progression in patients with congenital heart disease-related aortopathy.<sup>7-11</sup> Different studies have shown that aortic flow eccentricity, defined as the displacement of peak systolic flow from the aortic center, is related to aortic morphology in bicuspid valve-related dilated aortopathy.<sup>11,12</sup> Another comprehensive hemodynamic parameter that can be derived from 4D flow MRI is wall shear stress (WSS). WSS is defined as the viscous shear force of flowing blood acting tangentially to the vessel wall. Areas of high WSS have been associated with marked histological changes in the ascending aortic vessel wall in patients with bicuspid aortic valves.<sup>13</sup> In addition, abnormal WSS has been suggested to have potentially contributing effects on vessel dilatation and aneurysm formation; for example, on the thoracic aorta and on intracranial aneurysms.<sup>14,15</sup> In TGA patients after ASO, abnormal flow patterns in the ascending aorta are present in the majority of patients.<sup>4</sup> Assessment of aortic flow displacement and



detection of areas of high WSS may be helpful in unravelling flow alterations and their relationship with altered arterial geometry and aortic dilatation. We hypothesized that the specific geometry of the ascending neo-aorta after ASO including the Lecompte maneuver is related to altered ascending aortic flow hemodynamics. Therefore, the aim of this study was to evaluate aortic flow displacement and regional WSS in relation to ascending neo-aortic geometry in patients after ASO for TGA.

## Materials and methods

### Study population

All patients or their legal guardians and all healthy subjects gave written informed consent for the study. The study protocol was approved by the institutional Medical Ethical Committee. Twenty-eight patients with simple TGA or TGA with ventricular septal defect (VSD) were included in this study between December 2015 and March 2018. TGA patients (simple TGA or TGA with VSD) aged 10-25 years that underwent regular MRI examinations of the heart and large vessels as part of the standardized clinical follow-up protocol for early detection of well-known sequelae after ASO (typically performed shortly after birth) were asked for participation in the study. Aortic 4D flow acquisitions were performed additionally to a standard-of-care cardiac MRI. To ensure morphologic homogeneity, patients with complex TGA including Taussig-Bing anomaly, prior left ventricular outflow tract obstruction, bicuspid neo-aortic valve, aortic arch obstruction, moderate-to-severe neo-aortic insufficiency, or prior neo-aortic valve or root re-operations were not included in the study. All patients underwent 4D flow MRI in addition to the clinically indicated standard-of-care MRI assessment of the heart and large vessels. Ten healthy subjects with a tricuspid aortic valve and without history of cardiovascular disease were included as a healthy reference group. All healthy subjects underwent the same MRI assessment of the heart and great vessels including 4D flow aortic imaging as part of a validation study.<sup>16</sup>

### MRI acquisition

MRI examinations including aortic 4D flow imaging of all patients and healthy subjects were performed at the same 3T scanner (Ingenia, Philips Medical Systems, the Netherlands; Software Stream 4.1.3.0) using a combination of FlexCoverage Posterior coil in the table top with a dStream Torso coil, providing up to 32 coil elements for signal reception. The standard-of-care MRI exam of the heart and large vessels included dynamic ECG gated two-dimensional (2D) cine steady state free precession (SSFP) imaging for the evaluation of cardiac anatomy and function, as well as a non-contrast enhanced three-dimensional (3D) free-breathing navigator-gated MR angiography (NCE-MRA) images for the assessment of thoracic aorta diameters.<sup>17</sup> For the NCE-MRA imaging, a Dixon sequence with prospective triggering and gated to end diastole, respiratory navigator gating was used with following sequence parameters: spatial resolution = 1.6 x 1.6 x 3.2 mm, echo time/repetition time = 2.3/3.6-3.9

msec, field of view = 300 x 300 x 99 mm; reconstructed voxel size = 0.8 x 0.8 x 1.6 mm. 4D flow MRI was a segmented fast spoiled-gradient echo technique with standard 4-point velocity encoding in all three directions. The 4D flow MRI was acquired during free breathing using a hemidiaphragm respiratory navigator and retrospective ECG gating. Scan parameters were as follows: velocity-encoding of 200-300 cm/s in three directions, acquired spatial resolution = 2.5 x 2.5 x 2.5 mm, temporal resolution = 33.6-36.8 msec, echo time/repetition time = 2.4-2.7/4.2-4.6 msec, flip angle = 10°, field of view = 350 x 250 x 75 mm, segmentation factor = 2, sensitivity encoding (SENSE) was used with SENSE factor 2.5 in anterior-posterior direction. Acquisition time was on average 12 minutes. Concomitant gradient correction and initial phase offset correction was performed from standard available scanner software.

## Data analysis

### *Aortic dimensions and cardiac function*

Left ventricular ejection fraction was measured from short-axis SSFP images by a radiologist with over 20 years of experience in MR imaging (L.K.). From NCE-MRA, ascending aortic diameters were measured at five standardized anatomic landmarks according to international guidelines,<sup>18</sup> consisting of the neo-aortic valve (AoV), neo-aortic root (Root), STJ, for TGA patients defined as the aortic level 5-7 mm below the pulmonary artery bifurcation; mid-ascending aorta at the level of the pulmonary artery bifurcation (mid-AAo) and the distal ascending aorta, just proximal to the origin of the brachiocephalic trunk (AAo-BCT) (Figure 1). All diameters were measured from edge to edge and obtained from a sagittal-axis orientation. The mean neo-aortic root diameters (i.e. average of three cusp-to-commissure diameters) were measured perpendicular to the aortic axis on NCE-MRA double oblique transversal angulated multiplanar reconstructions. A second observer (independent radiologist with 10 years of experience in cardiovascular MR imaging) remeasured all ascending aortic diameters in a random subset of healthy volunteers ( $n = 5$ ) and patients ( $n = 10$ ) to assess interobserver reproducibility. To take into account differences in age and body size between individuals, aortic Z-scores were determined for each individual using MRI-derived normative data of aortic diameters in children and adolescents.<sup>19</sup> Body surface area was calculated using the Mosteller formula. The Z-score represents the deviation of a given measurement to the body size or age-specific population mean. A Z-score between -2 and +2 is considered normal. Aortic diameter ratio between the neo-aortic root diameter and the mid-AAo diameter was calculated for each subject  $\left(\frac{\text{Root}}{\text{mid-AAo}}\right)$ .

### *4D Flow - Aortic flow displacement & WSS assessment*

4D flow MRI data were imported into the software program CAAS MR 4D flow v2.0 (Pie Medical Imaging BV, Maastricht, the Netherlands). Additional phase offset correction and antialiasing was performed in the CAAS MR software package. The 4D flow segmentation was performed as previously described.<sup>16</sup> In short, from the 4D flow raw data (Figure 1A) the peak systolic phase was automatically detected by the CAAS MR Flow software program by identification of the cardiac phase with the highest variance in the 3D velocity dataset.

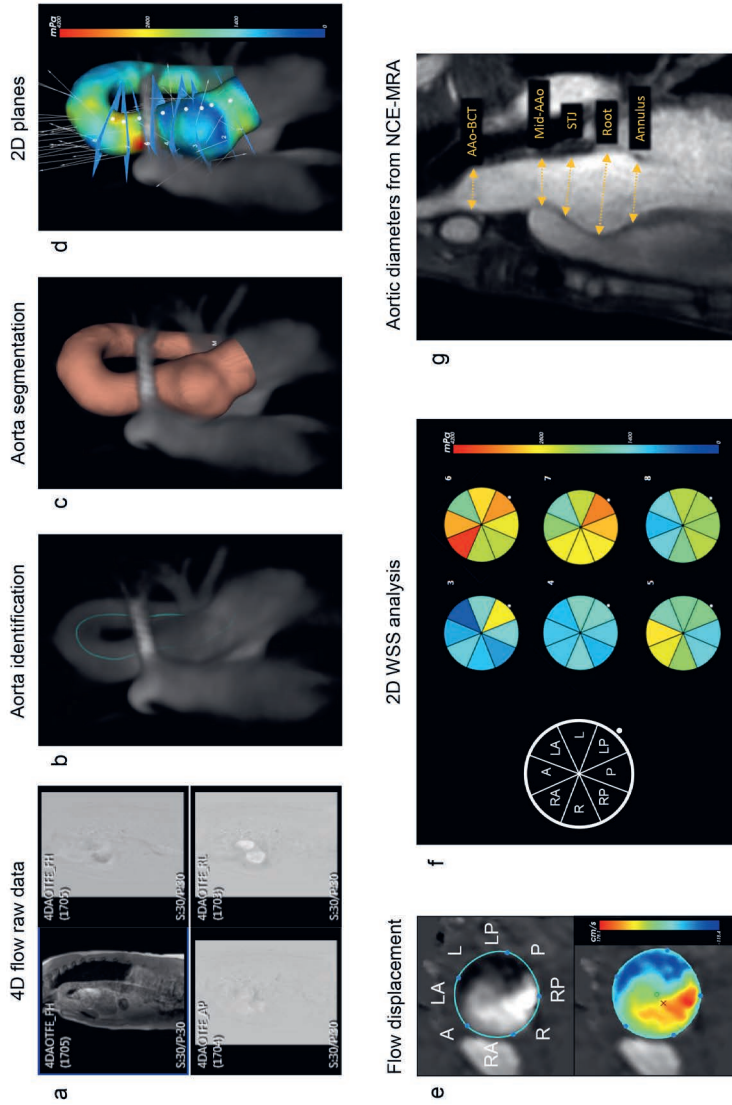


**Figure 1.** Measurement of aortic diameters and workflow 4D flow analysis for flow displacement and wall shear stress. 4D flow dataset (A). Identification of the thoracic aorta and automatic computation of aortic centerline (B). 3D segmentation of the thoracic aorta (C). Positioning of eight cross-sectional planes perpendicular to the centerline: 1. left ventricular outflow tract, 2. aortic valve, 3. neo-aortic root, 4. sinotubular junction, 5. mid-ascending aorta, 6. distal ascending aorta-1 (dAAo-1), 7. distal ascending aorta-2 (dAAo-2), 8. proximal to the origin of the brachiocephalic trunk (D). Determining flow displacement and direction,  $\odot$  = center of vessel,  $\times$  = center of vessel. Planar 2D WSS analysis (E). Aortic diameter measurements from non-contrast enhanced magnetic resonance angiography (G). AAo-BCT, distal ascending aorta proximal to the origin of the brachiocephalic trunk; A, anterior; LA, left-anterior; L, left; LP, left-posterior; mid-AAo, mid-ascending aorta; NCE-MRA, non-contrast enhanced magnetic resonance angiography; P, posterior; RP, right-posterior; R, right; RA, right-anterior; Root, neo-aortic root; STJ, sinotubular junction; WSS, wall shear stress.

For this phase (Figure 1B), the segmentation was initialized by manually placing two points (start and endpoint): one in the left ventricular outflow tract and one in the descending aorta, at the same level as the start point (Figure 1B). A centerline was automatically created (Figure 1B) and a phase-specific 3D aortic volume was automatically segmented for this peak systolic phase (Figure 1C) plus two consecutive phases before and two phases after this peak systolic phase. For the ascending aorta, the peak systolic 3D aortic segmentation was selected, visually checked and manually adapted when necessary in case of segmentation incorrectness. Eight cross-sectional planes were manually positioned along the ascending aorta perpendicular to the centerline (Figure 1D). The 2D analysis planes were placed from the LVOT to the origin of the brachiocephalic trunk at anatomic locations: 1. left ventricular outflow tract (LVOT), 0.5 cm beneath the neo-aortic valve (AoV) level; 2. AoV; 3. neo-aortic root (Root); 4. STJ, for TGA patients defined as the aortic level 5-7 mm below the pulmonary artery bifurcation; 5. mid-AAo, at the level of the pulmonary artery bifurcation; 6. distal ascending aorta-1 (dAAo-1), at 1/3 distance between plane 5 and plane 8, calculated from plane 5; 7. distal ascending aorta-2 (dAAo-2), at 2/3 distance between plane 5 and plane 8, calculated from plane 5; 8. proximal to the origin of the brachiocephalic trunk (AAo-BCT) (Figure 1D).

Normalized systolic flow displacement (FD) was calculated in each of the cross-sectional planes according to a method previously described by Sigovan et al.<sup>20</sup> (Figure 1E). Briefly, FD is defined as the distance between the anatomical center of the vessel and the center velocity ( $C_{vel}$ ) of the flow at peak systole, normalized to the vessel lumen diameter. The vessel lumen diameter was automatically identified on 2D analysis planes by the CAAS MR software and manual delineation of the vessel lumen boundary was performed with the available adaptation tool from the software in case of incorrectness. To determine the center of velocity the next equation was used:

$$C_{vel,j} = \frac{\sum_i r_{i,j} |v_i|}{\sum_i |v_i|}, i = \text{lumen pixels}; j = x, y, z \text{ positions}; v_i = \text{velocity}$$

The vessel circumference was divided into eight equally-sized segments (octants) and for each patient the direction of FD in each cross-sectional plane was qualitatively assessed (A = anterior, LA = left-anterior, L = left, LP = left-posterior, P = posterior, RP = right-posterior, R = right, RA = right-anterior) (Figure 1E).

Peak systolic WSS was calculated for eight aortic wall segments from the cross-sectional planes 3-8 (i.e. from the neo-aortic root to the origin of the brachiocephalic trunk) (Figure 1F). The systolic WSS was calculated based on the extracted velocity profile perpendicular to the phase-specific 3D aortic surface. After factorizing the velocity profile into its component parallel to the aortic lumen wall, the systolic WSS was computed by the first derivative of a quadratic approximation of that velocity profile at the location of the aortic lumen wall.<sup>16</sup>

Similarities between the location of FD and the location of the highest systolic WSS were evaluated by determining the absolute difference between these locations. The number of octant positions clockwise or counterclockwise away from the position of the FD location

was calculated and categorized as follow: 0 = no difference in location; 1 = difference of 1 octant position; 2 = difference of 2 octant positions; 3 = difference of 3 octant positions; 4 = difference of 4 octant positions. A difference  $\leq 1$  octant position was defined as good to excellent. In case of no relationship, a Gaussian (nonskewed) distribution of the absolute differences is expected, with a nonsignificant result from the normality test.

### **Statistical analysis**

Statistical analyses were performed using IBM SPSS Statistics version 23 (IBM, Chicago, IL, USA). Variables are presented as mean  $\pm$  standard deviation or median [interquartile range, IQR] if not normally distributed. A Shapiro-Wilk test was used to test variables for normal distribution. A chi-square test was performed to investigate differences in gender distribution between TGA patients and healthy subjects. To compare normally distributed parameters between TGA patients and healthy subjects an unpaired *t*-test was used. An interobserver reproducibility analysis was performed for the aortic diameter measurements. For comparison of differences in magnitude of FD and regional aortic WSS between the TGA patients and healthy subjects a Mann Whitney test was used. A chi-square test was performed to investigate differences in FD directionality between TGA patients and healthy subjects and within the TGA patients based on the preoperative spatial position of the great arteries. The relationship between aortic Z-score and FD was investigated using correlation analysis based on linear regression (Spearman's correlation). Correlation analysis based on linear regression (Spearman's correlation) was also performed to assess the effect of aortic geometry (aortic diameter ratio between neo-aortic root and mid-AAo) and WSS parameters. To evaluate distribution normality on the absolute differences in octant location between flow displacement in root, STJ and mid-AAo and location of highest peak systolic WSS at mid-AAo level, a Shapiro-Wilk test was performed and skewness and kurtosis markers were calculated.  $P < 0.05$  was considered significant for all statistical tests. A Bonferroni correction was performed to adjust for the multiple comparisons for the planar WSS analysis along the AAo and differences between groups were considered significant for  $P < 0.00104$ .

## **Results**

Baseline and surgical characteristics are presented in Table 1. No significant differences between TGA patients and healthy subjects were observed except for age. All patients and healthy subjects had a normal systolic left ventricular function. The proximal ascending aorta in TGA patients, including the indexed neo-aortic valve annulus, neo-aortic root and STJ, was significantly larger and dilated compared with healthy subjects. Using a Z-score  $>2.0$  to define aortic dilatation, 25 patients (89%) had neo-aortic root dilatation and 19 of the TGA patients (68%) had dilatation of the STJ. In contrast, the diameter of the mid-AAo, the location where the pulmonary arteries embrace the ascending aorta from anterior in TGA patients, was significantly smaller in TGA patients compared with healthy subjects (mid-AAo: 17.0 [16.0-18.3] vs 20.5 [18.0-21.6] mm/m<sup>2</sup>,  $P = 0.001$ ; mid-AAo Z-score  $0.32 \pm 3.06$

**Table 1.** Baseline characteristics and MRI measurements

	TGA patients (n = 28)	Healthy subjects (n = 10)	P value
<b>Patient and surgical characteristics</b>			
Male, n (%)	18 (64.3)	5 (50.0)	0.473
Age, years	16.0 ± 3.3	27.3 [24.9-28.4]	<0.001
Weight, kg	60.5 ± 14.0	68.3 ± 12.7	0.129
Height, cm	170.8 ± 12.2	175.6 ± 6.6	0.250
Body surface area, m <sup>2</sup>	1.7 ± 0.2	1.8 ± 0.2	0.137
LV ejection fraction, %	59.1 ± 5.7	62.0 ± 2.5	0.155
<b>Surgical variables</b>			
Age at ASO, days	6.0 [4.0-10.0]		
Weight at ASO, kg	3.5 ± 0.5		
Lecompte maneuver, n (%)	28 (100)		
<b>Transposition type, n (%)</b>			
TGA-IVS	21 (75.0)		
TGA-VSD	7 (25.0)		
<b>Great artery position, n (%)</b>			
Aorta right anterior to PA	15 (53.6)		
Aorta right side to PA	3 (10.7)		
Aorta anterior to PA	7 (25.0)		
Aorta left anterior to PA	3 (10.7)		
<b>Aortic diameters (mm/ BSA<sup>0.5</sup>)<sup>a</sup></b>			
Neo-aortic valve annulus	18.8 [17.4-20.1]	15.2 [13.9-17.4]	<0.001
Neo-aortic root sagittal	28.0 [25.7-29.7]	23.1 [21.0-24.2]	<0.001
Neo-aortic root short-axis, mean	27.2 [26.3-30.6]	22.4 [21.5-22.9]	<0.001
Sinotubular junction	20.6 [19.7-24.0]	19.2 [17.2-20.2]	0.008
Mid ascending aorta	17.0 [16.0-18.3]	20.5 [18.0-21.6]	0.001
Origin of BCT	17.2 [15.5-18.1]	18.0 [16.3-18.9]	0.142
<b>Aortic Z-scores<sup>b</sup></b>			
Neo-aortic root short-axis, mean	4.38 ± 1.96	1.52 ± 0.70	<0.001
Sinotubular junction	3.48 ± 2.67	1.38 ± 1.30	0.010
Mid ascending aorta	0.32 ± 3.06	1.69 ± 1.24	0.001
Origin of BCT	-0.52 ± 1.21	0.20 ± 1.29	0.122

<sup>a</sup>Data are presented as median [interquartile range]. <sup>b</sup>Data are presented as mean ± SD. ASO, arterial switch operation; BCT, brachiocephalic trunk; BSA, body surface area; IVS, intact ventricular septum; LV, left ventricular; PA, pulmonary artery; TGA, transposition of the great arteries; VSD, ventricular septal defect.

vs  $1.69 \pm 1.24$ ,  $P = 0.001$ ). The interobserver reproducibility analysis showed an excellent agreement between the aortic measurements of the observers: mean difference 0.18 mm, limits of agreement ( $\pm 2$  SD) of 3.9 mm; coefficient of variation 3.2%; intraclass correlation coefficient: 0.979 (95% confidence interval [CI] 0.969-0.986); correlation:  $r = 0.96$ ,  $P < 0.001$ .

### Aortic flow displacement

The group-averaged magnitude of FD along the entire ascending aorta for both TGA patients and healthy subjects is illustrated in Figure 2. Flow displacement magnitude was significantly higher in TGA patients compared with the healthy subjects at the level of the neo-aortic root (FD  $0.048 \pm 0.027$  vs  $0.021 \pm 0.006$ ,  $P < 0.001$ ) and STJ (FD  $0.054 \pm 0.037$  vs  $0.029 \pm 0.013$ ,  $P < 0.05$ ). No differences in FD magnitude were found at the mid-AAo level (TGA vs healthy subjects: FD  $0.050 \pm 0.034$  vs  $0.033 \pm 0.021$ ,  $P = 0.083$ ).

Flow displacement direction and magnitude for all individual patients and healthy subjects were depicted for three adjacent aortic planes (root, STJ, and mid-AAo) in Figure 3. The FD direction in the ascending neo-aorta in TGA patients (root and mid-AAo) was different compared with healthy subjects (Figure 3; Root  $P = 0.024$ , mid-AAo  $P = 0.002$ ).

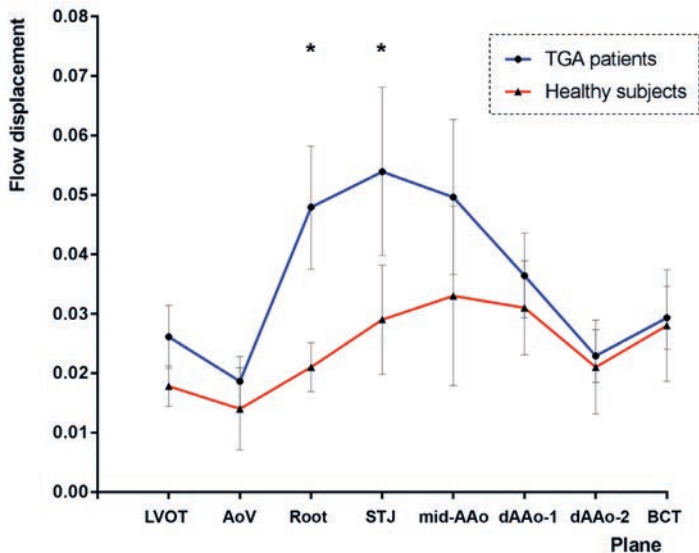


**Figure 2.** Flow displacement along the ascending aorta.

Group averaged flow displacement along the ascending aorta (mean, 95% CI) at aortic levels as stated in Figure 1D. \*  $P < 0.05$ .

AoV, neo-aortic valve; BCT, distal ascending aorta proximal to the origin of the brachiocephalic trunk; dAAo-1, distal ascending aorta at 1/3 distance between 'mid-AAo plane' and 'BCT plane'; dAAo-2, distal ascending aorta at 2/3 distance between 'mid-AAo plane' and 'BCT plane'; LVOT, left ventricular outflow tract; mid-AAo, mid ascending aorta; Root, neo-aortic root; STJ, sinotubular junction.

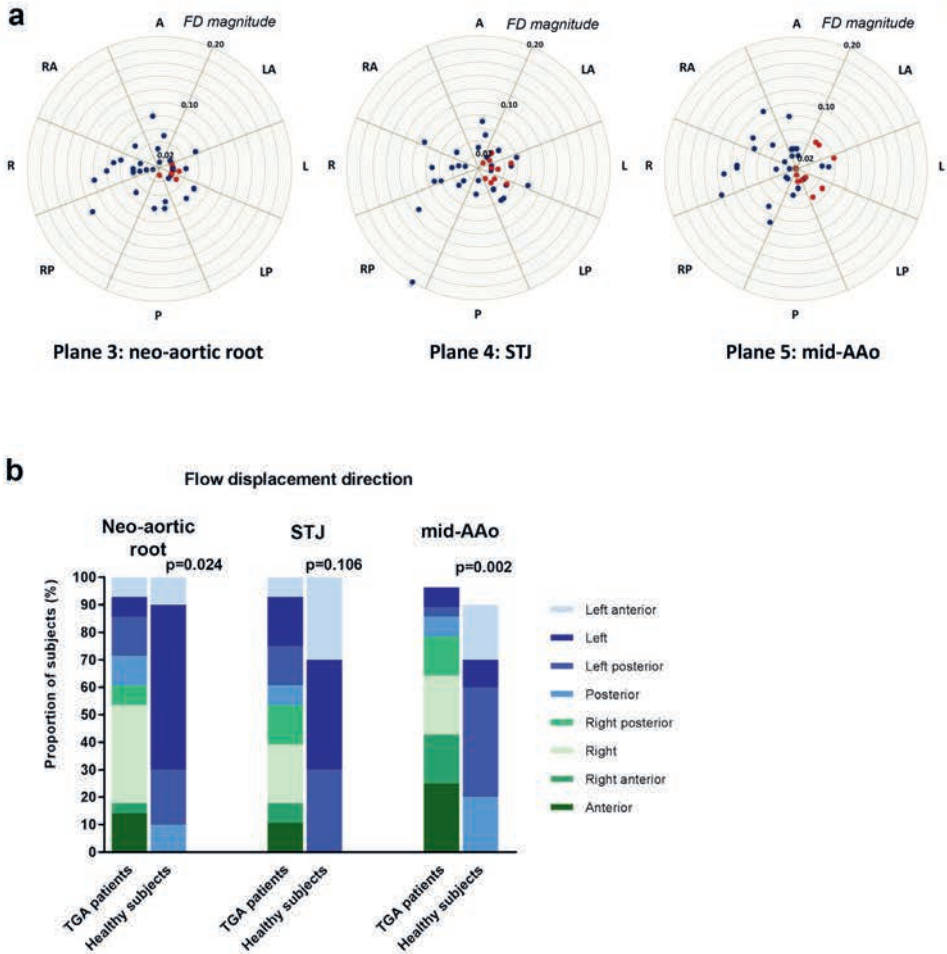


**Figure 3.** Flow displacement magnitude and direction profiles.

Each dot represents the peak systolic flow displacement direction (i.e. octant location) and magnitude per subject (i.e. FD magnitude increasing from inner (0) to outer circle (0.20)): TGA patients (blue dots), healthy subjects (red dots) (A). Flow displacement direction per octant in TGA patients ( $n = 28$ ) vs healthy subjects ( $n = 10$ ) (B). Of note, FD direction analysis for the mid-AAo plane is presented for 27 TGA patients and nine healthy subjects because of no FD in two subjects, one in each group.

FD, normalized flow displacement; mid-AAo, mid-ascending aorta; STJ, sinotubular junction; TGA, transposition of the great arteries.



Healthy subjects showed a primarily central and central-left orientated (left-anterior, left or left-posterior) aortic flow at the root, STJ and mid-AAo levels, whereas the TGA patients showed a more heterogeneous flow direction, both left- and rightward orientated in the root that shifted more to anterior and right side from root to the mid-AAo (Figure 3). Differences in FD direction between TGA patient subgroups based on preoperative great artery position were observed in the neo-aortic root (Figure 4). TGA patients with a right-anterior or right-sided position of the aorta related to the pulmonary artery ( $n = 18$ ) showed more FD to the right-side of the AAo, whereas a left-anterior or anterior position of the aorta ( $n = 10$ ) resulted in more FD to the left-side of the aortic wall at the level of the neo-aortic root ( $P = 0.025$ ) (Figure 4). At the level of the STJ and mid-AAo this difference in FD direction could not be statistically detected (STJ,  $P = 0.148$ ; mid-AAo,  $P = 0.738$ ).

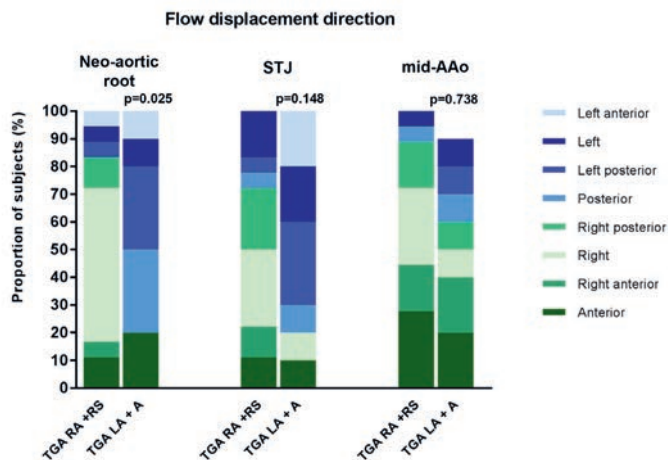


**Figure 4.** Flow displacement direction per octant in TGA subgroups.

TGA patients are divided into subgroups based on great artery position before arterial switch operation (aorta related to pulmonary trunk). Group 1 (TGA RA + RS) consists of TGA patients with the aorta right-anterior (RA) or right-sided (RS) to the pulmonary trunk ( $n = 18$ ). Group 2 (TGA LA + A) consists of TGA patients with the aorta anterior (A) or left-anterior (LA) to the pulmonary trunk ( $n = 10$ ). Of note, FD direction for the mid-AAo plane is presented in nine TGA LA+A patients because of no FD in 1 TGA LA+A patient.

A, anterior; LA, left-anterior; RA, right anterior; RS, right-sided; TGA, transposition of the great arteries.

### Ascending aortic WSS assessment

The systolic WSS distribution along the ascending aorta showed distinct differences between the TGA patients and the healthy subjects. In the proximal ascending aortic segment (plane 3-4: root and STJ) the systolic WSS in the TGA patients was evenly distributed along the circumference of the aortic wall and WSS was low. In specific regions at these levels (root and STJ) significantly lower WSS was found compared with the healthy subjects (Figure 5, plane 3-4: root and STJ).

In TGA patients, significantly higher and highly asymmetric peak systolic WSS was detected in the distal ascending aortic segments, at and beyond the level of the embracement of the ascending aorta by the pulmonary artery branches (plane 6-8: dAAo-1, dAAo-2, and AAO-BCT) (Figure 5). At these distal AAO planes, the distribution of the systolic WSS in the TGA patients was uneven, with the most pronounced significantly increased peak systolic WSS in the anterior regions (right-anterior, anterior and left-anterior,  $P \leq 0.001$ ). In healthy subjects there was no increase in systolic WSS in the distal part of the ascending aorta (Figure 5).

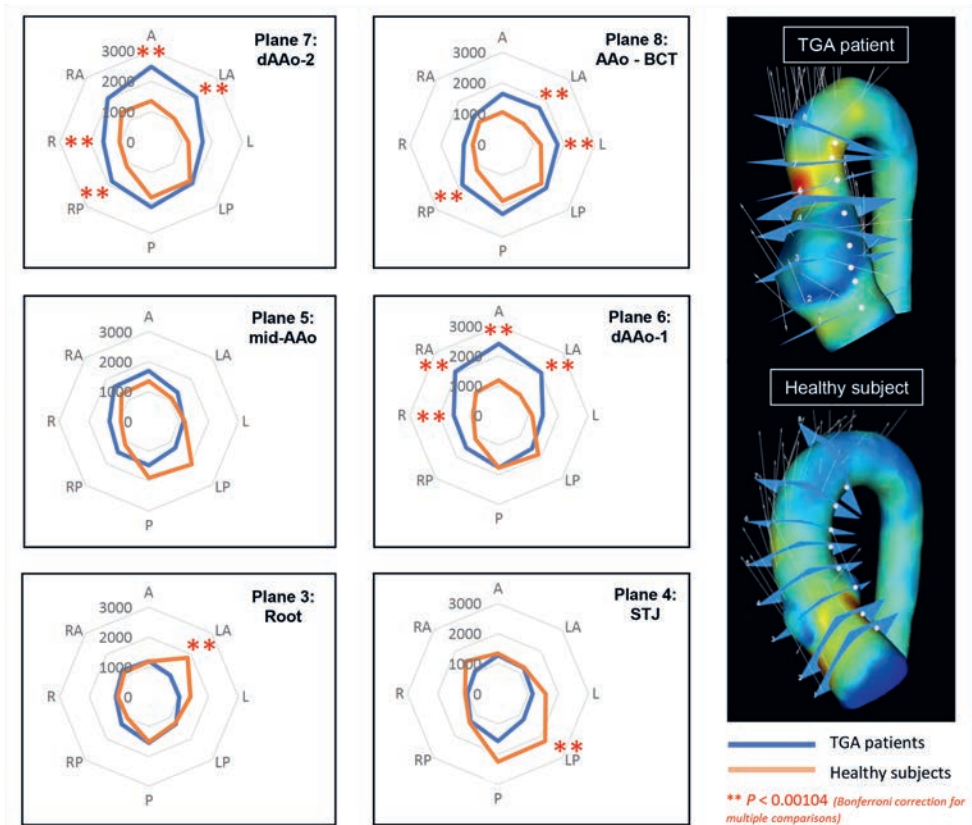


**Figure 5.** Planar aortic WSS assessment along the ascending aorta in TGA patients and healthy subjects. Wall shear stress in mPa. Mann Whitney test for comparison of differences in regional aortic WSS between the TGA patients and healthy subjects. Differences between the groups were considered significant for  $P < 0.00104$  (Bonferroni correction for multiple comparisons). AAO-BCT, distal ascending aorta proximal to the origin of the brachiocephalic trunk; dAAo-1, distal ascending aorta at 1/3 distance between plane 5 'mid-AAo' and plane 8 'AAo-BCT'; dAAo-2, distal ascending aorta at 2/3 distance between plane 5 'mid-AAo' and plane 8 'AAo-BCT'; mid-AAo, mid ascending aorta; Root, neo-aortic root; STJ, sinotubular junction; TGA, transposition of the great arteries.

### Flow displacement, WSS and correlations with aortic geometry

In the entire study cohort (TGA patients and healthy subjects), FD magnitude showed a moderate positive linear relationship with the neo-aortic Z-score at the level of the neo-aortic root and STJ ( $r = 0.54$ ,  $P < 0.001$  and  $r = 0.54$ ,  $P < 0.001$ , respectively; Figure 6).

The octant location of FD in the root, STJ, and mid-AAo matched the location of maximum systolic WSS at mid-AAo level. The distribution of absolute differences in FD location (root, STJ, and mid-AAo) vs WSS location at mid-AAo level was skewed. In approximately 60% of the TGA patients, absolute differences in location between FD and WSS were 0 or 1 octant, representing no differences (Figure 7). TGA patients showed a predominant FD direction in the anterior and rightward orientation (right, right-anterior, anterior) from root to mid-AAo plane levels with elevated maximum systolic WSS in the anterior to right anterior locations from the mid- to distal AAo planes (Figure 3 and 7A). Wall shear stress magnitude in the distal ascending aortic planes showed a moderate positive linear relationship with the change in aortic dimension between the root and mid-AAo in TGA patients (Figure 8). A more pronounced increase in peak systolic WSS in those regions was detected in the patients with relatively small mid-AAo diameter compared with the neo-aortic root. The association between WSS magnitude and vessel diameter change was found for the right, right-anterior and anterior regions from the distal AAo planes (dAAo-1 and dAAo-2) (Figure 8), which corresponds with the regions where TGA patients showed highly asymmetric and elevated peak systolic WSS.

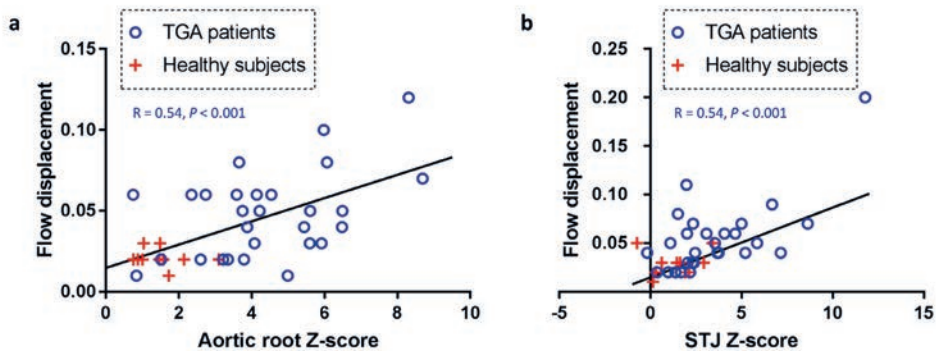


**Figure 6.** Relationship between aortic Z-score and normalized flow displacement in the proximal ascending aorta.

Aortic root: Z-score vs FD (A). STJ: Z-score vs FD (B).

STJ, sinotubular junction; TGA, transposition of the great arteries.

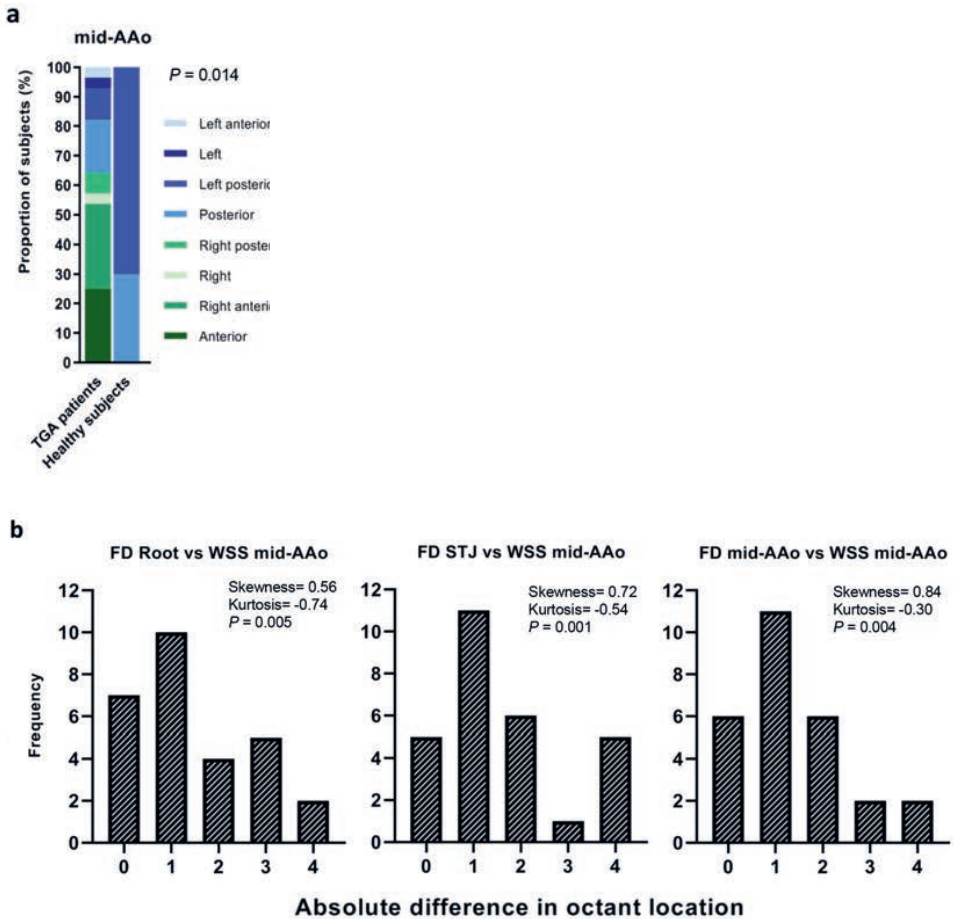


**Figure 7.** Location of peak systolic WSS (mid-AAo) and the relation with flow displacement direction in the proximal ascending aorta.

Location of peak systolic WSS at mid-AAo level in TGA patients and healthy subjects (A). Frequency histograms on the distribution of the absolute differences in octant location between FD (root, STJ, and mid-AAo) and the location peak systolic WSS (mid-AAo) in TGA patients (B). Normality tested by Shapiro-Wilk test. Of note, absolute differences in octant location between FD and WSS at the mid-AAo are presented for 27 TGA patients because of no FD in one TGA patient.

FD, normalized flow displacement; mid-AAo, mid-ascending aorta; Root, neo-aortic root; STJ, sinotubular junction; TGA, transposition of the great arteries; WSS, wall shear stress.

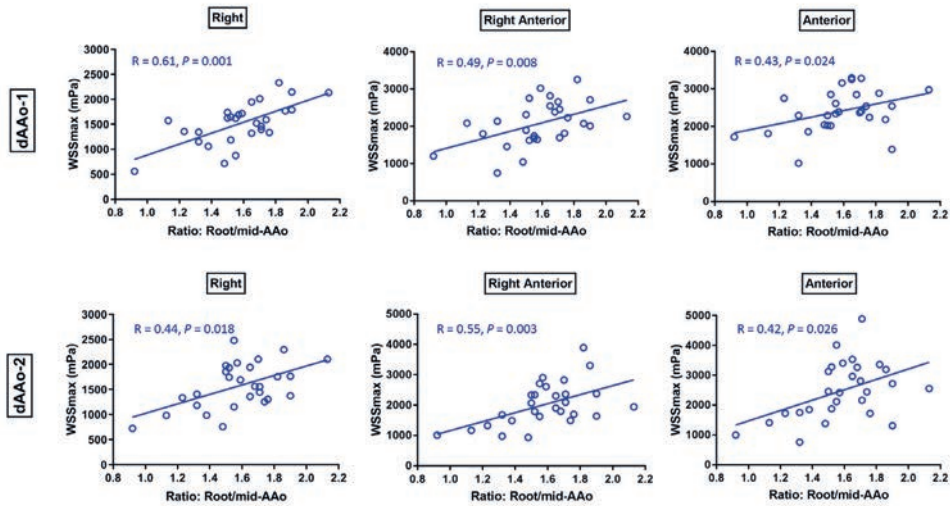


**Figure 8.** Relationship between aortic diameter change and wall shear stress along the distal ascending aorta. Diameter change between neo-aortic root and mid-ascending aorta represented as Root/mid-AAo ratio. Peak systolic wall shear stress (WSSmax) for the right, right-anterior and anterior regions along the distal ascending aorta (cross-sectional plane 6: dAAo-1 and plane 7: dAAo-2, as illustrated in Figure 1D).

## Discussion

The results of this study demonstrate a more eccentric aortic flow in the proximal ascending aorta in TGA patients compared with healthy subjects. TGA-specific preoperative position of the great arteries showed different directionality of the eccentric flow profiles and the magnitude of the eccentric flow was linearly related with the local aortic Z-scores. The ASO-specific geometry consisted of neo-aortic root dilatation and a sudden change in vessel diameter at mid-ascending aortic level, the level of anterior aortic compression by the pulmonary trunk. This sudden change in aortic diameter was associated with increased and asymmetric peak systolic WSS distribution along the distal ascending aorta, most pronounced in the right and anterior aortic wall regions (right, right-anterior and anterior regions). The flow displacement direction from root to mid-AAo also corresponded to the peak systolic WSS distribution in the mid-AAo, but the contribution of FD on WSS distribution more upstream in the distal AAO was less compared with the effect of vessel tapering. The regions of abnormal increased WSS in the distal AAO clinically correlates with the location of the paper-thin and fragile anterior wall of the AAO that has been found in ASO patients during root reoperations.<sup>21, 22</sup>

Neo-aortic root dilatation is a key problem in long-term follow-up in patients after ASO for TGA because of its ongoing progression beyond the age of 18 years.<sup>2, 3, 23</sup> The neo-aortic root after ASO dilates and elongates and the STJ becomes more distally-displaced over time.<sup>24</sup> Similar to previous findings,<sup>2, 5</sup> the geometric alterations in the proximal ascending

aorta with neo-aortic root dilatation were accompanied by the relatively narrow mid-ascending aortic segments in this study, due to the anterior impression of the ascending aorta by the pulmonary trunk following Lecompte maneuver.

Mechanisms leading to progressive dilatation and elongation are not fully understood. Based on unoperated heart specimen with TGA, it is suggested that the arterial root in TGA patients has a diminished amount and altered distribution of collagen and that the root and left-sided semilunar valve are less firmly embedded in the myocardium,<sup>25</sup> which potentially makes the arterial root of these patients more susceptible for aortic dilatation after ASO. Semilunar valve diameters in TGA fetus are proven to be larger than in normal fetal hearts and the prenatal pulmonary valve size has been associated with neo-aortic root dilatation in the first years post-ASO.<sup>26</sup> Furthermore, it is known that abnormal blood flow may affect vessel wall tissue and may impact neo-aortic root dilatation as well.<sup>13</sup> Hemodynamic factors derived from 4D flow MRI, including flow eccentricity and WSS, have been associated with aortic diameter progression and vascular wall remodeling in patients with bicuspid aortic valve related aortopathy respectively.<sup>12,13</sup> This study shows that children and adolescent TGA patients after ASO have an eccentric systolic flow in the ascending aorta: regions of most prominent flow eccentricity were detected at the level of the neo-aortic root and STJ. Consistent with the results of studies in patients with a bicuspid aortic valve,<sup>12,27</sup> we found a close linear relationship between aortic dimensions and the normalized FD. In one of these studies, systolic FD was correlated with future ascending aortic growth in patients with bicuspid valve anatomy.<sup>12</sup> Despite the correlations found in this and other studies, longitudinal studies in patients after ASO are needed to assess the causative role of systolic FD for progressive neo-aortic root dilatation. Furthermore, the TGA-specific preoperative spatial position of the great arteries showed to be a factor for different directionality of the eccentric flow profiles in the neo-aortic root. Most likely this is the result of a different angulation between the neo-aortic valve and the newly formed STJ, depending on the location from where the aorta needs to be transposed on top of the neo-aortic root, stressing the influence of geometry on flow deviation within the ascending aorta. Next to this, a cardiac MRI study showed that a more acute aortic arch angulation, as is typical in post-ASO aortic geometry, is a risk factor for the development of root dilatation and valve regurgitation.<sup>28</sup>

A comparative computational fluid dynamic (CFD) and *in vitro* 4D flow MRI phantom study on the thoracic aorta from a single TGA case after ASO supports the findings of our study.<sup>29</sup> In the TGA model (derived from a 15-year-old patient) appreciable less symmetrical flow, with a skewed peak of flow velocity in the ascending aorta, was observed compared with the aortic model of a healthy subject, in which the higher velocities were clustered around the center of the neo-aortic root. In line with the finding of our study, there was a flow jet impingement at the top of the TGA anterior root with a higher WSS in the anterior ascending aortic wall.

In TGA patients, WSS analysis showed in general a more evenly distributed and regionally lower WSS in the dilated root compared with the healthy subjects and clear areas of higher WSS at the right and anterior aortic wall regions from the mid-aortic level and above. The

displacement of flow away from the aortic centerline and directed more towards the vessel wall in the proximal ascending aorta, together with a sudden change in vessel geometry at mid-ascending aortic level, most likely causes an increase in velocity with a higher near-wall velocity gradient resulting in elevated WSS in the right and anterior wall regions of the distal AAO.

The geometric shape of the aorta with its typical appearance after ASO has proved to be one of the most influential factors on blood flow and WSS in aortic flow simulations.<sup>30</sup> The CFD investigation on TGA models after ASO about the influence of geometric changes in the thoracic aorta on the blood flow and WSS reported a large curvature near the aortic root as a distinctive characteristic of the post-ASO geometry.<sup>30</sup> The WSS assessment in the TGA aortic models of that study revealed significantly higher maximum WSS values than in the healthy aortic model, comparable with the findings in this study. The maximum WSS was located in either the ascending aorta or the aortic arch, depending on the degree of aortic torsion and curvature of the two assessed TGA models.<sup>30</sup> The relationship between the degree of aortic diameter reduction at mid-AAo level and WSS in the anterior regions of the distal ascending aorta found in our study supports the hypothesis that in TGA patients after ASO aortic blood flow physiology (expressed in advanced hemodynamic parameters) is altered due to a changed geometry.

Currently, no cases have been documented with aortic rupture or dissection after ASO, but in several re-operated patients the anterior wall of the aneurysmatic aorta was observed to be paper-thin and fragile.<sup>21,22</sup> These regions correspond to the areas of elevated WSS, as found in our study, and the combined CFD and *in vitro* 4D flow study by Biglino et al.<sup>29</sup> Whether this hemodynamic parameter may add to the prediction of progressive aortic dilatation, aortic wall thinning, or imply a higher lifetime risk on adverse aortic events (aortic rupture or dissection) at that site is unknown and requires further longitudinal follow-up. This is of high importance as, to date, indications for reoperation for neo-aortic root dilatation after ASO to prevent rupture, dissection or progressive neo-aortic regurgitation are unclear. Moreover, extending knowledge on pathophysiologic mechanisms of altered flow hemodynamics on disease progression is necessary, to get better insight and to think about alternative surgical techniques solving long-term residual sequelae in patients with TGA. In this regard, an alternative surgical technique has been described for TGA which preserves a more physiologic spiral anatomy of the great arteries, without applying Lecompte maneuver.<sup>31</sup> Although not frequently applied worldwide and technically not applicable for every TGA patient, results from *in vivo* 4D flow studies in these patients 20 years after ASO reported more physiological aortic blood flow in the great arteries compared with patients who underwent a Lecompte procedure during ASO.<sup>32</sup> These results, together with the results of this study, in which we showed already the presence of abnormal aortic flow hemodynamics in young patients after ASO, suggest aortic geometry as an important factor for altered flow hemodynamics. Although aortic geometry seems to contribute to altered flow hemodynamics, due to the measurements at a single timepoint, it is unknown if the altered FD and WSS are the result of progressive aortic dilatation, or if in any way these

altered hemodynamics were causative to the dilatation. Additional 4D flow studies evaluating the interindividual differences in aortic hemodynamics between TGA patients with different anatomy (i.e. with or without VSD, with different spatial position of the great arteries) and between TGA patients with different surgical ASO techniques (i.e. with and without Lecompte maneuver) need to be performed to optimize management strategies for the best long-term outcomes.

The current study is subject to some limitations. Healthy subjects who were used as a reference group were older compared with the TGA patients included in this study. This might have an impact on the Z-scores that were somewhat larger than expected in the healthy subjects group by the use of the MRI-derived normative data with an age range up to 20 years.<sup>19</sup> While the MRI-derived normative dataset is based on a small population of children and uses nongated contrast-enhanced MRA images, there is currently no larger combined pediatric and adolescent MRI-specific database and this method of normalization is the best available alternative. In addition, the velocity of the aortic flow will decrease with increasing age,<sup>33</sup> which could have lowered the WSS results in healthy subjects, as WSS is closely related to velocity since it is a derivative of velocity.<sup>34, 35</sup> However, the relative small age difference between the adolescent TGA patient group and the healthy young adult subjects is not expected to lead to large differences in mean velocity according to the study on the distribution of velocity in the normal aorta over age by Garcia et al.<sup>33</sup> Therefore, only small differences in WSS are to be expected based on the age difference. These differences do not exceed the WSS differences that have been found between younger TGA patients and healthy subjects, neither will they explain the WSS asymmetry results in this study. Moreover, in healthy adolescents and young adults flow velocity distribution descriptors indicating velocity symmetry and shape (i.e. skewness and kurtosis) only started to increase significantly beyond the age of 40 years.<sup>33</sup> Hence, small differences in age between TGA patients and the healthy control group in this study will not have affected normalized FD measures.

Because of the limited spatial resolution of 4D flow MRI, WSS is known to be underestimated. However, all MR acquisitions in both TGA and healthy subjects were made at the same MR scanner with the same imaging parameters, so differences between groups remain useful. Moreover, patients were analyzed with the software for which a 3D WSS reproducibility analysis study showed robustness of the segmentation and WSS analysis method.<sup>16</sup> Furthermore, the robustness and reproducibility of 2D WSS analysis in cross-sectional planes has been previously demonstrated.<sup>36</sup> However, WSS determination in the neo-aortic root remains a challenge because of the aortic motion and the presence of slow and recirculating flow. Although we did perform a time-resolved segmentation method to account for aortic motion,<sup>16</sup> small border errors may be present for the calculated WSS in the neo-aortic root region, implying that it may not actually reflect the stress on the wall.

In conclusion, TGA patients after ASO have more flow asymmetry in the proximal AAO evidenced by a higher magnitude and directionality of FD, related to increased proximal AAO Z-scores. TGA-specific geometry related to the ASO, with neo-aortic root dilatation and



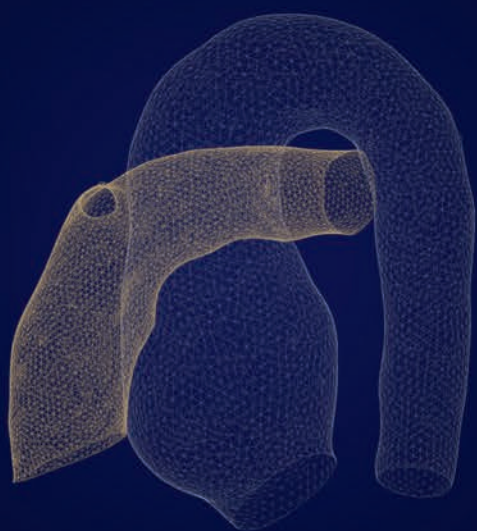
a sudden change in vessel diameter at mid-AAo level, leads to specific WSS distribution along the AAo in TGA patients that is different with higher WSS compared with healthy subjects. Our observations only start to unravel the interaction between the post-ASO geometry and hemodynamics within the ascending aorta and how the hemodynamics may be involved in the (progression of) neo-aortic root dilatation. Therefore, longitudinal follow-up studies are needed for correlation between changes in systolic WSS and progression of dilatation and to assess the consequence of the increased WSS and its WSS extent on the distal AAo.

## References

1. Jatene AD, Fontes VF, Paulista PP, de Souza LC, Neger F, Galantier M, Souza JE. Successful anatomic correction of transposition of the great vessels. A preliminary report. *Arq Bras Cardiol.* 1975;28(4):461-64.
2. Shepard CW, Germanakis I, White MT, Powell AJ, Co-Vu J, Geva T. Cardiovascular Magnetic Resonance Findings Late After the Arterial Switch Operation. *Circ Cardiovasc Imaging.* 2016;9(9).
3. van der Palen RLF, van der Bom T, Dekker A, Tsonaka R, van Geloven N, Kuipers IM, Konings TC, Rammeloo LAJ, Ten Harkel ADJ, Jongbloed MRM, et al. Progression of aortic root dilatation and aortic valve regurgitation after the arterial switch operation. *Heart.* 2019;105(22):1732-40.
4. Geiger J, Hirtler D, Burk J, Stiller B, Arnold R, Jung B, Langer M, Markl M. Postoperative pulmonary and aortic 3D haemodynamics in patients after repair of transposition of the great arteries. *Eur Radiol.* 2014;24(1):200-8.
5. Ntsinjana HN, Capelli C, Biglino G, Cook AC, Tann O, Derrick G, Taylor AM, Schievano S. 3D morphometric analysis of the arterial switch operation using in vivo MRI data. *Clin Anat.* 2014;27(8):1212-22.
6. Dyverfeldt P, Bissell M, Barker AJ, Bolger AF, Carlhall CJ, Ebberts T, Francios CJ, Frydrychowicz A, Geiger J, Giese D, et al. 4D flow cardiovascular magnetic resonance consensus statement. *J Cardiovasc Magn Reson.* 2015;17:72.
7. Frydrychowicz A, Markl M, Hirtler D, Harloff A, Schlensak C, Geiger J, Stiller B, Arnold R. Aortic hemodynamics in patients with and without repair of aortic coarctation: in vivo analysis by 4D flow-sensitive magnetic resonance imaging. *Invest Radiol.* 2011;46(5):317-25.
8. van der Palen RL, Barker AJ, Bollache E, Garcia J, Rose MJ, van Ooij P, Young LT, Roest AA, Markl M, Robinson JD, et al. Altered aortic 3D hemodynamics and geometry in pediatric Marfan syndrome patients. *J Cardiovasc Magn Reson.* 2017;19(1):30.
9. van Ooij P, Markl M, Collins JD, Carr JC, Rigsby C, Bonow RO, Malaisrie SC, McCarthy PM, Fedak PWM, Barker AJ. Aortic Valve Stenosis Alters Expression of Regional Aortic Wall Shear Stress: New Insights From a 4-Dimensional Flow Magnetic Resonance Imaging Study of 571 Subjects. *J Am Heart Assoc.* 2017;6(9).
10. Bissell MM, Hess AT, Biasioli L, Glaze SJ, Loudon M, Pitcher A, Davis A, Prendergast B, Markl M, Barker AJ, et al. Aortic dilation in bicuspid aortic valve disease: flow pattern is a major contributor and differs with valve fusion type. *Circ Cardiovasc Imaging.* 2013;6(4):499-507.
11. Mahadevia R, Barker AJ, Schnell S, Entezari P, Kansal P, Fedak PW, Malaisrie SC, McCarthy P, Collins J, Carr J, et al. Bicuspid aortic cusp fusion morphology alters aortic three-dimensional outflow patterns, wall shear stress, and expression of aortopathy. *Circulation.* 2014;129(6):673-82.
12. Burris NS, Sigovan M, Knauer HA, Tseng EE, Saloner D, Hope MD. Systolic flow displacement correlates with future ascending aortic growth in patients with bicuspid aortic valves undergoing magnetic resonance surveillance. *Invest Radiol.* 2014;49(10):635-9.
13. Guzzardi DG, Barker AJ, van Ooij P, Malaisrie SC, Puthumana JJ, Belke DD, Mewhort HE, Svystonyuk DA, Kang S, Verma S, et al. Valve-Related Hemodynamics Mediate Human Bicuspid Aortopathy: Insights From Wall Shear Stress Mapping. *J Am Coll Cardiol.* 2015;66(8):892-900.
14. Bousset L, Rayz V, McCulloch C, Martin A, Acevedo-Bolton G, Lawton M, Higashida R, Smith WS, Young WL, Saloner D. Aneurysm growth occurs at region of low wall shear stress: patient-specific correlation of hemodynamics and growth in a longitudinal study. *Stroke.* 2008;39(11):2997-3002.
15. Burk J, Blanke P, Stankovic Z, Barker A, Russe M, Geiger J, Frydrychowicz A, Langer M, Markl M. Evaluation of 3D blood flow patterns and wall shear stress in the normal and dilated thoracic aorta using flow-sensitive 4D CMR. *J Cardiovasc Magn Reson.* 2012;14:84.
16. van der Palen RLF, Roest AAW, van den Boogaard PJ, de Roos A, Blom NA, Westenberg JJM. Scan-rescan reproducibility of segmental aortic wall shear stress as assessed by phase-specific segmentation with 4D flow MRI in healthy volunteers. *MAGMA.* 2018;31(5):653-63.

17. van Kesteren F, Elattar MA, van Lienden KP, Baan J, Jr., Marquering HA, Planken RN. Non-contrast enhanced navigator-gated balanced steady state free precession magnetic resonance angiography as a preferred magnetic resonance technique for assessment of the thoracic aorta. *Clin Radiol*. 2017;72(8):695 e1- e6.
18. Hiratzka LF, Bakris GL, Beckman JA, Bersin RM, Carr VF, Casey DE, Jr., Eagle KA, Hermann LK, Isselbacher EM, Kazerooni EA, et al. 2010 ACCF/AHA/AATS/ACR/ASA/SCA/SCAI/SIR/STS/SVM Guidelines for the diagnosis and management of patients with thoracic aortic disease. A Report of the American College of Cardiology Foundation/American Heart Association Task Force on Practice Guidelines, American Association for Thoracic Surgery, American College of Radiology, American Stroke Association, Society of Cardiovascular Anesthesiologists, Society for Cardiovascular Angiography and Interventions, Society of Interventional Radiology, Society of Thoracic Surgeons, and Society for Vascular Medicine. *J Am Coll Cardiol*. 2010;55(14):e27-e129.
19. Kaiser T, Kellenberger CJ, Albisetti M, Bergstrasser E, Valsangiacomo Buechel ER. Normal values for aortic diameters in children and adolescents--assessment in vivo by contrast-enhanced CMR-angiography. *J Cardiovasc Magn Reson*. 2008;10:56.
20. Sigovan M, Hope MD, Dyverfeldt P, Saloner D. Comparison of four-dimensional flow parameters for quantification of flow eccentricity in the ascending aorta. *J Magn Reson Imaging*. 2011;34(5):1226-30.
21. Koolbergen DR, Manshanden JS, Yazdanbakhsh AP, Bouma BJ, Blom NA, de Mol BA, Mulder BJ, Hazekamp MG. Reoperation for neo-aortic root pathology after the arterial switch operation. *Eur J Cardiothorac Surg*. 2014;46(3):474-9.
22. Vida VL, Zanotto L, Zanotto L, Stellin G, European Congenital Heart Surgeons Association Study G, Padalino M, Sarris G, Protopapas E, Prospero C, Pizarro C, et al. Left-Sided Reoperations After Arterial Switch Operation: A European Multicenter Study. *Ann Thorac Surg*. 2017;104(3):899-906.
23. van der Bom T, van der Palen RL, Bouma BJ, van Veldhuisen SL, Vliegen HW, Konings TC, Zwinderman AH, Blom NA, Koolbergen DR, Hazekamp MG, et al. Persistent neo-aortic growth during adulthood in patients after an arterial switch operation. *Heart*. 2014;100(17):1360-5.
24. Jhang WK, Shin HJ, Park JJ, Yun TJ, Kim YH, Ko JK, Park IS, Seo DM. The importance of neo-aortic root geometry in the arterial switch operation with the trap-door technique in the subsequent development of aortic valve regurgitation. *Eur J Cardiothorac Surg*. 2012;42(5):794-9.
25. Lalezari S, Mahtab EA, Bartelings MM, Wisse LJ, Hazekamp MG, Gittenberger-de Groot AC. The outflow tract in transposition of the great arteries: an anatomic and morphologic study. *Ann Thorac Surg*. 2009;88(4):1300-5.
26. van der Palen RLF, van der Zee C, Vink AS, Knobbe I, Jurgens SJ, van Leeuwen E, Bax CJ, du Marchie Sarvaas GJ, Blom NA, Haak MC, et al. Transposition of the great arteries: Fetal pulmonary valve growth and postoperative neo-aortic root dilatation. *Prenat Diagn*. 2019;39(12):1054-63.
27. Raghav V, Barker AJ, Mangiameli D, Mirabella L, Markl M, Yoganathan AP. Valve mediated hemodynamics and their association with distal ascending aortic diameter in bicuspid aortic valve subjects. *J Magn Reson Imaging*. 2018;47(1):246-54.
28. Martins D, Khraiche D, Legendre A, Boddaert N, Raisky O, Bonnet D, Raimondi F. Aortic angle is associated with neo-aortic root dilatation and regurgitation following arterial switch operation. *Int J Cardiol*. 2019;280:53-6.
29. Biglino G, Cosentino D, Steeden JA, De Nova L, Castelli M, Ntsinjana H, Pennati G, Taylor AM, Schievano S. Using 4D Cardiovascular Magnetic Resonance Imaging to Validate Computational Fluid Dynamics: A Case Study. *Front Pediatr*. 2015;3:107.
30. Fukui T, Asama H, Kimura M, Itoi T, Morinishi K. Influence of Geometric Changes in the Thoracic Aorta due to Arterial Switch Operations on the Wall Shear Stress Distribution. *Open Biomed Eng J*. 2017;11:9-16.
31. Chiu IS, Wu SJ, Chen MR, Lee ML, Wu MH, Wang JK, Lue HC. Modified arterial switch operation by spiral reconstruction of the great arteries in transposition. *Ann Thorac Surg*. 2000;69(6):1887-92.
32. Rickers C, Kheradvar A, Sievers HH, Falahatpisheh A, Wegner P, Gabbert D, Jerosch-Herold M, Hart C, Voges I, Putman LM, et al. Is the Lecompte technique the last word on transposition of the great arteries repair for all patients? A magnetic resonance imaging study including a spiral technique two decades postoperatively. *Interact Cardiovasc Thorac Surg*. 2016;22(6):817-25.

33. Garcia J, van der Palen RLF, Bollache E, Jarvis K, Rose MJ, Barker AJ, Collins JD, Carr JC, Robinson J, Rigsby CK, et al. Distribution of blood flow velocity in the normal aorta: Effect of age and gender. *J Magn Reson Imaging*. 2018;47(2):487-98.
34. Allen BD, van Ooij P, Barker AJ, Carr M, Gabbour M, Schnell S, Jarvis KB, Carr JC, Markl M, Rigsby C, et al. Thoracic aorta 3D hemodynamics in pediatric and young adult patients with bicuspid aortic valve. *J Magn Reson Imaging*. 2015;42(4):954-63.
35. van Ooij P, Garcia J, Potters WV, Malaisrie SC, Collins JD, Carr JC, Markl M, Barker AJ. Age-related changes in aortic 3D blood flow velocities and wall shear stress: Implications for the identification of altered hemodynamics in patients with aortic valve disease. *J Magn Reson Imaging*. 2016;43(5):1239-49.
36. Markl M, Wallis W, Harloff A. Reproducibility of flow and wall shear stress analysis using flow-sensitive four-dimensional MRI. *J Magn Reson Imaging*. 2011;33(4):988-94.



## **CHAPTER 8**

# Wall shear stress in the thoracic aorta at rest and with dobutamine stress after arterial switch operation

European Journal of Cardio-Thoracic Surgery. 2021;59:814-22

Roel L.F. van der Palen  
Joe F. Juffermans  
Lucia J.M. Kroft  
Mark G. Hazekamp  
Hildo J. Lamb  
Nico A. Blom  
Arno A.W. Roest  
Jos J.M. Westenberg

## Abstract

### Objectives

Progressive root dilatation is an important complication in patients with transposition of the great arteries (TGA) after arterial switch operation (ASO) that may be caused by altered flow dynamics. Aortic wall shear stress (WSS) distribution at rest and under dobutamine stress (DS) conditions using 4D flow magnetic resonance imaging (MRI) were investigated in relation to thoracic aorta geometry.

### Methods

4D flow MRI was performed in sixteen adolescent TGA patients after ASO (rest and DS condition) and in ten healthy controls (rest). The primary outcome measure was the WSS distribution along the aortic segments and the WSS change with DS in TGA patients. Based on the results, we secondary zoomed in on factors (aortic geometry and left ventricular (LV) function) parameters) that might relate to these WSS distribution differences. Aortic diameters, arch angle, LV function parameters (stroke volume, LV ejection fraction, cardiac output) and peak systolic aortic WSS were obtained.

### Results

TGA patients had significantly larger neo-aortic root and smaller mid-ascending aorta (AAo) dimensions and aortic arch angle. At rest, patients had significantly higher WSS in the entire thoracic aorta, except for the dilated root. High WSS levels beyond the proximal AAo were associated with the diameter decrease from the root to the mid-AAo (correlation coefficient  $r = 0.54-0.59$ ,  $P = 0.022-0.031$ ), not associated with the aortic arch angle. During DS, WSS increased in all aortic segments ( $P < 0.001$ ), most pronounced in the AAo segments. The increase in LV ejection fraction, stroke volume and cardiac output as a result of DS showed a moderate linear relationship with the WSS increase in the distal AAo (correlation coefficient  $r = 0.54-0.57$ ,  $P = 0.002-0.038$ ).

### Conclusions

Increased aortic WSS was observed in TGA patients after ASO, related to the ASO-specific geometry, which increased with DS. Stress-enhanced elevated WSS may play a role in neo-aortic root dilatation and anterior aortic wall thinning of the distal AAo.

## Introduction

The arterial switch operation (ASO) is the current treatment for patients with transposition of the great arteries (TGA). This surgical intervention restores the ventriculoarterial concordance by reconnecting the great arteries to the correct ventricles leaving the semilunar valves and the native root in its original position. The relocation of the great arteries following ASO results in an altered spatial great artery relationship and geometry of the thoracic aorta. With the Lecompte maneuver, the pulmonary artery bifurcation is positioned in front of the ascending aorta with the pulmonary artery branches embracing the ascending aorta resulting in a more posterior location of the ascending aorta post-ASO. Consequently, an acute angulation of the curvature of the aortic arch is often present after ASO.<sup>1,2</sup>

In the long term, progressive neo-aortic root dilatation occurs accompanied by an increasing incidence of neo-aortic valve leakage in these patients.<sup>3,4</sup> Furthermore, cardiothoracic surgeons have observed thinning of the anterior wall of the ascending aorta in adult post-ASO patients who underwent reoperation for the aneurysmatic neo-aortic root dilatation,<sup>5,6</sup> closely related to the location of the pulmonary arteries. It is largely unknown what mechanisms contribute to the progression of neo-aortic root dilatation and anterior wall thinning, but geometry-driven alterations in aortic flow might have its impact on the (neo-)aortic wall. This relationship has been shown in bicuspid aortic valve-related aortopathy<sup>7</sup> but has not been extensively evaluated in TGA patients post-ASO so far.<sup>8</sup>

With 4D flow magnetic resonance imaging (MRI), blood flow and hemodynamic parameters in large vessels can be visualized and quantified and this imaging modality facilitates studying the relation and interaction of aorta geometry and blood flow on the aortic wall (i.e. wall shear stress, WSS). Currently, almost all patient studies using 4D flow MRI have been performed in rest states. However, it is unknown how aortic blood flow hemodynamics behave with an increase in cardiac output (CO) and whether changes in stroke volume (SV) may add to changes in hemodynamic parameters. Low-dose dobutamine increases heart rate, myocardial contractility and ventricular ejection by stimulating  $\beta$ -1 receptors on the heart and allows studying aortic hemodynamics under increased SV conditions using MRI.

We hypothesize that evaluation of hemodynamics of the thoracic aortic reveals specific areas with abnormal WSS that increase under pharmacological-induced stress conditions and may help to better understand blood flow interactions on the aortic vessel wall in patients with repaired congenital heart diseases with altered aortic geometry. Therefore, the aim of this study was to evaluate aortic WSS in the thoracic aorta of patients with TGA after ASO with comparative rest and pharmacological stress 4D flow MRI investigations.



## Methods

### Study population

The study protocol was approved by the local Medical Ethics Committee and informed consent was obtained from all patients and their legal guardians. Sixteen patients with TGA and intact ventricular septum or TGA with ventricular septal defect were prospectively included in the study between January 2016 and December 2017. Patients from outpatient pediatric and congenital cardiology clinics who needed a standard-of-care MRI of the heart and large vessels as regular clinical follow-up for early detection of well-known sequelae after ASO from the age of 10 years were invited to participate. To ensure morphologic homogeneity, exclusion criteria were Taussig-Bing anomaly, prior left ventricular (LV) outflow tract obstruction, bicuspid neo-aortic valve, aortic arch obstruction, presence of branch pulmonary artery stent(s), moderate-to-severe neo-aortic insufficiency or prior neo-aortic valve or root reoperations. All patients underwent aortic 4D flow MRI at rest and during dobutamine-induced stress immediately following the standard-of-care MRI assessment. The healthy subjects were recruited from a prior 4D flow MRI validation study<sup>9</sup> and served as a reference group. They underwent the same MRI protocol including 4D flow aortic imaging (only at rest).

### Magnetic resonance imaging acquisition

All MRI examinations were performed on a 3T scanner (Ingenia, Philips Healthcare, the Netherlands). The protocol included ECG-gated two-dimensional cine steady-state free precession (SSFP) imaging for ventricular and functional analysis at rest and during dobutamine stress. At rest, a three-dimensional (3D) non-contrast-enhanced magnetic resonance angiography (NCE-MRA) was performed for the assessment of thoracic aorta diameters and aortic arch geometry. 4D flow MRI covering the thoracic aorta was acquired at rest and during dobutamine stress condition. MRI acquisitions details are summarized in supplementary Table S1. Dobutamine was administered intravenously starting at a dose of 5.0 µg/kg/min, and the dose was increased to 7.5 µg/kg/min after 3 min followed by a 5-10 min observation period waiting for a steady state of patients' heart rate and blood pressure.

### Aortic geometry and cardiac function

Left ventricular indices [end-systolic and end-diastolic volume (LVESV and LVEDV)] and LV function parameters [SV, LV ejection fraction (LVEF), CO and cardiac index] were obtained from short-axis SSFP-images:

$$\begin{aligned} \text{Stroke volume} &= \text{LVEDV} - \text{LVESV}; & \text{LVEF} &= 100 * \frac{\text{stroke volume}}{\text{LVEDV}}; \\ \text{CO} &= \text{SV} * \text{heart rate}; & \text{Cardiac Index} &= \frac{\text{CO}}{\text{Body Surface Area}} \end{aligned}$$

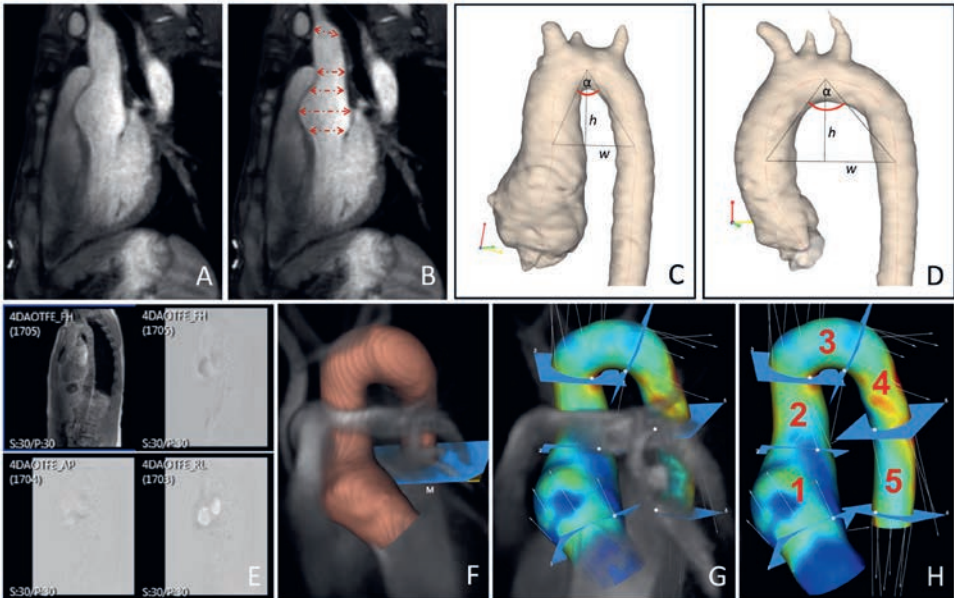


**Figure 1.** Workflow aortic geometry and 4D flow analysis.

Non-contrast enhanced magnetic resonance angiography (NCE-MRA) (A) with aortic diameter measurements (B). Aortic segmentation from NCE-MRA of a TGA patient (C) and healthy subject (D) with centerline creation, aortic width ( $w$ ), height ( $h$ ) and aortic arch angle ( $\alpha$ ) measurement. Raw 4D flow MRI data (E) used to create a 3D aortic segmentation (F). Visualization of anatomical great artery relation with the peak systolic aortic WSS (G). Thoracic aorta subdivision into 5 segments (H).

Aortic diameters were measured from NCE-MRA at 6 anatomic landmarks: 1. neo-aortic root (Root); 2. sinotubular junction, defined as the aortic level 5-7 mm below the pulmonary artery bifurcation; 3. mid-ascending aorta at the level of the pulmonary artery bifurcation (mid-AAo); 4. aorta at the origin of the innominate artery; 5. aortic isthmus; 6. mid-descending aorta (Figure 1A-B). Aortic dimensions were measured from external-to-external edges from a sagittal-axis orientation. Average neo-aortic root diameters (average of three cuspto-commissure dimensions) were measured perpendicular to the aortic axis on NCE-MRA double oblique transversal angulated multiplanar reconstructions. Diameters were indexed to body surface area and converted into Z-scores.<sup>10</sup> Aortic diameter ratio between the neo-aortic root diameter and the mid-AAo diameter was calculated:  $\left(\frac{\text{Root}}{\text{mid-AAo}}\right)$ .

Aortic arch geometry was obtained from NCE-MRA. After aortic segmentation using Enterprise Suite v6.5 (Vital Images, Minnetonka, USA) and automatic computation of the centerline of the aorta segmentations, the aortic arch width ( $w$ ), maximal height ( $h$ , perpendicular to the width) and aortic arch angle ( $\alpha$ , between mid-AAo, maximal height and mid-descending aorta) were quantified (Figure 1C-D) using an in-house developed software (Python Software Foundation, Wolfeboro Falls, NH, USA). Width-height ( $w/h$ ) ratio was calculated accordingly.

### Segmental WSS assessment

The software program CAAS MR 4D flow v2.0 (Pie Medical Imaging BV, Maastricht, the Netherlands) was used for post-processing of the 4D flow MRI data, for which a 3D WSS reproducibility analysis study showed robustness of the segmentation and WSS analysis method.<sup>9</sup> A summary of the workflow analysis is depicted in Figure 1E-H, and was previously described in detail.<sup>9</sup> Briefly, from the 4D flow dataset peak systolic thoracic aortic segmentations were performed and provided with an aortic centerline (Figure 1E-F). For the regional aortic wall shear stress (WSS) assessment, the thoracic aorta was manually subdivided into 5 segments based on anatomic landmarks by placing planes perpendicular to the aortic centerline (Figure 1G): segment 1: proximal ascending aorta (pAAo, from aortic valve level to mid-AAo); segment 2: distal ascending aorta (dAAo, from mid-AAo to innominate artery); segment 3: aortic arch (Arch, from the innominate artery until left subclavian artery); segment 4: proximal descending aorta (pDAo, beyond the left subclavian artery to the mid-descending thoracic aorta); and segment 5: distal descending aorta (dDAo, from mid-descending thoracic aorta to the descending aorta at the level of the aortic valve). For every aortic segment, mean 3D systolic WSS (WSS<sub>mean</sub>) and maximum 3D systolic WSS (WSS<sub>max</sub>) values were calculated as described previously (Figure 1H).<sup>9</sup> Wall shear stress is defined as the derivative of the axial velocity  $u$  at the vascular wall in the direction perpendicular to the vascular wall times the dynamic viscosity  $\mu$  ( $WSS = \mu \frac{\partial u}{\partial y} \Big|_{y=0}$  (in mPa)). The surface of the 3D segmented aorta was divided into wall points, and for all wall points, a 3D systolic WSS vector was calculated based on a quadratic approximation of the axial velocity profile perpendicular to the surface of the 3D segmented aorta.<sup>9</sup> WSS<sub>max</sub> was then defined as the maximum WSS vector of all wall points within the defined aortic segment (in mPa). WSS<sub>mean</sub> was defined as the average of all WSS vectors of all wall points within the defined aortic segment (in mPa). Differences in WSS ( $\Delta WSS$ ) and percentage WSS changes (%WSS) between rest and stress state were calculated for each segment:

$$\Delta WSS = WSS_{stress} - WSS_{rest}; \quad \%WSS = \frac{WSS_{stress} - WSS_{rest}}{WSS_{rest}}$$

### Statistical analysis

Statistical analyses were performed using IBM SPSS Statistics version 23 (IBM, Chicago, IL, USA). Variables are presented as mean  $\pm$  standard deviation or median (interquartile range, IQR) depending on the normality of the distribution. The normality of the distribution was tested using the Shapiro-Wilk test. The primary outcome measure was the WSS distribution along the aortic segments and the WSS change with dobutamine stress in TGA patients. Based on the results, we secondary zoomed in on factors (aortic geometry and LV function parameters) that might relate to these WSS distribution differences. A power calculation was performed to determine the power to detect differences in the WSS values between the rest and dobutamine stress measurements (primary outcome measure). Based on the WSS magnitude known in the healthy pediatric and adult population, study sample sizes to

show a 20% difference (difference of clinical interest; estimated mean difference in WSSmean 400 Pa; estimated standard deviation 100 Pa) in these variables with a power of 90% and a  $\alpha$  error of 0.01 (to correct for multiple comparison according to the Bonferroni correction) must contain a minimum of 6 TGA patients. The power analysis was performed for the paired t-test (because of the unknown shape of the underlying distribution) (Division of Biomathematics/Biostatistics, Columbia University Medical Center, New York, USA; <http://biomath.info/power>). Using the rule of thumb because of using a non-parametric test, we added 15% to the sample size required for a parametric test, resulting in a study sample size of at least 7 to 8 patients.

A chi-square test was performed to investigate differences in sex distribution between TGA patients and healthy subjects. Differences between groups were compared using the independent sample t-test or a Mann Whitney test based on the normality of the distribution. Differences in cardiac parameters between rest and dobutamine stress were tested by a paired t-test; in case of non-normality, the Wilcoxon signed-rank test was performed. A Friedman test was performed to test for differences in the percentage increase in WSS from rest to stress state between the 5 aortic segments. A Bonferroni correction was performed to adjust for the multiple comparisons for the WSS analysis along aortic segments between groups, between rest and dobutamine stress in TGA patients and for the percentage WSS increase from rest to stress between the 5 aortic segments. Correlation between aortic geometry measures (root/mid-AAo diameter ratio, arch angle and *w/h* ratio) and segmental aortic WSS were calculated using Spearman rank correlation. Correlation between percentage WSSmean increase and percentage increase in LV function parameters (EF, SV, CO) were calculated using Pearson's correlation. A *P* value <0.05 was considered statistically significant.

## Results

### Aortic geometry

Patient characteristics are shown in Table 1. Indexed neo-aortic root and sinotubular junction dimensions (Z-scores) were significantly larger in TGA patients compared to healthy subjects. Neo-aortic root and sinotubular junction were dilated (Z-score >2.0) in 94% and 81% of the TGA patients respectively. Patients without aortic Z-score >2.0 had also large indexed neo-aortic root and sinotubular junction dimensions with Z-scores  $\geq 1.7$ , except for one patient. The mid-AAo diameter was significantly smaller in TGA patients. Other thoracic aortic dimensions were within the normal range compared with the MRI-based healthy reference population (Z-score <2.0). Aortic arch geometry descriptors showed that the aortic arch height was comparable between TGA patients and healthy subjects. The aortic arch angle, aortic width and *w/h* ratio were significantly smaller in TGA patients.

**Table 1.** Baseline characteristics and MRI measurements

	TGA patients (n = 16)	Healthy subjects (n = 10)	P value
<b>Patient and surgical characteristics</b>			
Male, n (%)	11 (68.8)	5 (50.0)	0.339
Age, years <sup>a</sup>	16.5 [14.4-18.8]	27.3 [24.9-28.4]	<0.001
Weight, kg	63.8 ± 14.0	68.3 ± 12.7	0.419
Height, cm	173.4 ± 12.7	175.6 ± 6.6	0.571
BSA, m <sup>2</sup>	1.75 ± 0.25	1.8 ± 0.20	0.452
<b>Transposition type, n (%)</b>			
TGA-IVS	12 (75.0)		
TGA-VSD	4 (25.0)		
<b>Coronary artery anatomy, n (%)*</b>			
1LCx-2R	11 (68.8)		
1L-2CxR	2 (12.5)		
1L-2R, no Cx	2 (12.5)		
1RL-2Cx	1 (6.3)		
<b>Surgical variables</b>			
Age at ASO, days (range)	8 (1-70)		
Previous surgery prior to ASO, n (%)	1 (6.3)		
Lecompte maneuver, n (%)	16 (100)		
Coronary artery transfer technique, n (%)			
Double button	6 (37.5)		
Single button, single trapdoor	7 (43.8)		
Double trapdoor	3 (18.8)		
<b>Aortic diameters (mm/BSA<sup>0.5</sup>)</b>			
Neo-aortic root sagittal	21.4 ± 3.2	17.0 ± 1.5	0.001
Neo-aortic root short-axis, mean	21.7 ± 3.0	16.7 ± 0.9	<0.001
Sinotubular junction	16.9 ± 3.0	14.1 ± 1.6	0.013
Mid ascending aorta <sup>a</sup>	12.7 [12.0-14.9]	15.1 [13.6-16.3]	0.035
Origin of brachiocephalic trunk	13.0 ± 1.6	13.2 ± 1.2	0.755
Aortic isthmus	12.6 ± 1.6	11.1 ± 1.1	0.018
Mid descending aorta	10.0 ± 1.3	10.2 ± 0.6	0.526
<b>Aortic Z-scores</b>			
Neo-aortic root short-axis, mean	4.8 ± 1.6	1.5 ± 0.7	<0.001
Sinotubular junction	3.6 ± 2.3	1.4 ± 1.3	0.011
Mid-ascending aorta <sup>a</sup>	-0.3 [-1.0-0.3]	1.8 [0.2-2.7]	0.005
Origin of brachiocephalic trunk	-0.5 ± 1.5	0.2 ± 1.3	0.217
Aortic isthmus	2.2 ± 1.2	0.8 ± 1.4	0.013
Mid-descending aorta	-0.3 ± 0.9	0.2 ± 0.6	0.197
<b>Aortic arch geometry</b>			
Arch width	41.3 ± 5.1	58.4 ± 7.4	<0.001
Arch height	31.0 ± 5.5	34.0 ± 3.3	0.132
Arch angle (°)	66.6 ± 8.2	80.1 ± 7.4	<0.001
Width/Height ratio	1.4 ± 0.2	1.7 ± 0.2	0.001

<sup>a</sup> Data are presented as median [Interquartile range]. \* Coronary artery anatomy description according to the Leiden Convention coronary coding system. BSA, body surface area; IVS, intact ventricular septum; TGA, transposition of the great arteries; VSD, ventricular septal defect.

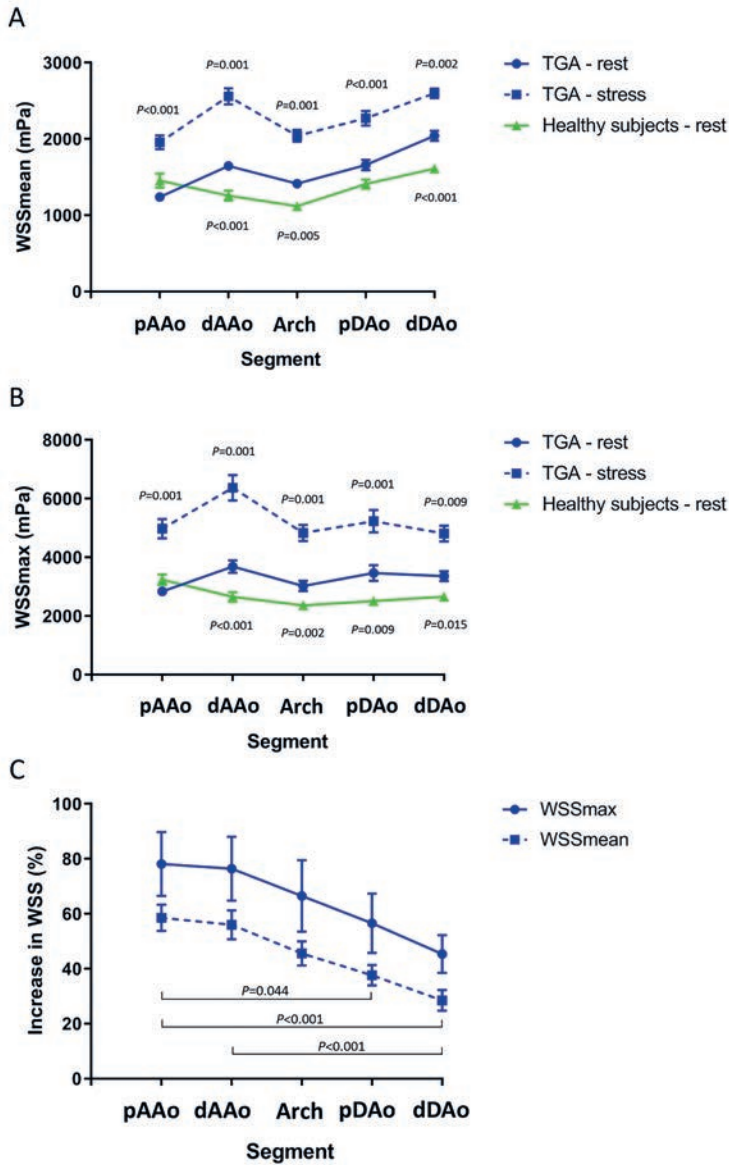


**Figure 2.** Aortic wall shear stress assessment at rest and during dobutamine stress. WSSmean (A) and WSSmax (B) values (mean  $\pm$  standard error of the mean) along the thoracic aortic segments in TGA patients (rest and stress) and compared with healthy subjects (rest). Adjusted *P* values (Bonferroni correction) of the corresponding lines represent the results of the WSS comparison with the TGA patients at rest (only significant *P* values are depicted). Percentage WSS increase between rest and dobutamine stress for each of the thoracic aortic segments (C). Differences in %WSS increase between the 5 segments for WSSmax: *P* = 0.19; for WSSmean: *P* < 0.001 (Friedman test). Brackets with adjusted *P* values (Dunn's pairwise post hoc test with Bonferroni correction) are depicted to indicate statistical significance for differences in %WSSmean increase between the aortic segments. dAAo, distal ascending aorta; dDAo, distal descending aorta; pAAo, proximal ascending aorta; pDAo, proximal descending aorta; TGA, transposition of the great arteries; WSS, wall shear stress.

### **Thoracic aortic WSS at rest and correlation with geometry**

Figure 2A-B illustrates the aortic WSS along the entire thoracic aortic segments and shows the regional differences in WSS<sub>mean</sub> and WSS<sub>max</sub> between TGA patients and healthy subjects. At rest, TGA patients showed significantly higher WSS in almost all thoracic aortic segments ( $P < 0.001 - P = 0.015$ ), except for the pAAo segment (for WSS<sub>mean</sub> and WSS<sub>max</sub>) and pDAo (for WSS<sub>mean</sub>) (Figure 2A-B). In TGA patients, WSS magnitude (WSS<sub>mean</sub> and WSS<sub>max</sub>) was lowest in the dilated pAAo while the highest WSS<sub>max</sub> levels were found in the dAAo segment. Along the thoracic aorta, the trend (i.e. increase or decrease) of the WSS<sub>mean</sub> and WSS<sub>max</sub> between the aortic segments also differed between TGA patients and healthy subjects. In the healthy subjects, there was a WSS decrease from the pAAo segment to the aortic arch segment, with a WSS increase beyond the aortic arch (Figure 2A-B). In TGA patients, there was a significant WSS increase from the pAAo to the dAAo segment ( $P < 0.001$  for WSS<sub>mean</sub>;  $P = 0.003$  for WSS<sub>max</sub>) with a concomitant WSS decrease in the aortic arch segment compared with the dAAo segment (Figure 2A-B). Beyond the aortic arch, in the descending thoracic aorta, there was overall an increase in WSS<sub>mean</sub> and WSS<sub>max</sub> between the consecutive segments comparable to the trend found in healthy subjects, but on a higher WSS level.

At rest, WSS<sub>mean</sub> in the dAAo segment, but also in the descending aortic segments, showed a moderate linear relationship with the change in aortic dimension between the neo-aortic root and mid-AAo, as expressed as the root/mid-AAo ratio (Figure 3). A higher systolic WSS<sub>mean</sub> was detected in the patients with relatively small mid-AAo diameters compared with the neo-aortic root dimensions. In general, the aortic arch geometry descriptors, arch angle and  $w/h$  ratio, did not show a relationship with the WSS parameters from the aortic arch and descending aortic segments (supplementary Table S2). Only for WSS<sub>max</sub> in the distal DAo segment, an association was observed with the arch geometry (angle: correlation coefficient  $r = 0.58$ ,  $P = 0.020$  and  $w/h$  ratio: correlation coefficient  $r = 0.54$ ,  $P = 0.032$ ).

### **Dobutamine-stress induced changes in LV function parameters**

At rest, no significant differences between TGA patients and healthy subjects were observed in cardiac parameters, except for heart rate and cardiac index (supplementary Table S3). All patients received maximum dobutamine dosage (7.5  $\mu\text{g}/\text{kg}/\text{min}$ ) without any adverse effects. In the entire TGA group, heart rate, blood pressure and the LV functional parameters derived from MRI, SV and CO, significantly increased from rest to stress state (supplementary Table S3). Fourteen TGA patients had a normal systolic LV function ( $\text{EF} \geq 55\%$ ) and two patients slightly below normal ( $\text{EF} 51\%$  and  $54\%$ ) without regional wall motion abnormalities. No significant neo-aortic regurgitation was present in the patients. All healthy subjects had an  $\text{EF} \geq 55\%$ .

### **Stress-induced changes in aortic WSS and correlation with LV function parameters**

During dobutamine stress, the trend in WSS between the aortic segments remained similar but with significantly higher WSS in all aortic segments compared with the levels at rest

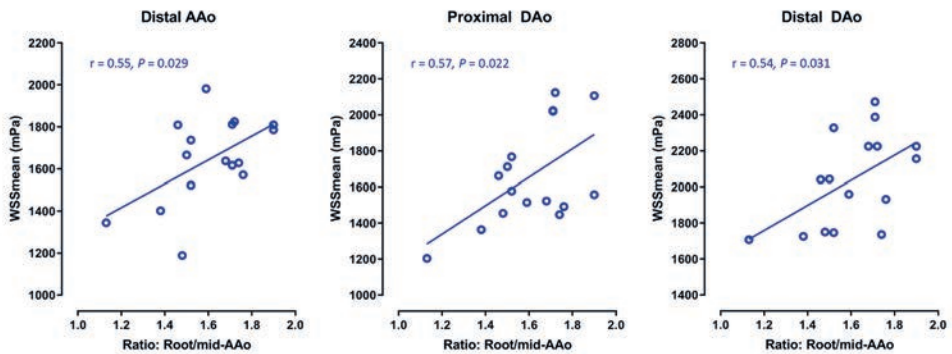


**Figure 3.** Relationship between ascending aortic diameter change and WSSmean at rest along the thoracic aorta. Spearman correlation coefficient ( $r$ ). AAO, ascending aorta; DAO, descending aorta; WSS, wall shear stress.

state ( $P < 0.001 - P = 0.009$ , for WSSmax and WSSmean) (Figure 2A-B). The highest absolute WSSmean and WSSmax values were detected in the dAAo segment. The percentage WSS increase from rest to stress state was highest for the ascending aortic segments (pAAo and dAAo) with a WSS increase between 56-78% (Figure 2C). The percentage WSS increase was the most pronounced for WSSmax and high but to a lesser extent present for WSSmean (for pAAo and dAAo: WSSmax 78% and 76%; WSSmean 58% and 56%, respectively). The dobutamine-induced percentage WSS increase diminished for the consecutive aortic segments beyond the ascending aortic segments (Figure 2C).

All TGA patients showed more or less similar WSS patterns with an increased WSS area at the anterior wall of the dAAo segment, on top of the anterior root. This area of high WSS was present at rest and during dobutamine stress and the area of high WSS also extended over the anterior wall of the dAAo (Figure 4, example of single patient). The WSS distribution in the dAAo segments was asymmetric and more expressed on the anterior wall, and more symmetrically distributed over the aortic wall of descending aortic segments as suggested by the lower magnitude of WSSmax and the higher magnitude of WSSmean in the descending aortic segments as compared with the ascending aortic segments (Figure 2A-B).

The percentage increase of peak systolic WSSmean in the dAAo segment with stress showed a moderate positive linear relationship with the percentage increase in parameters EF, SV and CO as a result of dobutamine (Figure 5). Cardiac output and EF showed the best association with the percentage increase in WSSmean (correlation coefficient  $r = 0.59, P = 0.016$  and correlation coefficient  $r = 0.70, P = 0.002$ , respectively). Arch geometric descriptors did not show significant associations with WSS in aortic segments during dobutamine stress (supplementary Table S2).



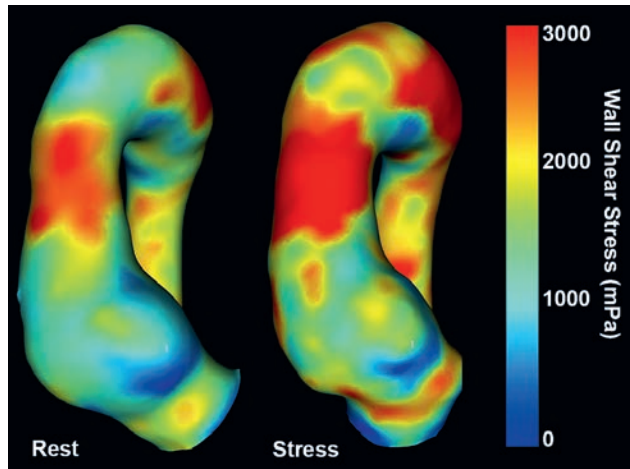


**Figure 4.** Peak systolic 3D wall shear stress visualization (anterior aortic view) in single a TGA case - rest vs stress

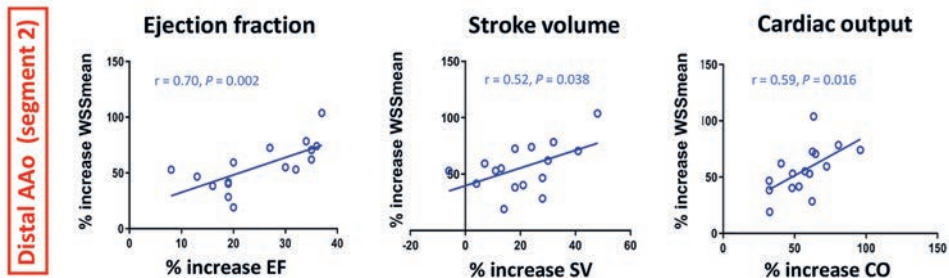


**Figure 5.** Correlation between increase in WSSmean in the distal AAo and ejection fraction, stroke volume, and cardiac output under dobutamine infusion.

Pearson correlation coefficient ( $r$ ).

AAo, ascending aorta; CO, cardiac output; EF, ejection fraction; SV, stroke volume; WSS, wall shear stress.

## Discussion

This study evaluated the thoracic aortic WSS in TGA patients after ASO. The effect of pharmacological-derived stress on aortic WSS was studied *in vivo* and was compared with the rest state. The main findings of this study demonstrate that patients after ASO have a significantly higher WSS magnitude in the entire thoracic aorta compared with healthy subjects at rest, except for the dilated proximal AAo. The regions of high peak systolic WSS were most pronounced in the distal AAo and located at the anterior aortic wall of that segment. The specific ascending aortic geometry post-ASO, reflected by the size discrepancy

between the dilated neo-aortic root and the smaller mid-AAo diameter, was associated with higher WSS levels in the aortic segments downstream this caliber change: the larger the size discrepancy, the higher the WSS levels in the distal AAO, but also in the descending aortic segments. In addition to this association, the geometry of the aortic arch did not further contribute to the high WSS levels in the aortic arch and the descending aortic segments. Dobutamine-induced cardiac stress did increase WSS magnitude significantly along all thoracic aortic segments, the most prominent in the AAO. The highest peak systolic WSS was present in the distal AAO segment during both rest and stress, but for stress, this was even more pronounced. The peak systolic WSS increase by dobutamine in that segment showed a positive correlation with the increase in the LVEF, SV and CO.

The results of this study extend the findings reported previously.<sup>8</sup> In addition to the increased WSS in the distal AAO segment, significantly higher WSS values at rest were observed in the aortic segments beyond the distal AAO (the arch and descending aortic segments), segments of the aorta remote from the dilated neo-aortic root and not directly affected by the surgical repair. The increased WSS in these descending aortic segments is most likely a perpetuation of the elevated WSS found in the distal AAO segment owing to the eccentric aortic outflow<sup>8</sup> and the abnormal ascending aortic geometry. This is supported by the observed relationship between the ascending aortic geometry and WSS in the descending thoracic aortic segments in this study. Local geometric changes of the aorta (i.e. changes in diameter, arch curvature, vessel torsion) are known to have effect on downstream hemodynamics.<sup>11</sup> In accordance with existing literature,<sup>1,2</sup> TGA patients in this study showed a more acute aortic arch angulation. However, the aortic arch geometry descriptors (angle and *w/h* ratio) were not associated with the high WSS magnitude in the aortic arch and descending aortic segments, on top of the aforementioned association with the ascending aortic geometry. This could also be related to the lack of power due to the relatively small sample size of TGA patients.

Impaired aortic bioelastic aortic wall properties have been described after ASO for TGA<sup>12</sup> and may also affect the blood flow propagation in the thoracic aorta (i.e. higher velocity), but these factors were not investigated in this study. In thoracic aortas of healthy volunteers, it has been reported that there is a significant slowing of blood flow velocity in the aortic arch compared with the velocity in the ascending aorta followed by an increase to higher velocities in the descending aorta due to vessel diameter reduction.<sup>13</sup> As WSS is a derivative of velocity, these observations are in accordance to the findings of the WSS trend along the thoracic aorta in the healthy subjects from this study, where WSS initially starts high in the proximal AAO, significantly diminishes in the aortic arch segment and subsequently increases in the descending aortic segments. This trend of WSS increase from the arch to the descending aortic segments was also observed in the TGA patients.

### **Aortic WSS during dobutamine stress**

Low-dose dobutamine administration resulted in a normal cardiac hemodynamic response in the TGA patients. Similar to previous findings from echocardiographic and MRI studies

in healthy subjects,<sup>14,15</sup> a significant increase in SV and LVEF, a decrease in end-systolic volume and no changes in end-diastolic volume were observed.

The dobutamine-induced increase in SV, EF, and CO enhanced the geometry-driven effects on WSS distribution. The SV in patients after ASO accumulates in the dilated aortic root and under stress may play a role in root dilatation negatively influenced by the smaller mid-AAo segment (vessel narrowing) on top of the dilated root. Notably, highest percentages of WSS increase under stress were found in the proximal and distal AAo segments. The increased WSS findings might introduce a risk with important clinical consequences in the long run as increased WSS is associated with elastic fiber alteration (thinning and degeneration) and dysregulation of the extracellular matrix in the aortic wall.<sup>7,16</sup> In healthy subjects, regular exercise-induced increases in blood flow and shear stress have been observed to enhance vascular function and structure.<sup>17</sup> However, in diseased aortas with altered flow phenomena and elevated regional WSS aggravated by increased SV, this may have negative effects on cardiovascular remodeling. In the arterial roots of unoperated TGA patients, already structural vessel wall abnormalities characterized by a diminished amount and altered distribution of collagen and a dedifferentiating of smooth muscle cells with increasing age have been observed,<sup>18</sup> making the neo-aortic root theoretically more vulnerable for altered WSS. So far, no reports have been described on histopathological changes in the distal AAo in TGA patients after ASO. However, cardiothoracic surgeons who performed reoperations on adult post-ASO patients have observed a thinner and more fragile anterior wall of the ascending aorta just behind the pulmonary artery bifurcation.<sup>5,6</sup> These anterior aortic regions clinically correlate with the regions of abnormal increased WSS in the distal AAo as found in this study.

Clinical implications of the altered WSS distribution over the aorta and the changes during stress are preliminary and consequences unknown, as we did not evaluate the effect of it on the aortic wall tissue itself. Correlation studies between 4D flow MR-derived aortic WSS and aortic vessel specimen after neo-aortic root and/or ascending aortic replacement are important next steps to consider. Furthermore, serial 4D flow MR evaluations are essential to assess the predictive value of hemodynamic parameters such as WSS on the progression of aortic dilatation, wall thinning or the development of adverse aortic events (aortic dissection or rupture). Ultimately, comparative hemodynamic studies between TGA patients after ASO performed with different techniques (i.e. conventional ASO with versus without Lecompte maneuver and conventional ASO versus spiral ASO technique) may provide insights for the optimization of surgical strategies for patients with different anatomy. Currently, based on our study, clinical recommendations related to these issues are not yet possible.

### **Limitations**

The study is limited by the small sample size but represents randomly selected TGA patients from the outpatient clinic that required MR investigation as part of their regular lifelong follow-up. Furthermore, healthy subjects in this study were older compared with the TGA

patients. As the velocity of aortic blood flow is known to decrease with increasing age,<sup>19</sup> older age could have lowered the WSS results in healthy subjects since it is a derivative of velocity. However, no large differences in mean velocity and thus in WSS are to be expected based on the small differences in age range between the groups based on a study on the velocity distribution in the normal aorta over age.<sup>19</sup> The comparison of the effect of pharmacological-induced stress on the aortic WSS could not be performed other than within the TGA group.

## Conclusion

In conclusion, increased aortic WSS was found in the distal ascending aortic segment and in the aortic segments beyond and was primary related to the ASO-specific geometry of the ascending aorta, not related to the steeper arch geometry. Dobutamine-induced stress further increased abnormal segmental WSS and showed a moderate positive correlation with the increase in left ventricular cardiac output parameters. Pharmacological-induced stress evaluations of aortic blood flow may better reflect location and expansion of vascular wall areas exposed to abnormal WSS with subsequent risks for vascular remodeling. Stress might play a role in neo-aortic root dilatation in TGA patients after ASO given the significant stress-induced WSS increase in the neo-aortic root, acting on root tissue with structural vessel wall abnormalities.

## ACKNOWLEDGEMENT

The authors thank Pieter J. van den Boogaard for help in providing support with the MRI acquisitions, dr. Monique R.M. Jongbloed for the assistance with adult patient enrollment and Alex Korenhof for the support in post-processing of the MRI data.

## References

1. Ntsinjana HN, Capelli C, Biglino G, Cook AC, Tann O, Derrick G, Taylor AM, Schievano S. 3D morphometric analysis of the arterial switch operation using in vivo MRI data. *Clin Anat*. 2014;27(8):1212-22.
2. Martins D, Khraiche D, Legendre A, Boddaert N, Raisky O, Bonnet D, Raimondi F. Aortic angle is associated with neo-aortic root dilatation and regurgitation following arterial switch operation. *Int J Cardiol*. 2019;280:53-6.
3. Lo Rito M, Fittipaldi M, Haththotuwa R, Jones TJ, Khan N, Clift P, Brawn WJ, Barron DJ. Long-term fate of the aortic valve after an arterial switch operation. *J Thorac Cardiovasc Surg*. 2015;149(4):1089-94.
4. van der Palen RLF, van der Bom T, Dekker A, Tsonaka R, van Geloven N, Kuipers IM, Konings TC, Rammeloo LAJ, Ten Harkel ADJ, Jongbloed MRM, et al. Progression of aortic root dilatation and aortic valve regurgitation after the arterial switch operation. *Heart*. 2019;105(22):1732-40.
5. Koolbergen DR, Manshanden JS, Yazdanbakhsh AP, Bouma BJ, Blom NA, de Mol BA, Mulder BJ, Hazekamp MG. Reoperation for neo-aortic root pathology after the arterial switch operation. *Eur J Cardiothorac Surg*. 2014;46(3):474-9.
6. Vida VL, Zanotto L, Zanotto L, Stellin G, European Congenital Heart Surgeons Association Study G, Padalino M, Sarris G, Protopapas E, Prospero C, Pizarro C, et al. Left-Sided Reoperations After Arterial Switch Operation: A European Multicenter Study. *Ann Thorac Surg*. 2017;104(3):899-906.
7. Guzzardi DG, Barker AJ, van Ooij P, Malaisrie SC, Puthumana JJ, Belke DD, Mewhort HE, Svystonyuk DA, Kang S, Verma S, et al. Valve-Related Hemodynamics Mediate Human Bicuspid Aortopathy: Insights From Wall Shear Stress Mapping. *J Am Coll Cardiol*. 2015;66(8):892-900.
8. van der Palen RLF, Deurvorst QS, Kroft LJM, van den Boogaard PJ, Hazekamp MG, Blom NA, Lamb HJ, Westenberg JJM, Roest AAW. Altered Ascending Aorta Hemodynamics in Patients After Arterial Switch Operation for Transposition of the Great Arteries. *J Magn Reson Imaging*. 2020;51(4):1105-16.
9. van der Palen RLF, Roest AAW, van den Boogaard PJ, de Roos A, Blom NA, Westenberg JJM. Scan-rescan reproducibility of segmental aortic wall shear stress as assessed by phase-specific segmentation with 4D flow MRI in healthy volunteers. *MAGMA*. 2018;31(5):653-63.
10. Kaiser T, Kellenberger CJ, Albisetti M, Bergstrasser E, Valsangiacomo Buechel ER. Normal values for aortic diameters in children and adolescents--assessment in vivo by contrast-enhanced CMR-angiography. *J Cardiovasc Magn Reson*. 2008;10:56.
11. PrahL Wittberg L, van Wyk S, Fuchs L, Gutmark E, Backeljauw P, Gutmark-Little I. Effects of aortic irregularities on blood flow. *Biomech Model Mechanobiol*. 2016;15(2):345-60.
12. Voges I, Jerosch-Herold M, Hedderich J, Hart C, Petko C, Scheewe J, Andrade AC, Pham M, Gabbert D, Kramer HH, et al. Implications of early aortic stiffening in patients with transposition of the great arteries after arterial switch operation. *Circ Cardiovasc Imaging*. 2013;6(2):245-53.
13. Hope TA, Markl M, Wigstrom L, Alley MT, Miller DC, Herfkens RJ. Comparison of flow patterns in ascending aortic aneurysms and volunteers using four-dimensional magnetic resonance velocity mapping. *J Magn Reson Imaging*. 2007;26(6):1471-9.
14. De Wolf D, Suys B, Verhaaren H, Matthys D, Taeymans Y. Low-dose dobutamine stress echocardiography in children and young adults. *Am J Cardiol*. 1998;81(7):895-901.
15. Parish V, Valverde I, Kutty S, Head C, Qureshi SA, Sarikouch S, Greil G, Schaeffter T, Razavi R, Beerbaum P. Dobutamine stress MRI in repaired tetralogy of Fallot with chronic pulmonary regurgitation: a comparison with healthy volunteers. *Int J Cardiol*. 2013;166(1):96-105.
16. Bollache E, Guzzardi DG, Sattari S, Olsen KE, Di Martino ES, Malaisrie SC, van Ooij P, Collins J, Carr J, McCarthy PM, et al. Aortic valve-mediated wall shear stress is heterogeneous and predicts regional aortic elastic fiber thinning in bicuspid aortic valve-associated aortopathy. *J Thorac Cardiovasc Surg*. 2018;156(6):2112-20 e2.

17. Niebauer J, Cooke JP. Cardiovascular effects of exercise: role of endothelial shear stress. *J Am Coll Cardiol.* 1996;28(7):1652-60.
18. Lalezari S, Mahtab EA, Bartelings MM, Wisse LJ, Hazekamp MG, Gittenberger-de Groot AC. The outflow tract in transposition of the great arteries: an anatomic and morphologic study. *Ann Thorac Surg.* 2009;88(4):1300-5.
19. Garcia J, van der Palen RLF, Bollache E, Jarvis K, Rose MJ, Barker AJ, Collins JD, Carr JC, Robinson J, Rigsby CK, et al. Distribution of blood flow velocity in the normal aorta: Effect of age and gender. *J Magn Reson Imaging.* 2018;47(2):487-98.

## Supplementary material

**Supplementary Table S1.** NCE-MRA and 4D flow MRI acquisition details

<b>MR scanner, field strength</b>	Ingenia - Philips Medical Systems, 3Tesla
<b>Coil</b>	Combination of FlexCoverage Posterior coil (table top) and dStream Torso coil, providing up to 32 coil elements for signal reception
<b>NCE-MRA</b>	
Sequence	Dixon
Respiratory compensation	Navigator gating
Cardiac gating	Prospective, to end diastole
Spatial resolution (mm)	1.6 x 1.6 x 3.2
Temporal resolution (ms)	31.4 ± 1.6
TE (ms)	2.3
TR (ms)	3.6-3.9
Field-of-view (mm)	300 x 300 x 99
Reconstructed voxel size (mm)	0.8 x 0.8 x 1.6
<b>Aortic 4D flow MRI</b>	
Sequence	Segmented fast-spoiled echo pulse
Respiratory compensation	Navigator gating
Cardiac gating	retrospective, 24-36 phases
Spatial resolution (mm)	2.5 x 2.5 x 2.5
Temporal resolution (ms)	34-36 (rest)
	33-34 (stress)
Flip angle (°)	10
TE (ms)	2.4-2.6 (rest)
	2.2-2.4 (stress)
TR (ms)	4.2-4.5 (rest)
	4.1-4.3 (stress)
VENC (cm/s)	200 (range 200-300) (rest)
	3000 (range 250-350) (stress)
Scan duration (minutes)	10-12
Acceleration methods	SENSE factor 2.5, AP direction; TFE factor 2
Gradient correction	Yes*
Phase offset correction	Yes*
Acquisition time	~ 12 minutes

\* from standard available scanner software.

AP, anterior-posterior; ms, milliseconds; NCE-MRA, non-contrast enhanced magnetic resonance angiography; SENSE, sensitivity encoding; TE, echo time; TFE, turbo field echo; TR, repetition time; VENC, velocity encoding.

**Supplementary Table S2.** Relationship between the aortic arch geometry and aortic WSS in TGA patients from the arch and beyond

		Arch angle (°)		w/h ratio	
		r	P value	r	P value
<b>Rest state</b>					
Arch	WSSmean	0.01	0.97	-0.08	0.76
	WSSmax	0.11	0.69	0.03	0.91
pDAo	WSSmean	0.24	0.36	0.19	0.49
	WSSmax	0.35	0.19	0.25	0.34
dDAo	WSSmean	0.13	0.64	0.13	0.63
	WSSmax*	0.58	0.02	0.54	0.03
<b>Stress state</b>					
Arch	WSSmean	-0.01	0.96	-0.08	0.77
	WSSmax	0.24	0.38	0.27	0.31
pDAo	WSSmean	0.004	0.99	-0.01	0.96
	WSSmax	-0.02	0.95	0.02	0.94
dDAo	WSSmean	-0.35	0.19	-0.25	0.35
	WSSmax	0.28	0.30	0.32	0.23

Spearman correlation coefficient (r). \* statistically significant.  
dDAo, distal descending aorta; pDAo, proximal descending aorta; WSSmax, maximum 3D systolic wall shear stress; WSSmean, mean 3D systolic wall shear stress.

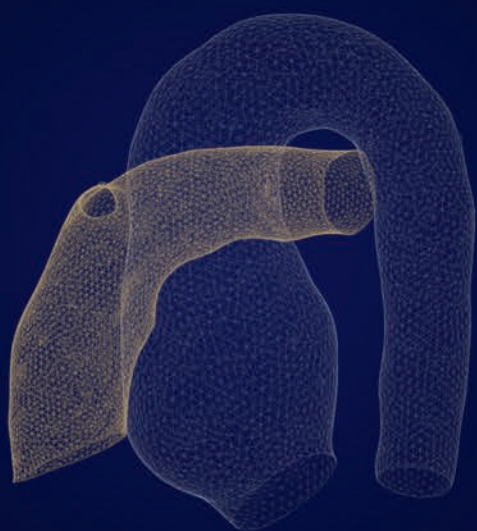


**Supplementary Table S3.** Blood pressure, heart rate and MRI measurements during rest and stress

	TGA patients				Healthy subjects		P value
	Rest		Stress		Rest Mean (SD)	TGA vs Healthy at rest	
	Mean (SD)	Difference $\Delta$ (SD)	Mean (SD)	Difference Rest-Stress % (SD)			
HR (bpm)	72.3 (12.3)	27.2 (14.6)	98.3 (17.8)	40.0 (22.0)	60.8 (7.7)	0.015	<0.001
SBP (mmHg)	123.4 (14.1)	41.8 (19.7)	165.8 (18.7)	35.1 (15.4)	NA	NA	<0.001
DBP (mmHg)	61.8 (9.7)	7.3 (10.9)	69.1 (10.1)	13.4 (18.7)	NA	NA	0.017
EDV (ml)	171.9 (44.7)	-6.3 (14.9)	165.7 (45.1)	-3.4 (8.8)	161.3 (35.9)	0.531	0.114
EDVi (ml/m <sup>2</sup> )	97.9 (18.5)	-3.1 (8.2)	94.7 (20.6)	-3.4 (8.8)	88.0 (12.5)	0.151	0.142
ESV (ml)	69.0 (23.7)	-25.6 (10.1)	43.4 (15.7)	-36.6 (9.3)	60.0 (13.1)	0.283	<0.001
ESVi (ml/m <sup>2</sup> )	38.9 (10.0)	-14.2 (4.5)	24.6 (7.1)	-36.6 (9.3)	32.8 (5.0)	0.051	<0.001
SV (ml)	101.7 (24.2)	20.4 (15.9)	122.1 (30.2)	20.6 (13.9)	100.3 (21.5)	0.882	<0.001
SVi (ml/m <sup>2</sup> )	58.3 (11.6)	11.6 (8.1)	70.0 (14.2)	20.6 (13.9)	54.7 (6.9)	0.382	<0.001
EF (%)	59.7 (5.5)	14.5 (4.6)	74.2 (3.4)	25.0 (9.2)	62.3 (2.5)	0.181	<0.001
CO (l/min)	7.2 (1.5)	4.0 (1.3)	11.2 (2.4)	56.7 (17.8)	6.1 (1.2)	0.066	<0.001
CI (l/min/m <sup>2</sup> )	4.2 (0.8)	2.3 (0.5)	6.4 (1.0)	56.7 (17.8)	3.4 (0.5)	0.011	<0.001

CO, cardiac output; CI, cardiac output indexed for body surface area; DPB, diastolic blood pressure; EDV, end-diastolic volume; EDVi, end-diastolic volume indexed for body surface area; EF, ejection fraction; ESV, end-systolic volume; ESVi, end-systolic volume indexed for body surface area; HR, Heart rate; NA, not available; SBP, systolic blood pressure; SV, stroke volume; SVi, stroke volume indexed for body surface area; TGA, transposition of the great arteries.





## **CHAPTER 9**

# Altered aortic 3D hemodynamics and geometry in pediatric Marfan syndrome patients

Journal of Cardiovascular Magnetic Resonance. 2017;19:30-41

Roel L.F. van der Palen  
Alex J. Barker  
Emilie Bollache  
Julio Garcia  
Michael J. Rose  
Pim van Ooij  
Luciana T. Young  
Arno A.W. Roest  
Michael Markl  
Joshua D. Robinson  
Cynthia K. Rigsby

## Abstract

### Background

Blood flow dynamics make it possible to better understand the development of aortopathy and cardiovascular events in patients with Marfan syndrome (MFS). Aortic 3D blood flow characteristics were investigated in relation to aortic geometry in children and adolescents with MFS.

### Methods

25 MFS patients (age  $15.6 \pm 4.0$  years; 11 females) and 21 healthy controls (age  $16.0 \pm 2.6$  years; 12 females) underwent magnetic resonance angiography and 4D flow CMR for assessment of thoracic aortic size and 3D blood flow velocities. Data analysis included calculation of aortic diameter and BSA-indexed aortic dimensions (Z-score) along the thoracic aorta, 3D mean systolic wall shear stress ( $WSS_{\text{mean}}$ ) in 10 aortic segments and assessment of aortic blood flow patterns.

### Results

Aortic root (root), ascending (AAo) and descending (DAo) aortic size was significantly larger in MFS patients than healthy controls (Root Z-score:  $3.56 \pm 1.45$  vs  $0.49 \pm 0.78$ ,  $P < 0.001$ ; AAo Z-score  $0.21 \pm 0.95$  vs  $-0.54 \pm 0.64$ ,  $P = 0.004$ ; proximal DAo Z-score  $2.02 \pm 1.60$  vs  $0.56 \pm 0.66$ ,  $P < 0.001$ ). A regional variation in prevalence and severity of flow patterns (vortex and helix flow patterns) was observed, with the aortic root and the proximal DAo (pDAo) being more frequently affected in MFS. MFS patients had significantly reduced  $WSS_{\text{mean}}$  in the proximal AAo (pAAo) outer segment ( $0.65 \pm 0.12$  vs  $0.73 \pm 0.14$  Pa,  $P = 0.029$ ) and pDAo inner segment ( $0.74 \pm 0.17$  vs  $0.87 \pm 0.21$  Pa,  $P = 0.021$ ), as well as higher  $WSS_{\text{mean}}$  in the inner segment of the distal AAo ( $0.94 \pm 0.14$  vs  $0.84 \pm 0.15$  Pa,  $P = 0.036$ ) compared to healthy subjects. An inverse relationship existed between pDAo  $WSS_{\text{mean}}$  and both pDAo diameter ( $r = -0.53$ ,  $P < 0.001$ ) and % diameter change along the pDAo segment ( $r = -0.64$ ,  $P < 0.001$ ).

### Conclusions

MFS children and young adults have altered aortic flow patterns and differences in aortic WSS that were most pronounced in the pAAo and pDAo, segments where aortic dissection or rupture often originate. The presence of vortex flow patterns and abnormal WSS correlated with regional size of the pDAo and are potentially valuable additional markers of disease severity.

## Background

Marfan syndrome (MFS) is an inherited autosomal dominant connective tissue disease, mostly related to mutations in the fibrillin-1 (FBN1) gene. Many organ systems can be involved, but most life-threatening complications are related to the cardiovascular system and include aortic dissection and aortic rupture. Although the entire aorta may dilate in MFS, specific aortic regions are prone for progressive dilation and dissection and represent the aortic root and the proximal descending aorta (pDAo).<sup>1-3</sup> Before the implementation of preventive surgical management strategies, two-thirds of dissections and ruptures occurred in the ascending aorta (AAo) while one-third occurred in the descending aorta (DAo). Recently, this ratio has shifted towards proportionally more DAo complications.<sup>4,5</sup> Thus, pathology of the aorta distal to the aortic root remains a cause of concern.

In the current guidelines, absolute aortic diameters and identification of changes in aortic dimension play an important role in risk stratification and decision making for preventive surgery.<sup>6</sup> However, it is known that aortic dissection may occur in only moderately dilated aortas, and recent literature has shown that only about 50% of MFS patients with pDAo dissections had pDAo diameters larger than the upper limit of normal.<sup>5</sup> These findings indicate that aortic dimension alone may not capture the predictive risk for adverse cardiovascular events.

It is not well known how aortic hemodynamics interact with the altered vascular structure of the aorta in MFS. Independent associations between hemodynamic markers and aortopathy have been presented in cardiovascular magnetic resonance (CMR) imaging studies.<sup>7-10</sup> These studies employed time-resolved 3D phase-contrast CMR with three-directional velocity encoding (4D flow CMR) to enable a comprehensive, non-invasive in-vivo investigation of cardiac and aortic hemodynamics. The technique allows for quantitative analysis of advanced hemodynamic parameters<sup>11-14</sup> such as wall shear stress (WSS), which is defined as the tangential force exerted by blood flow on the aortic wall. WSS has recently been correlated with evidence of molecular and architectural medial wall dysfunction in bicuspid aortic valve-related aortopathy.<sup>15</sup> WSS may also be a useful parameter to identify focal regions with wall dysfunction in MFS patients. The aim of the study was to investigate regional aortic WSS, flow patterns and aortic dimensions in a pediatric MFS cohort compared to a healthy age appropriate control cohort by using a novel 3D WSS technique.

## Methods

### Study population

Twenty-five patients with MFS (mean age  $15.6 \pm 4.0$  years, 11 females) were included in this Institutional Review Board (IRB) approved and HIPAA compliant study. All patients underwent 4D flow CMR immediately following a clinically ordered standard-of-care CMR assessment of the entire aorta. The diagnosis of MFS was based on clinical criteria according to the

international standards derived from the 2010 Revised Ghent Criteria.<sup>16</sup> In addition to the clinical criteria, conventional genetic testing for FBN1 mutation was performed in 23 MFS patients; in 22 of them a FBN1 mutation was proven. Patients with a bicuspid aortic valve or prior aortic surgery were excluded. Twenty-one healthy pediatric subjects (mean age 16.0 ± 2.6 years, 12 females) with a tricuspid aortic valve without history of cardiovascular disease and normal cardiac and aortic valve function, who underwent 4D flow CMR following a standard-of-care CMR examination, were collected from a retrospective chart review as approved by the IRB and were used as a healthy control group. The majority of these subjects underwent CMR for atypical chest pain after the inability of echocardiography to detect the origins of coronary arteries. The CMR revealed no morphological and functional cardiac or large vessel abnormalities in any of the healthy subjects. Written informed consent was obtained from all participants or their legal guardians for the addition of the 4D flow CMR to the standard-of-care CMR protocol.

### **Magnetic Resonance Imaging**

CMR examinations were performed on 1.5T systems (MAGNETOM Avanto or Area, Siemens, Germany). All patients and healthy subjects underwent a standard-of-care CMR exam that included dynamic ECG gated two-dimensional (2D) cine steady state free precession (SSFP) imaging, for the evaluation of cardiac anatomy and function, as well as ECG gated and navigator triggered time-resolved contrast-enhanced MR angiography (CE-MRA) after administration of blood pool contrast media (gadofosveset trisodium, ABLAVAR, 0.03 mmol/kg, Lantheus, N. Billerica, MA), for evaluation of aortic morphology and dimensions. Sequence parameters for CE-MRA: spatial resolution 1.3-1.5 x 1.3-1.5 x 1.3-1.7 mm<sup>3</sup>, echo time/repetition time: 1.2-1.6 ms/3.2-3.6 ms, flip angle: 18°. For assessment of aortic blood flow, 4D flow CMR was acquired during free breathing using respiratory navigator and prospective ECG-gating, with full volumetric coverage of the thoracic aorta in an oblique sagittal orientation. Standardized 4D flow sequence parameters were used throughout the study for age categories: 6-12 years and >12 years of age. Average 4D flow scan parameters were as follows: spatial resolution: 2.3-3.8 x 1.6-2.0 x 1.8-3.0 mm<sup>3</sup>, temporal resolution: 38.4-41.6 ms, echo time/repetition time: 2.4-2.7 ms/5.0-5.1 ms, flip angle: 15°, field of view: 250-320 x 141-250 mm<sup>2</sup>, matrix size: 160 x 70-130 and velocity sensitivity: 120-200 cm/s.

### **Data analysis**

#### *Thoracic aortic size*

Thoracic aortic diameters were determined from the CE-MRA exams using a 3D workstation with multiplanar reformatting capabilities (Vitreia, Vital Images, Minneapolis, MN). According to the international guidelines,<sup>17</sup> maximum orthogonal aortic diameters were measured along the aorta from inner-edge to inner-edge at the following levels: STJ: sinotubular junction; midAAo: mid-ascending aorta, at the level of the right pulmonary artery; dAAo: distal ascending aorta, prior to innominate artery; distal aortic arch, between left carotid artery and left subclavian artery; aortic isthmus, at the level direct beyond the left subclavian

artery; pDAo: proximal descending aorta, at the level of the ductal ampulla; midDAo: mid-descending aorta, at the level of the left atrium; dDAo: distal descending aorta, at the level of the diaphragm (Figure 1B).

Maximum aortic root (Root) diameter was measured on a short-axis cine SSFP plane across the aortic root at peak systole.<sup>18,19</sup> Change in aortic diameter along aortic segments was calculated and expressed as percentage change for the segments aortic root to midAAo and aortic isthmus to pDAo:

$$\left(\frac{|Aortic\ root - midAAo|}{Aortic\ root}\right) * 100 \text{ and } \left(\frac{|Aortic\ isthmus - pDAo|}{Aortic\ isthmus}\right) * 100.$$

To account for the range of patient age and body size, aortic Z-scores were calculated for each patient from the CMR aortic measurements (AAo through pDAo) and the body surface area (BSA; determined according to the method of Mosteller),<sup>20</sup> using EchoIMS (Merge Healthcare, Chicago, IL). The Z-score is a nomogram-based metric for assessing aortic dilatation in pediatric patients in which a Z-score between -2 and +2 is considered normal.<sup>21</sup> While EchoIMS provides ultrasound derived normative data, there is currently no CMR-specific database, and as such, this method of normalization is the best available alternative and supported by previous studies.<sup>22,23</sup> Particularly, Z-scores of the pDAo were calculated from the data on the aortic isthmus region of EchoIMS data. An aortic Z-score  $\geq 2.0$  indicates that the aortic diameter at that level is outside the upper normal range ( $\geq 2$  standard deviations from the mean). Based on pDAo Z-scores, MFS patients were divided into subgroups for additional analysis: group 1: MFS Z-score pDAo  $\geq 2.0$ ; group 2: MFS Z-score pDAo  $< 2.0$ .

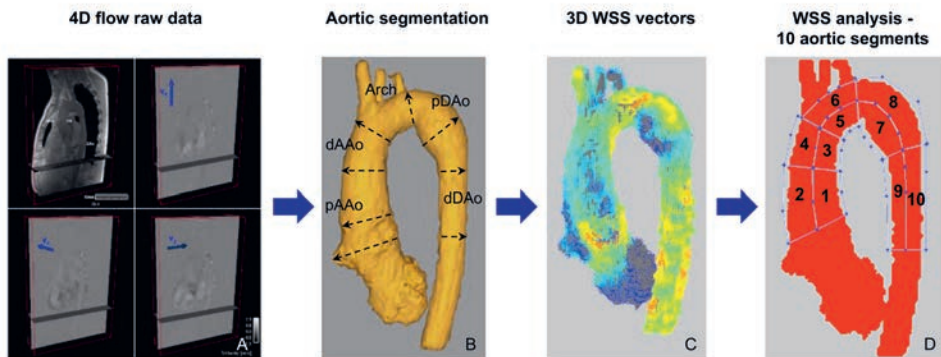


**Figure 1.** Aortic 4D flow data processing and analysis.

4D flow raw data including anatomical and flow data (A). Volumetric aorta segmentation; levels of aortic diameter measurements (B). Calculation of systolic 3D WSS vector maps (C). Regional WSS analysis in 10 aortic regions (D). Arch, aortic arch; dAAo, distal ascending aorta; pAAo, proximal ascending aorta; dDAo, distal descending aorta; pDAo, proximal descending aorta.



*4D flow data processing and 3D blood flow visualization*

All 4D flow CMR data (Figure 1A) were corrected for noise, velocity aliasing, Maxwell terms and eddy currents using Matlab-based in-house software (MathWorks, Natick, MA) as described previously.<sup>24</sup> A 3D phase-contrast MR angiogram was created from the corrected 4D flow CMR data and was used to semi-automatically define a 3D segmentation of the thoracic aorta (Mimics, Materialise, Leuven, Belgium) (Figure 1B). The 3D segmentation was used to mask the velocity field for the generation of time-resolved 3D pathlines to visualize aortic 3D blood flow (Enight, CEI, Apex, NC). Semiquantitative aortic flow pattern analysis using pathline movies was performed in MFS patients and healthy subjects in a blinded fashion and random order by two observers (CR and JR). A helical flow pattern was defined as rotational fluid motion around an axis parallel to the bulk fluid motion (i.e. along the longitudinal axis of the vessel). Vortical flow patterns were defined as revolving particles around a point within the vessel with a rotation direction deviating by  $>90^\circ$  from the physiological flow direction. Vortex and helix flow pattern grading was assessed in three aortic segments (AAo, Arch and DAo) on a 3-point ordinal scale: 0: no vortex/helix patterns; 1: flow rotation  $<360^\circ$ ; 2: flow rotation  $>360^\circ$  (Examples in Figure 2).

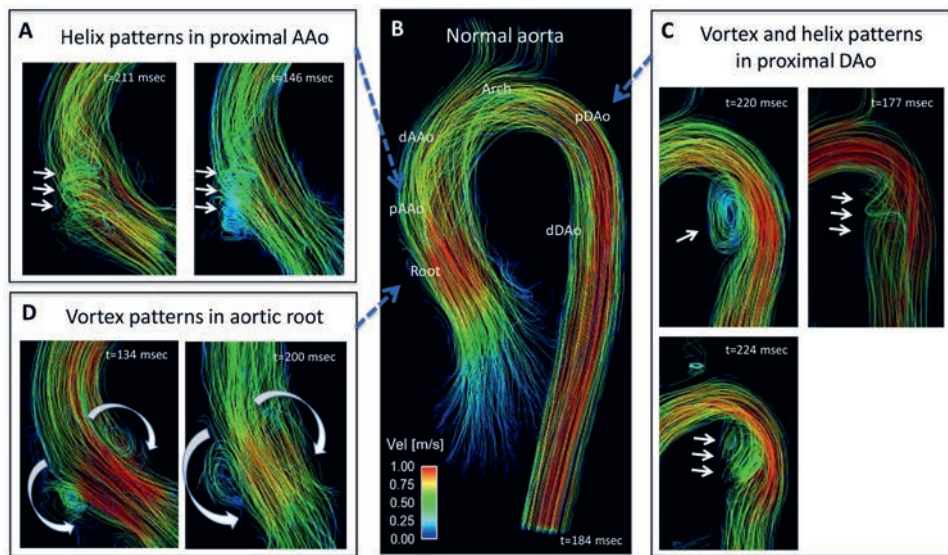


**Figure 2.** Aortic 3D blood flow characteristics (systolic streamlines).

Panel B represents systolic streamline visualization of a normal aorta from a healthy control. Panels A, C and D illustrate typical secondary flow patterns in Marfan syndrome patients during systole, like a helix flow pattern from the aortic root into the pAAo (A, grade 2) and vortex and helix flow patterns in the pDAo (C, grade 2). Prominent vortex flow patterns in the aortic root (D). Arch, aortic arch; dAAo, distal ascending aorta; pAAo, proximal ascending aorta; dDAo, distal descending aorta; pDAo, proximal descending aorta.

### *Regional wall shear stress assessment*

Based on the 3D segmentation, 3D mean systolic wall shear stress ( $WSS_{\text{mean}}$ ) along the entire aortic vessel wall was calculated from 4D flow velocity data (Figure 1C) using a previously described algorithm, which was shown to provide good reproducibility.<sup>25, 26</sup> Briefly, WSS vector was estimated for each wall point on the aortic surface based on the 3D velocity spatial gradient perpendicular to the vessel wall. Systolic WSS vector magnitude was defined as the average over five cardiac time frames centered on the peak systolic time frame (i.e., peak systolic phase  $\pm 2$  phases).  $WSS_{\text{mean}}$  was calculated within 10 aortic regions that were manually drawn based on anatomic landmarks (Figure 1D): 1) inner and outer proximal ascending aorta (pAAo, from STJ to midAAo); 2) inner and outer distal ascending aorta (dAAo, from midAAo to the origin of the innominate artery); 3) inner and outer aortic arch (from origin innominate artery until left subclavian artery); 4) inner and outer proximal descending aorta (pDAo, beyond the left subclavian artery to mid-descending thoracic aorta); 5) inner and outer distal descending aorta (dDAo, from mid-descending thoracic aorta to the level of the aortic valve). Of note, the supra-aortic arch branches were excluded from the regional WSS measurements.

### **Statistical analysis**

Statistical analysis was performed using IBM SPSS Statistics 20.0 (SPSS Inc., Chicago, IL, USA). Baseline characteristics are provided as mean  $\pm$  standard deviation for continuous variables and percentage for discrete variables. Shapiro-Wilk tests were performed to test for equal distribution of continuous variables. A chi-square test was used to investigate differences in gender distribution between the MFS and healthy subject groups. A non-paired t-test was performed to study differences in continuous variables from baseline characteristics between the two cohorts. For comparison of differences between aortic Z-scores as well as regional aortic WSS between the two cohorts a Mann Whitney test was used. A Kruskal-Wallis test was used to evaluate differences in aortic Z-score, size change and regional WSS between the two MFS subgroups, as well as between the MFS subgroup with a pDAo Z-score  $\geq 2.0$  and healthy subjects. The relationships between aortic dimensions and hemodynamic parameters were investigated using correlation analysis based on linear regression. A  $P$  value  $< 0.05$  was considered statistically significant for all statistical tests. Inter-observer agreement on qualitative assessment of helix and vortex flow formation between two observers was calculated using Cohen's  $\kappa$  statistics. A  $\kappa$  value of 0.61-0.80 corresponded to substantial interobserver agreement; values of 0.41-0.60 corresponded to moderate agreement.

## Results

Patient characteristics are summarized in Table 1. As expected, MFS patients were typically taller than healthy subjects. All patients and healthy subjects had normal systolic biventricular function and no significant regurgitation of the mitral valve or aortic valve, except for one MFS patient who showed moderate mitral valve regurgitation.

### Thoracic aorta dimensions

As summarized in Table 1, the aortic diameter Z-scores were significantly greater in MFS patients compared to healthy subjects at all thoracic aorta levels ( $P \leq 0.05$ ), except for the distal aortic arch ( $P = 0.155$ ). Aortic dilatation in the MFS population was most prominent in the aortic root and pDAo, with Z-scores of  $3.56 \pm 1.45$  and  $2.02 \pm 1.60$ , respectively. Using a Z-score  $\geq 2.0$  to define aortic dilatation,  $n = 21$  (84%) MFS patients had aortic root dilatation and  $n = 10$  (40%) had dilatation of the STJ. Seven MFS patients (28%) had a pDAo Z-score  $\geq 2.0$ .

### Aortic flow patterns

There was moderate to substantial inter-observer agreement for grading of flow patterns within the AAO (Kappa 0.54) and DAo (Kappa 0.84) between the two observers. Examples of 3D blood flow patterns found in MFS patients are depicted in Figure 2 (Panels A, C and D) and online supplementary Video 1. Marked vortex flow patterns were noted in the pDAo region of 14 MFS patients and in only two healthy subjects (56% vs 9.5% of total subjects,  $P = 0.002$ ), with an average pDAo vortex grading significantly higher in MFS patients than healthy subjects ( $0.82 \pm 0.83$  vs  $0.14 \pm 0.39$ ,  $P < 0.001$ ). These vortex flow patterns were most pronounced in MFS patients with a dilated pDAo (6 out of 7) (Figure 3; and online supplementary Video 1). Physiological vortex patterns in the sinuses of the aortic root were more often visible in MFS patients compared to healthy subjects (76.0% vs 23.8%,  $P < 0.001$ ; Figure 2, Panel D; and online supplementary Video 1 and 2). Non-physiological helical flow patterns with high strength (grade 2) originating from the aortic root were observed in 16% of the MFS patients and were not present in any of the healthy subjects ( $P < 0.05$ , Figure 2, Panel A). Finally, throughout the AAO, no difference in presence or strength of major flow patterns was observed between the MFS patients and healthy subjects (MFS vs healthy subjects: prevalence 76.0% vs 57.1%,  $P = 0.17$ ; average helix grading  $1.18 \pm 0.71$  vs  $0.86 \pm 0.76$ ,  $P = 0.14$ ). No helix or vortex flow patterns were present in the aortic arch for both MFS patients and healthy subjects.

### Segmental aortic WSS & correlations with diameter

Figure 4A illustrates regional differences in  $WSS_{\text{mean}}$  between MFS patients and healthy subjects. MFS patients showed reduced  $WSS_{\text{mean}}$  in the pAAo outer segment ( $0.65 \pm 0.12$  vs  $0.73 \pm 0.14$  Pa,  $P = 0.029$ ) and pDAo inner segment ( $0.74 \pm 0.17$  vs  $0.87 \pm 0.21$  Pa,  $P = 0.021$ ) compared to healthy subjects (Figure 4A). There was a higher  $WSS_{\text{mean}}$  in the inner segment of the dAAo in MFS patients ( $0.94 \pm 0.14$  vs  $0.84 \pm 0.15$  Pa,  $P = 0.036$ ). Moreover, in the entire

**Table 1.** Baseline characteristics

	Marfan	Healthy controls	P value
N (females)	25 (11)	21 (12)	0.375
Age (y)	15.6 ± 4.0	16.0 ± 2.6	0.720
Height (cm)	178.6 ± 17.3	161.2 ± 11.2	<0.001*
Weight (kg)	65.6 ± 20.2	58.8 ± 15.1	0.208
BSA (m <sup>2</sup> )	1.78 ± 0.36	1.61 ± 0.25	0.082
BMI (kg/m <sup>2</sup> )	20.1 ± 4.5	22.4 ± 4.0	0.081
LV ejection fraction (%)	55.7 ± 6.5	58.1 ± 3.7	0.243
Bilateral ectopia lentis (n, %)	5 (20)	0	
<b>Genetic mutation (n)</b>			
FBN1 gene	22	-	
Unknown	3	-	
<b>Cardiac medication (n, %)</b>			
1. Beta-blocker	20 (80)	0	
2. AT II-receptor antagonist	15 (60)	-	
3. ACE inhibitor	7 (28)	-	
4. Combination 1+2	3 (12)	-	
5. Combination 1+3	4 (16)	-	
5. Combination 1+3	1 (4)	-	
<b>Thoracic aortic size (Z-score)</b>			
Aortic Root	3.56 ± 1.45	0.49 ± 0.78	<0.001*
ST-junction	1.70 ± 1.28	-0.34 ± 0.77	<0.001*
Ascending aorta	0.21 ± 0.95	-0.54 ± 0.64	0.004*
Distal aortic arch	0.14 ± 0.90	-0.23 ± 0.66	0.155
Aortic isthmus	0.96 ± 0.94	0.43 ± 0.49	0.039*
Proximal descending aorta	2.02 ± 1.60	0.56 ± 0.66	<0.001*

The P value stems from non-paired t-test, for sex from chi-square test and for thoracic aorta dimensions from the Mann Whitney test. \* $P < 0.05$ .

ACE, angiotensin converting enzyme; AT, angiotensin; BMI, body mass index; BSA, body surface area; FBN1, fibrillin-1; LV, left ventricular; ST, sinotubular.

study cohort (MFS and healthy subjects),  $WSS_{mean}$  showed a strong inverse relationship with aortic dimensions, as well as with diameter changes along aortic segments. The most prominent association was found between the  $WSS_{mean}$  of the pDAo inner segment and both the pDAo Z-score ( $r = -0.53$ ,  $P < 0.001$ ) and the diameter change along the corresponding segment ( $r = -0.64$ ,  $P < 0.001$ ; Figure 5).

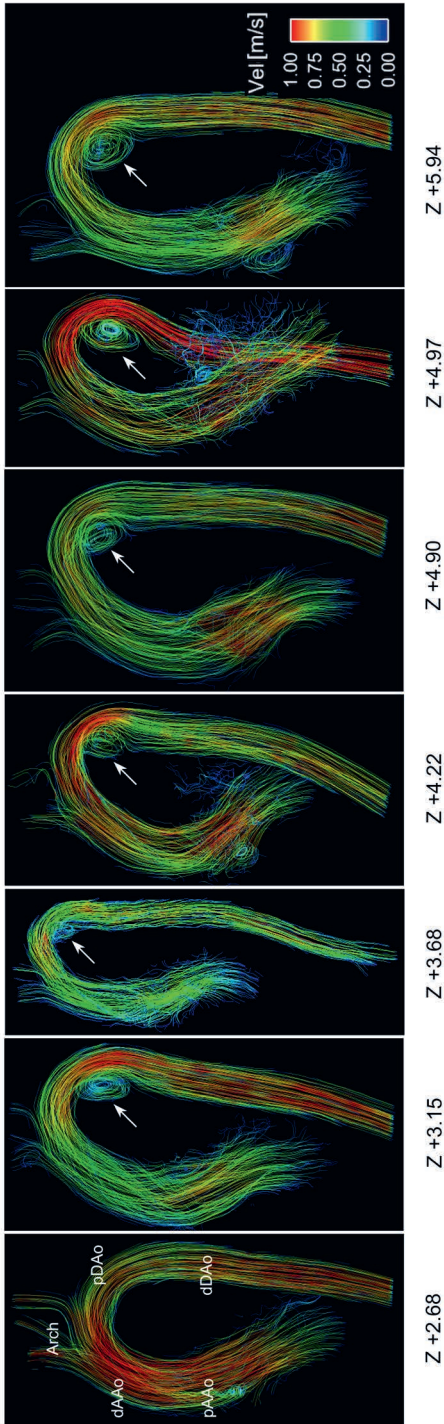


**Figure 3.** Aortic blood flow streamlines in MFS patients with Z-score  $\geq 2.0$  of the proximal descending aorta ( $n = 7$ ). Local vortex flow patterns at the inner curvature of the pDAo (arrows) in six out of the seven MFS patients with dilated pDAo (Z-score  $\geq 2.0$ ). Arch, aortic arch; dAAo, distal ascending aorta; pAAo, proximal ascending aorta; dDAo, distal descending aorta; pDAo, proximal descending aorta.

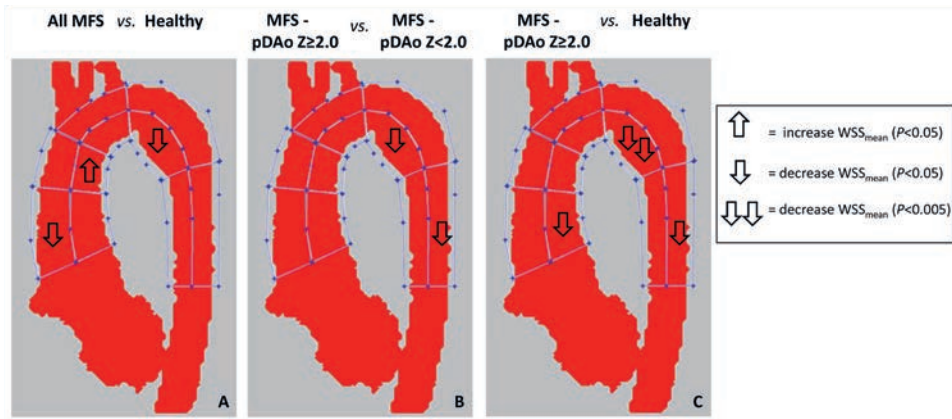


**Figure 4.** Comparison of mean systolic wall shear stress in the ten aortic regions between groups. Entire MFS cohort ( $n = 25$ ) vs healthy subjects ( $n = 21$ ) (A). MFS with a pDAo Z-score  $\geq 2.0$  ( $n = 7$ ) vs MFS with a pDAo Z-score  $< 2.0$  ( $n = 18$ ) (B). MFS with pDAo Z-score  $\geq 2.0$  ( $n = 7$ ) vs healthy subjects ( $n = 21$ ) (C). pDAo, proximal descending aorta.

### Subgroup analysis according to proximal DAo dilatation

Based on pDAo Z-scores, MFS patients were divided into subgroups for additional analysis. Seven MFS patients had a Z-score pDAo  $\geq 2.0$  (group 1), whereas 18 MFS patients had a Z-score pDAo  $< 2.0$  (group 2). Age, gender and BSA were comparable between the MFS subgroups with dilated pDAo (Z-score  $\geq 2.0$ ) and healthy subjects (Table 2). Differences in aortic diameter and segmental WSS between healthy subjects and MFS subgroups as well as between the 2 MFS subgroups are summarized in Table 2. Dimensions of the entire thoracic aorta in the MFS subgroup with dilated pDAo showed significantly greater Z-scores compared to both other groups, except for the aortic root (Table 2). MFS patients with a dilated pDAo showed significantly lower WSS<sub>mean</sub> in the inner pDAo aortic segment ( $P < 0.05$ ) compared to both the MFS patients with pDAo Z-score  $< 2.0$  and the group of healthy subjects (Figure 4B-C and Table 2). Furthermore, MFS patients with dilated pDAo also showed lower WSS<sub>mean</sub> at the inner pAAo segment ( $P < 0.05$ ) and outer dDAo ( $P < 0.05$ ) compared to healthy subjects.

## Discussion

The findings of this study demonstrate that pediatric MFS patients have significantly lower WSS<sub>mean</sub> in the pAAo and pDAo than age-matched healthy controls. These regions in the aorta correspond to the locations where aortic dissection and aortic rupture often originate.<sup>2, 4, 5</sup> The subgroup of MFS patients with already dilated pDAo showed more prominent local vortex flow patterns and markedly lower WSS<sub>mean</sub> in the dilated pDAo region, when compared to non-dilated pDAo MFS patients and healthy controls. Furthermore, an inverse relationship between regional aortic diameter and WSS<sub>mean</sub> was observed in the entire study group.

Aortic dilatation in MFS patients may start in early childhood, warranting close clinical follow up of the diameters in the entire thoracic aorta from the time of diagnosis. The average aortic size and the heterogeneous involvement of the pDAo regarding dilatation found in this study are in concordance with previous studies.<sup>27,28</sup> Although MFS is known to be prone to ascending aortic complications, a substantial part of the aortic dissections in MFS occur in the pDAo before reaching surgical cut-off levels. European studies reported the pDAo to be the site of the first aortic complications in 16-18% of the MFS patients.<sup>2,29</sup> This proportion will increase after elective surgery of the AAo.<sup>4,5</sup> Changes in WSS in the aorta caused by changes in flow may be the key to better understand aortic disease development in MFS.

### Aortic flow patterns and wall shear stress

Mechanisms leading to progressive aortic dilatation and elongation are not fully understood. Recently, aortic flow and derived hemodynamic factors derived from CMR, including WSS, have been associated with focal evidence of molecular and architectural tissue dysfunction in patients with bicuspid aortic valve and aortopathy.<sup>15</sup> This study confirms that children and adolescent MFS patients already have disturbed aortic flow patterns in the thoracic aorta. The regions of prominent flow alterations were the aortic root and pDAo, with a significantly higher prevalence and strength of vortex flow patterns found in the pDAo in MFS compared to healthy subjects. Although it is known that small vortex flow patterns in

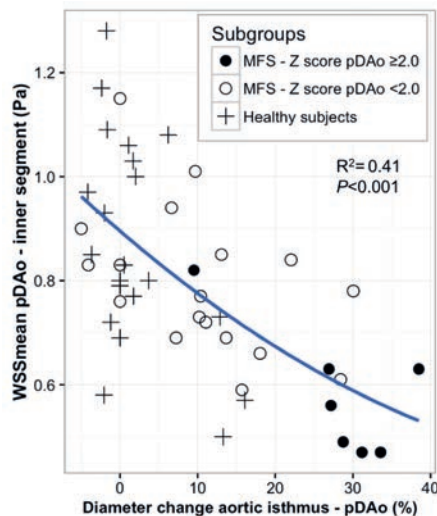


**Figure 5.** Relationship between size change and inner wall shear stress in the proximal descending aortic segment.

Inverse relation between diameter change between aortic isthmus and pDAo segment (in % of isthmus diameter) and  $WSS_{\text{mean}}$  of the pDAo segment in MFS patients and healthy subjects. pDAo, proximal descending aorta;  $WSS_{\text{mean}}$ , mean systolic wall shear stress.

the pDAo sometimes occur in normal aortas with an aortic spindle (i.e. a normal variation in the aortic contour not to be confused with an aneurysm),<sup>30</sup> the high prevalence and extensive nature found in these young MFS patients in this study is remarkable and consistent with observations by two previous CMR studies in MFS, with prevalence rates ranging from 54-70%.<sup>8,31</sup> Local aortic geometry seems to be related to the formation of these flow phenomena as the MFS subjects with most dilated pDAo segments (Z-score >2.0) showed the most extensive focal vortex flow patterns in this study.

**Table 2.** Comparison of aortic dimension and WSS between MFS groups and healthy subjects

	<b>Group 1</b> MFS - pDAo Z ≥2.0 (n = 7)	<b>Group 2</b> MFS - pDAo Z <2.0 (n = 18)	<b>Group 3</b> Healthy subjects (n = 21)
Age (y)	15.6 ± 4.5	15.6 ± 4.0	16.0 ± 2.6
Females (n)	3	8	12
BSA (m <sup>2</sup> )	1.6 ± 0.4	1.8 ± 0.3	1.6 ± 0.3
<b>Thoracic aortic size (Z-score)</b>			
Z-score Aortic Root**	4.4 ± 1.3	3.2 ± 1.4	0.5 ± 0.8
Z-score STJ**	3.0 ± 0.9	1.2 ± 1.0	-0.3 ± 0.8
Z-score AAo**	1.1 ± 0.7	-0.1 ± 0.8	-0.5 ± 0.6
Z-score distal Arch*	0.8 ± 0.7	-0.1 ± 0.9	-0.2 ± 0.7
Z-score Isthmus**	2.0 ± 0.7	0.6 ± 0.7	0.4 ± 0.5
Z-score proximal DAo**	4.2 ± 1.1	1.2 ± 0.6	0.6 ± 0.7
Δ diameter Root-AAo (%)**	30.9 ± 4.0	33.8 ± 7.0	19.0 ± 7.0
Δ diameter Isthmus-pDAo (%)**	27.9 ± 9.1	10.4 ± 10.1	1.9 ± 5.7
<b>WSS<sub>mean</sub> (Pa)</b>			
1. Inner pAAo*	0.69 ± 0.18	0.81 ± 0.09	0.86 ± 0.16
2. Outer pAAo	0.59 ± 0.11	0.67 ± 0.11	0.73 ± 0.14
3. Inner dAAo*	0.85 ± 0.18	0.97 ± 0.11	0.85 ± 0.15
4. Outer dAAo	0.75 ± 0.14	0.87 ± 0.11	0.83 ± 0.14
5. Inner Arch	0.83 ± 0.13	0.99 ± 0.13	0.91 ± 0.16
6. Outer Arch	0.71 ± 0.09	0.80 ± 0.11	0.79 ± 0.14
7. Inner pDAo*	0.58 ± 0.13	0.80 ± 0.14	0.87 ± 0.21
8. Outer pDAo	0.76 ± 0.13	0.89 ± 0.10	0.86 ± 0.12
9. Inner dDAo	0.75 ± 0.09	0.89 ± 0.16	0.89 ± 0.17
10. Outer dDAo*	0.78 ± 0.05	0.99 ± 0.18	0.97 ± 0.16

Significant across subgroups using a Kruskal-Wallis test. \*P < 0.05, \*\*P < 0.001.

Arch, aortic arch; dAAo, distal ascending aorta; pAAo, proximal ascending aorta; dDAo, distal descending aorta; pDAo, proximal descending aorta.



Several studies previously demonstrated that visibly pathologic flow patterns could lead to measurable alterations in WSS.<sup>32, 33</sup> Interestingly, the observed vortex flow patterns in the pDAo in MFS patients in this study corresponded to the reduced  $WSS_{\text{mean}}$  observed in the same segment. A similar relationship has been described in a longitudinal follow-up study of MFS patients after root replacement where vortex flow disturbances within the pDAo segment together with reduced local WSS measures developed.<sup>34</sup> In addition to the lower  $WSS_{\text{mean}}$  in the pDAo segment, considerable differences in  $WSS_{\text{mean}}$  were observed in the pAAo outer segment of the MFS patients compared to healthy subjects. However, no obvious flow pattern differences in the AAO were detected between MFS patients and the controls, except for local helix formation originating from the aortic root into the proximal AAO in 4 MFS patients. The significant difference in AAO size between the MFS and healthy controls could have contributed to this reduced regional  $WSS_{\text{mean}}$ .

Few studies have investigated aortic WSS in MFS disease cohorts so far<sup>9, 10</sup> and comparable investigations on aortic WSS were conducted in similar patients groups with dilative aortopathy of unknown origin (i.e. non-bicuspid valve related diseases).<sup>32, 35</sup> As in MFS patients, these patients have in common that the AAO is more or less dilated and these studies revealed similar aortic WSS results. In general, lower systolic WSS values were found along the dilated thoracic aorta in both these patient groups, as provided by 2D planar WSS quantification methods.<sup>9, 32, 35</sup> Similar to our findings, the specific locations of reduced systolic WSS were found at the outer curvature of the pAAo in most of these studies.<sup>9, 35</sup> Contrary to our results, one of the WSS studies in pediatric MFS patients showed inhomogeneous but relatively higher peak systolic WSS values at focal points on the vessel lumen circumference in the AAO compared to a healthy control group.<sup>10</sup> Although this is inconsistent to our findings, the higher WSS found in that study might be explained by the fact that the MFS patients were younger and had similar or even significantly smaller indexed aortic dimensions compared to the older healthy control group. Indeed, both factors (i.e. younger age and smaller vessel dimensions) have been proven to be associated with relatively higher WSS measures.<sup>36, 37</sup> The pDAo WSS in the MFS cohorts from these 4D flow CMR studies was equal or lower in MFS, but statistically similar compared to the WSS of healthy controls.<sup>9, 10</sup> It should be noted that the aortic WSS measurements in these comparative studies were all based on 2D planar WSS quantification methods, which means that WSS measurements are derived from single 2D cross-sectional planes along the thoracic aorta.

In this study, we used a novel approach providing 3D WSS along the entire aortic wall that was recently developed.<sup>25, 26</sup> The major advantage of this 3D WSS approach is that the entire aorta is included rather than sampling only a fraction of the vessel wall, thus reducing the chance of missing important regional variations in WSS. Moreover, it allows regional comparison to control references and no manual placement of 2D cross-sectional planes is needed, which is more subject to observer variability. In addition, the estimation of 3D WSS over a certain regional vessel surface enables to study relationships between regional hemodynamics and geometric measures, for instance aortic diameter or diameter changes between vessel segments.

### Aortic WSS and diameter

The findings of our study revealed a close interaction between altered aortic diameter and regional  $WSS_{mean}$  in MFS patients and healthy subjects. First, an inverse relationship between  $WSS_{mean}$  and aortic diameter was observed, which is congruent with existing literature.<sup>35, 36, 38</sup> The most obvious correlation was found for the pDAo segment, where both diameter and diameter change between the aortic isthmus and the largest pDAo dimension were inversely proportional to  $WSS_{mean}$ . Furthermore, subgroup analysis of MFS patients with a dilated pDAo showed the lowest  $WSS_{mean}$  in the corresponding region. Second, the dilation of the aortic root and STJ in MFS patients may have resulted in reduced  $WSS_{mean}$  values in the pAAo segment and might explain the  $WSS_{mean}$  asymmetry between the inner and outer pAAo segments. Such WSS asymmetry was also observed in the pAAo segment in another 4D flow CMR study on MFS patients.<sup>9</sup> Moreover, an *in-vitro* computational fluid dynamic (CFD) investigation about the effect of morphological changes in the aortic root on flow hemodynamics supports these findings. That CFD study, which was conducted with MFS-specific aortic root models of increasing size, showed that progressive root dilatation resulted in a different orientation of the blood stream jet in the aortic root and pAAo.<sup>39</sup> It is conceivable that a flow displacement from the sinus-side towards the commissure side has resulted in the altered distribution of  $WSS_{mean}$  that was observed in the pAAo in the MFS patients of this study.

### Clinical perspectives

Current management strategies for preventive aortic replacement in MFS are based on aortic diameters or rate of dilatation. However, this strategy remains imperfect and has led to a search for additional markers of disease severity and predictors of adverse vascular events, such as hemodynamic parameters. The results of this study showed already hemodynamic differences in young MFS patients compared to age-appropriate healthy subjects and determined close relationships between regional aortic geometry, flow patterns and 3D WSS over certain vessel regions. This relationship was most evident for the pDAo. Whether these hemodynamic parameters (i.e. flow and WSS) may add in the prediction of progressive dilatation, adverse events or optimization of management strategies in future in addition to the current diameter measurements is unknown and requires further longitudinal follow-up. In this regard and in line with our findings, a recent longitudinal 4D flow follow-up study on MFS patients after preventive valve-sparing aortic root replacement reported the occurrence of helical and vortex flow pattern formation along the inner curvature of the pDAo in 50% of the patients.<sup>34</sup> Additionally, in that report, a single case was described with newly derived regional vortex formation in the pDAo and altered WSS in that region prior to the development of an intramural hematoma with subsequent aortic dissection type B in the pDAo. This occurred 5 years after root replacement and the changes in flow and WSS parameters are noteworthy and suggest that these factors may play a role in the onset of the adverse event.<sup>34</sup> Together with our results, these observations show the clinical potential and future perspectives of comprehensive aortic flow hemodynamics assessments and monitoring of longitudinal changes by 4D flow imaging for optimization of preventive decision making.

Based on these and our data, one might speculate that at least the MFS patients with pDAo Z-score  $\geq 2.0$ , abnormal vortex flow patterns and decreased local  $WSS_{\text{mean}}$  are at higher risk for adverse cardiovascular events. Additional longitudinal studies are warranted to further elucidate the diagnostic value of inter-individual differences in MFS hemodynamics and the applicability of 4D flow parameters in prediction models.

### Study Limitations

The current study is subject to several limitations. In this observational study there might be some selection bias. Although MFS patients underwent CMR as a regular part of their lifelong clinical follow-up according to the MFS imaging guidelines, we cannot completely exclude the possibility that some of them received MR imaging based on previously abnormal findings on echocardiographic imaging. These results therefore may not be generalizable. However, it is known that the MFS patients individually can show a large heterogeneity in the involvement of heart and cardiovascular problems, e.g. the onset and the progression of disease over time.

To account for patient age and body size for aortic dimensions comparison in children, aortic Z-scores were calculated using EchoIMS. While EchoIMS provides ultrasound-derived normative data, there is currently no large pediatric CMR-specific database and this method of normalization is the best available alternative, is used in clinical practice and has been applied in previous CMR studies.<sup>22,23</sup>

Finally, potential sources of error, including the limited spatial resolution of 4D flow CMR, could have resulted in underestimation of 3D  $WSS_{\text{mean}}$  measurements. However, as both patient and healthy control groups underwent MR imaging at the same scanners with similar scan parameters, relative differences in  $WSS_{\text{mean}}$  between the two groups remain useful. Furthermore, 3D segmentation of the aorta based on the time-averaged systolic portion of the cardiac cycle is a potential source of error in this 4D flow study. However, averaging WSS over five systolic phases of the cardiac cycle with our algorithm, and using a well-defined segmentation protocol have been proven to produce low variability.<sup>26</sup>

### Conclusions

MFS children and young adults have altered aortic flow patterns and differences in WSS that were most pronounced in the pAAo and pDAo, which correspond to the locations where aortic dissection and aortic rupture often originate in these patients. Furthermore, close relationships between the regional aortic size and the presence of abnormal flow patterns and WSS were demonstrated and were more evident in the pDAo segment. These findings indicate that hemodynamic parameters may be discriminative and potentially valuable additional markers of disease severity. Additional longitudinal studies correlating changes in hemodynamic parameters (aortic flow profiles and WSS) with aortopathy are needed to establish the role of these parameters in disease progression and risk prediction of adverse events in MFS patients.

## References

1. Alpendurada F, Mohiaddin R. Prevalence of cardiovascular manifestations in patients with Marfan syndrome: a cardiovascular magnetic resonance study. *J Cardiovasc Magn Reson*. 2008;10(Suppl 1):A164.
2. Engelfriet PM, Boersma E, Tijssen JG, Bouma BJ, Mulder BJ. Beyond the root: dilatation of the distal aorta in Marfan's syndrome. *Heart*. 2006;92(9):1238-43.
3. Mariucci EM, Lovato L, Rosati M, Palena LM, Bonvicini M, Fattori R. Dilation of peripheral vessels in Marfan syndrome: importance of thoracoabdominal MR angiography. *Int J Cardiol*. 2013;167(6):2928-31.
4. Mimoun L, Detaint D, Hamroun D, Arnoult F, Delorme G, Gautier M, Milleron O, Meuleman C, Raoux F, Boileau C, et al. Dissection in Marfan syndrome: the importance of the descending aorta. *Eur Heart J*. 2011;32(4):443-9.
5. den Hartog AW, Franken R, Zwinderman AH, Timmermans J, Scholte AJ, van den Berg MP, de Waard V, Pals G, Mulder BJ, Groenink M. The risk for type B aortic dissection in Marfan syndrome. *J Am Coll Cardiol*. 2015;65(3):246-54.
6. Erbel R, Aboyans V, Boileau C, Bossone E, Bartolomeo RD, Eggebrecht H, Evangelista A, Falk V, Frank H, Gaemperli O, et al. 2014 ESC Guidelines on the diagnosis and treatment of aortic diseases: Document covering acute and chronic aortic diseases of the thoracic and abdominal aorta of the adult. The Task Force for the Diagnosis and Treatment of Aortic Diseases of the European Society of Cardiology (ESC). *Eur Heart J*. 2014;35(41):2873-926.
7. van Ooij P, Potters WV, Collins J, Carr M, Carr J, Malaisrie SC, Fedak PW, McCarthy PM, Markl M, Barker AJ. Characterization of abnormal wall shear stress using 4D flow MRI in human bicuspid aortopathy. *Ann Biomed Eng*. 2015;43(6):1385-97.
8. Geiger J, Markl M, Herzer L, Hirtler D, Loeffelbein F, Stiller B, Langer M, Arnold R. Aortic flow patterns in patients with Marfan syndrome assessed by flow-sensitive four-dimensional MRI. *J Magn Reson Imaging*. 2012;35(3):594-600.
9. Wang HH, Chiu HH, Tseng WY, Peng HH. Does altered aortic flow in marfan syndrome relate to aortic root dilatation? *J Magn Reson Imaging*. 2016;44(2):500-8.
10. Geiger J, Arnold R, Herzer L, Hirtler D, Stankovic Z, Russe M, Langer M, Markl M. Aortic wall shear stress in Marfan syndrome. *Magn Reson Med*. 2013;70(4):1137-44.
11. Wigstrom L, Ebbers T, Fyrenius A, Karlsson M, Engvall J, Wranne B, Bolger AF. Particle trace visualization of intracardiac flow using time-resolved 3D phase contrast MRI. *Magn Reson Med*. 1999;41(4):793-9.
12. Buonocore MH. Visualizing blood flow patterns using streamlines, arrows, and particle paths. *Magn Reson Med*. 1998;40(2):210-26.
13. Markl M, Frydrychowicz A, Kozerke S, Hope M, Wieben O. 4D flow MRI. *J Magn Reson Imaging*. 2012;36(5):1015-36.
14. Markl M, Schnell S, Wu C, Bollache E, Jarvis K, Barker AJ, Robinson JD, Rigsby CK. Advanced flow MRI: emerging techniques and applications. *Clin Radiol*. 2016;71(8):779-95.
15. Guzzardi DG, Barker AJ, van Ooij P, Malaisrie SC, Puthumana JJ, Belke DD, Mewhort HE, Svystonyuk DA, Kang S, Verma S, et al. Valve-Related Hemodynamics Mediate Human Bicuspid Aortopathy: Insights From Wall Shear Stress Mapping. *J Am Coll Cardiol*. 2015;66(8):892-900.
16. Loeys BL, Dietz HC, Braverman AC, Callewaert BL, De Backer J, Devereux RB, Hilhorst-Hofstee Y, Jondeau G, Faivre L, Milewicz DM, et al. The revised Ghent nosology for the Marfan syndrome. *J Med Genet*. 2010;47(7):476-85.
17. Hiratzka LF, Bakris GL, Beckman JA, Bersin RM, Carr VF, Casey DE, Jr., Eagle KA, Hermann LK, Isselbacher EM, Kazerooni EA, et al. 2010 ACCF/AHA/AATS/ACR/ASA/SCA/SCAI/SIR/STS/SVM Guidelines for the diagnosis and management of patients with thoracic aortic disease. A Report of the American College of Cardiology Foundation/American Heart Association Task Force on Practice Guidelines, American Association for Thoracic Surgery, American College of Radiology, American Stroke Association, Society

- of Cardiovascular Anesthesiologists, Society for Cardiovascular Angiography and Interventions, Society of Interventional Radiology, Society of Thoracic Surgeons, and Society for Vascular Medicine. *J Am Coll Cardiol*. 2010;55(14):e27-e129.
18. Burman ED, Keegan J, Kilner PJ. Aortic root measurement by cardiovascular magnetic resonance: specification of planes and lines of measurement and corresponding normal values. *Circ Cardiovasc Imaging*. 2008;1(2):104-13.
  19. Nejatian A, Yu J, Geva T, White MT, Prakash A. Aortic Measurements in Patients with Aortopathy are Larger and More Reproducible by Cardiac Magnetic Resonance Compared with Echocardiography. *Pediatr Cardiol*. 2015;36(8):1761-73.
  20. Mosteller RD. Simplified calculation of body-surface area. *N Engl J Med*. 1987;317(17):1098.
  21. Chubb H, Simpson JM. The use of Z-scores in paediatric cardiology. *Ann Pediatr Cardiol*. 2012;5(2):179-84.
  22. Johnson RK, Premraj S, Patel SS, Wahle A, Stolpen A, Sonka M, Scholz TD. Quantitative assessment of the entire thoracic aorta from magnetic resonance images. *Cardiol Young*. 2011;21(2):170-7.
  23. Allen BD, van Ooij P, Barker AJ, Carr M, Gabbour M, Schnell S, Jarvis KB, Carr JC, Markl M, Rigsby C, et al. Thoracic aorta 3D hemodynamics in pediatric and young adult patients with bicuspid aortic valve. *J Magn Reson Imaging*. 2015;42(4):954-63.
  24. Bock J, Kreher B, Henning J, Markl M. Optimized pre-processing of time-resolved 2D and 3D phase contrast MRI data. *Proceedings of the 15th Annual Meeting of ISMRM, Berlin, Germany*. 2007; Abstract 3138.
  25. Potters WV, van Ooij P, Marquering H, vanBavel E, Nederveen AJ. Volumetric arterial wall shear stress calculation based on cine phase contrast MRI. *J Magn Reson Imaging*. 2015;41(2):505-16.
  26. van Ooij P, Powell AL, Potters WV, Carr JC, Markl M, Barker AA. Reproducibility and interobserver variability of systolic blood flow velocity and 3D wall shear stress derived from 4D flow MRI in the healthy aorta. *J Magn Reson Imaging*. 2016;43(1):236-48.
  27. Faivre L, Masurel-Paulet A, Collod-Beroud G, Callewaert BL, Child AH, Steneur C, Binquet C, Gautier E, Chevallier B, Huet F, et al. Clinical and molecular study of 320 children with Marfan syndrome and related type I fibrillinopathies in a series of 1009 probands with pathogenic FBN1 mutations. *Pediatrics*. 2009;123(1):391-8.
  28. van Karnebeek CD, Naeff MS, Mulder BJ, Hennekam RC, Offringa M. Natural history of cardiovascular manifestations in Marfan syndrome. *Arch Dis Child*. 2001;84(2):129-37.
  29. Finkbohner R, Johnston D, Crawford ES, Coselli J, Milewicz DM. Marfan syndrome. Long-term survival and complications after aortic aneurysm repair. *Circulation*. 1995;91(3):728-33.
  30. Fisher RG, Sanchez-Torres M, Whigham CJ, Thomas JW. "Lumps" and "bumps" that mimic acute aortic and brachiocephalic vessel injury. *Radiographics*. 1997;17(4):825-34.
  31. Picher A, Cassar TE, Suttie J, Francis JM, Leeson P, Blair E, Wordsworth BP, Forfar JC, Myerson SG, Markl M, et al. Visualisation of aortic flow disturbance in Marfan syndrome by 4D phase-contrast CMR. *J Cardiovasc Magn Reson*. 2011;13(Suppl 1):P201.
  32. Biegling ET, Frydrychowicz A, Wentland A, Landgraf BR, Johnson KM, Wieben O, Francois CJ. In vivo three-dimensional MR wall shear stress estimation in ascending aortic dilatation. *J Magn Reson Imaging*. 2011;33(3):589-97.
  33. Frydrychowicz A, Arnold R, Hirtler D, Schlensak C, Stalder AF, Hennig J, Langer M, Markl M. Multidirectional flow analysis by cardiovascular magnetic resonance in aneurysm development following repair of aortic coarctation. *J Cardiovasc Magn Reson*. 2008;10:30.
  34. Hope TA, Kvitting JP, Hope MD, Miller DC, Markl M, Herfkens RJ. Evaluation of Marfan patients status post valve-sparing aortic root replacement with 4D flow. *Magn Reson Imaging*. 2013;31(9):1479-84.
  35. Burk J, Blanke P, Stankovic Z, Barker A, Russe M, Geiger J, Frydrychowicz A, Langer M, Markl M. Evaluation of 3D blood flow patterns and wall shear stress in the normal and dilated thoracic aorta using flow-sensitive 4D CMR. *J Cardiovasc Magn Reson*. 2012;14:84.
  36. Truong U, Fonseca B, Dunning J, Burgett S, Lanning C, Ivy DD, Shandas R, Hunter K, Barker AJ. Wall shear

stress measured by phase contrast cardiovascular magnetic resonance in children and adolescents with pulmonary arterial hypertension. *J Cardiovasc Magn Reson*. 2013;15:81.

37. van Ooij P, Garcia J, Potters WV, Malaisrie SC, Collins JD, Carr JC, Markl M, Barker AJ. Age-related changes in aortic 3D blood flow velocities and wall shear stress: Implications for the identification of altered hemodynamics in patients with aortic valve disease. *J Magn Reson Imaging*. 2016;43(5):1239-49.
38. Allen BD, Markl M, Barker AJ, van Ooij P, Carr JC, Malaisrie SC, McCarthy P, Bonow RO, Kansal P. Influence of beta-blocker therapy on aortic blood flow in patients with bicuspid aortic valve. *Int J Cardiovasc Imaging*. 2016;32(4):621-8.
39. Querzoli G, Fortini S, Espa S, Costantini M, Sorgini F. Fluid dynamics of aortic root dilation in Marfan syndrome. *J Biomech*. 2014;47(12):3120-8.

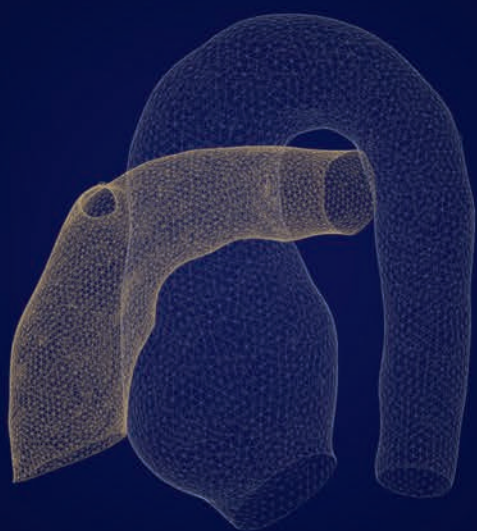
---

## Online supplementary videos

**Video 1.** Pathline visualization from a MFS patient's aorta with local vortex flow pattern in the proximal descending aorta during systole and early diastole. Note the prominent vortex flow patterns in the sinuses of the aortic root.

**Video 2.** Pathline visualization of a normal aorta from a healthy subject. No local flow pattern abnormalities are present.

<https://jcmr-online.biomedcentral.com/articles/10.1186/s12968-017-0345-7>



## **CHAPTER 10**

Summary and future perspectives



The aim of this thesis was to investigate the prevalence and evolution of neo-aortic root pathology and surgical cardiovascular outcomes in patients after arterial switch operation (ASO) for transposition of the great arteries (TGA). Furthermore, thoracic aortic blood flow hemodynamics were investigated in relation to post-ASO geometry and root pathology with advanced non-invasive 4D flow cardiovascular magnetic resonance imaging (MRI) techniques.

A brief introduction about the Leiden surgical history for TGA was given in **Chapter 1**, together with a description of the neo-aortic complications (i.e. neo-aortic root dilatation and neo-aortic valve regurgitation) patients may face during follow-up after ASO. The first ASO was successfully performed in 1975 and this approach has become the surgical procedure of choice for TGA worldwide since mid-eighties.<sup>1</sup> Cardiovascular imaging modalities such as echocardiography and cardiovascular MRI play an important role in the diagnosis of TGA and in monitoring and management of the neo-aortic root postoperatively. In the studies described in this thesis, echo and 4D flow MRI techniques were used to gain new insights into the progression of neo-aortic root pathology and on the aortic blood flow hemodynamics in TGA patients after ASO.

## **Part I**

### **The neo-aorta in TGA – outcome after arterial switch operation**

**Chapter 2** summarizes the long-term surgical cardiovascular outcomes of the TGA cohort after 43 years of experience with the ASO in the Center for Congenital Heart Disease Amsterdam-Leiden (1977-2020). Patients with TGA with intact septum or TGA with ventricular septal defect (TGA-VSD) and double outlet right ventricle with subpulmonary VSD (Taussig-Bing anomaly) were included. The entire cohort consisted of 490 patients who underwent ASO. Of them, 43 patients died in the first postoperative month and 34 overseas patients (surviving ASO) were lost to follow-up, leaving 413 early ASO survivors with known follow-up for the evaluation of long-term outcome. Median follow-up was 15.6 (IQR 7.0-22.4) years post-ASO. Hospital mortality rates decreased rapidly over decades to 3.3% for the last two decades. Late mortality was low with 12 out of 413 patients (2.9%) who died after hospital discharge post-ASO, at a median age of 10.6 (0.9-21.9) years post-ASO. Late mortality was not related to acute coronary artery problems in 5 patients with identified causes of death; in 7 patients the exact cause of death could not be retrieved retrospectively. During follow-up the need for one or more reoperations and one or more catheter interventions was 20.1% and 13.1% respectively. Most reoperations and interventions were performed for right ventricular outflow tract problems. Coronary artery reoperations or interventions were required in only nine patients (2.2%), suggesting that coronary problems do not frequently occur during follow-up. The neo-aortic root pathology however significantly impacts long-term outcome given that the incidence of neo-aortic root and aortic valve redo surgery increases over decades. Twenty-one surgical procedures and one catheter procedure for

neo-aortic valve insufficiency and/or root dilatation were performed in 15 patients (3.6%), approximately 20% of the total amount of reoperations. In two-third of the reoperated patients surgery was performed in the last decade (2009-2020). Between 1977 and 2009, only 5 patients needed reoperation for neo-aortic pathology of the 302 early survivors after ASO (1.7%). Although the total amount of reoperations for neo-aortic valve/root problems is still low and comparable to international surgical centers,<sup>2</sup> with longer follow-up times it is likely that the need for surgery for late neo-aortic root complications will further increase. Independent risk factors for the need of any reoperation or intervention were: a more complex TGA morphology (TGA-VSD), aortic arch repair associated to ASO and a non-usual coronary artery anatomy.

**Chapter 3** describes the natural growth of the *native* aortic valve and the pulmonary valve in fetuses with TGA from 20 weeks' gestation till birth. This growth was compared with normal fetal semilunar valve growth from reference data of fetuses without congenital heart defects.<sup>3,4</sup> In TGA fetuses, semilunar valves (i.e. both the pulmonary and the aortic valve) were larger compared with fetuses with normal hearts. Pulmonary valve annular diameters were larger than controls from 27 weeks' gestation, especially when a VSD was present, and were also significantly larger than control aortic valve annular diameters from 23 weeks' gestation. These observations suggest that other factors besides flow play a role in the growth of the semilunar valve annuli in fetal TGA. The indexed size of the pulmonary valve annulus (i.e. indexed to body surface area and expressed as Z-score) at 26 to 30 weeks correlated with the indexed size of the neo-aortic root at last follow-up visit post-ASO. However, this correlation was not strong enough and the postoperative follow-up relatively short to be clinically useful for a prenatal prediction of neo-aortic root dilatation (dilatation defined as Z-score >2.0) post-ASO. Findings from this study adds to our understanding of the pathophysiology of fetal semilunar growth. Furthermore, it provides insight in the origin of the differences between the morphological subtypes of TGA as starting point for the further course of neo-aortic valve and root growth in the years beyond the ASO.

**Chapter 4** reports the results of a retrospective longitudinal follow-up study on neo-aortic growth, neo-aortic valve function and reoperations for neo-aortic valve and/or root pathology from birth up to 39 years post-ASO for the various morphological subtypes of TGA. This study demonstrated that neo-aortic root dilatation is progressive over time and does not stabilize in adulthood. The neo-aortic annulus, root and the sinotubular junction all showed similar growth patterns: a rapid disproportional increase in the first year after ASO exceeding upper limits of normal dimensions (indexed to body surface area with on average Z-scores >2.0), followed by a nearly linear increase of neo-aortic dimensions in childhood comparable to normal somatic growth, with an ongoing progressive growth in adulthood. Complex morphological TGA subtype (TGA-VSD and Taussig-Bing anomaly) and male gender were found to be independent risk factors for neo-aortic root dilatation.

Furthermore, neo-aortic valve regurgitation continued to develop over time: freedom from moderate or more regurgitation during first 25 years post-ASO was 69%. Importantly, this study showed that the progression of neo-aortic root dilatation is a critical factor for impairment of the neo-aortic valve function: per millimeter increase in neo-aortic root dimension over time there was an average 9% increase in the hazard of moderate or more neo-aortic valve regurgitation. These data suggest that in this group of patients an important underlying mechanism for regurgitation is impaired leaflet coaptation due to progression of the neo-aortic root and valve dimensions. Bicuspid pulmonary valve morphology was not associated with a higher risk of regurgitation which endorses that a preoperative competent bicuspid valve itself is not a contraindication for ASO with regard to long-term valve function. The incidence of neo-aortic reoperations in this study was low and concerned 3% of the cohort. However, already 14% of the study cohort developed a neo-aortic root diameter  $\geq 40$ mm, with at least moderate neo-aortic valve regurgitation in 26% of them. Of note, one-quarter of these patients have not even reached adulthood. The ongoing neo-aortic dilatation also during adulthood, progression of neo-aortic valve regurgitation and its mutual relationship as demonstrated in this study is of concern and may imply an increased need of root and valve reoperations in the near future.

**Chapter 5** presents an extension of the results on the effect of changing neo-aortic dimensions over time on the risk of neo-aortic valve regurgitation as reported in Chapter 4. A reanalysis on the data was performed by a more comprehensive statistical analysis approach for the evaluation of longitudinal data with time-to-event data by means of joint modeling. From this approach, it was confirmed that the neo-aortic root dimensions showed a positive significant association with at least moderate neo-aortic valve regurgitation, but the association was much stronger than was previously determined (Chapter 4). Furthermore, with joint modeling the neo-aortic root dimension was also shown to be an independent risk factor for the development of at least mild neo-aortic valve regurgitation where previously no association was found. Moreover, also the neo-aortic annulus dimension was an independent risk factor for the development of both at least mild neo-aortic valve regurgitation and at least moderate neo-aortic valve regurgitation. Apart from this, neo-aortic annular growth rate as well as the neo-aortic root growth rate, in addition to the annular and root dimensions, were independently associated with the development of at least mild neo-aortic valve regurgitation. This means that a faster growth of the neo-aortic annulus and neo-aortic root, on top of the neo-aortic dimensions, was associated with a higher risk of neo-aortic valve regurgitation.

**Part II****Aortic 4D flow MR imaging - the arterial switch operation for TGA and beyond**

Recently, 4D flow MRI has been introduced as a novel non-invasive imaging method that can be used for comprehensive *in vivo* assessment of blood flow in the large vessels.<sup>5,6</sup> It provides information about the spatial and temporal distribution of vascular blood flow and enables the quantification of flow-related hemodynamic parameters. Therefore, 4D flow MRI is used to better understand cardiovascular physiology and pathophysiology and has led to improved knowledge of disease progression in patients with congenital heart disease-related aortopathy.<sup>6-10</sup> Advanced hemodynamic parameters such as wall shear stress (WSS) and flow displacement can be derived from 4D flow MRI. Several studies have shown that increased flow displacement, defined as the displacement of peak systolic flow from the aortic center, is related to aortic valve morphology and is correlated with future ascending aortic growth in bicuspid valve-related dilated aortopathy.<sup>9,11</sup> The parameter WSS represents the viscous shear force of flowing blood acting tangentially to the vessel wall. Areas of high WSS have been associated with marked histological changes in the ascending aortic vessel wall in patients with bicuspid aortic valves.<sup>12</sup> In addition, abnormal WSS has been suggested to have potentially contributing effects on vessel dilatation and aneurysm formation; for example, on the thoracic aorta and on intracranial aneurysms.<sup>13,14</sup>

The application of aortic 4D flow MRI can therefore be of great value for the evaluation of aortopathy in patients after ASO for TGA. However, validation of the applied 4D flow techniques and knowledge on the reproducibility and consistency of its output parameter(s) are necessary to interpret differences between patient groups and between longitudinal patient data. For that reason, a scan-rescan reproducibility and observer variability study for 3D systolic WSS in the thoracic aorta was performed in healthy subjects and summarized in **Chapter 6**. For the WSS analysis, the thoracic aorta was divided into 5 segments: proximal and distal ascending aortic segment, aortic arch and proximal and distal descending aortic segment. Consequently, the maximum peak systolic WSS (WSSmax) and the mean peak systolic WSS (WSSmean) in each of the segments were calculated. Scan-rescan reproducibility was good for WSSmean in all thoracic aortic regions but scan-rescan reproducibility for WSSmax was moderate with higher variability in the proximal ascending aorta. The intraobserver and interobserver reproducibility for segmental systolic WSS analysis of WSSmax and WSSmean was good to excellent. In general, the ascending aortic segments showed more variability in WSSmax and WSSmean measurements compared to aortic arch or descending aortic segments for scan-rescan, intraobserver and interobserver comparison. These WSS variations should be considered in patient studies and comparative rest-stress studies to avoid misinterpretation of data.

In **Chapter 7**, we investigated the ascending aortic hemodynamics in simple TGA patients after ASO compared to healthy subjects using 4D flow MRI. In these patients, neo-aortic

root dilatation is present and progressive over time and has been shown to be a critical factor in deterioration of the neo-aortic valve function (as stated in Chapter 4 and 5). Aortic dimensions from the ascending aorta and two quantitative hemodynamic parameters were assessed: normalized flow displacement (FD) and WSS. TGA patients after ASO showed more eccentric flow in the proximal ascending aorta (i.e. neo-aortic root) evidenced by a higher magnitude and directionality of FD, which was linearly related with local indexed aortic dimensions of the neo-aortic root and sinotubular junction (i.e. indexed by body surface area and expressed as Z-scores). Directionality of the eccentric flow profiles in the neo-aortic root were significantly different between patients with different TGA-specific preoperative position of the great arteries: a right-anterior or right-sided position of the aorta related to the pulmonary artery showed more FD to the right-side of the ascending aorta, whereas a left-anterior or anterior position of the aorta resulted in more FD to the left-side of the aortic wall at the level of the neo-aortic root. Furthermore, TGA patients showed abnormal regional WSS in the proximal ascending aorta: lower WSS compared to healthy subjects; in the distal ascending aorta: higher WSS compared to healthy subjects, with a focal increased WSS hotspot on the anterior-right anterior wall of the distal ascending aorta. The ASO-specific aortic geometry consisted of neo-aortic root dilatation and a sudden change in vessel diameter at the mid-ascending aortic level, the level of anterior aortic compression by the pulmonary trunk due to Lecompte maneuver as part of the ASO. This sudden change in aortic diameter was associated with increased and asymmetric peak systolic WSS distribution along the distal ascending aorta, most pronounced in the right and anterior aortic wall regions. The larger the size discrepancy between the neo-aortic root and mid-ascending aorta, the higher the WSS levels in the distal ascending aorta.

The regions of the abnormal increased WSS clinically correlate with the location of the paper-thin and fragile anterior wall of the ascending aorta that has been found in ASO patients during root reoperations, as described earlier by our center.<sup>15</sup> The flow displacement direction from root to mid-ascending aorta also corresponded to the peak systolic WSS distribution in the mid-ascending aorta, but the contribution of FD on WSS distribution more upstream in the distal ascending aorta was less compared with the effect of vessel tapering. The observations from this study start to unravel the interaction between the post-ASO geometry and hemodynamics within the ascending aorta and how the hemodynamics may be involved in the (progression of) neo-aortic root dilatation and/or anterior aortic wall thinning of the distal ascending aorta.

In **Chapter 8**, aortic WSS distribution was evaluated in the entire thoracic aorta of TGA patients after ASO compared to healthy subjects and was related to geometric thoracic aortic alterations post-ASO. Furthermore, the effects of dobutamine-induced stress on aortic WSS were studied *in vivo* in TGA patients and were compared with the rest state. The investigations were conducted to assess whether geometry-driven or pharmacological stress-induced alterations in aortic flow might have its impact on the aortic wall in patients with increased risk on progressive neo-aortic root dilatation over time. This is important

since progressive neo-aortic root dilatation has been proven to be a major factor for the impairment of neo-aortic valve function in these patients (as stated in Chapter 4 and 5). In concordance with literature,<sup>16-18</sup> specific geometric alterations of the thoracic aorta after ASO were observed and consisted of a large size discrepancy between the dilated neo-aortic root and the mid-ascending aortic diameter due to the anterior aortic position and compression by the pulmonary artery branches after ASO with Lecompte maneuver. Furthermore, a more acute angulation of the curvature of the aortic arch was determined. From the 4D flow analysis, pediatric and adolescent patients after ASO showed significantly higher WSS magnitude in the entire thoracic aorta compared with healthy subjects at rest, except for the dilated proximal ascending aorta. In agreement with the findings in Chapter 7, the regions of high peak systolic WSS were most pronounced in the distal ascending aorta and located at the anterior aortic wall of that segment. The specific ascending aortic geometry post-ASO, reflected by the size discrepancy between the dilated neo-aortic root and the smaller mid-ascending aorta diameter, was associated with higher WSS levels in all the aortic segments downstream this caliber change: the larger the size discrepancy, the higher the WSS levels in the distal ascending aorta, but also in the descending aortic segments. The geometry of the aortic arch, reflected by the sharper aortic arch angulation in TGA patients after ASO compared to healthy subjects, did not further contribute to the high WSS levels in the aortic arch and the descending aortic segments.

Dobutamine-induced cardiac stress did increase WSS magnitude significantly along all thoracic aortic segments, the most prominent in the ascending aortic segments. The highest peak systolic WSS was present in the distal ascending aortic segment during both rest and stress, but for stress, this was even more pronounced. The peak systolic WSS increase by dobutamine in that segment showed a positive correlation with the increase in the LV ejection fraction, stroke volume, and cardiac output. Based on the results from this study we concluded that pharmacological-induced stress evaluations of aortic blood flow might better reflect location and expansion of vascular wall areas exposed to abnormal WSS with subsequent risks for vascular remodeling. Stress might play a role in neo-aortic root dilatation in TGA patients after ASO given the significant stress-induced WSS increase in the neo-aortic root, acting on root tissue with structural vessel wall abnormalities.<sup>19, 20</sup>

Knowledge on the extent of the distribution and magnitude of aortic WSS is not only of interest in postoperative congenital heart disease patients such as in patients after ASO, but also in patients with inherited connective tissue disease such as Marfan syndrome. These patient groups have progressive root dilatation in common, but Marfan patients have proven to be at risk for aortic dissection and aortic rupture.<sup>21, 22</sup> In TGA patients after ASO root dilatation and valve insufficiency are well documented but aortic dissections have not been reported in literature so far. To learn from patients with aortopathy being more at risk for adverse cardiovascular events, we also performed a 4D flow MRI study in pediatric patients with Marfan syndrome. This study was performed in collaboration with the Lurie Children's Hospital of Chicago and the Northwestern University Feinberg School of Medicine,

Chicago, Illinois, USA and is summarized in **Chapter 9**. Thoracic aorta hemodynamics such as blood flow patterns, regional aortic WSS, and aortic dimensions were assessed in a pediatric Marfan syndrome cohort and were compared to a healthy age-appropriate control cohort. A substantial part of the children with Marfan syndrome showed altered aortic flow patterns, consisting of marked vortex flow in the proximal descending aorta and non-physiological helical flow patterns with high strength originating from the aortic root into the ascending aorta. Moreover, significant differences in aortic WSS were found in Marfan patients compared to the aged matched healthy subjects. These flow alterations and the detected lower WSS magnitude were most pronounced in the proximal ascending aorta and proximal descending aorta, segments where aortic dissection or rupture often originate. The presence of vortex flow patterns and abnormal WSS correlated with regional size of the proximal descending aorta and are potentially valuable additional markers of disease severity. Long-term follow-up of these patients will indicate the prognostication of these 4D flow imaging parameters on the progression of aortic dilatation and/or the occurrence of adverse aortic events at these predilection sites.

## Conclusions

In this thesis multiple aspects of aortopathy in patients with transposition of the great arteries were studied, both in fetal life and after the arterial switch operation, with a key role for aortic imaging and longitudinal follow-up. The development of the neo-aortic valve and root dimensions and the fate of the neo-aortic valve over time were investigated and showed progressive root dilatation without stabilization in adult life with the root diameter as critical factor for the impairment of neo-aortic valve function. Based on these findings, along with observations of an increased incidence of reoperations on the neo-aortic valve and/or root over the past decade, the need for surgery for late neo-aortic root complications is expected to further increase with longer follow-up times.

The pathophysiology of progressive root dilatation remains incompletely understood and is most likely multifactorial. In this thesis, it was demonstrated that more complex morphological TGA subtype (TGA-VSD and Taussig-Bing anomaly) and male gender were independent risk factors for neo-aortic root dilatation. Furthermore, insights from the present 4D flow studies suggest a contributing factor of flow hemodynamics associated with the ASO-specific thoracic aortic geometry. These insights from comprehensive aortic blood flow imaging may contribute in further understanding the mechanisms involved in the neo-aortic root dilatation and, ultimately, provide valuable information to guide personalized management of neo-aortic disease in TGA patients after ASO within the next decade.

## Recommendations and future prospects – personalized management

Three important areas of research impacting patient care for TGA patients after ASO in the near future should focus on personalized cardiovascular management to improve outcome.

### 1. Surveillance of valve and root complications – risk stratification models from serial data

Noninvasive imaging modalities are used for detection and surveillance of root dilatation and valve insufficiency. Longitudinal long-term follow-up data from standardized imaging protocols enables the assessment of risk factors for certain outcomes, as shown for the occurrence of neo-aortic valve leakage in this thesis. In addition, these data will also allow to predict outcome of adverse events or disease progression on an individualized basis. Development of such prediction models and risk stratification tools for physicians can serve for scientifically-based individual patient management. Using this information to direct care, identifies the right level of care for each patient, maximizes efficiency and may improve outcome at population level.

New statistical methodologies (e.g. joint modeling) can simultaneously model a longitudinal marker (neo-aortic root dilatation) with time-to-event data (the occurrence of certain degree of neo-aortic valve regurgitation). These models give more insight in patients: how they 'behave' compared to their peers. In addition, they have the potential to reduce costs, time and to better prognosticate. Since survival into adulthood is expected for almost all congenital heart diseases and prognostication is requested by patients and their parents, central registration of outcome data and longitudinal measures for residual abnormalities in large (local, national or even European controlled) databases is a recommended next step. We have the framework, but we have to critically choose patient categories for this investment and implement this in daily practice.

### 2. 4D flow imaging – surgical considerations (ASO technique & TGA morphology)

Extending knowledge on pathophysiologic mechanisms of altered flow hemodynamics on disease progression is necessary in TGA patients after ASO, to get better insight and to think about surgical techniques solving long-term residual sequelae in patients with TGA. Some surgical centers advocate for the preservation of the spiral relationship of the large arteries by the use of a direct spiral ASO instead of the application of the Lecompte maneuver with the neonatal ASO.<sup>23, 24</sup> Although it needs to be proved that direct spiral ASO has its advantages in functional outcome over the ASO with Lecompte maneuver in the long run, from semiquantitative evaluation of aortic flow patterns by 4D flow MR imaging in these patients with 20 year postoperative follow-up it is reported that more physiologically aortic blood flow profiles with less blood flow alterations (i.e. less vortex formation and lower relative helicity magnitude) are present using that technique.<sup>24</sup> These results, together with the results from the aortic 4D flow studies



reported in this thesis (Chapter 7 and 8) in which we showed already abnormal ascending aortic flow hemodynamics in young patients after ASO, suggest aortic geometry as an important factor for altered ascending aortic flow hemodynamics. The clinical relevance of these differences in blood flow profiles between the surgical ASO approaches for TGA patients later in life remains to be evaluated. Since all 4D flow studies in TGA patients after ASO have been performed at one single timepoint without serial follow-up, it is unknown whether the altered hemodynamics are either the result of progressive aortic dilatation, or whether the altered hemodynamics are in any way causative to the dilatation. Longitudinal 4D flow studies in these patients are necessary to gain more insight in these mechanisms. Moreover, additional 4D flow studies evaluating the interindividual differences in aortic hemodynamics between TGA patients with different ASO techniques (i.e. with and without the application of Lecompte maneuver) and between TGA patients with different anatomy (i.e. with or without VSD and TGA subgroups with different spatial position of the great arteries) need to be performed to ultimately optimize individual surgical management strategies for the best long-term outcomes.

### **3. 4D flow imaging – a guide for interventions**

Risk factors for neo-aortic root dilatation in TGA patients are most likely multifactorial, but insights from the present 4D flow studies suggest a contributing factor of flow hemodynamics related to the ASO-specific geometry of the thoracic aorta. Ultimately, advanced hemodynamic imaging parameters derived from 4D flow can serve in the prediction of aortic complications (root dilatation, aortic rupture or aortic dissection) and may aid in timing of interventions to optimize clinical outcome for dilative aortopathies as current management strategies are imperfect and based on just absolute diameters.<sup>25</sup> Therefore, efforts should be made to incorporate 4D flow MRI as standard follow-up examination in TGA patients after ASO, but also in other aortopathies like Marfan syndrome and after reconstructive aortic arch repair, to put the value of these novel imaging markers in clinical perspective. Moreover, 4D flow studies in all patients necessitating root replacement are required for the comparison of MR-derived biomarkers and histopathological aortic wall alterations to investigate flow-mediated wall changes contributing to root dilatation and anterior aortic wall thinning. Multi-institutional collaboration should be encouraged to move forward on this topic given the challenge of data collection with the relative low incidence of root replacements in single institutions.

Another potentially essential role for 4D flow imaging is its use in the preoperative planning for root and ascending aortic replacements. The integration of 4D flow-derived data from individual TGA-specific aortas in computational fluid dynamics enables the evaluation of the most optimal surgical approach for an intervention, by predicting the hemodynamic response and determining the best personalized aortic conduit fit (size, curvature and length) for implantation. Preoperative personalized surgical planning in a virtual platform with integrated computational fluid dynamic modeling of personalized

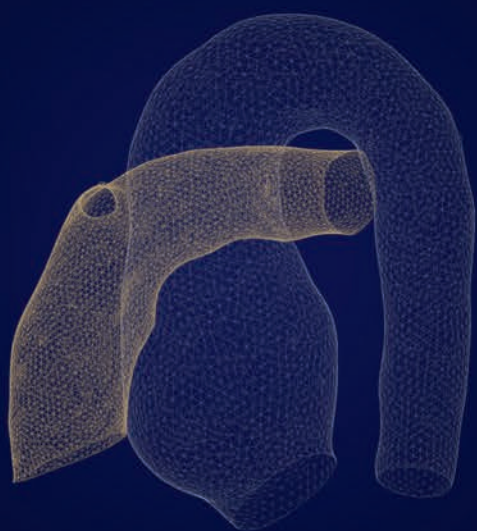
*in vivo* aortic 4D flow data will be the future, to tailor conduit characteristics, conduit production and implantation (i.e. model-based personalized management). It is expected that this application will not only become important for patients with aortopathy, but may also be relevant for a larger spectrum of growing patients with (repaired) congenital heart defects.

Technical advances in cardiovascular imaging are essential to promote cardiovascular science and medical management. However, one note has to be made. The rapidly advancing technology is striking, but validation of these new applications is essential before the implementation in daily clinical practice, and should not be underestimated. If proven to be robust (precise and reproducible), these techniques will ultimately change clinical practice and improve outcome for patients with TGA and other congenital heart diseases.

## References

1. Jatene AD, Fontes VF, Paulista PP, de Souza LC, Neger F, Galantier M, Souza JE. Successful anatomic correction of transposition of the great vessels. A preliminary report. *Arq Bras Cardiol.* 1975;28(4):461-64.
2. Vida VL, Zanotto L, Zanotto L, Stellin G, European Congenital Heart Surgeons Association Study G, Padalino M, Sarris G, Protopapas E, Prospero C, Pizarro C, et al. Left-Sided Reoperations After Arterial Switch Operation: A European Multicenter Study. *Ann Thorac Surg.* 2017;104(3):899-906.
3. Schneider C, McCrindle BW, Carvalho JS, Hornberger LK, McCarthy KP, Daubeney PE. Development of Z-scores for fetal cardiac dimensions from echocardiography. *Ultrasound Obstet Gynecol.* 2005;26(6):599-605.
4. Vigneswaran TV, Akolekar R, Syngelaki A, Charakida M, Allan LD, Nicolaidis KH, Zidere V, Simpson JM. Reference Ranges for the Size of the Fetal Cardiac Outflow Tracts From 13 to 36 Weeks Gestation: A Single-Center Study of Over 7000 Cases. *Circ Cardiovasc Imaging.* 2018;11(7):e007575.
5. Dyverfeldt P, Bissell M, Barker AJ, Bolger AF, Carlhall CJ, Ebbers T, Francios CJ, Frydrychowicz A, Geiger J, Giese D, et al. 4D flow cardiovascular magnetic resonance consensus statement. *J Cardiovasc Magn Reson.* 2015;17:72.
6. Kamphuis VP, Westenberg JJM, van der Palen RLF, Blom NA, de Roos A, van der Geest R, Elbaz MSM, Roest AAW. Unravelling cardiovascular disease using four dimensional flow cardiovascular magnetic resonance. *Int J Cardiovasc Imaging.* 2017;33(7):1069-81.
7. Bissell MM, Hess AT, Biasioli L, Glaze SJ, Loudon M, Pitcher A, Davis A, Prendergast B, Markl M, Barker AJ, et al. Aortic dilation in bicuspid aortic valve disease: flow pattern is a major contributor and differs with valve fusion type. *Circ Cardiovasc Imaging.* 2013;6(4):499-507.
8. Frydrychowicz A, Markl M, Hirtler D, Harloff A, Schlensak C, Geiger J, Stiller B, Arnold R. Aortic hemodynamics in patients with and without repair of aortic coarctation: in vivo analysis by 4D flow-sensitive magnetic resonance imaging. *Invest Radiol.* 2011;46(5):317-25.
9. Mahadevia R, Barker AJ, Schnell S, Entezari P, Kansal P, Fedak PW, Malaisrie SC, McCarthy P, Collins J, Carr J, et al. Bicuspid aortic cusp fusion morphology alters aortic three-dimensional outflow patterns, wall shear stress, and expression of aortopathy. *Circulation.* 2014;129(6):673-82.
10. van Ooij P, Markl M, Collins JD, Carr JC, Rigsby C, Bonow RO, Malaisrie SC, McCarthy PM, Fedak PWM, Barker AJ. Aortic Valve Stenosis Alters Expression of Regional Aortic Wall Shear Stress: New Insights From a 4-Dimensional Flow Magnetic Resonance Imaging Study of 571 Subjects. *J Am Heart Assoc.* 2017;6(9):e005959.
11. Burris NS, Sigovan M, Knauer HA, Tseng EE, Saloner D, Hope MD. Systolic flow displacement correlates with future ascending aortic growth in patients with bicuspid aortic valves undergoing magnetic resonance surveillance. *Invest Radiol.* 2014;49(10):635-9.
12. Guzzardi DG, Barker AJ, van Ooij P, Malaisrie SC, Puthumana JJ, Belke DD, Mewhort HE, Svystonyuk DA, Kang S, Verma S, et al. Valve-Related Hemodynamics Mediate Human Bicuspid Aortopathy: Insights From Wall Shear Stress Mapping. *J Am Coll Cardiol.* 2015;66(8):892-900.
13. Burk J, Blanke P, Stankovic Z, Barker A, Russe M, Geiger J, Frydrychowicz A, Langer M, Markl M. Evaluation of 3D blood flow patterns and wall shear stress in the normal and dilated thoracic aorta using flow-sensitive 4D CMR. *J Cardiovasc Magn Reson.* 2012;14:84.
14. Bousset L, Rayz V, McCulloch C, Martin A, Acevedo-Bolton G, Lawton M, Higashida R, Smith WS, Young WL, Saloner D. Aneurysm growth occurs at region of low wall shear stress: patient-specific correlation of hemodynamics and growth in a longitudinal study. *Stroke.* 2008;39(11):2997-3002.
15. Koolbergen DR, Manshanden JS, Yazdanbakhsh AP, Bouma BJ, Blom NA, de Mol BA, Mulder BJ, Hazekamp MG. Reoperation for neo-aortic root pathology after the arterial switch operation. *Eur J Cardiothorac Surg.* 2014;46(3):474-9.

16. Ntsinjana HN, Capelli C, Biglino G, Cook AC, Tann O, Derrick G, Taylor AM, Schievano S. 3D morphometric analysis of the arterial switch operation using in vivo MRI data. *Clin Anat.* 2014;27(8):1212-22.
17. Agnoletti G, Ou P, Celermajer DS, Boudjemline Y, Marini D, Bonnet D, Aggoun Y. Acute angulation of the aortic arch predisposes a patient to ascending aortic dilatation and aortic regurgitation late after the arterial switch operation for transposition of the great arteries. *J Thorac Cardiovasc Surg.* 2008;135(3):568-72.
18. Martins D, Khraiche D, Legendre A, Boddaert N, Raisy O, Bonnet D, Raimondi F. Aortic angle is associated with neo-aortic root dilatation and regurgitation following arterial switch operation. *Int J Cardiol.* 2019;280:53-6.
19. Lalezari S, Hazekamp MG, Bartelings MM, Schoof PH, Gittenberger-De Groot AC. Pulmonary artery remodeling in transposition of the great arteries: relevance for neo-aortic root dilatation. *J Thorac Cardiovasc Surg.* 2003;126(4):1053-60.
20. Lalezari S, Mahtab EA, Bartelings MM, Wisse LJ, Hazekamp MG, Gittenberger-de Groot AC. The outflow tract in transposition of the great arteries: an anatomic and morphologic study. *Ann Thorac Surg.* 2009;88(4):1300-5.
21. de Beaufort HWL, Trimarchi S, Korach A, Di Eusanio M, Gilon D, Montgomery DG, Evangelista A, Braverman AC, Chen EP, Isselbacher EM, et al. Aortic dissection in patients with Marfan syndrome based on the IRAD data. *Ann Cardiothorac Surg.* 2017;6(6):633-41.
22. Groth KA, Stochholm K, Hove H, Kyhl K, Gregersen PA, Vejlsstrup N, Ostergaard JR, Gravholt CH, Andersen NH. Aortic events in a nationwide Marfan syndrome cohort. *Clin Res Cardiol.* 2017;106(2):105-12.
23. Chiu IS, Wu SJ, Chen MR, Lee ML, Wu MH, Wang JK, Lue HC. Modified arterial switch operation by spiral reconstruction of the great arteries in transposition. *Ann Thorac Surg.* 2000;69(6):1887-92.
24. Rickers C, Kheradvar A, Sievers HH, Falahatpisheh A, Wegner P, Gabbert D, Jerosch-Herold M, Hart C, Voges I, Putman LM, et al. Is the Lecompte technique the last word on transposition of the great arteries repair for all patients? A magnetic resonance imaging study including a spiral technique two decades postoperatively. *Interact Cardiovasc Thorac Surg.* 2016;22(6):817-25.
25. Erbel R, Aboyans V, Boileau C, Bossone E, Bartolomeo RD, Eggebrecht H, Evangelista A, Falk V, Frank H, Gaemperli O, et al. 2014 ESC Guidelines on the diagnosis and treatment of aortic diseases: Document covering acute and chronic aortic diseases of the thoracic and abdominal aorta of the adult. The Task Force for the Diagnosis and Treatment of Aortic Diseases of the European Society of Cardiology (ESC). *Eur Heart J.* 2014;35(41):2873-926.



## **CHAPTER 11**

Nederlandse samenvatting

## Nederlandse samenvatting

Transpositie van de grote vaten (TGA) is een ernstige aangeboren hartafwijking waarbij in de aanleg van het hart de grote slagaders zijn verwisseld: de aorta komt uit de rechterkamer; de longslagader uit de linkerkamer. In Europa komt deze aandoening voor bij 3-4 op 10000 levend geboren kinderen. Operatief ingrijpen kort na geboorte is noodzakelijk anders overlijdt de patiënt. De huidige chirurgische behandeling van deze hartafwijking is de arteriële switch operatie (ASO). Deze operatie werd in 1975 voor het eerst succesvol uitgevoerd en sinds midden jaren '80 heeft het wereldwijd de daarvoor gebruikelijke operatieve techniek nagenoeg volledig vervangen. Tijdens de ASO worden de grote slagaders boven het niveau van de hartkleppen omgedraaid, zodat de grote bloedvaten weer op de juiste hartkamers aangesloten zijn. Tevens worden de kransslagaders omgezet. De longslagaderklep, aortaklep en het eerste deel van de slagaders blijven op hun oorspronkelijke plaats zitten. Hoewel deze nieuwe operatieve techniek de korte- en langetermijnoverleving voor kinderen met deze aandoening sterk heeft verbeterd, worden er in het beloop belangrijke restafwijkingen gevonden. Een van deze afwijkingen is een toenemende verwijding (dilatatie) van het eerste deel van de aorta (na ASO neo-aortawortel genoemd). Dilatatie van de neo-aortawortel komt bij het merendeel van de patiënten na ASO voor.

Dit proefschrift beschrijft de ontwikkeling van de neo-aortawortelproblematiek en de lange termijn cardiovasculaire uitkomsten bij patiënten na een ASO als behandeling voor TGA. Daarnaast worden de hemodynamische aspecten van de bloedstroom in de thoracale aorta in deze patiënten onderzocht in relatie met de aortageometrie en de neo-aortawortelpathologie door middel van geavanceerde cardiovasculaire beeldvormende techniek: vierdimensionale flow magnetische resonantie imaging (4D flow MRI).

**Hoofdstuk 1** geeft een korte introductie over de Leidse chirurgische geschiedenis van de behandeling van patiënten met TGA en de ontwikkeling van de ASO. De ASO werd voor het eerst succesvol uitgevoerd door dr. Jatene in 1975 en al in 1977 in het academisch ziekenhuis Leiden toegepast. Vanaf midden jaren '80 werd de ASO wereldwijd de beoogde operatieve techniek voor patiënten met TGA.<sup>1</sup> De belangrijkste aortacomPLICaties die op termijn na ASO kunnen optreden zijn dilatatie van de neo-aortawortel en neo-aortakleplekkage. Echocardiografie en cardiale MRI spelen een essentiële rol bij het diagnosticeren van deze hartaandoeningen en bij de monitoring en timing van de behandeling van neo-aortawortelproblemen na ASO. In de beschreven studies in dit proefschrift zijn echocardiografie en 4D flow MRI gebruikt om nieuwe inzichten te verkrijgen in zowel de ontwikkeling van neo-aortapathologie als de bloedstroomhemodynamica van de aorta na ASO.

**Deel I****De aorta in TGA – foetale groei & resultaten na de arteriële switch operatie**

Het eerste deel van dit proefschrift richt zich op de resultaten na ASO met focus op de aorta, alsmede op de groei van de aorta in patiënten met TGA, zowel tijdens de zwangerschap als na ASO. In **Hoofdstuk 2** worden de langetermijnnuitkomsten beschreven van het cohort TGA-patiënten geopereerd in het Centrum voor Aangeboren Hartafwijkingen Amsterdam-Leiden tussen 1977 en 2020. Dit cohort omvat 490 patiënten na ASO en bestaat uit TGA-patiënten met eenvoudiger anatomie, zoals TGA met intact ventrikel septum (TGA-IVS) en TGA met ventrikel septum defect (TGA-VSD), alsook uit patiënten met een complexere TGA-variant zoals double outlet rechterventrikel met subpulmonaal VSD (Taussig-Bing anomalie). Drieënveertig patiënten zijn direct of kort (<30 dagen) na de ASO overleden en van 34 patiënten is er geen follow-up omdat zij terugkeerden naar het land van verwijzing. Hierdoor is de langetermijnnuitkomst van 413 patiënten beoordeeld met een mediane follow-up van 15.6 (interkwartielafstand, IQR 7.0-22.4) jaar na ASO. De ziekenhuissterfte (overlijden in het ziekenhuis na hartoperatie) daalde snel na implementatie van de ASO tot 3.3% over de afgelopen twintig jaar. Twaalf van de 413 patiënten zijn gedurende follow-up (na ontslag uit het ziekenhuis na ASO) overleden, gemiddeld op een leeftijd van 10.6 (IQR 0.9-21.9) jaar na ASO. Voor 5 van de 12 patiënten kon de oorzaak van het overlijden worden achterhaald; geen van deze patiënten overleed door een probleem aan de kransslagaderen.

Het percentage van de patiënten dat in het beloop na ASO een nieuwe operatieve ingreep (heroperatie) of katheterinterventie heeft ondergaan is respectievelijk 20.1% en 13.1%. De meeste heroperaties betreffen operaties voor het herstellen van problemen in de rechterkamer uitstroombaan. Heroperaties of katheterinterventies aan kransslagaderen waren noodzakelijk in slechts 9 patiënten (2.2%), wat suggereert dat problemen aan kransslagaderen in het beloop niet veel voorkomen. Neo-aortaklep en/of neo-aortawortelpathologie lijkt een belangrijker probleem te worden op de lange termijn, gezien de toenemende incidentie van heroperaties voor deze problematiek. Eenentwintig chirurgische procedures en één katheterinterventie waren noodzakelijk bij 15 patiënten (3.6%) voor de behandeling van belangrijke neo-aortakleplekkage en/of neo-aortaworteldilatatie. Dit betreft 20% van het totaal aantal heroperaties. Bij twee derde van deze patiënten werd de operatie in de afgelopen 11 jaar uitgevoerd (2009-2020). Tussen 1977 en 2009 was slechts bij 5 van de 302 patiënten na ASO (1.7%) een heroperatie noodzakelijk voor neo-aortaproblematiek. Hoewel het totaal aantal heroperaties voor neo-aortapathologie nu nog laag is en vergelijkbaar met internationale centra voor kinderhartchirurgie,<sup>2</sup> is het te verwachten dat dit aantal zal toenemen bij langere follow-up. Onafhankelijke risicofactoren voor heroperatie of interventie, ongeacht de indicatie, zijn: 1. een meer complexe TGA-morfologie (TGA-VSD en Taussig-Bing anomalie), 2. een status na eerder chirurgisch herstel van de aortaboog en 3. een minder gebruikelijke kransslagader anatomie (anders dan *1LCx-2R*, *1L-2CxR* of *1L-2R,Cx afwezig*).



In **Hoofdstuk 3** wordt de intra-uteriene groei van de aortaklep en de longslagaderklep (ook wel semilunair kleppen genoemd) bij foetussen met een TGA beschreven (vanaf 20 weken zwangerschapstermijn tot aan de geboorte). Deze groei wordt vergeleken met de intra-uteriene groei van de semilunair kleppen bij foetussen zonder hartafwijking.<sup>3,4</sup> Gedurende deze periode is zowel de afmeting van de longslagaderklep als die van de aortaklep gemiddeld groter in foetussen met TGA dan in foetussen zonder deze hartafwijking. Vanaf een zwangerschapstermijn van 27 weken is de longslagaderklep in een TGA foetus gemiddeld groter dan de longslagaderklep in de controle groep, met name in aanwezigheid van een VSD. Bovendien is de longslagaderklep gemiddeld groter in vergelijking met de aortaklep in de controle groep vanaf een zwangerschapstermijn van 23 weken. Deze uitkomsten suggereren dat er naast de factor van een preferentiële bloedstroming (flow) ook andere factoren een rol spelen bij de groei van de semilunair kleppen in foetussen met TGA. De longslagaderklep tussen 26 en 30 weken zwangerschapstermijn (afmeting geïndexeerd voor lichaamsoppervlak en uitgedrukt als Z-score) correleerde met de geïndexeerde neo-aortawortel diameter na ASO gemeten bij het laatste kindercardiologische bezoek. Deze correlatie is relatief zwak en ook de follow-up van de patiënten in deze studie is relatief kort waardoor de longslagaderklep afmeting bij de foetus niet kan worden gebruikt als voorspeller van neo-aortaworteldilatatie na ASO. De bevindingen uit deze studie dragen bij aan het begrip van de pathofysiologie van foetale groei van de semilunair kleppen en geven bovendien inzicht in het ontstaan van de verschillen in semilunair klep afmetingen tussen TGA-patiënten met diverse morfologie.

In **Hoofdstuk 4** worden de resultaten beschreven van een retrospectieve longitudinale studie naar de groei en functie van de neo-aortaklep en neo-aortawortel in 345 patiënten vanaf ASO tot 39 jaar nadien. Tevens worden de heroperaties voor neo-aortawortel en kleppathologie geëvalueerd. Dit onderzoek toont aan dat de dilatatie van de neo-aortawortel progressief is en zich voortzet op volwassen leeftijd zonder tekenen van stabilisatie in tegenstelling tot de aortawortel van gezonde volwassenen die nauwelijks in diameter toeneemt met de leeftijd. De neo-aortaklep, neo-aortawortel en sinotubulaire junctie laten een identiek groeipatroon zien: er is een snelle disproportionele toename in het eerste jaar na ASO resulterend in geïndexeerde afmetingen boven de bovengrenzen van normaal (geïndexeerd voor lichaamsoppervlak met groepsgemiddelde Z-scores >2.0). De neo-aorta afmetingen op kinderleeftijd (1-18 jaar) laten een nagenoeg lineaire toename zien vergelijkbaar met de somatische groei in die periode, maar worden gevolgd door een progressieve groei op volwassen leeftijd. Onafhankelijke risicofactoren voor neo-aortadilatatie (dilatatie gedefinieerd als Z-score >2.0) zijn: mannelijk geslacht en een meer complexe TGA-morfologie (TGA-VSD en Taussig-Bing anomalie). De neo-aortakleplekkage toont eveneens een progressief beloop in de tijd: de kans op ontwikkelen van tenminste matige neo-aortakleplekkage 25 jaar na ASO is 31%. De progressie van neo-aortaworteldilatatie blijkt een kritische factor te zijn voor verslechtering van de neo-aortaklepfunctie in de loop van de tijd: per millimeter toename in de afmeting van de

neo-aortawortel is er een 9% toename in kans (hazard) op het ontwikkelen van tenminste matige neo-aortakleplekkage. Dit is een belangrijke bevinding en impliceert een verminderde coaptatie van de klepbladen door een toename van de neo-aortawortel en neo-aortaklepafmetingen als belangrijk onderliggend mechanisme voor het ontstaan van kleplekkage. Een bicuspide (tweeslippige in plaats van een meer gebruikelijke drieslippige) neo-aortaklep is niet geassocieerd met een hoger risico op kleplekkage. Op basis van deze resultaten kunnen we concluderen dat een competente bicuspide longslagaderklep bij een TGA-patiënt geen contra-indicatie is voor het verrichten van een ASO.

Het percentage patiënten met heroperaties aan de neo-aortaklep of neo-aortawortel in de studiegroep was laag, gemiddeld 3%. Echter, van de totale onderzoeksgroep heeft al 14% van de patiënten een neo-aortaworteldiameter  $\geq 40$  mm, waarbij in 26% van de gevallen tenminste een matige neo-aortakleplekkage is vastgesteld. Een kwart van de patiënten met een worteldiameter  $\geq 40$  mm is minderjarig ( $< 18$  jaar). Deze resultaten, samen met de voortgaande neo-aortadilatatie en neo-aortakleplekkage op volwassen leeftijd, en hun sterke onderlinge samenhang zoals aangetoond in dit onderzoek, zijn zorgwekkend en impliceren een te verwachten stijging van het aantal heroperaties voor neo-aortaklep en/of neo-aortawortelopathie in de nabije toekomst.

**Hoofdstuk 5** toont het resultaat van de aanvullende analyse naar het effect van veranderende aortadimensies in de tijd op het ontstaan van neo-aorta regurgitatie, zoals gerapporteerd in Hoofdstuk 4. Met een uitgebreidere statistische analyse (joint modeling) werd de sterke relatie tussen de neo-aortawortel afmeting en neo-aortakleplekkage bevestigd, maar deze was veel sterker dan eerder vastgesteld. Ook voor het ontwikkelen van tenminste milde neo-aortakleplekkage werd zowel de neo-aortaklep als neo-aortaworteldiameter als onafhankelijke risicofactor gekenmerkt. Bovendien werd gevonden dat naast de diameter ook de groeisnelheid van de neo-aortaklep en neo-aortawortel een onafhankelijke kritische factor is voor het ontwikkelen van tenminste milde neo-aortakleplekkage. Dit betekent dat een snellere groei van de neo-aortaklep en de neo-aortawortel, bovenop de neo-aortaklep en -wortelafmeting, een hoger risico op neo-aortakleplekkage geeft.

## Deel II

### Aorta 4D flow imaging in TGA patiënten na de ASO en daarbuiten

4D flow MRI is onlangs geïntroduceerd als een nieuwe niet-invasieve beeldvormingsmethode die wordt gebruikt voor beoordeling van de hemodynamische aspecten van de bloedstroom in de grote bloedvaten.<sup>5,6</sup> Het geeft informatie over het verloop van de bloedstroom binnen het bloedvat gedurende de hartcyclus (visualisatie van bloedstroom in 3 loodrechte richtingen in de ruimte (3D) als functie van de tijd (4D)) en maakt kwantificatie van flow-gerelateerde hemodynamische parameters mogelijk.

Om die reden wordt 4D flow MRI gebruikt om de cardiovasculaire fysiologie en pathofysiologie beter te begrijpen, wat heeft geleid tot een betere kennis van de progressie van aortaproblematiek in patiënten met aangeboren hartafwijkingen.<sup>6-10</sup> Hemodynamische parameters zoals 'wall shear stress' (WSS) en 'flow displacement' kunnen worden afgeleid van 4D flow MRI. Genormaliseerde flow displacement (FD) is een kwantitatieve maat voor de excentriciteit van de bloedstroom en is gedefinieerd als de afstand tussen het centrum van het bloedvat en het 'snelheidscentrum' van het golf front van de bloedstroom, genormaliseerd voor de diameter van het bloedvat. Door verschillende studies is aangetoond dat een toename in FD verband houdt met de morfologie van de aortaklep en gecorreleerd is met de mate van groei van de aorta in patiënten met een bicuspide aortaklep.<sup>9,11</sup> De parameter WSS, vrij vertaald wandschuifspanning, vertegenwoordigt de kracht van de bloedstroom die tangentieel (in de lengterichting van het verloop van het bloedvat) op de vaatwand inwerkt. Gebieden van de aorta blootgesteld aan hoge WSS zijn geassocieerd met kenmerkende histologische veranderingen in de aortavaatwand in patiënten met een bicuspide aortaklep.<sup>12</sup> Bovendien is beschreven dat een abnormale WSS een potentieel bijdragend effect heeft op vaatdilatatie en aneurysma vorming, bijvoorbeeld in de thoracale aorta en bij intracranieële aneurysmata.<sup>13,14</sup>

De toepassing van aorta 4D flow MRI kan daarom van belangrijke waarde zijn voor de evaluatie van aortaproblematiek bij TGA-patiënten na ASO. Validatie van de toegepaste 4D flow MRI-techniek door kennis over de reproduceerbaarheid en consistentie van de uitkomst parameter(s) is echter noodzakelijk om verschillen tussen patiëntgroepen en tussen longitudinale patiëntdata te kunnen interpreteren. Om die reden is een onderzoek ter beoordeling van de scan-rescan reproduceerbaarheid en beoordelaarsbetrouwbaarheid voor de hemodynamische parameter 3D WSS in de thoracale aorta uitgevoerd bij gezonde vrijwilligers. Hiervoor is er van de gezonde vrijwilligers tweemaal eenzelfde MRI-scan van het hart en de grote bloedvaten gemaakt met 10 minuten pauze tussen de twee scans (scan-rescan). De resultaten hiervan zijn samengevat in **Hoofdstuk 6**. Voor de beoordeling van de WSS is de thoracale aorta opgedeeld in vijf gelijke segmenten: proximale aorta ascendens, distale aorta ascendens, aortaboog, proximale aorta descendens en distale aorta descendens. De maximale pieksystolische WSS (WSSmax) en de gemiddelde pieksystolische WSS (WSSmean) is in elk van de segmenten berekend. De scan-rescan reproduceerbaarheid was goed voor WSSmean in alle thoracale aorta segmenten; de scan-rescan reproduceerbaarheid voor WSSmax was matig met een hogere variabiliteit in de proximale aorta ascendens. De reproduceerbaarheid van een identieke beoordelaar (intraobserver) en van twee onafhankelijke beoordelaars (interobserver) voor segmentale beoordeling van WSSmax en WSSmean was goed tot uitstekend. De segmenten van de ascenderende aorta tonen in het algemeen meer variabiliteit in WSSmax en WSSmean in vergelijking met de segmenten van de aorta descendens en aortaboog voor zowel de scan-rescan, intraobserver als interobserver beoordelingen. Met deze WSS-variaties moet rekening gehouden worden bij de interpretatie van onderzoeksresultaten tussen patiëntgroepen en bij rust-stress vergelijkingen binnen een patiëntengroep.

In **Hoofdstuk 7** zijn de resultaten van het 4D flow MRI-onderzoek naar de bloedstroom hemodynamica in de aorta ascendens in patiënten met TGA na ASO gerapporteerd. Deze resultaten zijn vergeleken met gezonde vrijwilligers. Naast de afmetingen van de aorta ascendens zijn er twee van 4D flow afgeleide hemodynamische parameters beoordeeld: FD en WSS. Patiënten na ASO tonen een meer excentrische bloedstroom in de proximale aorta ascendens (inclusief neo-aortawortel) zich uitend in een hogere FD en verschillende FD-richting. De mate van FD laat hierbij een lineair verband zien met geïndexeerde aortadimensies van de neo-aortawortel en de sinotubulaire overgang (dimensies geïndexeerd voor lichaamsoppervlak en uitgedrukt als Z-score). De richting van de excentrische flowprofielen in de neo-aortawortel is significant verschillend tussen de patiënten met verschillende TGA-specifieke preoperatieve positie van de grote vaten: in de groep TGA-patiënten met de aorta rechts of rechts-anterior gepositioneerd ten opzichte van de longslagader is de FD-richting meer gericht naar de rechterzijde in de aorta ascendens, terwijl een aorta positie links-anterior of anterior ten opzichte van de longslagader resulteert in een FD meer naar de linkerzijde van de aortawand van de aorta ascendens gericht ter hoogte van de neo-aortawortel. Daarnaast hebben TGA-patiënten een abnormale regionale WSS in het proximale segment aorta ascendens (lager in vergelijking met gezonde vrijwilligers) en in het distale segment van de aorta ascendens (hoger in vergelijking met gezonde vrijwilligers), met een lokaal gebied van maximaal verhoogde WSS aan de (rechter) voorzijde van de distale aorta ascendens. De geometrie van de aorta na ASO is erg specifiek en bestaat uit neo-aortaworteldilatatie en een vrij plotselinge overgang naar een smallere aortadiameter ter hoogte van het middendeel van de aorta ascendens (mid-aorta ascendens). Deze overgang is exact gelegen op het niveau van aortacompressie door de voorgelegen longslagaderstam als gevolg van de Lecompte manoeuvre als onderdeel van de ASO. De verandering in aortadiameter, uitgedrukt als ratio, is geassocieerd met een verhoogde WSS en een asymmetrische WSS-verdeling in het distale segment van de aorta ascendens. De relatie was lineair: hoe groter de discrepantie tussen de diameter van de neo-aortawortel en mid-aorta ascendens, des te hoger de WSS in het distale segment van de aorta ascendens.

Het gebied van de abnormaal verhoogde WSS correleert klinisch met de locatie van een papierdunne en fragiele voorwand van de aorta ascendens, een bevinding die frequent wordt gezien tijdens heroperaties aan de aorta in patiënten na ASO zoals eerder beschreven door ons centrum.<sup>15</sup> De richting van de FD vanaf de neo-aortawortel naar de mid-aorta ascendens komt ook overeen met de WSS-verdeling in de mid-aorta ascendens. De bijdrage van FD aan de WSS-distributie meer stroomopwaarts in de distale aorta ascendens is minder sterk vergeleken met de bijdrage van de tapering van het bloedvat hieraan. De observaties uit dit onderzoek zijn het begin van een verdere ontrafeling van de interactie tussen de aortageometrie na ASO en de hemodynamica en geven meer inzicht hoe de bloedstroom hemodynamica betrokken kan zijn bij de (progressie van) neo-aortaworteldilatatie en/of het dunner worden van de voorzijde van de aortavaatwand van het distale aorta ascendens segment.

**Hoofdstuk 8** beschrijft de bevindingen van de 4D flow MRI-studie naar de hemodynamische parameter WSS in de gehele thoracale aorta in TGA-patiënten na ASO. Deze WSS-analyse is uitgevoerd volgens de methode die is toegepast in het reproduceerbaarheidsonderzoek zoals beschreven in Hoofdstuk 6. TGA-patiënten zijn vergeleken met gezonde vrijwilligers en segmentale WSS-analyses zijn gerelateerd aan de geometrie van de thoracale aorta na de ASO. Daarnaast is het effect van dobutamine geïnduceerde stress op de WSS in de gehele thoracale aorta onderzocht.

Specifieke geometrische veranderingen van de thoracale aorta na ASO worden waargenomen conform de beschrijvingen in de literatuur.<sup>16-18</sup> De specifieke geometrie bestaat uit een grote diameter discrepantie tussen de verwijde neo-aortawortel en de relatief smallere mid-aorta ascendens, als gevolg van de anterieure positie van de longslagader en compressie van de longslagaderstam en -takken op de aorta na ASO met Lecompte manoeuvre. Daarnaast wordt in TGA-patiënten een scherpere hoek (angulatie) gezien van de aortaboog. Gebaseerd op de 4D flow analyse tonen zowel kinderen als jonge volwassenen na ASO significant hogere WSS-waarden in de gehele thoracale aorta vergeleken met de gezonde vrijwilligers, met uitzondering van de gedilateerde proximale aorta ascendens. In overeenstemming met de bevindingen in Hoofdstuk 7, worden de aorta regio's met hoge piek systolische WSS gevonden in het distale deel van de aorta ascendens, gelegen op de voorwand van dat segment. De specifieke geometrie van de aorta ascendens na ASO, uitgedrukt in een diameter discrepantie tussen de gedilateerde neo-aortawortel en het smallere mid-aorta ascendens deel, is geassocieerd met hogere WSS-waarden in alle aortasegmenten stroomafwaarts van deze kaliberandering: hoe groter de diameterdiscrepantie, des te hoger de WSS-waarden zowel in de distale aorta ascendens als in beide segmenten van de aorta descendens. De geometrie van de aortaboog, gekenmerkt door de meer acute aortaboog angulatie in TGA-patiënten na ASO in vergelijking met gezonde vrijwilligers, heeft geen additionele bijdrage aan de hoge WSS-waarden gevonden in zowel de aortaboog, het proximale en het distale segment van de aorta descendens boven op de WSS-verandering gerelateerd aan de ascendensgeometrie.

Dobutamine geïnduceerde cardiale stress verhoogt de WSS-waarden significant in alle segmenten van de thoracale aorta, met de hoogste procentuele WSS-stijging in de segmenten van de aorta ascendens. De hoogste pieksystolische WSS-waarde in de thoracale aorta is gelegen in het distale aorta ascendens segment, zowel in rust als tijdens dobutamine-stress, maar tijdens stress was dit nog meer uitgesproken. De dobutamine geïnduceerde WSS-stijging in dat segment toont een significante lineaire correlatie met de toename van de linkerkamer ejection fractie, het slagvolume en het hartminuutvolume (cardiac output). Gebaseerd op de resultaten van dit onderzoek kunnen we concluderen dat een beoordeling van aortale bloedflow tijdens dobutamine-stress mogelijk beter de locatie en uitgebreidheid van de vaatwand(en) blootgesteld aan abnormale WSS kan weergegeven; de gebieden die hierdoor meer risico lopen voor vasculaire modellering. Gezien de significante dobutamine-stress geïnduceerde toename van WSS in de neo-aortawortel, die een tangente kracht uitoefent op het neo-aorta weefsel met reeds structurele vaatwandafwijkingen,<sup>19,20</sup> is het voor te stellen dat stress een rol speelt bij de neo-aortaworteldilatatie in TGA-patiënten na ASO.

Kennis van de uitgebreidheid en verdeling van WSS in de aorta is niet alleen van belang voor patiënten met postoperatieve congenitale hartaandoeningen zoals patiënten na ASO, maar ook voor patiënten met erfelijke bindweefselziekten zoals het Marfan syndroom. Beide patiëntengroepen hebben een progressieve worteldilatatie als overeenkomstig kenmerk, maar het is bewezen dat Marfan patiënten risico lopen op het ontstaan van een dissectie en/of ruptuur van de aorta.<sup>21, 22</sup> In TGA-patiënten zijn neo-aortaworteldilatatie en kleplekkage bekend, maar aortadissecties zijn tot dusver niet in de literatuur gerapporteerd. Om te leren van patiënten met een aortopathie met verhoogd risico op ernstige cardiovasculaire events, hebben we ook een 4D flow MRI-onderzoek uitgevoerd bij pediatrie patiënten met het Marfan syndroom. Deze studie is uitgevoerd in samenwerking met het Amerikaanse Lurie Children's Hospital en de Northwestern University Feinberg School of Medicine uit Chicago en de resultaten zijn samengevat in **Hoofdstuk 9**. Zowel hemodynamische parameters afgeleid van 4D flow, semi-kwantitatieve karakterisering van bloedstroompatronen en segmentale WSS-analyse in de thoracale aorta, als de dimensies van de aorta zijn beoordeeld bij kinderen met het Marfan syndroom en zijn vergeleken met een voor de leeftijd geschikte controle groep. Een substantieel deel van de kinderen met het Marfan syndroom heeft opvallend andere aorta bloedstroom patronen in vergelijking met gezonde controles, bestaande uit opvallende vortices (vortexfenomenen) in de proximale aorta descendens en niet-fysiologische helix-vormige bloedstroom fenomenen, afkomstig van de aortawortel zich voortzettend naar de aorta ascendens. Deze veranderde bloedstroom patronen en de gedetecteerde lagere WSS-waarden zijn het meest uitgesproken in de proximale aorta ascendens en de proximale aorta descendens, segmenten waar aortadissecties of aortarupturen doorgaans ontstaan. De vortex patronen en abnormale WSS correleren met de regionale afmetingen van de proximale aorta descendens en zijn mogelijk waardevolle aanvullende hemodynamische markers voor de ernst van de ziekte. Langdurige follow-up van deze patiënten zal het onderscheidend vermogen van deze van 4D flow MRI-afkomstige parameters aangeven voor de progressie van aortadilatatie en/of het optreden van ernstige aortacomplicaties op deze voorkeurs locaties.

## Conclusie

In dit proefschrift zijn meerdere aspecten van de aortaproblematiek bij patiënten met TGA bestudeerd. Neo-aorta-afmetingen en de neo-aortaklepfunctie tonen in de loop van de tijd een progressieve neo-aortaworteldilatatie zonder stabilisatie op volwassen leeftijd waarbij de neo-aortaworteldiameter de kritische factor blijkt te zijn voor verdere achteruitgang in neo-aortaklepfunctie. Deze bevindingen, samen met de aangetoonde verhoogde incidentie van heroperatieve chirurgie aan de neo-aortaklep en/of de neo-aortawortel in het afgelopen decennium, impliceren dat het aantal heroperaties voor late neo-aortawortelcomplicaties verder zal toenemen met langere follow-up.

De pathofysiologie van de progressieve worteldilatatie is onvolledig begrepen en meest waarschijnlijk multifactorieel. In dit proefschrift wordt aangetoond dat een mannelijk geslacht en een meer complexe TGA-morfologie (TGA-VSD en Taussig-Bing anomalie) onafhankelijke risicofactoren zijn voor dilatatie van de neo-aorta. De inzichten uit de huidige 4D flow MRI-studies suggereren ook een bijdrage van hemodynamische factoren welke geassocieerd zijn met de ASO-specifieke thoracale aortageometrie.

## Perspectief voor de toekomst

Belangrijke onderzoeksgebieden die de patiëntenzorg na ASO in de nabije toekomst beïnvloeden moeten worden gericht op gepersonaliseerde cardiovasculaire behandeling ter optimalisatie van de langetermijntoekomst. Op basis van de inzichten verkregen uit dit proefschrift bieden de volgende gebieden perspectief voor verdere ontwikkeling met klinische relevantie:

- De ontwikkeling van predictie en risicostratificatie modellen op basis van seriële data door gestandaardiseerde imaging protocollen en het vastleggen van event data, zoals het volgen van aorta dimensies en het optreden van neo-aortakleplekkage in dit proefschrift. Deze kunnen dienen voor een wetenschappelijk onderbouwd individueel patiënt follow-up schema met adequaat zorgniveau voor elke patiënt, maximalisatie van efficiëntie en verbetering van het resultaat op populatieniveau.
- Inzetten op longitudinaal en aanvullend 4D flow MRI-onderzoek voor TGA-patiënten na ASO, door deze op te nemen als standaard onderzoek gedurende follow-up.
  - Hiermee kunnen vraagstukken rondom de interindividuele verschillen in aortahemodynamica tussen TGA-patiënten geopereerd met verschillende ASO-technieken (bijvoorbeeld met en zonder de toepassing van Lecompte manoeuvre) en tussen TGA-patiënten met verschillende anatomie (bijvoorbeeld met of zonder VSD en TGA-subgroepen met verschillende ruimtelijke positie van de grote slagaders) verder worden opgelost om uiteindelijk individuele chirurgische management strategieën te optimaliseren voor de beste langetermijnresultaten.
  - Daarnaast kan longitudinaal aorta 4D flow MRI-onderzoek helpen bij het voorspellen van aortacomplicaties (worteldilatatie, aortadissectie of aortaruptuur). Specifieke hemodynamische markers kunnen indicatief zijn voor het tijdig timen van interventies (wortelvervanging) en kunnen zo het klinische resultaat voor dilaterende aorta's optimaliseren, aangezien de huidige behandelstrategieën voor preventieve aortachirurgie onvolmaakt en enkel gebaseerd zijn op absolute aortadiameters.
  - Integratie van patiënt-specifieke aorta 4D flow informatie in computergestuurde modellen, geijkt op de simulatie van de effecten van bloedvatgeometrie en bloedstroom op de vaatwand (genaamd Computational Fluid Dynamics), maken het preoperatief mogelijk de hemodynamische respons van een chirurgische (her)ingreep te voorspellen. Met deze toepassing kan de meest optimale chirurgische aanpak van

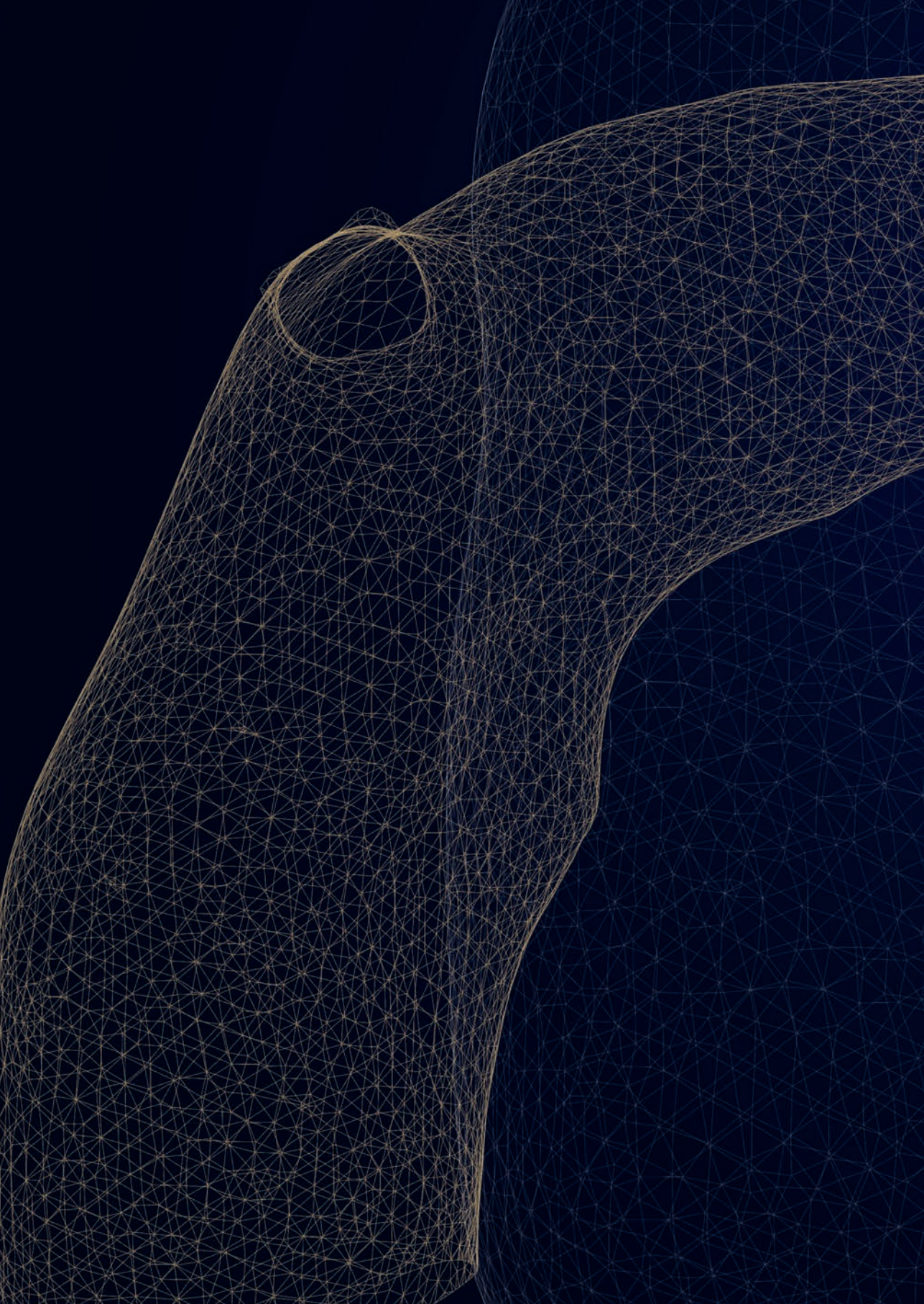
een probleem op voorhand worden bepaald. Voor patiënten na ASO kan bijvoorbeeld de beste gepersonaliseerde pasvorm van een aorta vaatprothese (grootte, kromming en lengte) voor implantatie worden bepaald, ter vervanging van het afwijkende deel van het bloedvat, met behoud van de meest optimale flow in en voorbij de geïmplanteerde vaatprothese.



## Referenties

1. Jatene AD, Fontes VF, Paulista PP, de Souza LC, Neger F, Galantier M, Souza JE. Successful anatomic correction of transposition of the great vessels. A preliminary report. *Arq Bras Cardiol.* 1975;28(4):461-64.
2. Vida VL, Zanotto L, Zanotto L, Stellin G, European Congenital Heart Surgeons Association Study G, Padalino M, Sarris G, Protopapas E, Prospero C, Pizarro C, et al. Left-Sided Reoperations After Arterial Switch Operation: A European Multicenter Study. *Ann Thorac Surg.* 2017;104(3):899-906.
3. Schneider C, McCrindle BW, Carvalho JS, Hornberger LK, McCarthy KP, Daubeney PE. Development of Z-scores for fetal cardiac dimensions from echocardiography. *Ultrasound Obstet Gynecol.* 2005;26(6):599-605.
4. Vigneswaran TV, Akolekar R, Syngelaki A, Charakida M, Allan LD, Nicolaidis KH, Zidere V, Simpson JM. Reference Ranges for the Size of the Fetal Cardiac Outflow Tracts From 13 to 36 Weeks Gestation: A Single-Center Study of Over 7000 Cases. *Circ Cardiovasc Imaging.* 2018;11(7):e007575.
5. Dyverfeldt P, Bissell M, Barker AJ, Bolger AF, Carlhall CJ, Ebbers T, Francios CJ, Frydrychowicz A, Geiger J, Giese D, et al. 4D flow cardiovascular magnetic resonance consensus statement. *J Cardiovasc Magn Reson.* 2015;17:72.
6. Kamphuis VP, Westenberg JJM, van der Palen RLF, Blom NA, de Roos A, van der Geest R, Elbaz MSM, Roest AAW. Unravelling cardiovascular disease using four dimensional flow cardiovascular magnetic resonance. *Int J Cardiovasc Imaging.* 2017;33(7):1069-81.
7. Bissell MM, Hess AT, Biasioli L, Glaze SJ, Loudon M, Pitcher A, Davis A, Prendergast B, Markl M, Barker AJ, et al. Aortic dilation in bicuspid aortic valve disease: flow pattern is a major contributor and differs with valve fusion type. *Circ Cardiovasc Imaging.* 2013;6(4):499-507.
8. Frydrychowicz A, Markl M, Hirtler D, Harloff A, Schlensak C, Geiger J, Stiller B, Arnold R. Aortic hemodynamics in patients with and without repair of aortic coarctation: in vivo analysis by 4D flow-sensitive magnetic resonance imaging. *Invest Radiol.* 2011;46(5):317-25.
9. Mahadevia R, Barker AJ, Schnell S, Entezari P, Kansal P, Fedak PW, Malaisrie SC, McCarthy P, Collins J, Carr J, et al. Bicuspid aortic cusp fusion morphology alters aortic three-dimensional outflow patterns, wall shear stress, and expression of aortopathy. *Circulation.* 2014;129(6):673-82.
10. van Ooij P, Markl M, Collins JD, Carr JC, Rigsby C, Bonow RO, Malaisrie SC, McCarthy PM, Fedak PWM, Barker AJ. Aortic Valve Stenosis Alters Expression of Regional Aortic Wall Shear Stress: New Insights From a 4-Dimensional Flow Magnetic Resonance Imaging Study of 571 Subjects. *J Am Heart Assoc.* 2017;6(9):e005959.
11. Burris NS, Sigovan M, Knauer HA, Tseng EE, Saloner D, Hope MD. Systolic flow displacement correlates with future ascending aortic growth in patients with bicuspid aortic valves undergoing magnetic resonance surveillance. *Invest Radiol.* 2014;49(10):635-9.
12. Guzzardi DG, Barker AJ, van Ooij P, Malaisrie SC, Puthumana JJ, Belke DD, Mewhort HE, Svystonyuk DA, Kang S, Verma S, et al. Valve-Related Hemodynamics Mediate Human Bicuspid Aortopathy: Insights From Wall Shear Stress Mapping. *J Am Coll Cardiol.* 2015;66(8):892-900.
13. Burk J, Blanke P, Stankovic Z, Barker A, Russe M, Geiger J, Frydrychowicz A, Langer M, Markl M. Evaluation of 3D blood flow patterns and wall shear stress in the normal and dilated thoracic aorta using flow-sensitive 4D CMR. *J Cardiovasc Magn Reson.* 2012;14:84.
14. Bousset L, Rayz V, McCulloch C, Martin A, Acevedo-Bolton G, Lawton M, Higashida R, Smith WS, Young WL, Saloner D. Aneurysm growth occurs at region of low wall shear stress: patient-specific correlation of hemodynamics and growth in a longitudinal study. *Stroke.* 2008;39(11):2997-3002.
15. Koolbergen DR, Manshanden JS, Yazdanbakhsh AP, Bouma BJ, Blom NA, de Mol BA, Mulder BJ, Hazekamp MG. Reoperation for neo-aortic root pathology after the arterial switch operation. *Eur J Cardiothorac Surg.* 2014;46(3):474-9.

16. Ntsinjana HN, Capelli C, Biglino G, Cook AC, Tann O, Derrick G, Taylor AM, Schievano S. 3D morphometric analysis of the arterial switch operation using in vivo MRI data. *Clin Anat.* 2014;27(8):1212-22.
17. Agnoletti G, Ou P, Celermajer DS, Boudjemline Y, Marini D, Bonnet D, Aggoun Y. Acute angulation of the aortic arch predisposes a patient to ascending aortic dilatation and aortic regurgitation late after the arterial switch operation for transposition of the great arteries. *J Thorac Cardiovasc Surg.* 2008;135(3):568-72.
18. Martins D, Khraiche D, Legendre A, Boddaert N, Raisy O, Bonnet D, Raimondi F. Aortic angle is associated with neo-aortic root dilatation and regurgitation following arterial switch operation. *Int J Cardiol.* 2019;280:53-6.
19. Lalezari S, Hazekamp MG, Bartelings MM, Schoof PH, Gittenberger-De Groot AC. Pulmonary artery remodeling in transposition of the great arteries: relevance for neo-aortic root dilatation. *J Thorac Cardiovasc Surg.* 2003;126(4):1053-60.
20. Lalezari S, Mahtab EA, Bartelings MM, Wisse LJ, Hazekamp MG, Gittenberger-de Groot AC. The outflow tract in transposition of the great arteries: an anatomic and morphologic study. *Ann Thorac Surg.* 2009;88(4):1300-5.
21. de Beaufort HWL, Trimarchi S, Korach A, Di Eusanio M, Gilon D, Montgomery DG, Evangelista A, Braverman AC, Chen EP, Isselbacher EM, et al. Aortic dissection in patients with Marfan syndrome based on the IRAD data. *Ann Cardiothorac Surg.* 2017;6(6):633-41.
22. Groth KA, Stochholm K, Hove H, Kyhl K, Gregersen PA, Vejlsstrup N, Ostergaard JR, Gravholt CH, Andersen NH. Aortic events in a nationwide Marfan syndrome cohort. *Clin Res Cardiol.* 2017;106(2):105-12.



A wireframe illustration of a human figure, primarily showing the head, neck, and upper torso. The figure is composed of a dense network of thin, light-colored lines forming a mesh that outlines the body's contours. The background is a dark, solid color. The text is positioned on the right side of the image, overlaid on the wireframe.

# APPENDICES

List of publications

Authors' affiliations

Dankwoord

Curriculum Vitae

## List of Publications

**van der Palen RLF**, Blom NA, Kuipers IM, Rammeloo LAJ, Jongbloed MRM, Konings TC, Bouma BJ, Koolbergen DR, Hazekamp MG. Long-term outcome after the arterial switch operation: 43 years of experience. *Eur J Cardiothorac Surg*. 2021. Online ahead of print.

**van der Palen RLF**, Juffermans JF, Kroft LJM, Hazekamp MG, Lamb HJ, Blom NA, Roest AAW, Westenberg JJM. Wall shear stress in the thoracic aorta at rest and with dobutamine stress after arterial switch operation. *Eur J Cardiothorac Surg*. 2021;59(4):814-822.

**van der Palen RLF**, Baart SJ, van Geloven N, Hazekamp MG, Blom NA. Neo-aortic growth rate and diameter as risk factors for neo-aortic valve regurgitation after arterial switch operation. *Heart*. 2020;106(24):1950.

**van der Palen RLF**, Deurvorst QS, Kroft LJM, van den Boogaard PJ, Hazekamp MG, Blom NA, Lamb HJ, Westenberg JJM, Roest AAW. Altered ascending aorta hemodynamics in patients after arterial switch operation for transposition of the great arteries. *J Magn Reson Imaging*. 2020;51(4):1105-1116.

**van der Palen RLF\***, van der Zee C\*, Vink AS, Knobbe I, Jurgens SJ, van Leeuwen E, Bax CJ, du Marchie Sarvaas GJ, Blom NA, Haak MC, Bilardo CM, Clur SA. \*Shared first authorship. Transposition of the great arteries: Fetal pulmonary valve growth and postoperative neo-aortic root dilatation. *Prenat Diagn*. 2019;39(12):1054-1063.

**van der Palen RLF**, van der Bom T, Dekker A, Tsonaka R, van Geloven N, Kuipers IM, Konings TC, Rammeloo LAJ, ten Harkel ADJ, Jongbloed MRM, Koolbergen DR, Mulder BJM, Hazekamp MG, Blom NA. Progression of aortic root dilatation and aortic valve regurgitation after the arterial switch operation. *Heart*. 2019;105(22):1732-1740.

**van der Palen RLF**, Roest AAW, van den Boogaard PJ, de Roos A, Blom NA, Westenberg JJM. Scan-rescan reproducibility of segmental aortic wall shear stress as assessed by phase-specific segmentation with 4D flow MRI in healthy volunteers. *Magn Reson Mater Phy*. 2018;31(5):653-663.

**van der Palen RLF**, Barker AJ, Bollache E, Garcia J, Rose MJ, van Ooij P, Young LT, Roest AA, Markl M, Robinson JD, Rigsby CK. Altered aortic 3D hemodynamics and geometry in pediatric Marfan syndrome patients. *J Cardiovasc Magn Reson*. 2017;19(1):30-42.

**van der Palen RLF**, van der Wal AC, Robles de Medina PG, Blom NA, Clur SA. Uhl's anomaly: Clinical spectrum and pathophysiology. *Int J Cardiol*. 2016;209:118-121.

**van der Palen RLF**, Westenberg JJ, Hazekamp MG, Kuipers IM, Roest AA. Four-dimensional flow cardiovascular magnetic resonance for the evaluation of the atrial baffle after Mustard repair. *Eur Heart J Cardiovasc Imaging*. 2016;17(3):353.

**van der Palen RLF**, Bulten BF, Mavinkurve-Groothuis AM, Bellersen L, van Laarhoven HW, Kapusta L, de Geus-Oei LF. Catecholamines influence myocardial <sup>123</sup>I MIBG uptake in neuroblastoma patients. *Nuklearmedizin*. 2013;52(6):228-234.

Baart SJ, **van der Palen RLF**, Putter H, Tsonaka R, Blom NA, Rizopoulos D, van Geloven N. Joint Modeling Tutorial - Application of neo-aortic root dilatation after arterial switch operation. *Submitted*.

Škorić-Milosavljević D, Tadros R, Bosada FM, Tessadori F, van Weerd JH, Odilia I, Woudstra, Tjong FVY, Lahrouchi N, Bajolle F, Cordell HJ, Agopian AJ, Pickardt T, Blue GM, Barge-Schaapveld DQCM, Preuss C, Lodder EM, Goodship JA, Mitchell LE, Beekman L, Bökenkamp R, Müller-Nurasyid M, KORA-Study Group, Vliegen HW, Konings TC, van Melle JP, van Dijk APJ, van Kimmenade RRJ, Roos-Hesselink JW, Sieswerda GT, Galan P, Lathrop M, Munter M, Al-Chalabi A, Shaw CE, Shaw PJ, Morrison KE, Veldink JH, van den Berg LH, Radivojkov-Blagojević M, Meitinger T, Bouma BJ, Chaix MA, Kline J, Bassett AS, Andelfinger G, **van der Palen RLF**, Bouvagnet P, Clur SAB, Breckpot J, Kerstjens-Frederikse WS, Winlaw DS, Bauer U, Mital S, Goldmuntz E, Keavney B, Bonnet D, Mulder BJ, Tanck MWT, Bakkers J, Christoffels VM, Postma AV, Bezzina CR. Common genetic variants contribute to risk of transposition of the great arteries. *Submitted*.

Perinajová R, Juffermans JF, Westenberg JJM, **van der Palen RLF**, van den Boogaard PJ, Lamb HJ, Kenjereš S. Geometrically induced wall shear stress variability in CFD-MRI coupled simulations of blood flow in the thoracic aortas. *Comput Biol Med*. 2021. Online ahead of print.

Heijstek V, Habib M, **van der Palen RLF**, van Doorn R, Hissink Muller P. Macrophage activation syndrome in a newborn: report of a case associated with neonatal lupus erythematosus and a summary of the literature. *Pediatr Rheumatol Online J*. 2021;19(1):13.

Terol Espinosa de Los Monteros C\*, **van der Palen RLF\***, Hazekamp MG, Rammeloo L, Jongbloed MRM, Blom NA, ten Harkel ADJ. \*Shared first authorship. Oxygen uptake efficiency slope is strongly correlated to  $VO_{2peak}$  long-term after arterial switch operation. *Pediatr Cardiol*. 2021. Online ahead of print.

Juffermans JF, Westenberg JJM, van den Boogaard PJ, Roest AAW, van Assen HC, **van der Palen RLF**, Lamb HJ. Reproducibility of aorta segmentation on 4D flow MRI in healthy volunteers. *J Magn Reson Imaging*. 2020;53(4):1268-1279.

van Broekhoven I, Kroft LJM, **van der Palen RLF**. Imaging large arteries after arterial switch operation. *Heart*. 2020;106(12):891-950.

Bruyndonckx L, Kroft LJM, Bekker V, Roest AAW, **van der Palen RLF**. Umbilical vein catheter protruding through a pulmonary vein in a patient with an infracardiac type total abnormal pulmonary venous drainage. *Pediatr Cardiol*. 2019;40(4):878-879.

Kamphuis VP, Westenberg JJM, **van der Palen RLF**, van den Boogaard PJ, van der Geest RJ, de Roos A, Blom NA, Roest AAW, Elbaz MSM. Scan-rescan reproducibility of diastolic left ventricular kinetic energy, viscous energy loss and vorticity assessment using 4D flow MRI: analysis in healthy subjects. *Int J Cardiovasc Imaging*. 2018;34(6):905-920.

Kamphuis VP, **van der Palen RLF**, de Koning PJH, Elbaz MSM, van der Geest RJ, de Roos A, Roest AAW, Westenberg JJM. In-scan and scan-rescan assessment of LV in- and outflow volumes by 4D flow MRI versus 2D planimetry. *J Magn Reson Imaging*. 2018;47(2):511-522.

Garcia J, **van der Palen RLF**, Bollache E, Jarvis K, Rose MJ, Barker AJ, Collins JD, Carr JC, Robinson J, Rigsby CK, Markl M. Distribution of blood flow velocity in the normal aorta: Effect of age and gender. *J Magn Reson Imaging*. 2018;47(2):487-498.

Kamphuis VP, Westenberg JJM, **van der Palen RLF**, Blom NA, de Roos A, van der Geest R, Elbaz MSM, Roest AAW. Unravelling cardiovascular disease using four dimensional flow cardiovascular magnetic resonance. *Int J Cardiovasc Imaging*. 2017;33(7):1069-1081.

Bökenkamp R, Aguilar E, **van der Palen RLF**, Sojak V, Bruggemans EF, Hruda J, Kuipers IM, Hazekamp MG. Reoperation for right ventricular outflow tract obstruction after arterial switch operation for transposition of the great arteries and aortic arch obstruction. *Eur J Cardiothorac Surg*. 2016;49(5):e91-96.

van der Bom T\*, **van der Palen RLF\***, Bouma BJ, van Veldhuisen SL, Vliegen HW, Konings TC, Zwinderman AH, Blom NA, Koolbergen DR, Hazekamp MG, Mulder BJ. \*Shared first authorship. Persistent neo-aortic growth during adulthood in patients after an arterial switch operation. *Heart*. 2014;100(17):1360-1365.

Nijkamp A, **van der Palen RLF**, Draaisma JM, Jacobs BS, Burger DM. Inadvertent intravenous polyethylene glycol 4000 infusion in a child. *Clin Toxicol (Phila)*. 2012;50(9):866.

ten Dam K, **van der Palen RLF**, Tanke RB, Schreuder MF, de Jong H. Clinical recognition of mid-aortic syndrome in children. *Eur J Pediatr*. 2013;172(3):413-416.

Bulten BF, **van der Palen RLF**, van Laarhoven HW, Kapusta L, Mavinkurve-Groothuis AM, de Geus-Oei LF. Interobserver variability of heart-to-mediastinum ratio in I-123 MIBG sympathetic imaging. *Curr Cardiol Rep.* 2012;14(4):389-390.

**van der Palen RLF**, Bok LA. A boy with a red swelling of the lower leg. *Ned Tijdschr Geneeskd.* 2010;154:A549.

Bannink EM, **van der Palen RLF**, Mulder PG, de Muinck Keizer-Schrama SM. Long-term follow-up of GH-treated girls with Turner syndrome: metabolic consequences. *Horm Res.* 2009;71(6):343-349.

Bannink EM, **van der Palen RLF**, Mulder PG, de Muinck Keizer-Schrama SM. Long-term follow-up of GH-treated girls with Turner syndrome: BMI, blood pressure, body proportions. *Horm Res.* 2009;71(6):336-342.



## Authors' affiliations

### **Leiden University Medical Center**

*Department of Pediatrics, division of Pediatric Cardiology*

Nico A. Blom

Arno A.W. Roest

Arend D.J. ten Harkel

Roel L.F. van der Palen

*Department of Cardiothoracic Surgery*

Mark G. Hazekamp

David R. Koolbergen

*Department of Radiology*

Hildo J. Lamb

Albert de Roos

Jos J.M. Westenberg

Lucia J.M. Kroft

Joe F. Juffermans

Pieter J. van den Boogaard

*Department of Cardiology and the department of Anatomy & Embryology*

Monique R.M. Jongbloed

*Department of Obstetrics and Fetal Medicine*

Monique C. Haak

*Department of Biomedical Data Sciences, Section Medical Statistics*

Nan van Geloven

Roula Tsonaka

*Medical students*

Annika Dekker

Quirine S. Deurvorst

### **Amsterdam University Medical Centers**

*Department of Pediatrics, division of Pediatric Cardiology – location AMC*

Nico A. Blom

Irene M. Kuipers

Sally-Ann B. Clur

*Department of Pediatrics, division of Pediatric Cardiology – location VUmc*

Lukas A.J. Rammeloo

Ingmar Knobbe

*Department of Cardiothoracic Surgery*

David R. Koolbergen

Mark G. Hazekamp

*Department of Cardiology – location AMC*

Berto J. Bouma

Barbara J.M. Mulder

Arja S. Vink

Teun van der Bom

*Department of Cardiology – location VUmc*

Thelma C. Konings

*Department of Radiology*

Pim van Ooij

*Department of Obstetrics and Gynaecology – location AMC*

Elizabeth van Leeuwen

*Department of Obstetrics and Gynaecology – location VUmc*

Caroline J. Bax

*Medical students*

Carlijn van der Zee

Sean J. Jurgens

**University Medical Center Groningen**

*Department of Pediatric Cardiology*

Gideon J. du Marchie Sarvaas

*Department of Obstetrics and Fetal Medicine*

Caterina M. Bilardo

**Erasmus Medical Center**

*Department of Biostatistics*

Sara J. Baart

**Northwestern University Feinberg School of Medicine, Chicago, Illinois, USA**

*Department of Radiology*

Michael Markl

Alex J. Barker

Cynthia K. Rigsby

Joshua D. Robinson

Emilie Bollache

Julio Garcia

Pim van Ooij

**Ann & Robert H. Lurie Children's Hospital of Chicago, Chicago, Illinois, USA**

*Department of Pediatrics, division of Pediatric Cardiology*

Joshua D. Robinson

Luciana T. Young

*Department of Pediatrics, division of Medical Imaging*

Cynthia K. Rigsby

Michael J. Rose

**McCormick School of Engineering, Northwestern University, Chicago, Illinois, USA**

*Department of Biomedical Engineering*

Michael Markl

## Dankwoord

Dit proefschrift is het resultaat van een fijne samenwerking, inzet en steun van enthousiaste collega's, patiënten en vrijwilligers. Allereerst wil ik alle patiënten en vrijwilligers bedanken: zonder jullie bereidheid was er geen onderzoek naar de bloedstroom in de aorta mogelijk geweest.

Prof. dr. Blom, beste Nico, bedankt voor het vertrouwen dat je me gaf door mij als jonge fellow kindercardiologie mee te nemen naar de kinderhartmissie in Suriname en me ruimte te geven voor het onderzoeksproject. De start met het bijeenzoeken van echodata uit de handgeschreven schriftjes en stoffige videobanden was een evenzo geduldige activiteit als het vissen op het Brokopondostuwmeer. Beide onvergetelijk met een mooie vangst als resultaat. Jij bent een voorbeeld in vele opzichten, bedankt voor de mogelijkheden die je me hebt gegeven binnen de kindercardiologie.

Prof. dr. Hazekamp, beste Mark, hartelijk dank voor de begeleiding rondom het proefschrift. Jouw ervaring en input maakt wetenschappelijke papers krachtiger en vernieuwend.

Mijn co-promotor, dr. Roest, beste Arno, als directe begeleider sta jij aan de basis van dit proefschrift. Jouw enthousiasme en positivisme werken stimulerend en je snelle beoordeling van manuscripten zorgt voor behoud van de juiste flow en klinische twist. Dank daarvoor. Je bull-ride was onvergetelijk, evenals vele andere congressmomenten.

Prof. dr. Lamb, beste Hildo, hartelijk dank voor de goede samenwerking met de afdeling Radiologie. Jullie rol in het verkrijgen van uniek inzicht in pathologie en pathofysiologie door imaging van congenitale hartziekten is essentieel.

Dr. Westenberg, beste Jos, het 4D flow MRI-onderzoek was niet mogelijk geweest zonder jouw hulp en betrokkenheid. Je schakelde snel zodat kwantitatieve analyse van geavanceerde hemodynamische parameters voor de aorta mogelijk werd. Bedankt voor je ideeën en wetenschappelijke adviezen.

Dr. Kroft, beste Lucia, bedankt voor het uitwerken van MRI-data en je waardevolle bijdrage aan het schrijven van de artikelen.

Pieter van den Boogaard, veel dank ben ik jou verschuldigd voor het scannen van de patiënten en vrijwilligers. Niemand is meer toegewijd dan jij om de kindercardiologische patiënt door de MRI-scansessies te begeleiden. Gelukkig vond jij de real time control errors tijdens de 4D flow acquisities even vervelend als ik.

Dr. Clur, beste Sally, jouw bevoegenheid voor de foetale cardiologie is inspirerend en resulteerde in twee papers samen, waarvan een te vinden in dit proefschrift. Veel dank hiervoor.

Dr. Kuipers, beste Irene, jouw tomeloze enthousiasme en inzet zorgden voor state-of-the-art echocardiografie. Dank voor je steun tijdens fasen van geluk en verdriet.

Dr. van Geloven, dr. Tsonaka en dr. Baart, beste Nan, Roula en Sara, jullie inzicht en bijdrage aan de statistische analyses mag niet onderschat worden. Bedankt voor de prettige samenwerking.

Mijn kindercardiologie roots liggen in meerdere centra: Veldhoven, Nijmegen, Utrecht, Amsterdam en Leiden. Dank aan diegenen die mij vanuit die basis gevormd hebben.

Kindercardiologen, kinderhartchirurgen, fellows, PA's, echocardiografisten en betrokkenen uit het Centrum voor Aangeboren Hartafwijkingen Amsterdam-Leiden (CAHAL), de academische zorg die we dagelijks leveren aan de patiënten is een teamprestatie en is het belangrijkste in ons werk. Ik ben trots om van deze groep deel te mogen uitmaken. Speciale dank aan de Leidse kindercardiologen, voor de gelegenheid die ik heb gekregen dit proefschrift af te ronden.

Researchers of the Northwestern Cardiovascular MR Imaging Group and Lurie Children's Hospital of Chicago. Prof. dr. Markl, dear Michael, thank you for having me, for educating me, and making me part of such an impressive research program and team during my stay. Dear Alex, Cynthia, Joshua, Julio, Emilie, Susanne, Michael Rose and (former associate) Pim, the way in which you are engaged in developing novel advanced imaging (analysis) techniques to better understand complex congenital cardiovascular diseases is outstanding. I felt right at home and you introduced me to beautiful Chicago. Many thanks for the great time and for the paper we wrote together.

Mijn waardering gaat ook uit naar voorgaande en huidige promovendi. Joe, voor de geometrische analyse van de aortaboog. Friso, voor je hulp bij het creëren van de cover afbeelding. Vivian, Ineke, Lisette en Covadonga, voor jullie photoshop kunsten, koffie, zoetheid en congresgezelligheid.

Gabriella, I am grateful for your drawings for the Introduction of this thesis.

Mijn paranimfen, Ingmar Knobbe en Sander Cretier: Ingmar, een interessante discussie over verhoogde rechterkamerdruk als eerste kennismaking leidde later tot een overlappend fellowship kindercardiologie. Geweldig was dat, met hoogtepunten als het poolbiljart in Vegas en hardlopen aan Dockweiler Beach in LA. Gelukkig vonden we allebei een plek binnen

het CAHAL en werden we in die tijd beide trotse vader. Sander, kindergeneeskunde en beeldvorming zijn de kernwoorden die brachten waar we beide nu staan. Dank voor alle steun en gezelligheid, veelal onder culinair genot. Medical imaging is key to patient understanding, keep up the good clinical work. Dank dat jullie mijn paranimf zijn.

Vrienden van het academische jaar 2000. Na het volbrengen van de studie Geneeskunde werd de Rotterdamse hunkering door velen van jullie (tijdelijk of permanent) geruild voor een buitenlands avontuur of een tintje Amsterdamse bravoure. Zo ook voor mij als zuiderling. Dank voor de vele gezellige momenten samen.

Lieve familie, schoonfamilie en vrienden, ik prijs mij enorm gelukkig met jullie. Ook al wonen we niet bij elkaar om de hoek, jullie zijn immer geïnteresseerd en staan altijd voor me klaar.

Mijn allerliefste ouders en broer Mark, dank voor jullie onvoorwaardelijke liefde en steun, voor alles wat jullie voor me doen en gedaan hebben. Woorden kunnen niet genoeg uitdrukken hoeveel jullie voor me betekenen. Mam, je mag dit helaas niet meer meemaken, maar wat zou je trots zijn.

Lieve Linda, bedankt voor jouw liefde, steun en Brabantse nuchterheid, voor onze prachtige kinderen Rein en Sophie en voor onze derde spruit die we oktober dit jaar verwachten. Niets is belangrijker dan jullie.

## Curriculum Vitae

Roel Laurens Frederik van der Palen was born on the 29<sup>th</sup> of March 1982 in Valkenswaard. After graduation from secondary school in 2000 (Hertog Jan College, Valkenswaard), he studied medicine at the Erasmus University of Rotterdam and passed the doctorate exam in 2006 (cum laude). He started his training in Pediatrics (2007) at the Radboud University Medical Center, Nijmegen (under supervision of dr. Jos Draaisma) after a successful residency (not-in-training) and peripheral internship (in training) at the Maxima Medical Center, Veldhoven (under supervision of dr. Martin de Kleine). At these centers, he became intrigued by the clinical subspecialty Pediatric Cardiology and it was not surprising that he completed his training Pediatrics with a profiling internship Pediatric Cardiology (Wilhelmina Children's Hospital, Utrecht). Thereafter, a 3-year clinical fellowship Pediatric Cardiology was pursued at the Amsterdam Medical Center in Amsterdam, part of the Center for Congenital Heart Disease Amsterdam–Leiden (CAHAL), under supervision of prof. dr. Nico Blom (2012-2015). In the final year of his fellowship, he started with his PhD project and submitted a research proposal to the Dutch Heart Foundation focusing on the aorta hemodynamics in patients with transposition of the great arteries after arterial switch operation. This research proposal was awarded a dr. E. Dekker grant (2014T087) and the research project was conducted in collaboration with the department of Radiology of the Leiden University Medical Center. A subpart of the project was performed in Chicago (USA), at the departments of Pediatric Cardiology and Radiology of the Ann & Robert H. Lurie Children's Hospital of Chicago and the Northwestern University Feinberg School of Medicine. Since 2016, he works as a staff pediatric cardiologist at the Leiden University Medical Center. Roel married Linda in May 2015 and together they have two children, Rein (2016) and Sophie (2018). They are expecting their third child October 2021.





